Gent University
Faculty of Sciences

SHALLOW MARINE ACOUSTIC IMAGING IN ENVIRONMENTAL INVESTIGATIONS

ONDIEPE MARIENE AKOESTISCHE BEELDVORMING IN MILIEUSTUDIES

Tine Missiaen
2008

Dissertation submitted for the degree of Doctor of Science: Geology
Promotor: Prof. Dr. Jean-Pierre Henriet

ISBN 978-90-9022828-0

Dankwoord

Het is schier onmogelijk om alle mensen te bedanken die op een of andere manier, direct of indirect, hebben bijgedragen aan dit proefschrift. Ik wil er hier dan ook alleen een paar uitpikken, en hoop dat de anderen mij dit vergeven.

In eerste instantie wil ik graag Koen De Rijcker bedanken voor zijn niet aflatende steun tijdens de vele campagnes op zee. De ontelbare uren die we samen hebben doorgebracht bij het ontwerpen, bouwen en uittesten van het 3D opnamesysteem staan in mijn geheugen gegrift. Je enthousiasme en onuitputtelijke energie (waar blijf je het vandaan halen?) maakt samenwerken met jou een groot plezier.

Beste Wim Versteeg, jij was, en bent nog steeds, een grote steun en toeverlaat. En dat geldt niet alleen voor de nauwe samenwerking tijdens de seismische campagnes, maar ook – en vooral – de vele technische discussies die ik met jou gevoerd heb. Je leerrijke en constructieve opmerkingen tijdens het schrijven van dit proefschrift heb ik ontzettend gewaardeerd. Ik hoop nog lang ook met jou te kunnen samenwerken.

Vadim Paka en Salle Kroonenberg, het was en is een waar genoegen om met jullie te mogen werken. Jullie bezieling voor de wetenschap, gecombineerd met een niet aflatend plezier in het werk en de bereidheid om ook buiten de lijntjes te kleuren, hebben mij zeker beïnvloed. Nigel Wardell, ik hoop dat onze fijne samenwerking van de afgelopen jaren in de toekomst wordt voortgezet. Ook aan Tom McGee, een van mijn eerste ‘mentors’ in Utrecht, ben ik veel dank verschuldigd. Ik kan nog veel van jullie leren.

Zonder mijn promotor, Jean-Pierre Henriet, zou dit proefschrift er niet geweest zijn. Hij heeft me, jaren geleden, enthousiast gemaakt voor de mariene geofysica en dat enthousiasme werkt door tot op de dag van vandaag. Zijn onstuitbare wetenschappelijke nieuwschierigheid, brede vakkennis en grote gedrevenheid zijn altijd een grote inspiratiebron geweest voor mij.

Last but not least, wil ik hier graag een mij zeer dierbare persoon postuum bedanken. Zij heeft in de eerste plaats mijn postgraduaatopleiding in de kwartairgeologie mogelijk gemaakt, maar boven alles is zij steeds een lichtend voorbeeld geweest voor mij. Ik draag dan ook van harte dit proefschrift aan haar op.

Opgedragen aan Tine Velzeboer

Dedicated to Tine Velzeboer

Shallow marine acoustic imaging in environmental investigations

Ondiepe mariene akoestische beeldvorming in milieustudies

CONTENTS

CHAPTER 1
INTRODUCTION

1.1 Detailed seismic imaging in shallow water

Shallow water environments are among the most dynamic coastal zones, subject to rapid sedimentary fluxes and a prominent focus for human activities. They therefore represent a stratigraphic archive of short-term environmental changes and human activity. The rapid increase in the development of coastal areas has resulted in increased stress on the marine environment. A thorough knowledge of these areas is essential for both land and marine use planning. However, these shallow environments present serious technological challenges, not only related to the setting (surf zone, high tidal amplitudes, shallow water depths) and the nature of the sediments (very soft sediments, presence of shallow gas), but also regarding the man-made influences and environmental pressure (Missiaen et al. 2005).

Geophysical investigations, and in particular seismic imaging techniques, form a perfect tool in obtaining a detailed description of the shallow subsurface. Due to its reliability and resolving power, the seismic method has become a major investigation tool in both environmental and geo-technical studies in nearshore areas, and increasingly also in archaeological studies. In this thesis we will focus on a few of the most recent developments in very high resolution (VHR)* shallow seismic imaging in marine environments, with special emphasis on 3D seismic techniques and the challenges involved in munition dumpsite research and archaeological site investigations. The term "VHR" here refers to mean source frequencies ≥1 kHz and vertical and horizontal resolution in the sub-meter range.

The last decade has seen a significant development in VHR 2D seismic acquisition in shallow water environments. Careful attention with regard to the source, receiver, their geometrical arrangement and the operational conditions is needed to match the target under study and survey requirements. However the seabed and shallow subsurface are by nature three-dimensional structures and ideally should be treated as such. This requires the use of 3D techniques. The design of VHR 3D surveys in shallow water environments however requires specific strategies and the optimum approach will necessarily be a compromise: on the one hand there is the need for high resolution requiring the use of high frequencies, on the other hand there are the constraints placed on sampling and positioning accuracy (Gardner 1993, Missiaen 2005). In many cases the survey design will also be dictated by the field conditions and the cost-effectiveness (Henriet et al. 1992, Abdulah et al. 1997, Marsset et al. 2001).

VHR seismic techniques play an increasingly prominent role in environmental and engineering assessments. An important application concerns the investigation of chemical munition dumpsites. Sea-dumped chemical weapons have been the subject of growing concern, as their amount in the North European seas alone runs into hundreds of thousand of tons at least (Missiaen & Henriet 2002). The "Paardenmarkt" dumpsite offshore Knokke-Heist is one well-known example. Over the last years this old WW1 munition dumpsite off the Belgian coast has been the subject of detailed research (Missiaen et al. 2001, 2002c, Henriet & Missiaen 2004, 2005). Most recently, detailed investigations have focused on a large WW2 chemical munition dumpsite east of Bornholm in the southern Baltic Sea (Missiaen & Paka 2007, Missiaen & Feller 2008).

The investigation of submerged archaeological sites using VHR acoustic techniques is receiving more and more attention. With an ever-increasing number of wrecks and other archaeological structures being discovered, the necessity for management and preservation of underwater cultural heritage is recognised internationally (Arnott et al. 2005). It is nowadays well recognised that buried artefacts are often best protected if left alone. Non-intrusive high-resolution techniques capable of locating and identifying wooden materials buried in the seabed, possibly also assessing their state of preservation/decay, are therefore becoming increasingly important (Bull et al. 1998, Quinn et al. 2000, Missiaen et al. 2004, Missiaen & Versteeg 2006). The study of submerged prehistoric (terrestrial) landscapes and their archaeological potential forms an important new challenge (Missiaen et al. 2008b).

Coastal areas are marked by the widespread occurrence of gassy sediments. Shallow gas renders the acquisition of high-quality seismic images particularly difficult. The potential impact on the marine environment and on human activities (with regard to geotechnical and engineering works) stresses the need for a better knowledge of shallow gassy sediments. Over the years shallow gas has become the subject of detailed studies focused on a qualitative description of the acoustic characteristics (e.g. Hart & Hamilton 1993, Figuerido et al. 1996). Recent advances in seismic techniques allow a more quantitative approach to the analysis of the acoustic responses in the presence of shallow gas (Best et al. 2004, Robb et al. 2006). A study of the shallow gassy sediments offshore the Belgian coast based on very high resolution seismic data focuses on various aspects of the gas such as seismic evidence, origin, distribution, quantification, and bubble resonance effects (Missiaen et al. 2002b).

A particular challenge is the transition environment that marks the land-sea boundary, such as intertidal flat areas and lagoons. The extremely shallow water depths demand an adapted seismic strategy and specific operational techniques have to be developed to achieve sea-land data continuity without loss of coverage (Zgur et al. 2003). This can optimally be done by using both land and marine sources. A recent study was carried out in the Verdronken Land van Saeftinge in the Westerschelde estuary, where high tidal amplitudes enabled the application of different techniques on land and on water (seismic, geo-electric, electromagnetic, CPT, coring). The results of this study indicate that no single technique can provide all the answers, and only an integrated use of complementary methods will allow to get a better grip on the sedimentary architecture (Missiaen et al. 2008a). This specific topic will not be further discussed in this thesis, as it focuses largely on non-marine and non-seismic methods.

1.2 VHR 2D seismic imaging

The main objective of VHR 2D seismic research is to image the shallow sedimentary sequence with the highest possible detail. For munition dumpsite studies and archaeological site investigations the detection of buried objects becomes an important additional goal. The acoustical detection of buried objects or archaeological artefacts, however, is not always straightforward due to a number of reasons: (1) unknown size of the objects – possibly too small for acoustic imaging, (2) unfavourable object depth near layer boundaries, (3) weak acoustic signals due to shallow gas, and (4) insufficient impedance difference due to a high degree of corrosion or decay. The main requirements for successful VHR 2D seismic imaging are a high vertical and lateral resolution. This has implications for the type of source that is used for these investigations.

1.2.1 Vertical resolution

Vertical resolution is the ability to separate two layers, which are very close together, as two separate features (Sheriff 1996). In order for a seismic wavelet to resolve thin layers, the wavelength must be sufficiently small. The dominant wavelength λ of a seismic wave depends on velocity V and dominant frequency f_m ($\lambda=V/f_m$). The vertical resolvable limit can be approximated by one quarter of the dominant wavelength (¼λ), as shown by the following equation :

$$\Delta R_z = V / 4 f_m \cos\alpha \qquad (1.1)$$

where α is the angle of incidence (Vermeer 1999, Mosher et al. 2002). The minimum resolvable distance is thus reached when the angle of incidence is near vertical, in other words for the near offset traces. Since velocity will increase with depth, also the wavelengths will increase with depth, and resolution will generally decrease. However this effect will be almost negligible for shallow applications.

In reality, the best resolution requires a spectrum of frequencies. If seismic wavelets were extremely sharp, resolution would not be a problem, but in fact only a limited range of frequencies are involved. The temporal bandwidth will not only depend on the source spectrum but also on the noise level of the data (Yilmaz 1987). Vertical resolution is also determined by absorption and attenuation. Due to the attenuation of higher frequencies/shorter wavelengths the practical separable limit is much lower, often half the dominant wavelength. Last but not least vertical resolution will also depend highly on signal repeatability – an important factor in very high resolution seismics. Indeed an event can be identified more reliably from one trace to another and its location in time or depth becomes less ambiguous as the pulse becomes more repeatable.

1.2.2 Horizontal resolution

Horizontal resolution refers to how close two reflection points can be situated horizontally yet be recognized as two separate points (Yilmaz 1987). Similar to vertical resolution, horizontal resolution will also depend on the dominant signal wavelength and broader bandwidths incorporating higher frequencies will yield a higher resolution. However, horizontal and vertical resolution will change at different rates, and and for unmigrated data horizontal resolution will always be less than vertical resolution (Sheriff 1996).

Horizontal resolution is generally described in terms of the first Fresnel zone. This is defined as the radius of the area of an interface circumscribed by the passage of ¼λ of the spherical wavefront (Sheriff 1996). Within the Fresnel zone reflection contributions will add up constructively; outside this zone peaks and troughs tend to cancel each other. The smaller the Fresnel zone, the easier it is to differentiate between two reflecting points. For a plane reflector and small offsets the first Fresnel radius is given by $(V/2)\ (t / f_m)^{1/2}$ where t denotes the two-way traveltime.

Horizontal resolution can be reduced by migration, which seeks to collapse the Fresnel zone to approximately the dominant wavelength, either along 2D lines of the profile or fully for 3D data (Yilmaz 1987). Whereas two-dimensional migration will shorten the Fresnel zone in the direction parallel to the line orientation but does not affect the perpendicular direction, 3D migration will collapse the Fresnel zone to a small circle. Horizontal resolution will also be favoured by seismic sources with a high directivity and a narrow beam footprint, as the latter

will result in a reduced reverberation and increased signal-to-noise ratio (Wunderlich et al. 2005).

1.2.3 Source options

VHR seismic technology offers a wide range of high-frequency acoustic sources, including piezo-electric transducers, sparker, watergun, and boomer sources. Watergun sources mostly lack high frequencies ($f_m \approx 700$ Hz) and are marked by a low repeatability. Sparker sources have a fairly broad bandwidth but their dominant frequency is rather limited ($f_m = 0.6$-1 kHz) and they often show low repeatability (Verbeek 1995). Transducer sources are generally marked by a high dominant frequency ($f_m = 4$-10 kHz) and good repeatability, but have a limited penetration depth. Their built-in receiver system often has the disadvantage that it records the envelope of the data, which contains amplitude information only and no phase information.

Boomer sources combine high frequencies ($f_m \approx 2$ kHz) with a broad power spectrum, and seem to offer a good compromise between resolution (order of 20-25 cm) and penetration (tens of meters at least) for shallow water site surveys. They generally have a good repeatability, although this will depend on the sea state (a rough sea will constantly change the source direction, thus reducing the repeatability). The Seistec Boomer also supports a line-in-cone receiver, and is marked by a large operational bandwidth, ranging from roughly 1 kHz to well over 8 kHz (dominant frequency 3-4 kHz). The suitability of boomer sources in VHR 2D and 3D seismic work has been shown on various occasions (e.g. Henriet et al. 1992, Missiaen et al. 1996, Davies & Austin 1997, Mosher & Simpkin 1999, Missiaen et al. 2002a, Müller et al. 2002).

The parametric echosounder is a non-linear transducer source which combines high resolution (10-15 cm) with a narrow beam and short pulse length. The source simultaneously transmits two signals of slightly different high frequencies (e.g. 100 and 110 kHz) at high sound pressures. Nonlinear interactions generate new frequencies in the water, one of them being the difference frequency which has a bandwidth similar to the primary frequency. Detailed technical aspects of this source are described in Wunderlich et al. (2005). Penetration can reach up to a few tens of meters in soft sediments. The narrow beam and small footprint make this source very suitable for buried object detection. In recent years parametric echosounder sources have been used very successfully in a wide range of geotechnical, environmental and archaeological studies (e.g. Wunderlich et al. 2005, Missiaen & Feller 2008, Missiaen et al. 2008a).

1.3 Moving from 2D to 3D seismic imaging

Up to this day the principal VHR marine seismic acquisition technique involves single- and multi-channel arrays. Although these allow detailed imaging of the shallow subsurface, still they remain inaccurate due to the 2D approximation - since the data are interpreted in a vertical plane along the direction of the ship's movement. The use of a 3D field layout can overcome this problem. Although it is perfectly feasible to acquire densely spaced 3D data above oil fields, in view of the economic importance and commercial interests, it is still too expensive to do this in (academic) VHR 3D exploration.

In the early nineties the Renard Centre of Marine Geology (RCMG) played a pioneering role in scaling down the shallow marine 3D method to very high resolution, thereby entering the world of small-scale geological structures (Henriet et al. 1992). In a modest and cost-effective way VHR 3D seismic data were acquired using a compact field system. Despite the good results, the

data were not of optimal quality due to a number of shortcomings. Further adaptation and optimisation of the 3D acquisition method were therefore required.

Based on this past experience a new 3D acquisition system was developed at RCMG in the framework of an EC project (Missiaen et al. 2002a). The new 3D array is flexible, which allows it to be tailored to the specific site characteristic. The system is designed for studies in shallow water (< 20 m), providing limited penetration (< 50 m bsf) and aimed at small target sites (order of magnitude 100x100 m). The desired resolution (both horizontal and vertical) is in the sub-meter range.

Until recently no well-established practice for marine VHR 3D survey design seemed to exist. The relationship between geophysical, operational and cost restraints is not always clearly understood, and often leads to conflicting requirements. Guidelines available in literature often relate to survey design optimisation for deep exploration 3D seismics, and seldom cater for very high resolution and shallow water specifications. One of the goals was therefore to come up with some practical specifications and guidelines for VHR 3D survey design in shallow water environments (Missiaen 2005).

Still we should keep in mind that there is not one unique VHR 3D seismic methodology. The optimal seismic strategy will depend on the geological target, sampling laws, desired resolution, acquisition and processing costs, and water depth. Shallow water environments are complex areas (river mouths, estuaries, shorelines, swamps) and surveys often have to deal with varying water depths, wind and wave action, surf, and heavy ship traffic. The development of a cost-effective VHR 3D seismic method for small-scale site investigations in shallow water proved to be a challenge, and called for creative design.

1.4 Thesis outline

This thesis will focus on the applications of very high resolution shallow seismic imaging for environmental, geotechnical and archaeological site investigations. Chapters 2 and 3 discuss the development of a flexible 3D seismic acquisition system for small-scale, very high resolution 3D investigations and its application to a geotechnical site study on the river Schelde. The next three chapters focus on munition dumpsite research. A discussion of the problems related to chemical munition dumpsites is presented in chapter 4. The following chapters 5 and 6 focus on two different case studies in munition dumpsite research from the North Sea (Paardenmarkt dumpsite) and the Baltic Sea (Bornholm dumpsite). Chapter 7 deals with the application of seismic techniques for archaeological investigations and presents two case studies over buried wooden shipwrecks on the river Schelde and the Dutch Wadden Sea. Finally chapter 8 focuses on shallow gas, a major problem in nearshore acoustic investigations. Summary and conclusions are presented in the final chapter 9.

The results presented here are by no means a one-man project but they are the fruit of close national and international collaboration. Basically, all seismic data acquisition, processing and interpretation discussed in this thesis were carried out by the author, except for the 1996 seismic survey at the Paardenmarkt dumpsite. Processing of the 3D Wadden Sea data was carried out in close collaboration with TNO-TPD in The Netherlands. MSc student Lieselot Noppe helped in processing the Bornholm data, a huge task seen the sheer quantity of data. The design and development of the prototype inflatable 3D system were done together with Koen De Rijcker; the final lay-out of the system was manufactured by a small private company. The development of its ‘predecessor’, the Seiscat system, and initial processing of the Schelde data in the early nineteen nineties was done by Henriet et al. (1990). Advanced processing of these data was done

by the author at Ifremer, France. Literature study and existing data synthesis of chemical munition dumpsites in general, and in specific the Bornholm and Paardenmarkt dumpsites, were carried out by the author. Side-scan, multibeam, magnetic and geo-electric data were acquired and processed by various project partners, often in close collaboration. Correlation and integration with the seismic data was carried out by the author.

The results of chapters 2 and 3 were largely published in Missiaen et al. 2002a and Missiaen 2005. Chapter 4 is based on the studies published in Missiaen et al. 2001 and Missiaen & Paka 2007. Different aspects of the Paardenmarkt study in chapter 5 have been covered in Missiaen et al. 2001, Missiaen et al. 2002c and Henriet & Missiaen 2005. Publication of the most recent seismic data (2007) is envisaged for the near future. The results of chapter 6 are the subject of two recently submitted articles (Missiaen & Noppe 2008, Missiaen & Feller 2008) and should be published in 2008. The results of chapter 7 were partly discussed in different project reports (a.o. Missiaen et al. 2004, van den Brenk et al. 2003). The shallow gas study presented in chapter 8 is published in Missiaen et al. 2002b. The results of two international workshops on VHR shallow marine seismic and chemical munition dumpsites were published in Missiaen, Wardell & Dix (eds) 2005 and Missiaen & Henriet (eds) 2002.

CHAPTER 2
VHR 3D SEISMIC IMAGING

2.1 Introduction

Very high resolution (VHR) marine seismic technology has progressed quickly over the last decades, and constant evolution towards better equipment and more powerful computers is making VHR multichannel recording more and more popular. Till recently however 2D surveys were common use and 3D acquisition was mainly carried out in the hydrocarbon exploration realm involving complex field and processing procedures, making it very costly and time-consuming (e.g. Yilmaz 2001). Since the early nineties there has been a constant development in high resolution (HR) and very high resolution (VHR) 3D marine seismic acquisition. One of the early attempts of 3D survey design was the development of the 'Kite' seismic system consisting of a source and hydrophone array (24 channels) towed perpendicular to the direction of propagation (Rogers et al. 1993). This resulted in a 3D 'strip' approx. 20 m wide, i.e. the width of the receiver array. In 1993 a 3D seismic study was carried out on the New Jersey shelf, using a boomer source and 10-element receiver in water depths of roughly 70 m (Pulliam et al. 1996). Maximum resolution was in the order of 0.5 m vertically and 10 m laterally.

In the mid-nineties an experimental 3D survey was carried out by Rice University (Houston, Texas) involving a source and two single-channel streamers. This set-up yielded bin sizes ≥ 15x15m, and clearly demonstrated the resolution constraints due to spatial sampling (Abdulah et al. 1997). More recently a number of 3D experiments were carried out by Kiel University (Germany) using a boomer source and two streamers (24 and 48 channels respectively) (Müller et al. 2002). Due to the large streamer spacing (15 m) and cross-line distances involved the data did not provide full lateral continuity (binning was only applied in the inline direction) and it therefore seems more appropriate to call this a 2,5D survey rather than an actual 3D survey.

In the framework of the EC project 'VHR3D' a 3D system for very high resolution investigations was developed at Ifremer (France) for surveys in water depths up to 100 m, using four streamers with 6 channels each spaced between 4 and 10 m apart (Marsset et al. 2001, Marsset et al. 2003). Targeted vertical resolution was 1 m, with bin sizes ≥ 2x2 m. Difficulties in streamer positioning forced to abandon this approach, and research is now aimed on high resolution instead of very high resolution work (Thomas et al. 2004). Recent studies at the University of Lausanne also focus on high resolution investigations. A new acquisition system was developed for lake studies (water depths > 200 m) using three 24-channel streamers (2.5 m channel interval), which yielded bin sizes in the order of 1.5x3.5 m (Scheidhauer et al. 2005). Additional DGPS receivers attached at the tail of each streamer provided the necessary positioning accuracy.

Most recently advances have been made in the development of rigid 3D arrays for small-scale site investigation. Research at the University of Southampton (UK) has resulted in the development of an ultra-high resolution 3D Chirp system containing 4 source transducers and 60 hydrophones groups spaced 25 cm apart. Source and receivers are fixed on a rigid grid (2.75 m wide and 2.3 m long) with four RTK positioning antennas, allowing absolute positioning with cm precision (Vardy et al. 2006). The size and form of the array limits survey work to sheltered areas of restricted size. Recent developments at the University of Kiel (Germany) involve a pseudo-rigid 3D receiver array. The array contains 16 active hydrophones (spaced 0.5 m apart) and its construction restricts all horizontal movement of the receivers. The seismic source

(boomer), which is kept within a wooden frame, holds the positioning antenna. First test results from Turkey are very encouraging but also show the high sensitivity of the system to wind and wave action, restricting the work to sheltered areas and fair weather (Müller et al. 2006).

At RCMG a first important step in scaling down the shallow marine 3D method to very high resolutions was taken in 1990. In the framework of the EC Hydrocarbons Project 'An integrated approach to the stability evaluation of prospective offshore sites' a test survey was carried out on the Schelde river using a simple and compact 3D acquisition system (SEISCAT). Data processing resulted in a resolution never achieved previously in true 3D practice (Henriet et al. 1992). In the framework of the EC MAST-II Fellowship Research Project 'Very high resolution 3D seismic reflection imaging' the 3D data volume was subjected to advanced processing (Missiaen 1997). A detailed description of the acquisition system and the results of data processing are given in the Annex.

In the framework of the EC MAST-II project "VHR3D" a new acquisition system (OPUS3D) was developed at RCMG. Past experience with the SEISCAT system had learned that a compact field system with close streamer and channel spacing renders good results, but still there were a number of shortcomings. For one the array proved very rigid and deployment was only possible from relatively large-sized vessels. A more flexible acquisition system was required to allow deployment from smaller vessels, and also to work autonomously. Furthermore higher sampling rate and broader frequency range, as well as improved coverage, were needed.

2.2 The OPUS3D acquisition system

The approach in the development of a new 3D acquisition array was chosen in function of a number of factors: the geological target, water depth, resolution, and - last but not least - the available budget. The new 3D array is aimed at small geological or geotechnical targets (< few hundred m) with a limited depth (<< 100 m) and shallow water areas (< 20 m water depth). Short survey times (ranging from a few days to 1 week) and a limited data volume (few hundred Mb) should allow cost-effective acquisition and processing of the data.

To obtain maximum flexibility a modular, inflatable system seemed the best solution. An inflatable array will need limited space and allows convenient deployment and recovery, simply through inflation and deflation, even on smaller vessels. A central floating platform offers the necessary stability and rigidity to the inflatable system. The modular approach furthermore allows to adjust the array to specific site characteristics (survey area, target size, target depth). In areas of difficult navigation such as nearshore areas, high traffic access lanes to harbours or harbour development areas, the width of the acquisition array can be adapted by decreasing the number of modules. For deeper targets the streamer spacing may be increased.

Channel and streamer spacing were fixed at 2 m. This makes it easier to cover larger and/or deeper targets than the previously used 1 m spacing. The number of modules and streamers was initially set at 6 and 8 respectively. This guarantees sufficient rigidity, but also has a practical purpose: fewer modules make the system easier to handle. Extra modules may always be added at a later stage, and if needed the streamer spacing could be decreased. The number of channels per streamer was fixed at two. Apart from being cost-effective, this dual-channel layout had proven to be efficient for shallow research. Furthermore it allowed the use of short streamers which will help to minimise the movement of the receivers and allow a high manoeuvrability. With the total number of streamers at 8, this also allowed simultaneous recording of the source signal and long-offset on a 24 channel seismic recording system.

2.2.1 Development of the prototype

A first prototype of the new 3D acquisition system was developed in 1998. It contained two sets of 3 modular inflatable frames, each frame 4 m long and 2 m wide, joined in the middle by a zodiac boat (Figure 2.1). The frames provide the necessary spacing for the streamers, which are attached to the frames, and result in a total 'wing span' of roughly 14 m. The inflatable frames were kept under constant air pressure (~0.5 bar) through air supply cables connected to a divider system. The prototype inflatable frames were made of flexible fire-hose with a diameter of 10 cm. Each frame consisted of two length floaters and 3 cross floaters (Figure 2.2). The connection between the floaters was done using PVC pipes. These were fit tightly to the fire hose using special straps. In order to avoid contact with the water surface the cross floaters were curved upward using a tight rope. The prototype frames were first tested on a shallow lake (Figure 2.2). The streamers are 7.5 m long (active section) and contain 2 channels each (two hydrophones per channel), with a channel spacing of 2 m. Depending on the desired offset the streamers can be towed far behind the frames or close to the frames. The seismic source can be towed from the central zodiac.

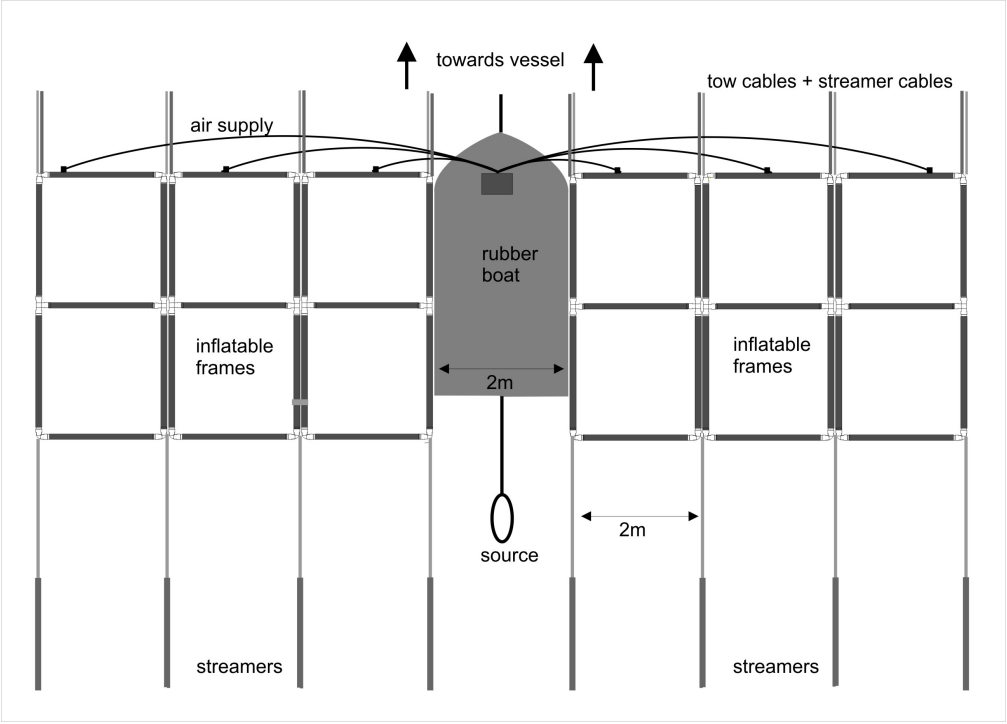

Figure 2.1 *Schematic overview of the first prototype of the new VHR 3D acquisition array. Two sets of 3 modular inflatable frames are joined in the middle by a zodiac boat. The streamers are towed from the frames. Constant air supply keeps the inflatable frames under pressure.*

Sea trials were carried out offshore Knokke-Heist in September 1998 on board the R/V Belgica (see chapter 5). During these trials the acquisition system was towed some 15 m behind the vessel. Deployment and recovery operations were practiced. The inflatable frames were folded into the zodiac boat which was then put over board (Figure 2.3-top). Once behind the ship the frames were let into the water and inflated one by one (Figure 2.3-bottom). Towing ropes were attached to the frames to prevent deformation while turning. In general the inflatable array kept well aligned; the frames remained rigid but at the same time were flexible enough to follow the movement of the water. During turning the frames were occasionally bent but the full layout was resumed as soon as a straight course was regained. The large number and heavy weight of the streamer cables leading towards the junction box on board the tow vessel proved to be very impractical.

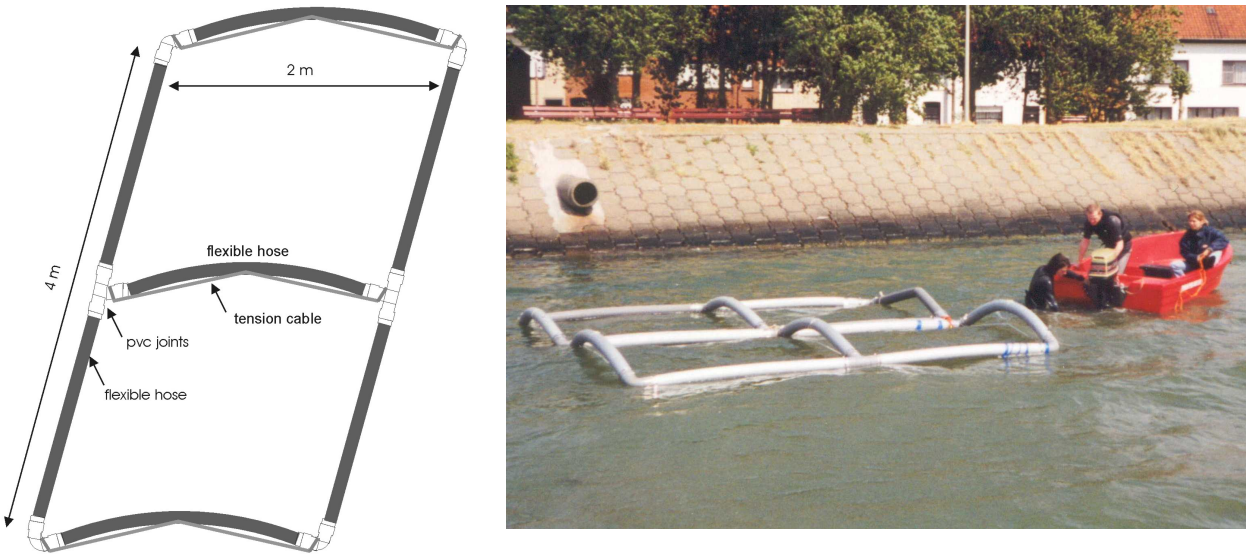

Figure 2.2 *Left: Schematic overview of a single prototype frame. The inflatable frame is 4 x2 m. A tight rope keeps the cross floaters curved upward. Right: testing the prototype frames on a small lake.*

Figure 2.3 *Sea trials with the prototype acquisition system. Top: Putting the acquisition system over board. Bottom: Setting up the inflatable array.*

The sea trials revealed a number of weaknesses of the acquisition system. Some of the most important shortcomings include the following:

- PVC joints are vulnerable and break down easily under increased stress;
- the central zodiac needs more stability;
- the central zodiac should be large enough to easily hold the deflated modules;
- air pressure valves on the inflatable frames are very vulnerable;
- the large number of cables and ropes (towing, streamer, source, air supply, positioning) make the array difficult to handle;
- module and streamer connections need further simplification;
- absolute (x,y,z) positioning needs at least dm-range precision and a fast data link;
- the source should be towed close to the central zodiac to avoid a swaying movement;

Additional tests carried out at the streamer manufacturer SIG revealed that the streamers have a tendency to sink in brackish or fresh water at low vessel speeds (80 cm submersion for a speed of 2 knots). In order to avoid this effect during future surveys on lakes, rivers or estuaries the streamers were adapted with light-weight connections and lighter streamer oil. Finally, the heavy streamer cables were replaced by a thin cable which can be strapped easily onto the modules. The part of the streamer cables close to the active streamer section was replaced by a thick, floating cable for maximum buoyancy.

2.2.2 Final lay-out

Based on the experience with the prototype a definite model of the acquisition array was constructed. Modular frames were designed without PVC connections. The frames were made from Hypalon rubber (1.2 mm thick) and 'pre-shaped' to increase their rigidity (Figure 2.4). Special attention was paid to the air pressure valves: to minimize the chance of rupture the valves were built into the frames. The modular frames were equipped with fixed connections to allow easy construction and dismantling of the array. The frames were tested on a small lake before the final model was manufactured.

A new catamaran-type central zodiac (so-called RIB) assured optimum stability at sea (Figure 2.5). The RIB is wide enough to allow convenient deployment and recovery of the inflatable frames; furthermore it is sufficiently large to allow stand-alone use of the system. A number of tests were carried out with the RIB and the inflatable modules. Different modes to attach the modules to the RIB were tested to assure minimal friction. A simple, flexible system using small fenders turned out to give the best results.

Also the streamer array was simplified to facilitate the deployment and recovery operations. The thin streamer cables were attached to the module frames and led to the junction box in the RIB, thus reducing the number of streamer cables leading to the tow vessel to one single cable. The thin streamer cables and the air-supply cables were easily strapped onto the modules with flexible Velcro strips. Cable and module suspensions were further simplified to allow easier deployment. The final layout of the acquisition array is shown in Figure 2.5. The modular inflatable array allows easy deployment from small to medium-sized vessels, optimally with an A-frame or small crane (in the absence of an A-frame or crane the inflatable array is set up in the harbour, and then towed behind the vessel to the survey site). Towing takes place with a central rope attached onto the RIB and additional ropes towards the module tips allow additional control of the array rigidity (Missiaen et al. 2002a).

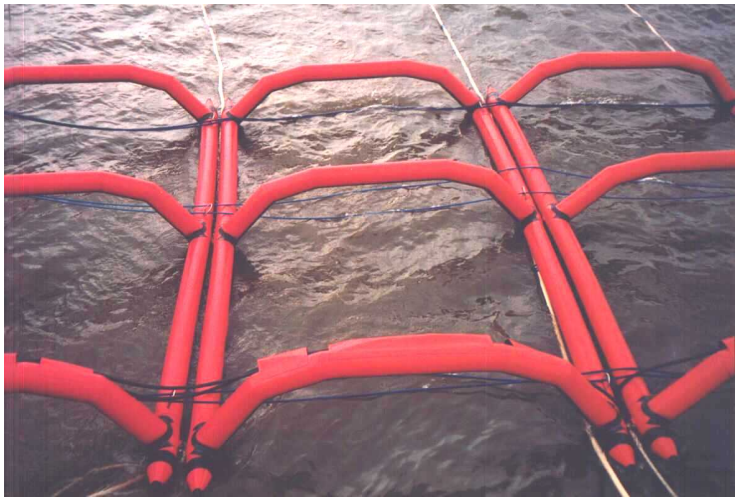

Figure 2.4 *Final version of the inflatable frames. The rigidity of the frames was enhanced by their pre-shaped upward curved form.*

Figure 2.6 illustrates the different steps in the set-up of the array. First all components are folded into the RIB, which is set over board. Once deployed at the right distance behind the vessel, the deflated frames and the streamers are then lowered on either side, and finally the frames are inflated one by one. After the survey the frames are again deflated one by one and rolled with the streamers into the RIB, which is then hauled back on board.

Figure 2.5 *Final lay-out of the seismic acquisition system OPUS3D.*

Figure 2.6 *Different steps in the deployment of the inflatable array OPUS3D.*

2.2.3 Stand-alone use

The central RIB is a rugged and stable boat that can easily be converted into an autonomous survey vessel unit. Rail-mounted modules include a seismic, navigation and positioning console, as well as two storage boxes hosting adequate generators and fuel supply. Twin engines, hydraulically controlled, provide both smooth low-speed surveying operational modes and if needed power for safe navigation under any emergency situation.

In protected waters (inshore, harbour areas, rivers, lakes) and in the absence of strong wind or waves this opens perspectives for a 3D survey capacity. The behaviour of the inflatable array under autonomous propulsion was tested successfully for the first time during a survey on Lake Geneva (Figure 2.7). Additional test surveys were carried out on a crater lake in the Massif Central (France) and in the Venice lagoon (Italy). The use of a stand-alone 3D acquisition system offers a unique flexibility, with easy transport to any site on a trailer behind a standard van. It also allows to make optimal use of good weather windows for performing high quality 3D data acquisition without expensive survey vessels' standby costs (Missiaen et al. 2002a).

Figure 2.7 *The 3D acquisition array used in stand-alone mode on Lake Geneva.*

2.3 Positioning strategy

The success of any water-borne VHR 3D seismic method will highly depend on accurate positioning of the acquisition array. Wave motion, swell, currents, tide and changes in the ship's heading will cause movement of the acquisition array away from the nominal (theoretical) geometry, resulting in horizontal and vertical variations in the theoretical (x,y,z) positions of the source and receiver elements (Figure 2.8).

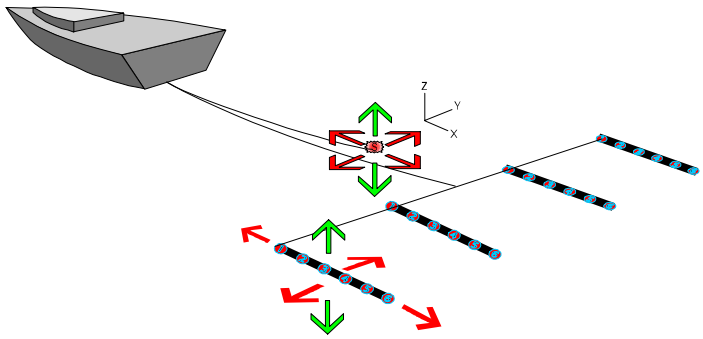

Figure 2.8 *Schematic illustration of the possible array movements involved in marine 3D seismic operations (after Diviacco & Wardell 2003).*

In conventional high resolution surveys these horizontal and vertical movements are small compared to the dimensions of the system and therefore do not form a major problem. For very high resolution data, with frequencies well above 1-2 kHz, the positioning uncertainty can easily reach the same order of magnitude (or even larger) as the main signal wavelengths (Missiaen et al. 2002a). Considering the bin size dimensions and the desired resolution (dm range), these variations can severely degrade the data quality. Accurate positioning with sub-meter accuracy is therefore needed in order to carry out correct processing without destructive stacking.

In developing a suitable VHR 3D positioning strategy - one that allows the necessary positioning accuracy in a cost-effective way - we have to distinguish between: (1) navigation positioning, i.e. absolute positioning of the mother vessel; (2) seismic positioning, i.e. absolute positioning of the acquisition array; and (3) relative positioning, i.e. positioning of source and receivers with respect to each other.

2.3.1 Navigation positioning

With a total 'wing span' of the inflatable 3D array of 14 m, midpoint coverage in bands 7 m wide is obtained on the seafloor (Figure 2.9). In order to assure sufficient overlap of the trace midpoints in the 3D area an average line spacing of 5-6 m is therefore needed. This necessitates track-line navigation with sub-meter range accuracy. In practice, however, precise vessel steering along pre-calculated tracks is often very difficult due to currents, wind, ship traffic, etc.

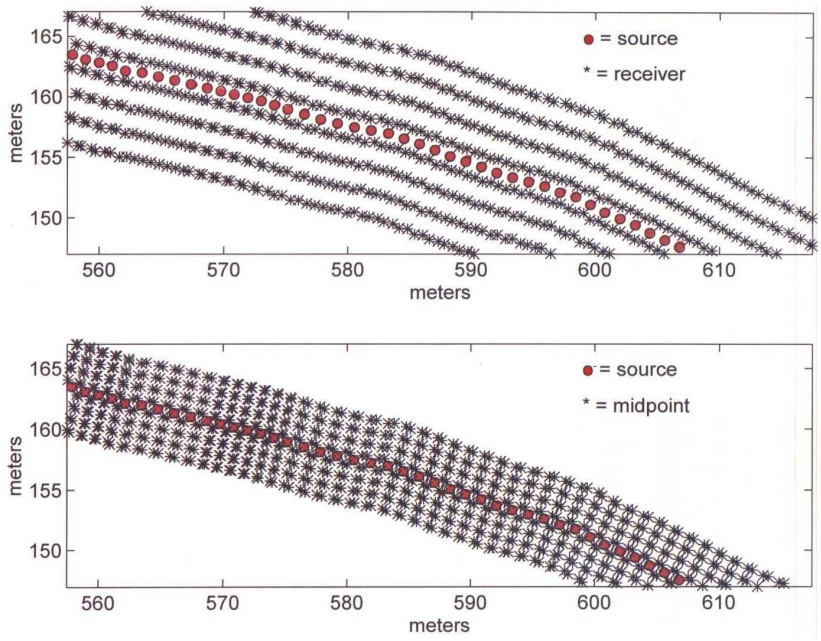

Figure 2.9 *Navigation geometry and shot-receiver-midpoint coverage of the inflatable acquisition array.*

Vessel navigation nowadays relies on GPS (Global Positioning System). The precision depends on the quality of the pseudo distance measurements, but in general a raw GPS receiver can deliver positions with 10 m accuracy. Differential GPS (DGPS) goes one step further. The basic idea is that two receivers observing the same satellites will take similar measurements with similar errors if they are close to one another. By placing a reference receiver at a known position, it is possible to evaluate the theoretically correct measurement values according to the known position, and then to compare these theoretical values with the actual ones taken. The difference (error) can then be used to provide corrections to receivers that are placed at unknown positions.

DGPS generally has a positioning accuracy in the order of 1 meter. The corrections in DGPS can be made either by post-processing (raw measurements are recorded and then processed by software) or in real-time (corrections are calculated on-line and immediately transmitted by a radio link to the roving receiver which applies them prior to calculating their position). This is needed to allow the necessary accuracy for vessel navigation during VHR 3D survey work.

2.3.2 Absolute positioning

Taking into account the frequency range and the desired resolution in VHR 3D seismics absolute real-time positioning of the acquisition array with cm or dm accuracy is required. This does not only apply to the lateral positions but also to vertical positioning, especially in areas with high tidal amplitudes. The accuracy of the vertical data should be at least of the same order as the horizontal accuracy (Missiaen 2005).

Real-time DGPS does not allow the necessary positioning accuracy for the acquisition array. In recent years a new short-range DGPS positioning system has been developed based on real-time kinematic positioning (RTK), where GPS signal corrections are transmitted in real time from a reference receiver at a known location to one or more remote rover receivers. The RTK method assures real-time cm accuracy in (x,y,z) for nearshore studies, and is marked by a fast update rate, low latency (calculation delay), high data link continuity, fast correction rate, and high data output frequency. These qualities make it ideal for VHR 3D shallow water studies.

There are two different applications of the RTK method: the KART (Kinematic Applications in Real Time) method for single-frequency receivers and LRK (Long Range Kinematic) method for dual-frequency receivers. The KART method allows coverage over a distance of 10 to 15 km. The LRK (Long Range Kinematic) method allows coverage over distances up to 40 km even with a reduced number of visible satellites.

Using an acquisition array with a central RIB made it possible to mount the positioning antenna on the central RIB. Still a certain amount of antenna movement due to waves and currents cannot be avoided, especially during offshore work. The horizontal and vertical displacement amplitudes of the antenna receiver will depend on the height of the antenna and the angle of movement (Figure 2.10).

In general the vertical displacement will be much less than the lateral displacement. For an antenna of 1 m height the vertical and horizontal displacement will be resp. 2 cm and 18 cm for an angle of 10 degrees, going up to resp. 4 cm and 30 cm for an angle of 20 degrees. Reducing the antenna height to 0.5 m will lead to displacements of resp. 1 cm and 7 cm for an angle of 10 degrees, and resp. 2 cm and 12 cm for an angle of 20 degrees. Bearing in mind the required positioning accuracy (dm or cm range) this means that the antenna height should be kept as small as possible (while still assuring an optimum radio link of course) in order to reduce the horizontal and vertical displacement to an acceptable level.

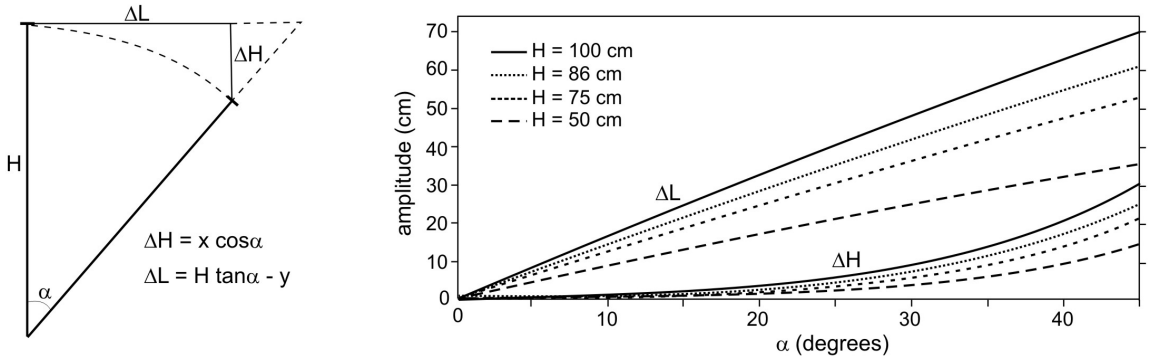

Figure 2.10 *Dependency between antenna height (H), angle of movement (a), and lateral/vertical displacement (ΔL,ΔH). For movement angles of 20 degrees the horizontal amplitude can reach up to 30 cm for an antenna height of 1 m.*

2.3.3 Relative positioning

The antenna positions, no matter how accurate, do not give us information on the actual position of the different elements of the seismic array and their movement away from the nominal lay-out. One of the main advantages of the OPUS3D system is the use of short streamers and the possibility to mount the positioning antenna close to the source and receivers. When acquiring 3D data in a marine environment however, it is impossible to avoid movement of the source and streamers. Although these variations in the shot-to-shot positions tend to be small (in the order of decimeters) they can be critical (Missiaen et al. 2002a).

The relative source and receiver positions can vary both in horizontal and vertical directions. Tides, swell and wave motion cause a vertical movement of the seismic array which introduces constant (static) shifts to the seismic data (Figure 2.11-top). Currents, waves and changes in the course of the vessel will cause a horizontal movement of the seismic array which will result in variations in offset and produce dynamic shifts to the seismic data (Figure 2.11-bottom).

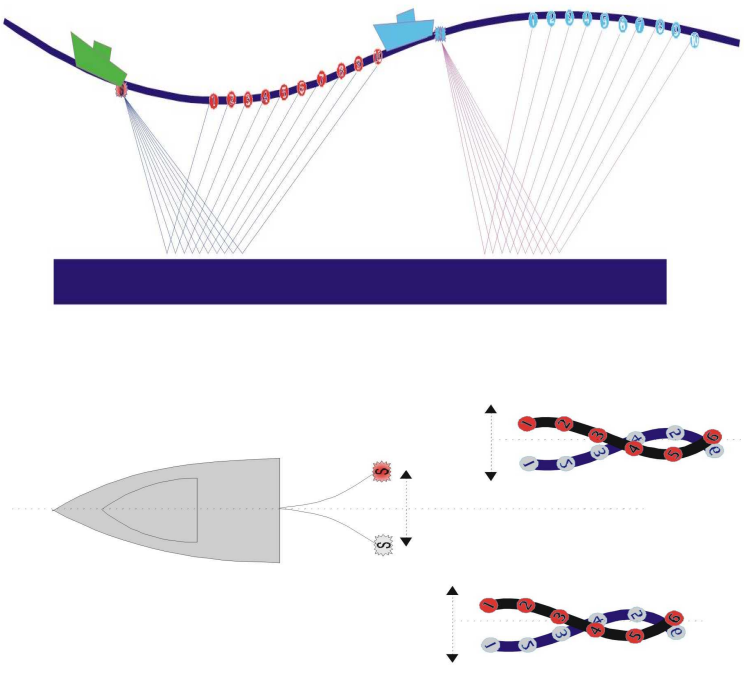

Figure 2.11 *Schematic illustration of possible movement of the 3D acquisition array. Top: Vertical movement due to swell and tides.*

Bottom: Lateral movement due to wave action, currents and change in course (after Diviacco & Wardell. 2003).

A number of technical solutions exists which allow lateral steering and depth control of seismic streamers, including so-called 'birds', compasses and acoustic positioning systems. Most of these techniques, however, have been developed in the 3D exploration realm. Taking into account the cost-effectiveness of these devices (they are often very expensive) and the OPUS3D specifications (short streamers, limited streamer diameter), and also the accuracy level required (dm range), these techniques are not realistic in our VHR 3D work. Pulling the source and streamers close to the array, or, if possible, attaching the streamers underneath the frames can help to reduce the uncertainty in positioning. Although this improves the control of the receiver positions (both lateral and vertical) one has to be careful about any additional disturbance in the water caused by the frames and possible deterioration of the direct arrival signals. However the main drawback is that it will limit the maximum offset and the use of this set-up therefore depends on the water and target depths.

2.3.4 Source movement

To reduce source movement to a minimum the source frame is best towed close to the RIB. In the absence of waves and strong currents the source frame may also be attached in front of the RIB. The Seistec boomer frame (and also the echosounder frame) proved very stable and allowed installation of the positioning antenna on the source, thus further reducing relative positioning errors (Missiaen et al. 2002a). The antenna positions recorded with this set-up showed that there is relatively little lateral source movement between consecutive shots, even in offshore conditions (Figure 2.12-left). Vertical source movement proved to be highly dependent of the state of the sea, but mostly fell within the limits of the positioning accuracy (Figure 2.12-right).

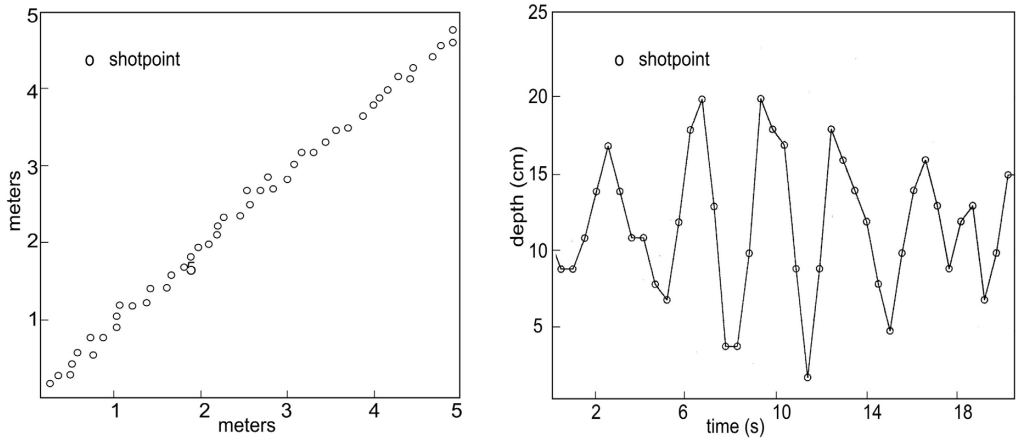

Figure 2.12 *Source-mounted antenna movement at sea. Left: lateral movement. Right: vertical movement.*

2.3.5 Streamer movement

Trials on the Schelde river indicated that the inflatable frames yield a stable acquisition layout. Indeed the absence of wave action and the presence of a strong current parallel to the track lines kept the array straight and well aligned (Figure 2.13-top). In offshore environments, however, the array alignment is not always optimal. This was visible during the survey (Figure 2.13-bottom) as well as on the seismic data (Figure 2.14). In some cases streamer movement led to a difference of up to 0.7 ms between theoretical and observed arrival times (Missiaen et al. 2002a).

Strong currents or changes in vessel heading can result in an inclined position of the acquisition array behind the tow vessel (this was the case for the 3D survey on the Wadden Sea, see chapter 7). This is not expected to result in important relative positioning errors since source and receivers follow the same 'path'. The deviation from the nominal geometry can be calculated using the course of the tow vessel and the acquisition array. Still, it can give rise to an irregular seismic coverage that may affect the overall quality of the processed data.

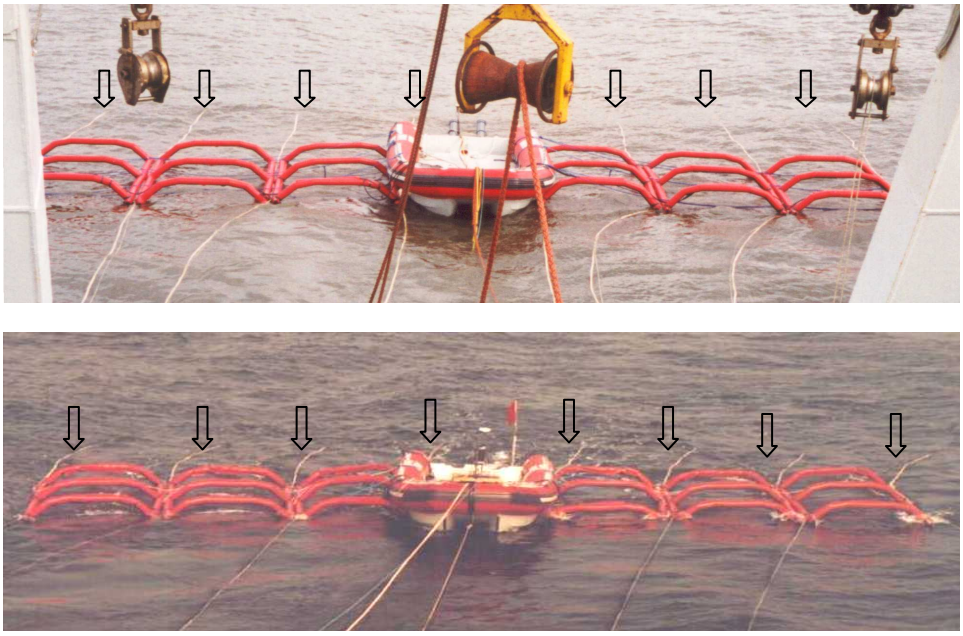

Figure 2.13 *Top: Array stability in a river environment, with good streamer alignment. Bottom: Array stability in offshore conditions, with swaying movement of the streamers. Blue arrows indicate streamer positions.*

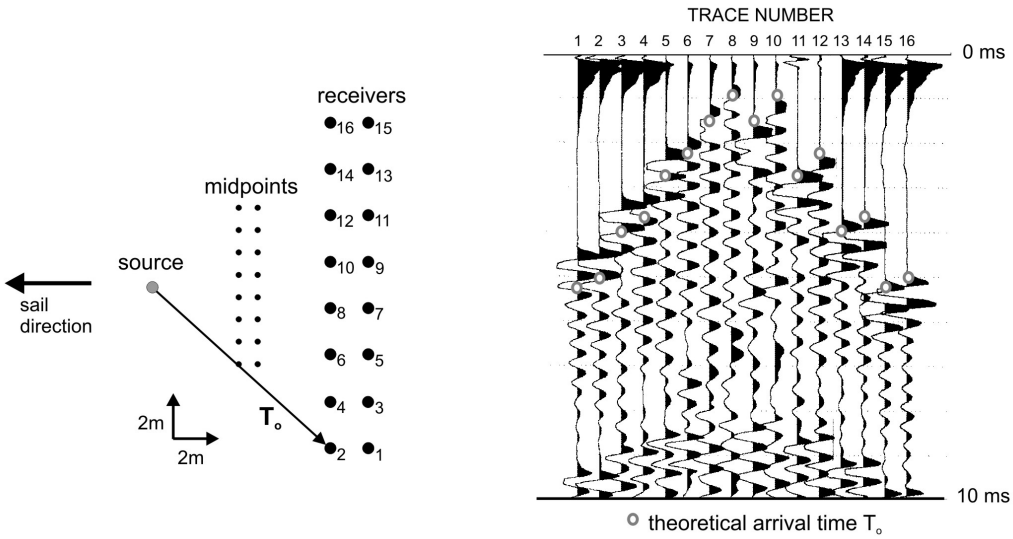

Figure 2.14 *Deviation between theoretical and real (recorded) arrival times due to streamer movement. Left: Theoretical shot geometry (T_0 = theoretical arrival time). Right: shot gather recorded at sea.*

Variations between theoretical and real (= recorded) arrival times can be due to several factors:

- Lateral streamer displacement due to currents & wave action. Both individual movement (curling) as well as 'aligned' movement (diversion to one side) (Figure 2.15);
- Vertical streamer movement caused by swell or by variations in streamer immersion depth. Due to the very short length of the streamers this is expected to be negligible;
- Streamer vibration, often observed at high vessel speeds (> 4kn). Rather than causing positioning inaccuracies this will lead to general deterioration of the data quality.

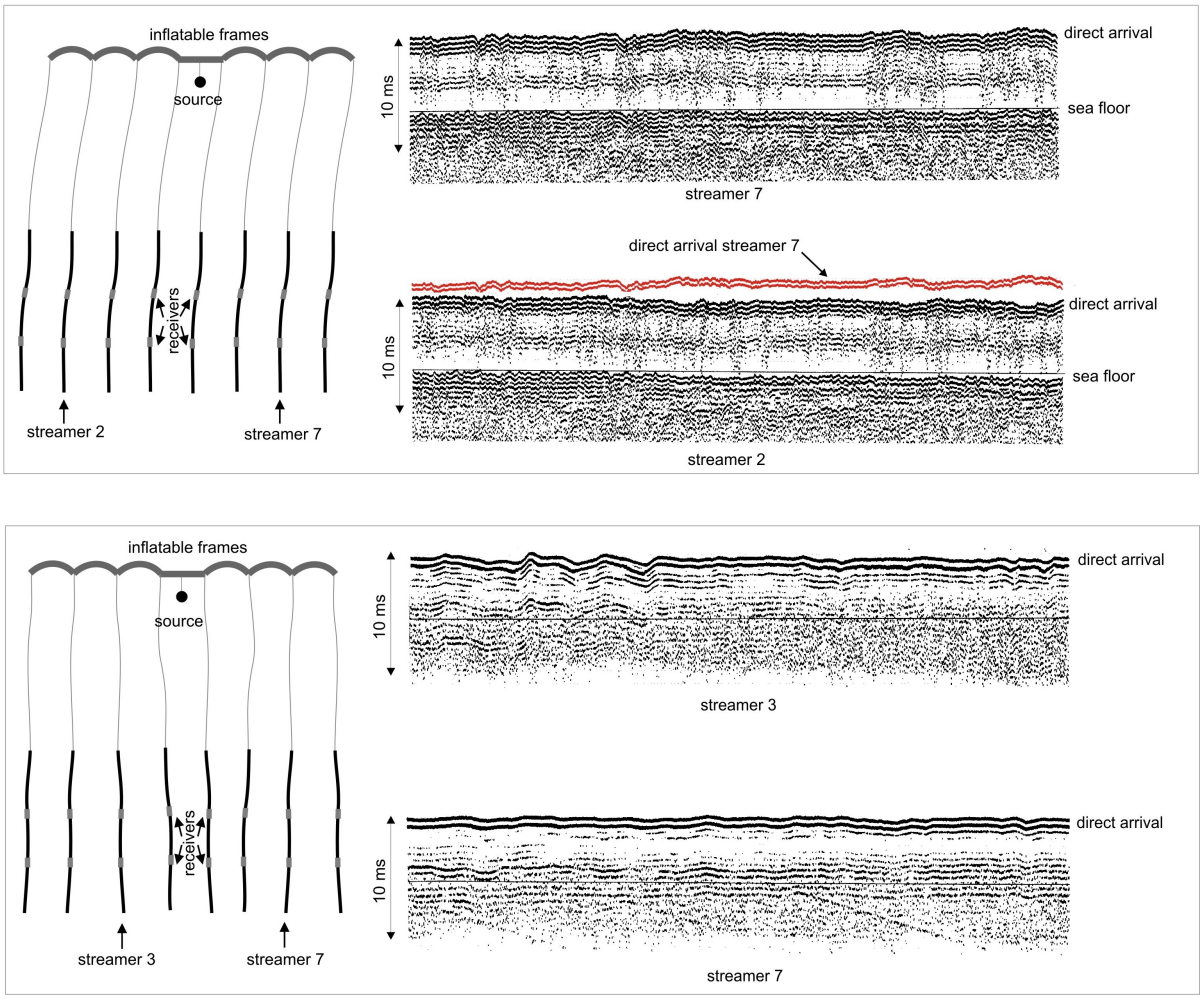

Figure 2.15 *Schematic presentation of the 3D array (left) and single-channel recording of two streamers (right). Top: Uniform streamer movement. The direct arrivals of 'mirror' streamers are symmetrical. Bottom: Individual streamer movement. The direct arrivals suggest an uncorrelated streamer movement.*

2.3.6 Swell and positioning accuracy

Working in an offshore environment the effect of swell can be considerably. Often a swell filter is used to remove the wave motion from the data prior to any processing. But swell filtering can also be done in the processing phase by applying a spatial filter to picked reflector times and removing the unfiltered residual times from the data (Marsset et al. 2001). In the case of VHR data, however, this may be tricky for more than one reason. First of all picking of the first break (seafloor) arrivals is a tedious job that often involves manual interference. Most automatic

picking routines have been developed for medium to high resolution data and they are not able to correctly handle very high resolution data with marked amplitude variations. Secondly the danger exists that the swell filter will also flatten out small structures or irregularities in the seabed which are smaller than the length of the filter, eventually causing a miss-stack of the seismic data.

The vertical movement of source and receivers induced by swell will lead to variations in the trace midpoint positions. These variations result in a horizontal and vertical displacement of the trace midpoints, but the magnitude of their effect will vary. The most pronounced effect will be on the vertical displacement of the trace midpoint. This can reach up to several dm for a wave height of 0.5 m. The lateral displacement of the trace midpoint however will generally be very small (in the order of a few cm) and can thus be neglected.

2.4 Seismic strategy

Moving towards very high and ultra high resolutions in 3D seismics does not simply involve a mere downscaling problem, but it also requires specific strategies (Henriet et al. 1992, Pulliam et al. 1996, Abdulah et al. 1997, Marsset et al. 2001, Missiaen et al. 2002a). Because VHR 3D surveys are focused on (often complex) shallow water areas and transition zones they require special - and creative - planning. Each survey demands careful design of the acquisition geometry with respect to the target to be imaged and the questions to be addressed by the 3D volume.

Much of the success of the 3D method will depend on acquiring high-quality data. This involves three basic requirements: good signal-to-noise ratio, high resolving power, and adequate subsurface coverage of the target. Along with a number of geophysical guidelines, a.o. related to bin size, data fold and offset, they form the basis of survey design (Ashton et al. 1994). For VHR 3D surveys, the main geophysical constraints related to seismic imaging include the depth of the target, maximum dip of the layers, horizontal resolution, and vertical resolution. These in turn are related to a number of factors in the acquisition geometry such as signal frequency, trace interval, streamer spacing, line spacing, and shot interval. These survey parameters have to satisfy the physical laws including time and depth sampling, spatial sampling, and array directivity.

The optimum acquisition strategy will necessarily be a compromise. On the one hand there is the need for high resolution (both vertical and horizontal) and this requires high dominant frequencies. On the other hand there are the constraints placed on spatial sampling - very high frequencies require very small sampling intervals, not only in time, but also in space (Gardner 1993). An important factor in VHR 3D survey design is cost-effectiveness. Acquiring good seismic data is expensive.

In Chapter 1 a number of source options have already been discussed. Since 3D acquisition involves the use of a spread of receivers, a certain beam width is required to cover the entire receiver array (Figure 2.16). Seismic sources marked by a high directivity will often display a decrease in dominant frequency and bandwidth for high offset angles (Verbeek 1995). The source directivity should therefore be such that the entire receiver array can be covered without a significant loss in signal quality. Although the Seistec boomer source cannot be considered as a perfect point source, the limited array dimensions of the OPUS3D system will limit the possible directivity effects and make this source a good option for 3D survey work.

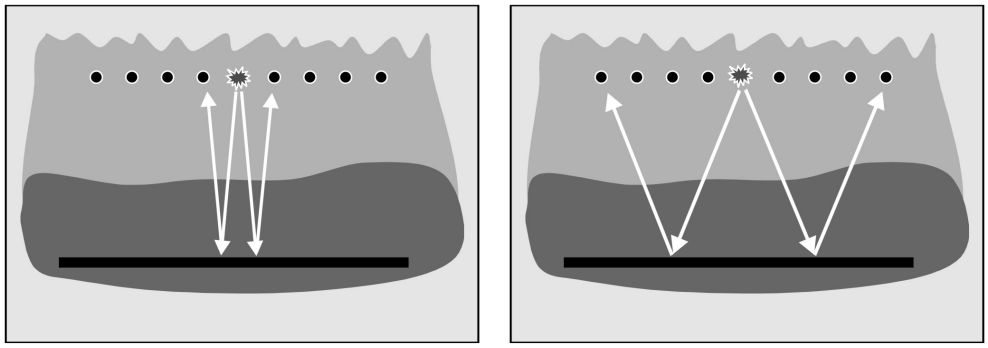

Figure 2.16 *Cartoon illustrating the need of a certain beam width in VHR 3D acquisition. A narrow beam will be unable to cover the entire receiver spread. A wider beam will also cover the outermost receivers.*

2.4.1 Frequency and spatial aliasing

Frequency aliasing is related to digital sampling: in order to allow complete recovery of the waveform a minimum sampling frequency is required. Aliasing occurs when frequencies higher than half the sampling frequency (so-called Nyquist frequency f_N) are present. Frequency aliasing can be tackled by using a low pass filter prior to digital sampling, but this will limit the sampled frequency band. This was the case for the 1990 Schelde survey (see Annex), where the low anti-alias filter restricted the possible achieved imaging resolution. To avoid frequency aliasing the digital sampling rate should be twice the value of the highest frequency component. In practice, often a sampling rate of four times is applied.

Aliasing does not only apply to the sampling of discrete time intervals but also to the sampling that is done by the source and receiver elements in the 3D array. This so-called spatial sampling is more delicate to grasp than frequency aliasing as it will not be obvious during acquisition, yet it is an important limiting factor in the imaging processing. Spatial aliasing occurs if the spatial sampling interval (i.e. distance between two consecutive reflection points) leads to a time lag, for a common wave front, greater than half the main time period (Sheriff & Geldart 1982). This means that, for a dip angle θ, wave numbers k_N greater than $f \sin(\theta) / V$ will be aliased to $-f \sin(\theta) / V$, thus blurring the frequency content over f (Figure 2.17).

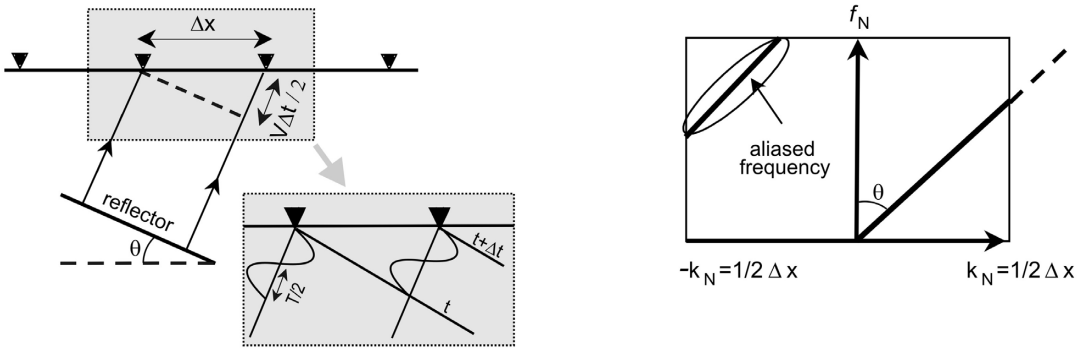

Figure 2.17 *Spatial aliasing aspect in the time domain (left) and wavenumber domain (right).*

To avoid spatial aliasing a compromise must therefore be found between the spatial sampling interval Δx, maximum imaged reflector dip θ_{max} and maximum signal frequency f_{max}:

$$sin(\theta_{max}) \leq V / [4 f_{max} \Delta x] \quad (2.1)$$

From this formula it is clear that the steeper the dip, the lower the frequency at which spatial aliasing occurs. It also implies that as the maximum frequency and/or the maximum dip decreases, the receiver group interval ($2\Delta x$) can be increased (Figure 2.18). For instance, decreasing the maximum frequency from 2 to 1 kHz allows to double the group interval for the same dip angle.

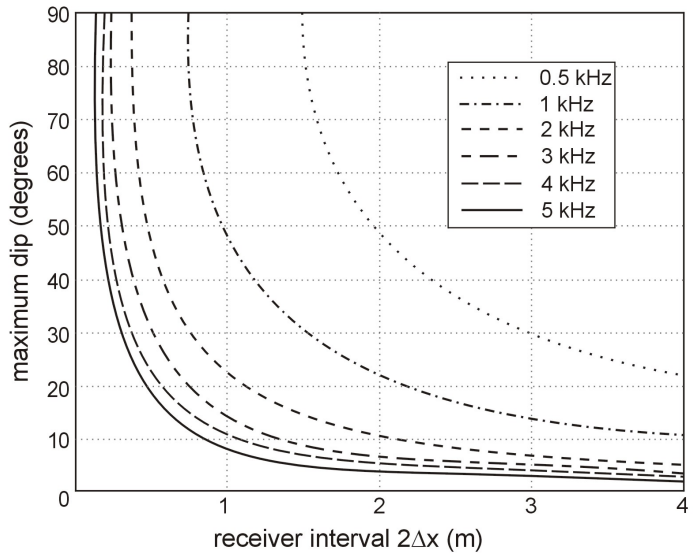

Figure 2.18 *Maximum non-aliased dip as a function of the receiver interval and signal frequency.*

For the OPUS3D layout, and with a shot interval of 0.5 s and a vessel speed of 3-4 knots, the receiver interval in the inline direction will be between 0.75 and 1 m. In the absence of crossline profiles (i.e. perpendicular to the sail direction) and assuming no line overlap the receiver interval in the crossline direction will be 2 m (Figure 2.19). Using formula 2.1, for a maximum frequency of 2 kHz this set-up should allow to correctly image dips up to roughly 24 degrees in the inline direction and roughly 11 degrees in the crossline direction. For a maximum frequency of 3 kHz the maximum dip values will reduce to 15 and 6 degrees respectively.

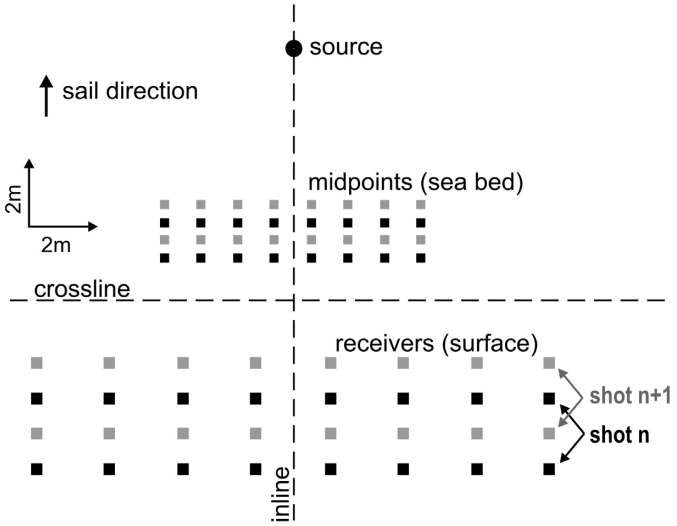

Figure 2.19 *Schematic overview of the spatial dimensions of the OPUS3D array for a sail speed of 4 kn and shot interval 0.5 s. The receiver interval amounts to twice the spatial sampling interval Δx (i.e. the midpoint interval).*

The imaging restrictions can be improved for a perpendicular network with profiles sailed in inline and crossline directions instead of only one direction. Indeed this will yield a spatial sampling interval of 0.37 to 0.5 m both directions. For maximum frequencies of resp. 2 and 3 kHz this will allow to image dips in the inline and crossline direction of resp. 24 and 15 degrees.

It is clear that there is a relation between the vertical resolution desired to image the target and the horizontal resolution required to achieve the desired vertical resolution. Indeed the source option does not only affect the vertical resolution and penetration depth, but it will also have implications for the acquisition geometry, since the highest frequency of interest gives the minimum wavelength which should be used in the array design. A compromise is therefore necessary between the source frequency and the desired vertical and horizontal resolution.

2.4.2 Receiver array directivity

The directivity of the receiver array* plays an important role in seismic acquisition as it affects the levels of noise that are registered in the hydrophones. In order to avoid strong signal deterioration optimal hydrophone geometry is therefore essential. If the receiver array is organised incorrectly, the directivity will reduce the signal quality and increase the amount of noise present. The array directivity has two main constraints: (1) it has to be in agreement with the spatial aliasing requirements, and (2) it has to filter out events on an azimuth basis.
(array refers to the pattern of a group of hydrophones which feed a single channel)*

The receiver array directivity function (A), also called array response, will depend on the hydrophone spacing (Δy), number of hydrophones (n) per channel, signal wavelength (λ), and angle of incidence (θ) (Sheriff & Geldart 1982):

$$A = \frac{\sin(\sin(\theta)\, n\, \Delta y\, \pi/\lambda)}{n \sin(\sin(\theta)\, \Delta y\, \pi/\lambda)} \qquad (2.2)$$

The array response is often expressed as a measure of the relative intensity (amplitude) versus direction of an outgoing seismic wave. The graph usually consists of a series of maxima (lobes) separated by small values. Beyond the alias lobe (given by Δx = apparent wavelength $\lambda/\sin\theta$), the pattern repeats. The region between the points where the response is down to 3 dB is called the reject region (Sheriff & Geldart 1982). Array response can also be plotted as a polar diagram where the radius vector gives the amplitude value as a function of the incidence angle.

Figures 2.20 and 2.21 show array response for different angles of incidence and frequencies for two hydrophones spaced 50 and 25 cm apart. As expected, attenuation of the seismic signal will increase for high angles of incidence. A hydrophone spacing of 50 cm will not filter out extreme high angles of incidence, so-called grazing rays, for higher frequencies (>> 1 kHz). Instead angles of 20-30 degrees, which may correspond to reflected signals in shallow water, will be attenuated. Decreasing the hydrophone spacing to 25 cm will avoid much of the signal deterioration. For frequencies of 2-3 kHz the secondary lobes have disappeared and attenuation of the seismic signal for relevant angles is less than -3 dB. For lower frequencies (≤ 1 kHz) this set-up will not attenuate noise signals at grazing angles, whereas for higher frequencies the signals arriving at high angles (> 40°) will be attenuated.

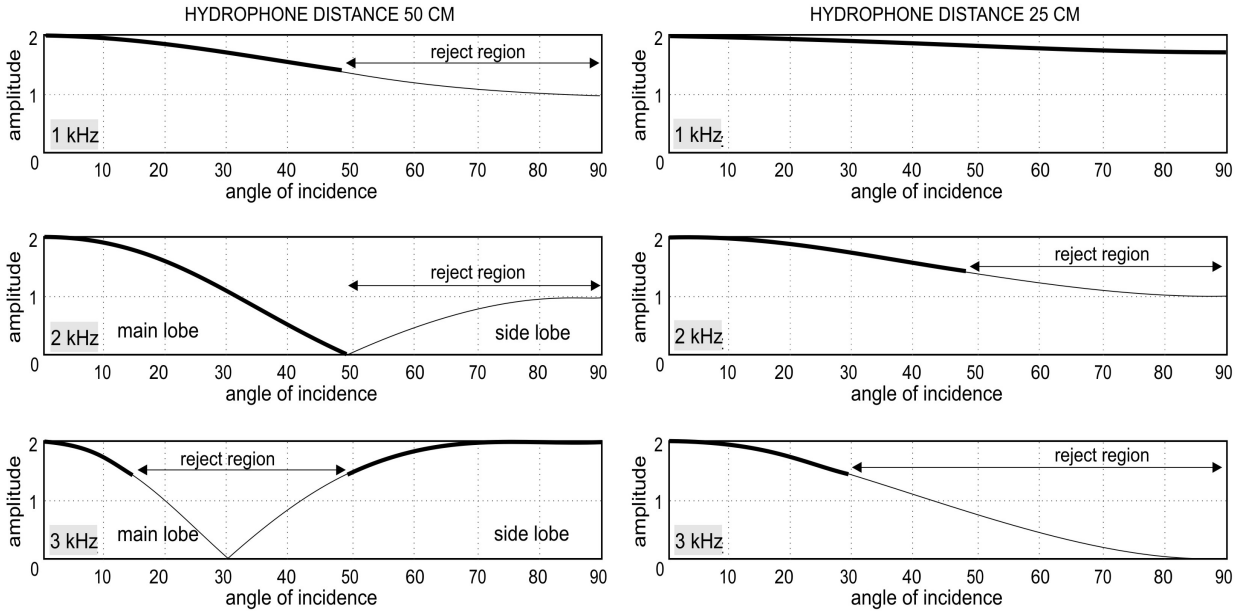

Figure 2.20 *Signal amplitude as a function of angle of incidence for different frequencies and hydrophone spacing. The thick black line indicates angles with attenuation less than -3 dB.*

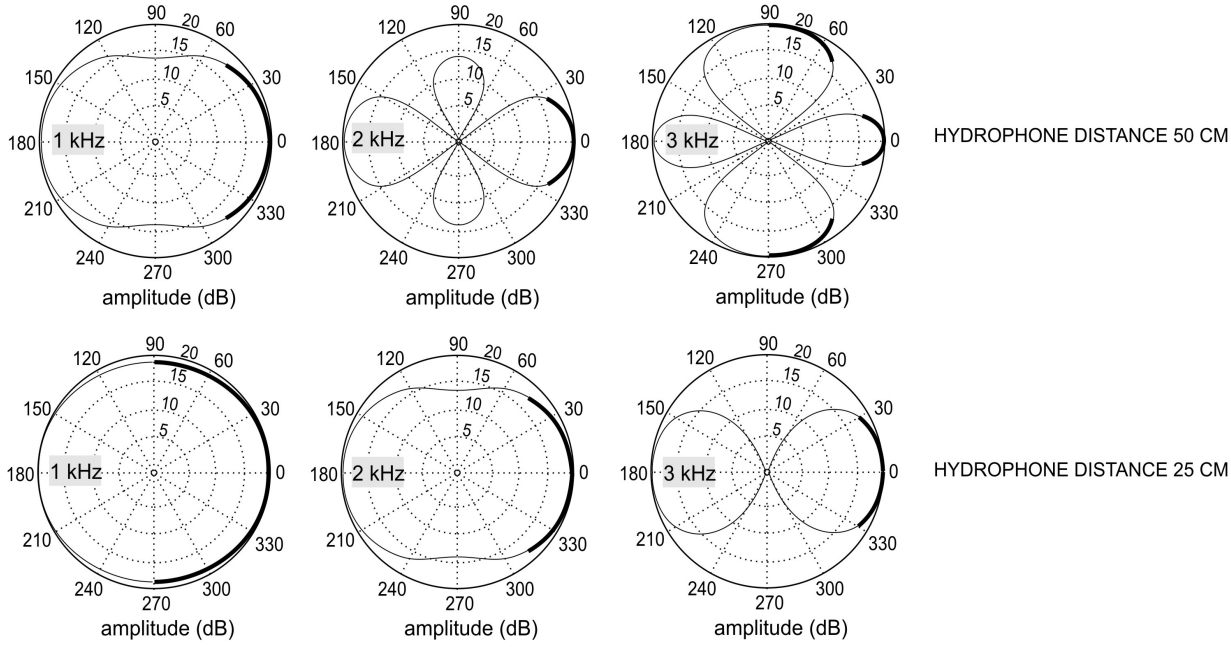

Figure 2.21 *Corresponding polar plots showing the sensitivity of the amplitude to different angles of incidence for varying frequencies and hydrophone spacing. The thick black line indicates angles with attenuation less than -3 dB.*

2.4.3 Receiver array length

In order to allow constructive stacking of the hydrophone signals in one receiver channel the signals must be in phase - i.e. the difference in travel distance of the seismic signal between the first and last hydrophone in the receiver must be smaller than a quarter wavelength of the wavelength of the signal (Sheriff & Geldart 1982). The relation between maximum array length (L), water depth (d), offset (x) and minimum wavelength (λ) can be derived from simple geometry (Figure 2.22):

$$L = -x \pm \tfrac{1}{2} [4x^2 + \lambda^2/4 + 2\lambda (4d^2 + x^2)^{1/2})]^{1/2} \quad (2.3)$$

The optimal receiver array geometry will therefore be a compromise between signal frequency, water depth and offset. Figure 2.22 shows the relation between hydrophone array length and source-receiver offset for various water depths and wavelengths. It is clear that shallower water and increasing offset will require shorter hydrophone spacing. For the OPUS3D layout 25 cm hydrophone spacing will assure good results for high frequency work (2-3 kHz) in shallow water (< 20 m) and using short offsets (< 15 m). Deeper water will allow the use of larger offsets. Moving towards extremely shallow water (<< 10 m) the offset should be reduced in order to avoid signal deterioration.

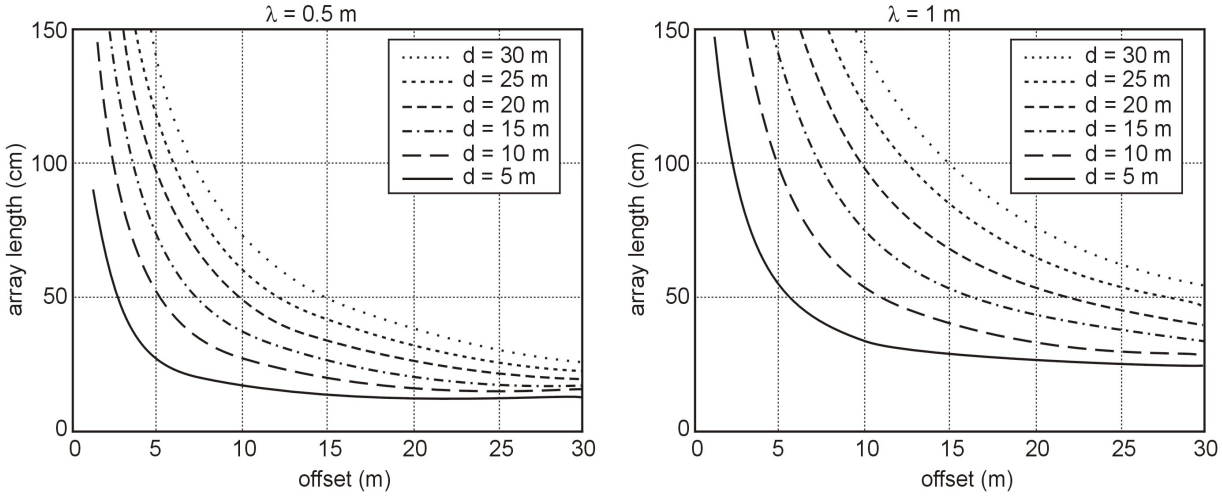

Figure 2.22 *Maximum array length and offset for varying wavelength (λ) and water depth (d).*

2.4.4 Binning and spatial resolution

Binning forms the heart of the 3D processing sequence. It refers to the stacking operation where the trace midpoints (from each source-receiver pair) falling within one grid cell, or bin, are summed. The optimum bin size dimension will depend on the positioning accuracy, spatial sampling and horizontal resolution (Missiaen et al. 2002a). Whereas a small bin size will increase the chance for low fold (i.e. the number of traces stacked per bin) and thus reduce the effect of stacking, a large bin size will decrease the resolution as it smears the events since traces are summed over a larger subsurface area.

The bin dimension must satisfy the spatial resolution requirements. The number of traces per bin should not only be sufficiently high - the general rule is that 2-3 samples are required to resolve a target (Mosher et al. 2002) - but the traces within one bin should also add up constructively. In

other words, the bin size will also depend on the Fresnel zone. For a target located at 20 ms the (first) Fresnel zone will be ~2.5 m for a main frequency of 2 kHz (V = 1550 m/s). A bin size dimension of 1x1 meter should therefore assure accurate imaging of the target.

In the presence of dipping layers and non-constant velocity the bin size required to prevent aliasing of the frequency f_{max} will depend on the interval velocity (immediately above the zone of interest) and the subsurface dip (Yilmaz 1987):

$$bin\ size = V_{int} / 4 f_{max} \sin(\theta) \quad (2.4)$$

As the maximum frequency and/or the dip decreases the bin size can be increased. For V = 1550 m/s, f_{max} = 2 kHz, and θ = 12 degrees the bin size is slightly bigger than 1x1 m.

2.5 Summary and conclusions

VHR 3D seismic acquisition requires specific strategies. The optimal strategy will depend on the target depth and dip, water depth, sampling laws, desired resolution. In practice though the survey design will not only depend on the theoretical considerations of seismic imaging but it will also be dictated by the field conditions and the available budget. The new flexible array OPUS3D developed at RCMG is aimed at small geological or geotechnical targets with a limited depth in shallow water areas. To obtain maximum flexibility a modular, inflatable array is used allowing convenient deployment and recovery.

Accurate positioning is a crucial factor. In view of the high frequencies involved even very small movements of the source and streamers can lead to a degradation of the seismic signal. A fast update rate of the positions is therefore crucial. In order to ensure that the traces are assigned their correct geometry the source-receiver positions should be known with decimeter precision. Short streamers and a positioning antenna near the source and streamers will reduce the positioning uncertainty. In sheltered areas the deviation will be very small and can be reasonably neglected. In offshore areas waves and currents will reduce the array stability and geometry corrections need to be applied.

To avoid spatial undersampling a compromise between the sampling interval, reflector dip and signal frequency is needed. In order to prevent aliasing of the high frequencies the hydrophone array should be short. Working in very shallow water environments requires small offsets to avoid signal deterioration related to high angles of incidence. Bin dimension will depend on positioning accuracy, spatial sampling and frequency content. Increasing the target dip will require a reduction in bin size.

In short the main conclusions regarding the acquisition array, positioning strategy and resolution & aliasing requirements can be summarized as follows:

Acquisition array

- modular array is adaptable to site characteristics;
- inflatable frames require limited space and can be deployed on small ships;
- central RIB allows to use the system as stand-alone in sheltered areas;
- 6 modular frames and 8 streamers;
- dual-channels streamers allow short streamer length and are cost effective;
- 2 m streamer and channel spacing allows to cover larger and deeper targets.

Positioning strategy

- real-time kinematic (RTK) positioning in (x,y,z) with cm/dm range
- compromise between antenna height and optimal radio link
- short source towing distance to minimise source deviation
- positioning antenna on the source frame
- short streamers to minimise streamer deviation
- small positioning uncertainty in sheltered environment:
- geometric corrections needed in offshore areas.

Resolution & aliasing

- vertical resolution 0.5 - 1 m;
- horizontal resolution ≤ 1 m;
- shot interval ≤ 0.5 s to allow imaging of medium target dips;
- hydrophone array ≤ 25 cm to avoid spatial aliasing);
- offsets ≤ 15 m to avoid signal deterioration in shallow water;
- bin size ~ 1 m to allow correct imaging of medium target dips.

CHAPTER 3
SCHELDE RIVER CASE STUDY

3.1 Introduction

In the framework of the EC-MASTII project "VHR3D" a 3D seismic survey was carried out in September 1999 with the newly developed inflatable acquisition system 'OPUS3D'. The target of the 3D study was a small diapir in the Boom Clay (Rupelian Formation) under the Schelde river near Antwerpen (Figure 3.1). The clay diapir had been discovered during a seismic survey in 1982 (Henriet et al. 1986). Detailed site investigations in the area related to metro tunnel works and the construction of a storm surge barrier (Schittekat et al. 1983, Heldens 1983) have turned the site into a well-documented test ground. The clay diapir had also been the subject of a previous test survey with the SEISCAT acquisition system to evaluate the potential of the VHR 3D technique (Henriet et al. 1992). The results of this test survey are discussed in the Annex.

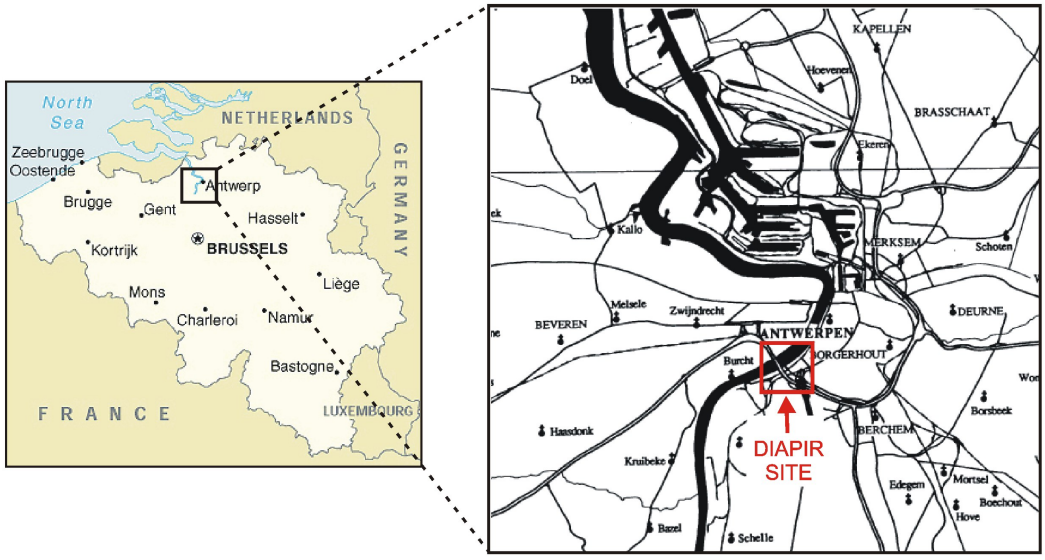

Figure 3.1 *Location of the diapir in the Boom Clay under the Schelde river near Antwerpen.*

3.2 The target

The clay diapir has an apparent diameter of 60 m, and a vertical amplitude ranging from a few decimeters at 50 m depth to a few meters at about 25 m depth (Figure 3.2). Its geotechnical properties prove not to be significantly different from those of the surrounding undisturbed clay (Schittekat et al 1983). The superposition of the clay diapir and a small depression in the river bed may suggest an origin related to differential decompaction, the sediment load being reduced by erosion of the river bed (Verschuren 1992).

The Boom Formation, or Boom Clay, is marked by a regular sequence of silt-rich and clay-rich layers. The thickness of the silty layers varies roughly between 0.2 and 0.4 m, except for the basal layers which can reach thicknesses of up to 2 m. The clayey layers are generally thicker, with a thickness between 0.3 and 2 m (Heldens 1983). Typical for the Boom Formation is the presence of calcareous-rich horizons marked by carbonate concretions (so-called "septaria")

containing internal cavities (septae) (Figure 3.3). The position of the calcareous horizons is not related to grain size or organic matter as they occur both in silty and clayey layers (Vandenberghe 1978). They represent originally marly sedimentation horizons which were modified by later diagenesis (after a few meters of burial a slight pH decrease remobilises and redistributes the carbonates into nodules and as these lithify, under vertical overburden, vertical cavities are formed) (Vandenberghe & Laga 1986). The concretions often stand out as diffraction hyperbolae on analog profiles (Schittekat et al. 1983, Henriet et al. 1986) (Figure 3.2).

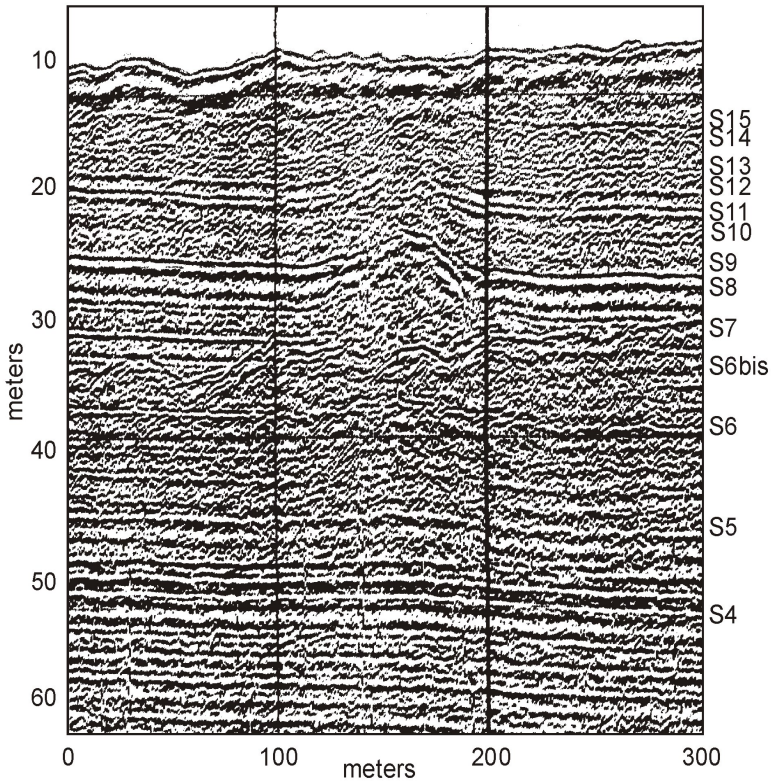

Figure 3.2 *Analog boomer profile obtained in 1982 across the clay diapir (after Henriet et al. 1992). Age number of diffraction hyperbolae can be observed, most likely related to calcareous concretions. The numbers on the right refer to the different concretion levels identified in the area by Heldens (1983).*

Figure 3.3 *Carbonate concretion in the Boom Clay.*

Heldens (1983) identified over 15 septaria horizons in the vicinity of the diapir (Figure 3.2). The septaria are marked by a flattened spherical shape with an average diameter between 0.3 and 1 m and a thickness between 10 and 30 cm (Vandenberghe 1978). The form, size and distribution of the septaria can vary largely between the horizons. Whereas certain beds are marked by very large (1 to 2 m, occasionally up to 3 m) and thick (up to 50 cm) septaria, other beds contain small (< 30 cm diameter) and flat (10 cm thick) concretions.

In general the distribution of the septaria within each horizon is fairly regular, with an average spacing between 3 and 6 m (Heldens 1983). It is not unlikely that the formation of the diapir will have caused some displacement of the septaria. In particular it was a challenge to see whether the new acquisition system would allow us to assess the 3D spatial distribution of the septaria. Whereas the diapir itself is not expected to form a major geotechnical hazard - the geotechnical properties inside the diapir are not significantly different from those of undisturbed clay (Schittekat et al. 1983) - this may no longer be true for the septaria (Laga 1966). Detailed information on the septaria and their local distribution can be crucial for geotechnical construction works that involve drilling operations (Henriet et al. 1992).

3.3 Seismic acquisition

The 3D survey on the river Schelde was carried out on board R/V Belgica. During the first day of the survey strong wind and currents (due to spring tide conditions) made it difficult to deploy the inflatable array. The following day weather conditions improved and the 3D array was deployed without any problem. The comportment of the inflatable frames was very good, and thanks to the simplified lay-out the frames were easy to handle. During the survey the inflatable array was towed 15 meters behind the vessel (Figure 3.4). Offset between the source (Seistec boomer) and nearest receivers was ±7 m. Each shot generated 16 subsurface reflection points in a swath 7 m wide. Theoretical line spacing was set at 6 m in order to assure full spatial coverage.

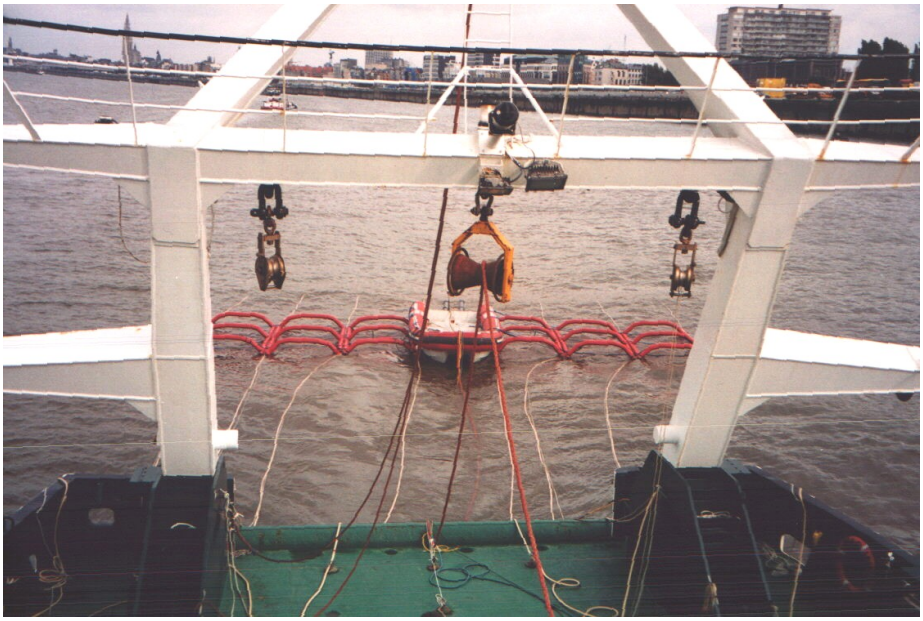

Figure 3.4 *The inflatable seismic acquisition system Opus3D towed behind the R/V Belgica during the survey on the river Schelde.*

In two days time a network of 48 seismic profiles was recorded over the diapir, with an average profile length of 300 m (Figure 3.5). To reduce the noise level the vessel sailed on electrical propulsion. Recording of the seismic data was done using the Elics Delph24 multichannel seismograph (shot interval 0.5 s, record length 100 ms). Sampling rate was 16 kHz which should avoid possible aliasing effects. The total recorded data volume amounted to ±3.5 Gbytes.

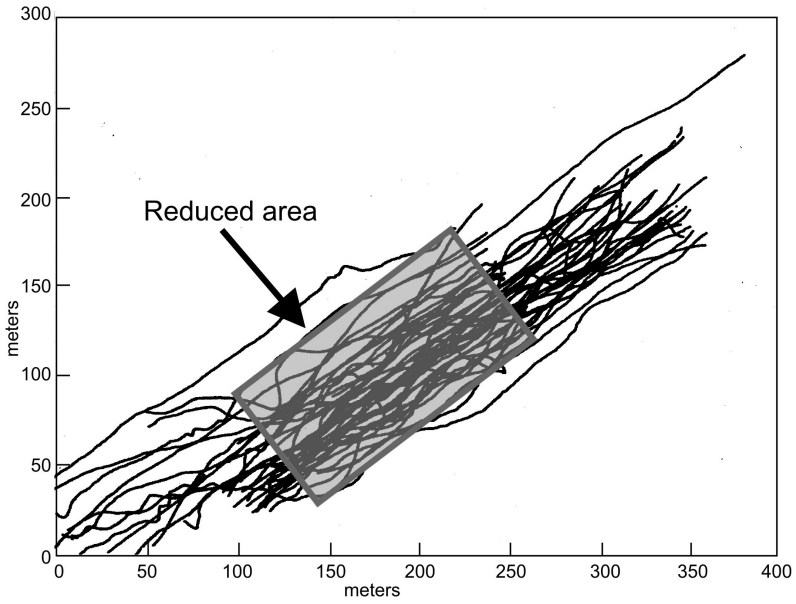

Figure 3.5 *3D seismic network recorded during the Schelde survey. The grey rectangle marks the reduced area over the clay diapir (Missiaen et al. 2002a).*

Positioning was done using a short-range DGPS system based on RTK positioning. The reference antenna was located on a high building close to the survey area. Thanks to the fast update rate real-time (x,y,z) positions could be acquired for each shot with cm accuracy. Because the Seistec boomer frame proved very stable in the river environment the positioning antenna was installed on the Seistec, which further helped to minimise relative positioning errors. In order to keep the inflatable array well stretched the vessel did not turn but instead seismic tracks were sailed against the current, alternatively forward and backwards. This method had already proven its efficiency in 1990 (see chapter 2). However this resulted in a highly variable vessel speed and regular profile spacing could therefore not always be achieved (Missiaen et al. 2002a).

3.4 Geometry processing

The vertical antenna positions were occasionally marked by small high-frequency variations, a.o. caused by wave movement due to passing ships. The effect of these small 'vibrations' was clearly visible on the seismic data, and the variations were therefore filtered out (Figure 3.6). Profiles of inferior data quality were left out. The seismic network was rotated and reduced to a 150x80 m area covering the clay diapir (see Figure 3.5), resulting in a final data volume of 1.5 Gbytes.

The source, receiver and midpoint positions were calculated from the antenna positions taking into account the ship's heading and assuming a rigid and well-aligned array (Figure 3.7). This seemed to be justified by the observations during the survey, indicating that the streamers remained well stretched. This was not only due to the protected river environment showing

relatively little wave motion, but also to the fact that all profiles were sailed parallel to the current, thereby keeping the streamers well aligned (Missiaen et al. 2002a).

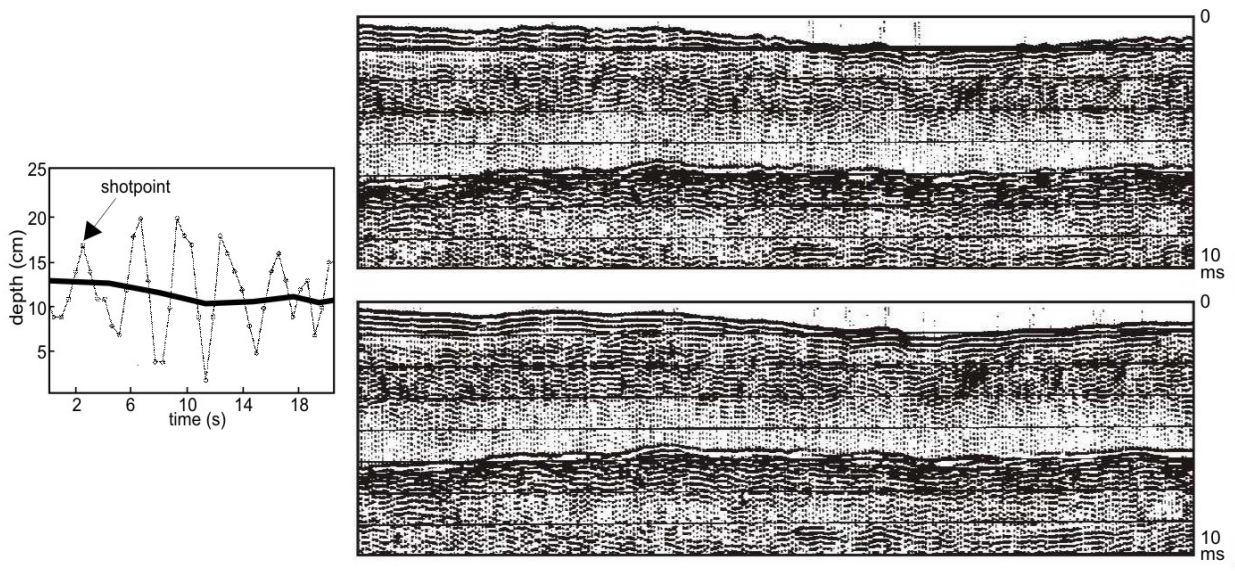

Figure 3.6 *Left: small high-frequency variations in the vertical antenna data, Schelde survey (thick black line = filtered data). Right: effect on common offset section. Top = unfiltered data, bottom = filtered data.*

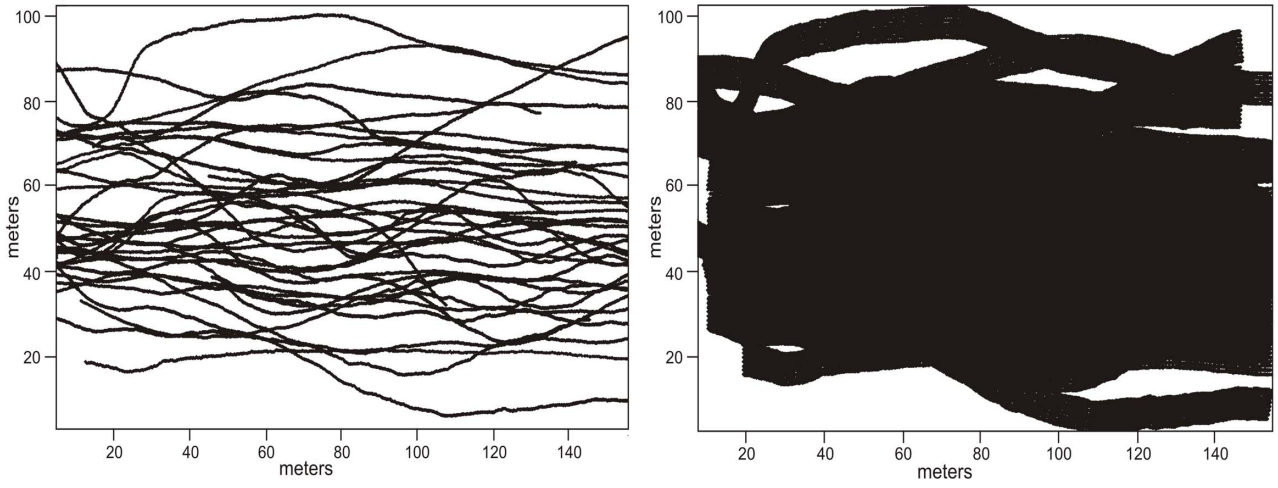

Figure 3.7 *Seismic coverage in the reduced area over the clay diapir, Schelde survey. Left: shotpoint distribution. Right: midpoint distribution.*

Close inspection of the first break arrivals showed that this theoretical approach did not always match reality. Occasionally changes in the shot gather pattern could be observed, especially at very low vessel speed, indicating a slight swaying movement of the streamer array. Still, the effect of this movement was quite small (offset deviations << 50cm) and therefore it seemed reasonable not to apply geometrical corrections.

3.5 Data processing

Since tidal action on the river Schelde is quite large (with amplitudes >5 m) tidal correction was a crucial step. This was done by adding a time shift based on the vertical coordinates of the antenna. Tidal shifts were applied to the zero-offset data, after NMO correction(velocities ranging from 1500 to 1650 m/s, based on the velocity model extracted from geotechnical site investigations, see Annex) (Figure 3.8). The tidal corrections also resulted in suppression of the seabed multiple in the process of stacking. Additional data processing included bandpass filtering, agc and deconvolution (Missiaen et al. 2002a).

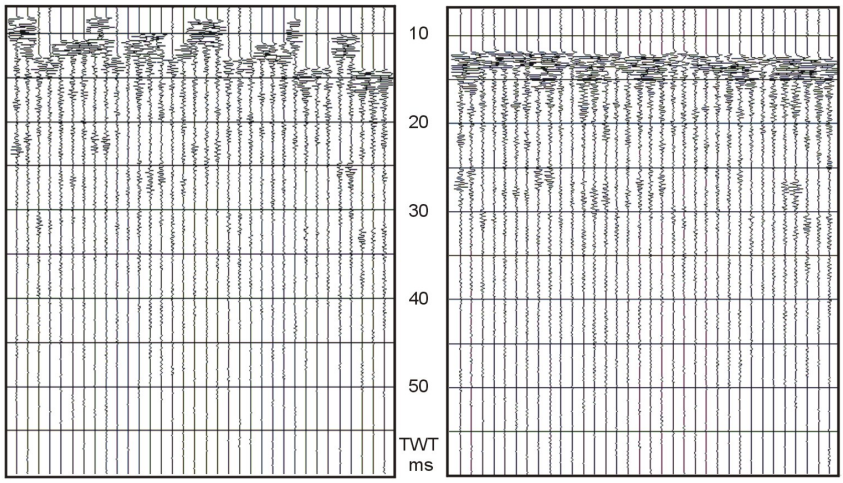

Figure 3.8 *Bin traces from the Schelde survey. Left: before NMO and tidal correction. Right: after NMO and tidal correction, showing good line-up of traces in the stack bin.*

With the depth of the target being shallow, a stack grid of 1x1 m bins was set out. This would adequately oversample the first Fresnel zone (see chapter 2). Trace midpoint positions were set out in the bin grid and the resulting stack fold coverage calculated. Due to the irregular navigation pattern the fold coverage was somewhat variable. Still it was generally good in the area of interest with an average of 20 to 30 traces per bin, reaching up to 120 traces in areas of extreme low vessel speed (Figure 3.9). The actual stacking process was carried out per bin, resulting in a total of over 16,000 stacks. The good line-up of traces in the stack bins (see Figure 3.8) justified the geometrical correction approach discussed above (Missiaen et al. 2002a).

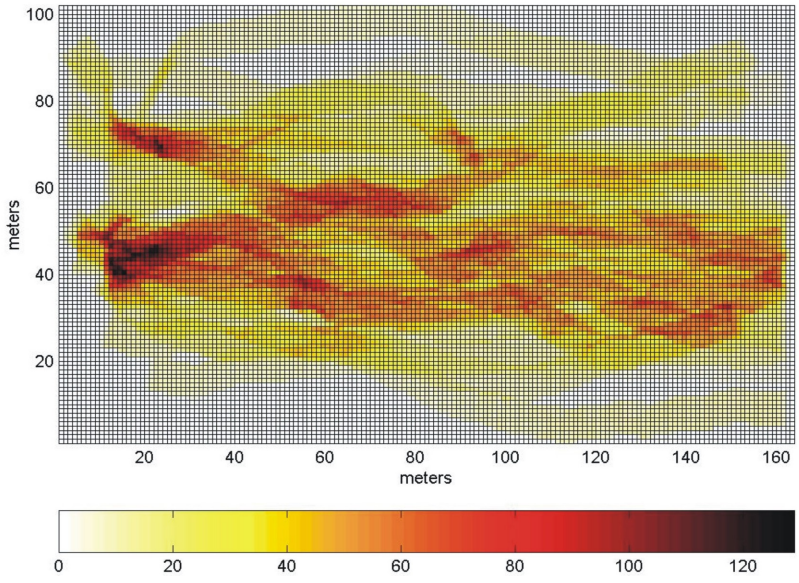

Figure 3.9 *Stack fold coverage in the reduced area over the clay diapir, Schelde survey. Grid bin size 1x1 m.*

3.6 Imaging results

The quality of the stacked 3D data was generally very good. The vertical inline sections show a great coherency, and are marked by a large number of continuous and highly energetic reflectors (Figure 3.10). Although the upper part of the clay diapir remains largely disturbed, weak internal reflectors can now be observed on a number of inline sections (Figure 3.10-left) (Missiaen et al. 2002a).

Figure 3.11 shows a series of consecutive time slices (10 cm interval, ~0.13 ms) taken from the lower part of the diapir. The time slices reveal a sharply defined concentric reflector pattern growing towards the base of the diapir. As can be expected the time slices from the upper part of the diapir become less coherent, although the concentric pattern can still be clearly observed (Figure 3.12) (Missiaen et al. 2002a). The slight dip towards the northeast observed on the time slices corresponds to the general dip of the Tertiary strata in this area.

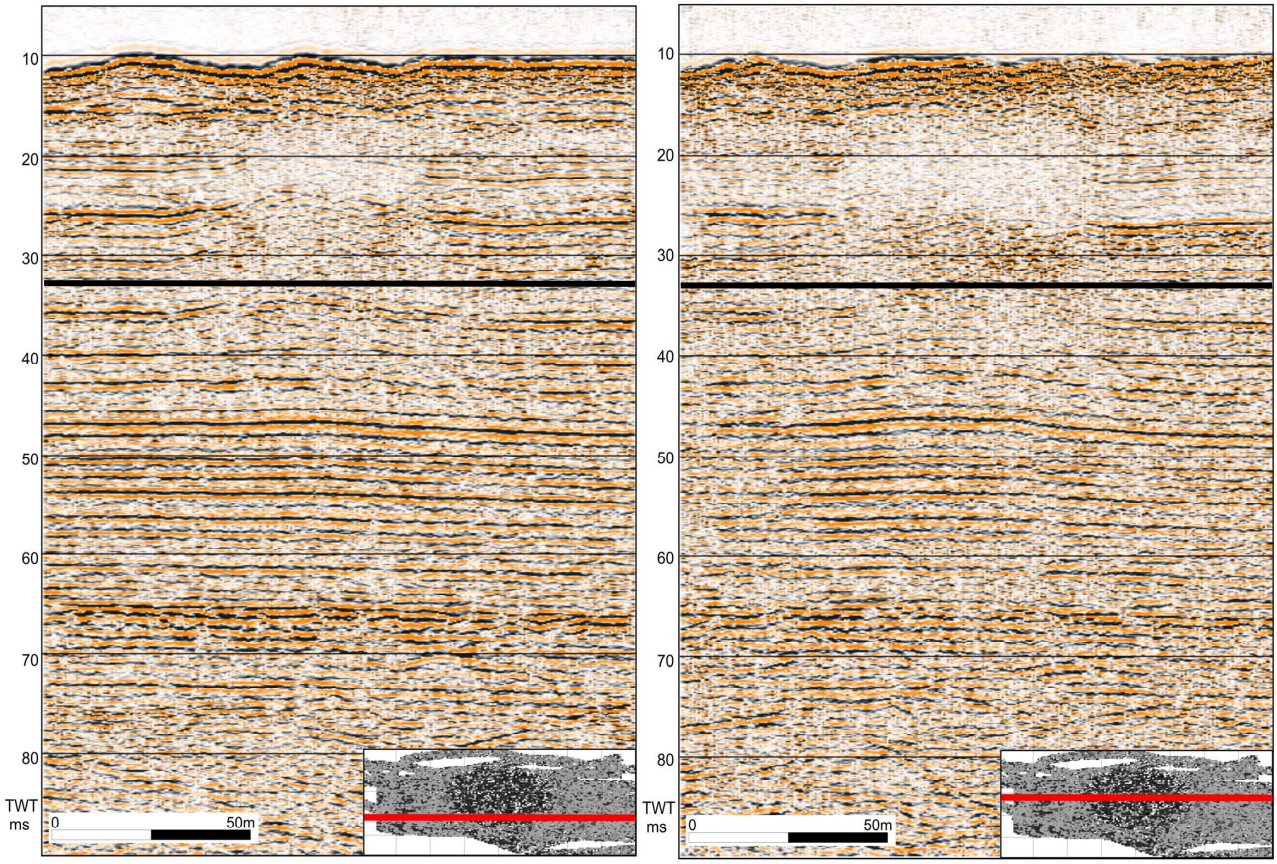

Figure 3.10 *Two inline vertical stack sections through the 3D volume over the clay diapir, Schelde survey. The location of the sections is indicated in the lower right corner (red line). The sections are marked by a large number of continuous reflectors. Although the internal facies of the clay diapir remains chaotic a number of weak internal reflectors are now visible (left profile). The horizontal black line at ~32 ms TWT marks the location of the time slices shown in Figure 3.11.*

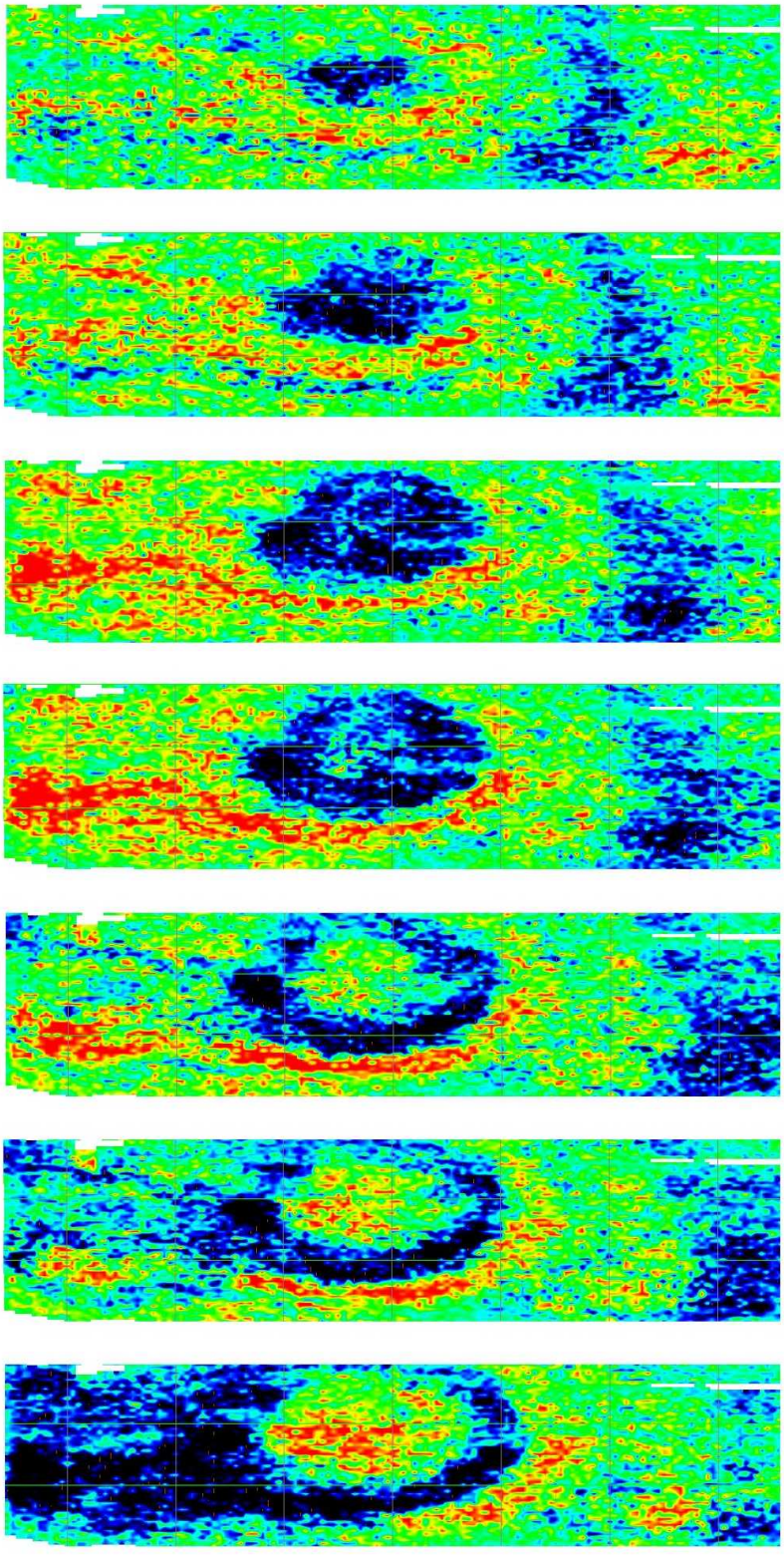

Figure 3.11 *Series of consecutive time slices (10 cm interval, ~0.13 ms) through the 3D volume of the Schelde survey showing the concentric reflector pattern over the clay diapir and a slight dip to the NE. The latter corresponds to the general dip of the Tertiary strata in this area. Area dimensions approx. 140 x 60 m. The location of the time slices is indicated in Figure 3.10.*

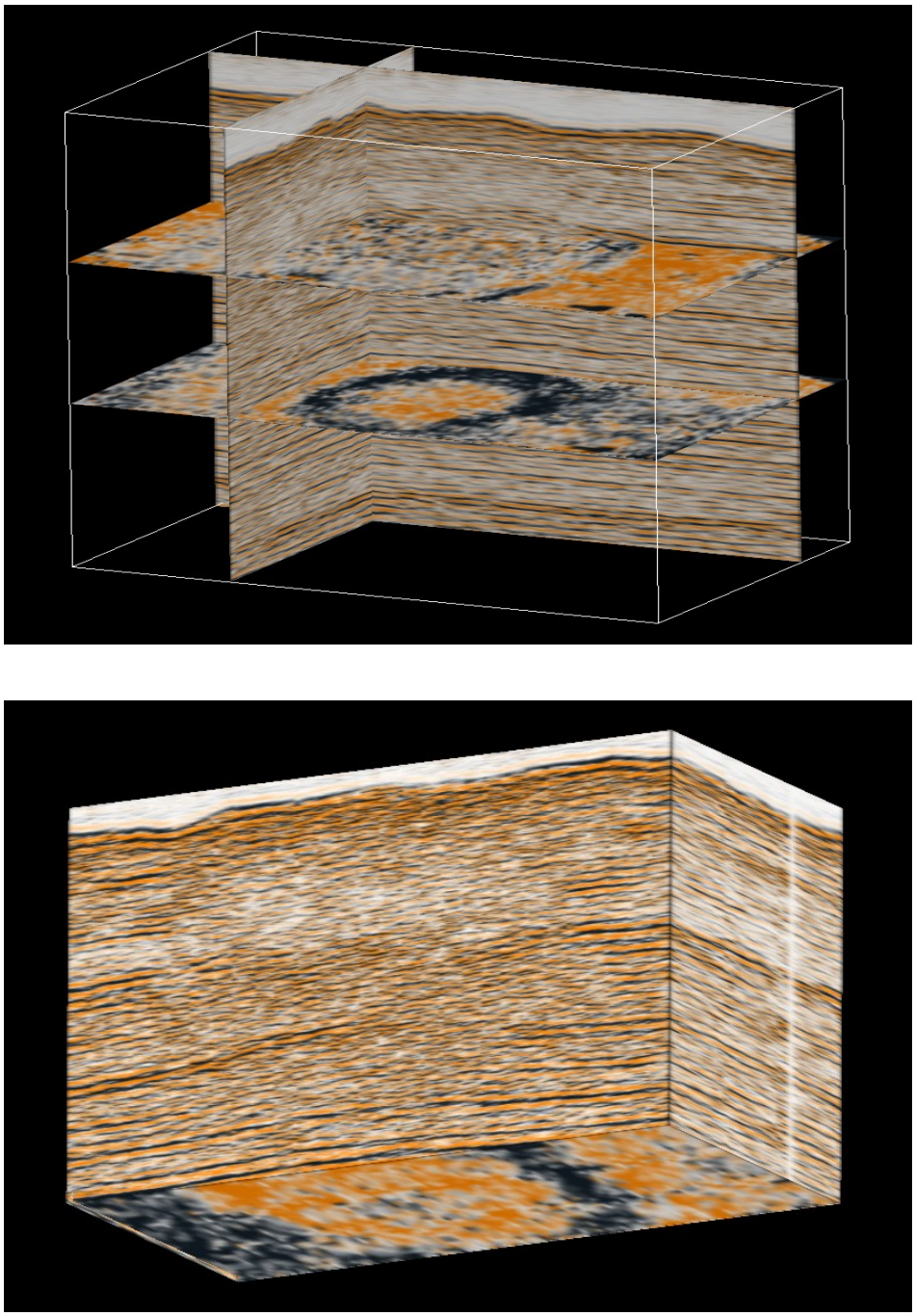

Figure 3.12 *Top: Panel section combining time slices and vertical sections through the 3D volume over the clay diapir, Schelde survey (panel dimensions approx. 140x60x35 m). Although less clear, the concentric reflector pattern can still be observed in the upper part of the clay diapir. Bottom: 3D cube of the clay diapir, Schelde survey (cube dimensions approx.120x60x20 m).*

3.7 Comparison with 1990 survey

Figure 3.13 shows a comparison between the results of the 1990 SEISCAT survey (right, see Annex) and the 1999 OPUS3D survey (left) over the same clay diapir. Both data sets were binned with 1x1 m bin cells. The results clearly illustrate that the vertical stack sections obtained in 1999 show greater detail, with better defined and more continuous reflectors, also in the upper part of the diapir where most reflectors showed up weak and incoherent on the 1990 data. Also the time slices resulting from the 1999 data volume are marked by a distinct increase in resolution of the concentric reflector pattern.

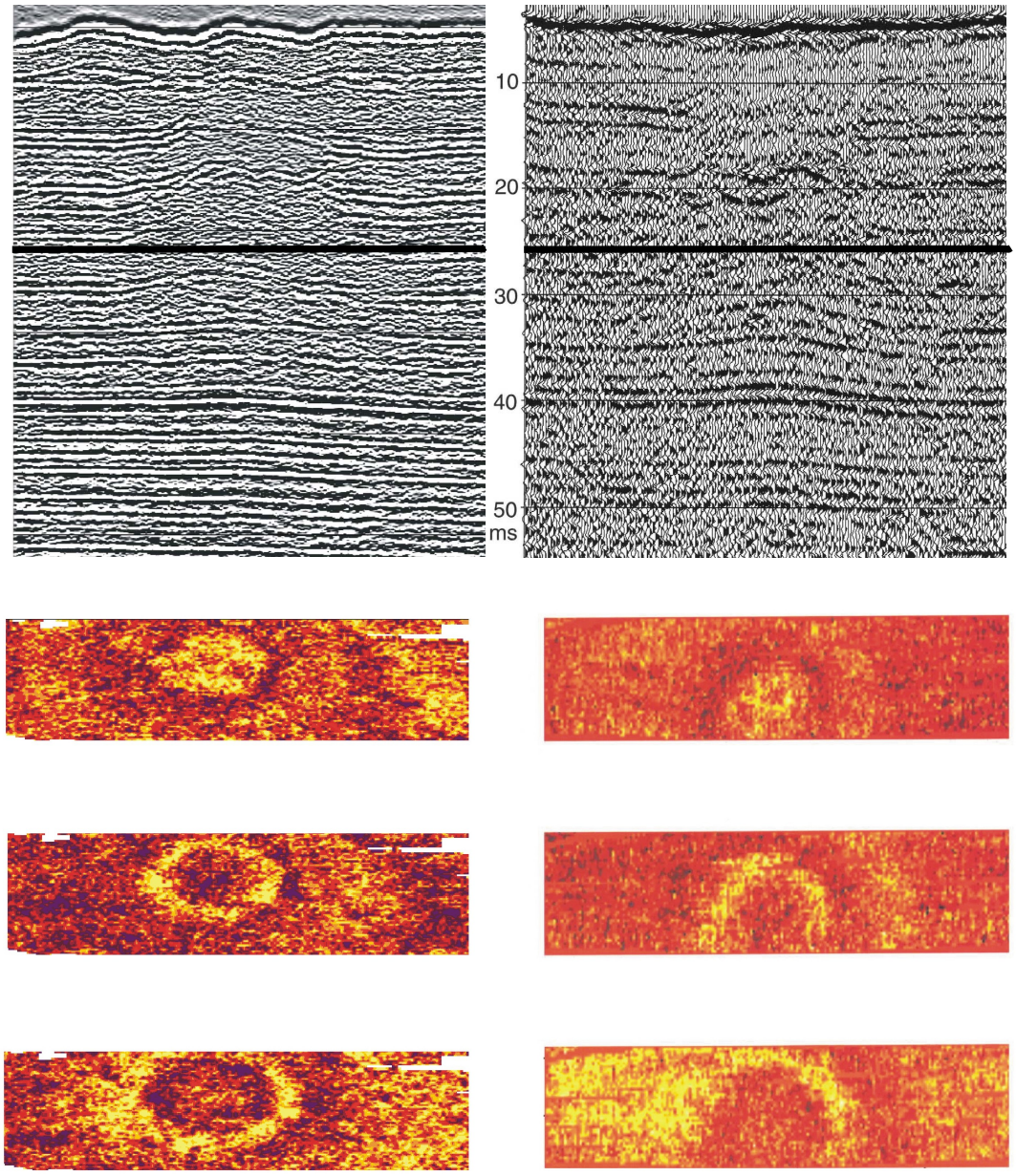

Figure 3.13 *Comparison between results from the 1990 SEISCAT survey (right) and 1999 OPUS3D survey (left) over the same clay diapir. Top: Vertical stack sections, taken from the central part of the diapir (profile width 150 m). The full black line marks the location of the time slices. Bottom: Horizontal time slices (50 cm interval, ~0.6 ms) taken from the lower part of the diapir (area dimensions 140 x 60 m). The improvement in image quality of the 1999 data compared to the 1990 data is clearly visible.*

3.8 Septaria horizons

The vertical stack sections through the 3D data volume over the clay diapir show the presence of numerous diffraction hyperbolae, indicating a possible relation with the septaria (or clusters of septaria) in the clay sequence. Up to now these septaria had only been observed on analog seismic recordings (see §3.1). Based on the results of detailed geotechnical site investigations, carried out in the framework of metro tunnel works and the construction of a storm surge barrier, at least 15 different septaria horizons (so-called "S"-horizons) were identified in the clay diapir area (Heldens 1983) (see Figure 3.2).

The size of the septaria and their distribution will differ from horizon to horizon. Certain horizons are marked by large, thick septaria whereas others are marked by small, flat septaria. It therefore seems likely that not all horizons can be easily traced on the 3D data, e.g. due to the limited size of the septaria or the sparse distribution in some horizons. As mentioned in §3.1, the distribution of the septaria within each horizon is fairly regular, although some local displacement (related to the clay diapir) cannot be ruled out.

In order to try and resolve the spatial distribution of the septaria beds a number of reflectors identified with different horizons were carefully picked. The horizons were known to be marked by relatively large septaria (very small septaria will most likely not show up on the 3D data due to the bin size limitations). Horizon S4 was chosen from an undisturbed section in the lower part of the clay diapir. A number of parallel horizon slices were made at very small intervals (4 cm or ~0.03 ms) just below the picked septaria horizon (4-5 cm).

Figures 3.14 and 3.15 show the results for septaria horizon S4. The vertical stack section (Figure 3.14) shows the presence of numerous diffraction hyperbolae which can most likely be linked to individual septaria within each horizon. The series of corresponding horizon slices (Figure 3.15-left), taken at very small intervals, are marked by a slowly appearing and disappearing blotchy pattern. Figure 3.15-right shows an enlargement, over an area of 60 x 40 m, of the third horizon slice of septaria level S4. The distribution of the "spots" (average spacing < 4 m) suggests that we are likely dealing here with the actual septaria.

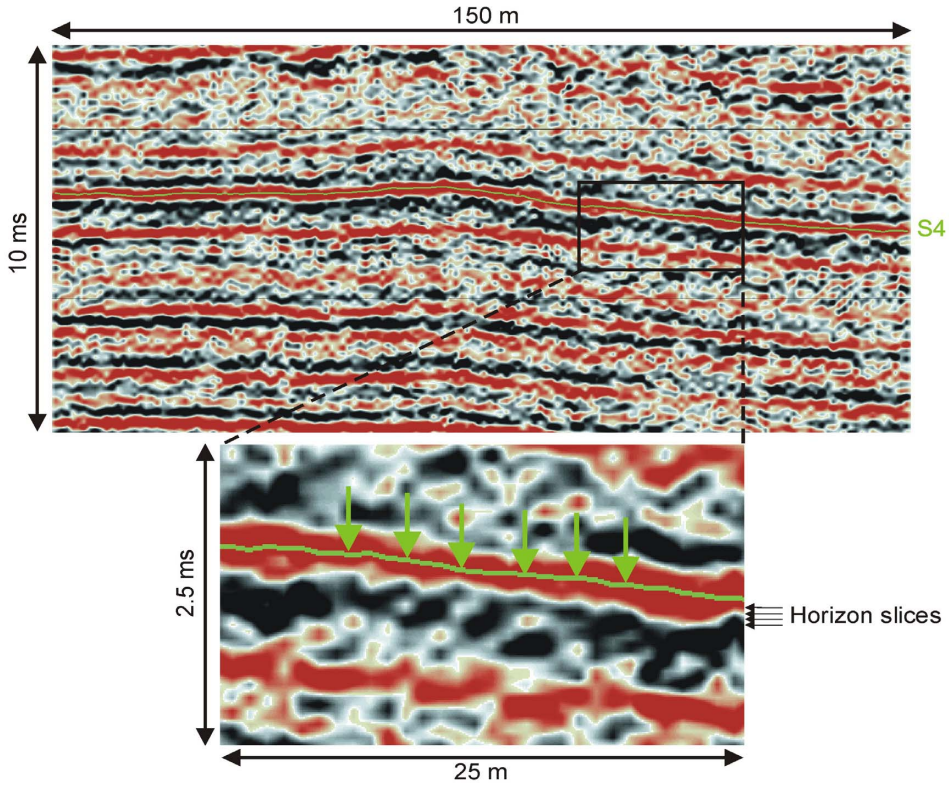

Figure 3.14 *Top: Vertical stack section through the lower part of the clay diapir. Bottom: Detailed close-up of septaria horizon S4 showing the presence of numerous diffraction hyperbolae (marked by green arrows). The small black arrows on the right mark the location of horizon slices shown in Figure 3.15-left.*

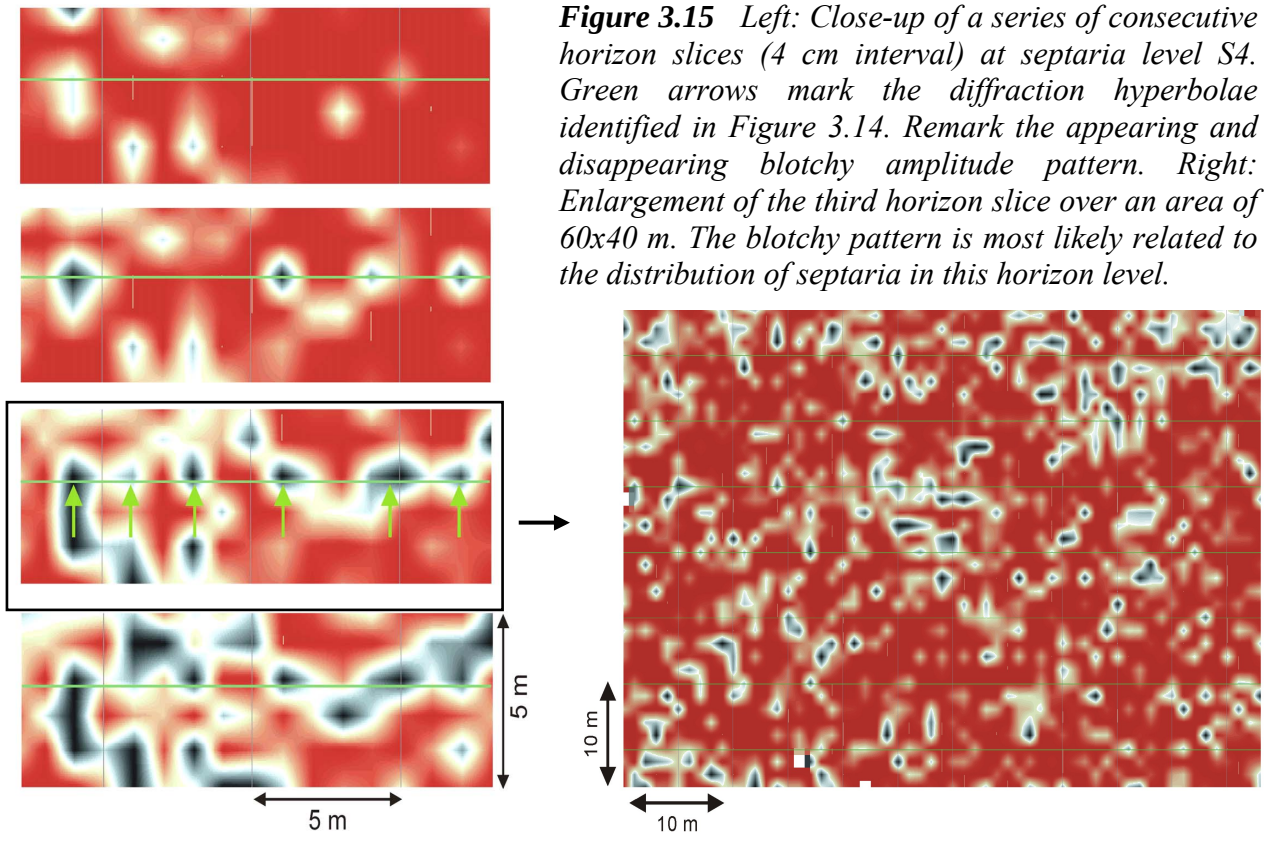

Figure 3.15 *Left: Close-up of a series of consecutive horizon slices (4 cm interval) at septaria level S4. Green arrows mark the diffraction hyperbolae identified in Figure 3.14. Remark the appearing and disappearing blotchy amplitude pattern. Right: Enlargement of the third horizon slice over an area of 60x40 m. The blotchy pattern is most likely related to the distribution of septaria in this horizon level.*

3.9. Summary and conclusions

A 3D seismic survey was carried out on the river Schelde with the inflatable acquisition array OPUS3D. The target was a diapir in the Boom Clay. The diapir had been the subject of previous investigations and formed a well-documented test ground. The inflatable array was easily deployed and due to the sheltered environment the array and streamers stayed well aligned. Source and receiver movement away from the nominal geometry were minimal and no geometry corrections were required. A dense network of 48 seismic profiles was recorded over the diapir, with an average profile length of 300 m and spacing of roughly 6 m. Positioning was done using a short-range RTK antenna mounted on the Seistec frame resulting in real-time (x,y,z) positions with cm accuracy.

Source and receiver coverage were calculated from the antenna positions taking into account the ship's heading and assuming a rigid and well-aligned array. Since tidal action was very large (> 5 m) static corrections were essential. A stack grid of 1x1 m bins was used, which would adequately oversample the first Fresnel zone. The quality of the stacked data was very good, and vertical time sections were marked by a large number of continuous reflectors that showed up less coherent on earlier data. Although the upper part of the clay diapir remained disturbed (most likely due to a loss of internal structure caused by gravitational collapse) some internal reflectors were now observed. Time slices revealed a sharply defined concentric reflector pattern growing towards the base of the diapir.

The Boom Clay is marked by the presence of calcareous-rich horizons containing carbonate concretions (so-called "septaria"). They often show up as diffraction hyperbolae on the seismic data. The size of the septaria and their distribution differs from horizon to horizon. It was a challenge to see whether the 3D approach would allow us to assess the spatial distribution of the septaria. Several horizons, known to be marked by relatively large septaria (very small septaria may be acoustically invisible), were carefully picked and a number of parallel horizon slices were made at very small intervals (4 cm or ~0.03 ms). The results showed a slowly appearing and disappearing blotchy pattern which probably reflects the distribution of the septaria within the horizon.

The results of this survey illustrate the importance of VHR 3D shallow seismic investigations for engineering geophysics and geological and geotechnical site investigations. The study also shows that it is feasible to acquire high-quality VHR marine 3D data in a modest and cost-effective way, without requiring complex field procedures. The inflatable acquisition system OPUS3D allowed to improve the imaging resolution, even when based on relatively simple processing, and so further scale down the shallow 3D method to ultra-high resolutions and dm scale.

CHAPTER 4
CHEMICAL MUNITION DUMPSITES: A BORDER-TRANSGRESSING PROBLEM

4.1 Introduction

The problem posed by sea-dumped chemical weapons (CW) deserves considerable international attention: the amount dumped in the North European seas alone since the end of WW1 runs into hundreds of thousand of tons at least (Kaffka 1995, Stock & Lohs 1997). The toxic war material, often dumped in relatively shallow waters and areas of active fishing, not only represents a serious threat to the marine environment but also to the often densely populated coastlines. The chemical weapons have time and again showed up, for instance when retrieved in fishing nets or when washed ashore on beaches, attracting local media coverage only. Nevertheless, the problem has received little attention and was neglected for a long time at the international level.

There were a number of reasons for the decades of delay in addressing this problem. For one thing the issue is politically sensitive as it raises the problem of accountability. Many dumping operations were carried out secretly and it is not always clear who can be held responsible. Some dumpsites are located in international waters, although more often dumping operations were carried out in territorial waters near the borders of neighbouring states. The government bodies of both the states that carried out the operations and those bordering the dumping areas have been long reluctant to tackle this sensitive problem (especially during the Cold War), but these political obstacles have mostly been removed now.

Another factor is the complexity of the problem which requires a large expertise in different scientific fields, and therefore involves a huge commitment of financial and technological resources. In recent years, however, sea-dumped chemical weapons have been the subject of growing concern in a number of international conferences and workshops. Although the full extent of the dumping operations still remains unclear – often due to a lack of documentation and loss or destruction of records - an increasing number of dumpsites have been and still are being documented.

4.2 Historical background and international treaties

Chemical weapons were first used on a large scale in the battle of Ypres in April 1915. During the entire WW1 a wide range of toxic warfare agents was produced (at least 40 different compounds) and employed on the battlefields. An estimated 1.45 billion shells were fired during the war, about 66 million of these contained toxic agents (Prentiss 1937). The most common chemical agents included tear agents (e.g. bromides and chloropicrin), choking agents (e.g. phosgene and diphosgene), vomiting agents (e.g. Clark) and blistering agents (e.g. mustard gas*, also known as Yperite after the battle of Ypres in Flanders where mustard gas was deployed for the first time in July 1917).
(The word "gas" is misleading. Mustard gas commonly appears under solid form or as a viscous liquid).*

Outrage at the effects of chemical warfare led to the signing of the Geneva Protocol for the "Prohibition of the Use of Asphyxiating, Poisonous or Other Gases, and Bacteriological Methods of Warfare" in 1925. Strangely enough the treaty did not forbid the development, production and possession of these weapons. A large number of nations signed the treaty, but

also expressed that they should maintain the right to retaliate any chemical attack on their territory with the same means, as well as the right to use chemical weapons against non-signatories of the protocol (SIPRI 1997).

In the nineteen thirties and forties the invention of nerve agents (e.g. Sarin, Tabun and Soman) and blood agents (e.g. hydrogen cyanide (so-called “Zyklon B”) and cyanogen chloride) gave a new dimension to chemical warfare. During WW2 chemical weapons were not used in mass quantities, although large stocks were produced by the US, Germany, Japan, USSR and the UK. In Germany alone 65,000 tons (net weight) of toxic warfare compounds, for the larger part mustard gas, were produced before and during WW2 (Duursma 1999). After WW2 in total some 300,000 tons (gross weight) of CW were discovered in the German occupation zones of the US, UK, France and USSR (Figure 4.1) (Duursma 1999). At that time dumping at sea was considered the best and most practical solution to get rid of these old CW stocks, thereby completely ignoring the consequences for the environment. An estimated 80% of the WW2 stocks were dumped in the Baltic Sea and the North Sea (Duursma 1999).

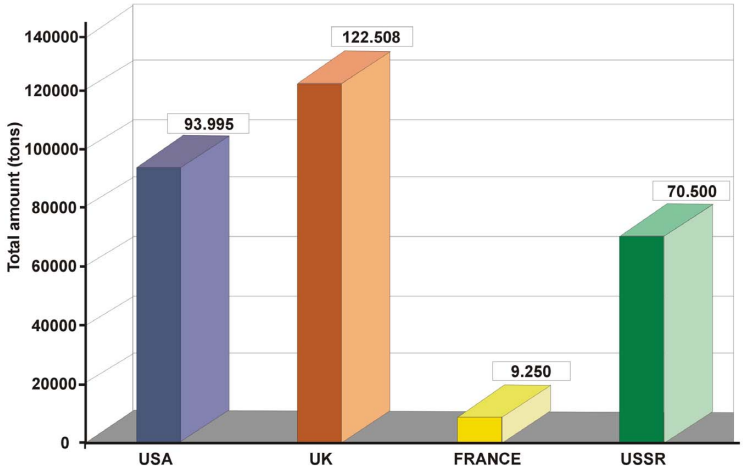

Figure 4.1 *Amount of chemical warfare (tons gross weight) discovered by the Allied Forces on German territory after WW2 (after Duursma 1999).*

Also after WW2 the production of CW continued. For decades dumping at sea remained a widely used method to reduce old or obsolete stocks. Growing environmental protest in the seventies led to the "Convention for the Prevention of Marine Pollution by Dumping from Ships and Aircraft" (so-called Oslo Convention) in 1972. In 1974 this was followed by the "Convention for the Prevention of Marine Pollution from Land-Based Sources" (so-called Paris Convention). In 1992 both conventions merged into the "Oslo-Paris Convention for the Protection of the Marine Environment of the Northeast Atlantic" (so-called OSPAR Convention). Equivalent with the OSPAR convention, the "Convention for the Protection of the Marine Environment of the Baltic" was signed in 1974 (so-called Helsinki Convention).

During the nineteen eighties further steps were taken towards a general convention banning chemical weapons. This finally led to the "Chemical Weapons Convention" (CWC) in 1993 which prohibits the development, production and use of chemical war material for military purposes and calls for the destruction of the present stocks. The treaty does not provide any incentives to recover chemical weapons that were sea-dumped before 1985. Member states are obliged to report within 30 days the presence of weapons from WW1 and WW2 (so-called "old and abandoned CW") on their own territory or on the territory of another member state, and pass on all necessary information.

It is generally accepted that chemical weapons cannot be openly dumped at sea today. The CWC explicitly forbids the dumping of CW in any body of water for its state parties (Verification Annex, Part IV(A), §13). The OSPAR and HELCOM Conventions forbid the dumping of toxic waste at sea. However in these treaties no explicit reference is made to war material. Still, there is no other way than considering a chemical warfare agent as a toxic substance: this characteristic is at the heart of the definition of chemical weapons.

4.3 Major CW dumpsites worldwide

4.3.1 North Sea, Mediterranean and NE Atlantic

Although sea-dumping of chemical weapons already started after WW1, the main dumping operations were carried out after WW2. In total over 140 munition dumpsites (of which 30 involve chemical war material) have been reported in the North Sea and Northeast Atlantic (OSPAR 2005) (Figure 4.2). Yet it seems likely that this list is not complete (for instance Portugal has not yet reported to OSPAR). In this thesis we will mainly focus on the chemical munition dumpsites. The dumpsites located in the Skagerrak Strait will be discussed in §4.2 (Baltic Sea).

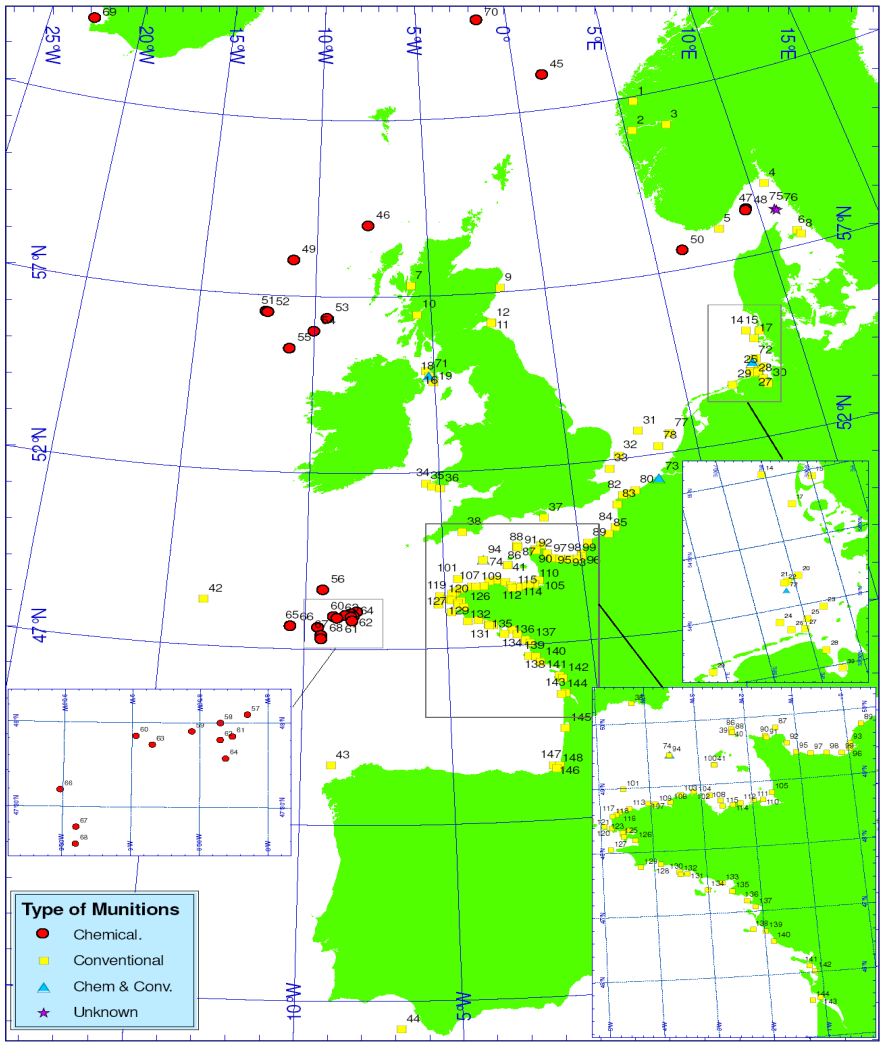

Figure 4.2 *Location of conventional and chemical munition dumpsites in the North Sea and NE Atlantic (after OSPAR 2005). Chemical munition dumpsites are marked in red. Conventional munition dumpsites are marked in yellow.*

Large quantities of conventional war material, and to lesser extent chemical weapons, were dumped off the German coast after WW2 (some chemical weapons are known to have been dumped already after WW1 near Helgoland) (Nehring 2005). The total amount of dumped war material is estimated at roughly 1.5 million tons, spread over 16 dumpsites ranging from the Wadden Sea to the North Friesian islands (Rapsch & Fischer 2000, Nehring 2005). Many of these dumpsites are located in very shallow water, in some cases even surfacing at low tide. In the fifties and sixties between 250,000 and 300,000 tons of dumped munition were recovered for recycling purposes (Figure 4.3), a result of increased demands for steel production (an estimated 50,000 tons was dumped again) (Nehring 2005). In 1964, 462 Tabun shells were recovered from Wolgast harbour (former GDR), set in concrete blocks and dumped in the Norwegian Sea (BSH 1993).

After WW2 the UK conducted extensive dumping operations in the NE Atlantic to dispose of its stockpile of chemical weapons as well as captured German war material (Beddington & Kinloch 2005). Between 1945 and 1956 at least 100,000 tons of CW (this is a conservative estimate) were dumped on different locations in the NE end of the Atlantic Deep, west of the Hebrides, and west of Northern Ireland (a.o. operation "Sandcastle", where three ships loaded with 68,000 tons of Tabun shells were sunk off Northern Ireland) (Beddington & Kinloch 2005).

Figure 4.3 *Munition recovery in the North Sea using electro-magnets (left) and large grab (right) (Rapsch & Fischer 2000).*

In the Irish Sea over 1.2 million tons (according to some sources up to 2 million tons) of chemical and conventional weapons have been dumped since 1945, possibly from as early as 1920 (SOAEFD 1996, Hart 2000). The weapons were dumped in a 200 to 300 m deep trench between Scotland and Northern Ireland called Beaufort Dyke and consists mainly of artillery rockets filled with phosgene gas. Most likely also small quantities of low and intermediate radioactive waste were dumped in the fifties. The last dumping operation probably took place in 1976. A detailed survey undertaken in the mid-nineties showed that large quantities of war material were dumped outside the charted dumpsite area (SOAEFD 1996).

In the North Sea offshore Norway and Scotland the US authorities sunk two vessels containing 4500 tons of unspecified German CW in 1948, in water depths over 1000 m (HRRT 2001). This dumping was part of the operation "Davey Jones Locker" during which also 9 other vessels were dumped in the Skagerrak Strait (see §4.3.2) (HRRT 2001). Further south, between the Doggerbank and Fladengrund, twelve ships loaded with mustard gas were sunk after WW2 (Kulturtechnik 1990).

In Belgium an estimated 35,000 tons of war material were dumped after WW1 on a shallow sand flat one mile off the coast (so-called “Paardenmarkt”), in water depths less than 6 m. One third of the dumped munition is believed to contain chemical warfare agents, for the most part Clark and mustard gas (Missiaen et al. 2001). The war material is nowadays completely covered under a few meters of fine-grained sediments. A detailed study of this dumpsite is presented in chapter 5.

After WW2 the Soviet authorities have dumped large amounts of chemical weapons in the arctic seas. On this subject there is hardly any official information. According to an American study a maximum of approximately 115,000 tons of mustard gas and Lewisite were dumped into the White Sea, the Barents Sea and Kara Sea (MEDEA 1997). In addition, a maximum of 32,000 tons of Tabun and Sarin is estimated to have been dumped in these seas. In total 5 potential dumpsites have been identified in the area (MEDEA 1997).

Little official information is available regarding possible chemical munition dumpsites off the French coast. Unofficial sources report the clearing of stocks of WW1 ammunition, a.o. at the mouth of the Somme river, where war material was dumped in big pits at low tide and brought to explode at high tide. According to Laurin (1997) at least 3 vessels loaded with chemical weapons were sunk by the Allies in the Bay of Biscay after WW2. For many years large amounts of chemical (and also nuclear) material have been dumped there by different countries. In 1960, Tabun shells recovered from the Little Belt in the Baltic Sea were set in concrete and dumped in the Bay of Biscay (BSH 1993, Glasby 1997).

A large amount of chemical weapons were dumped by the US in 1945 and 1946 in the Mediterranean and Adriatic Sea. The majority of the dumped material came from Allied Forces arsenals in southern Italy (ICRAM 2006). Offshore St. Raphael (southern France) 1700 mustard gas bombs and 1700 Lewisite bombs were dumped (HRRT 2001). Offshore Naples (Italy) an unknown quantity of mustard gas shells, phosgene and cyanide bombs, and drums filled with mustard gas were dumped (HRRT 2001, ICRAM 2006).

During WW2, both the Germans and Allied Forces dumped CW (mainly filled with mustard gas and phosgene) in the southern Adriatic Sea (ICRAM 2006). Two official dumping areas have been located, in water depths of resp. 1000 m and 300-500 m. In 1943 the American vessel SS J. Harvey, loaded with 2000 mustard gas bombs, was sunk in the port of Bari during a German air raid (HRRT 2001). Two years later the SS C. Henderson was also sunk here after an accidental explosion, carrying with it 800 bombs mainly filled with mustard gas (ICRAM 2006). From 1947 to 1953 recovery operations were carried out, mainly in the port of Bari (Figure 4.4) but also in other Apulian ports (the main part of this recovered warfare was dumped again). In 2005 the Italian navy recovered 150 WW1 mustard gas munitions filled from Monfalcone harbour, in the northern Adriatic (ICRAM 2006).

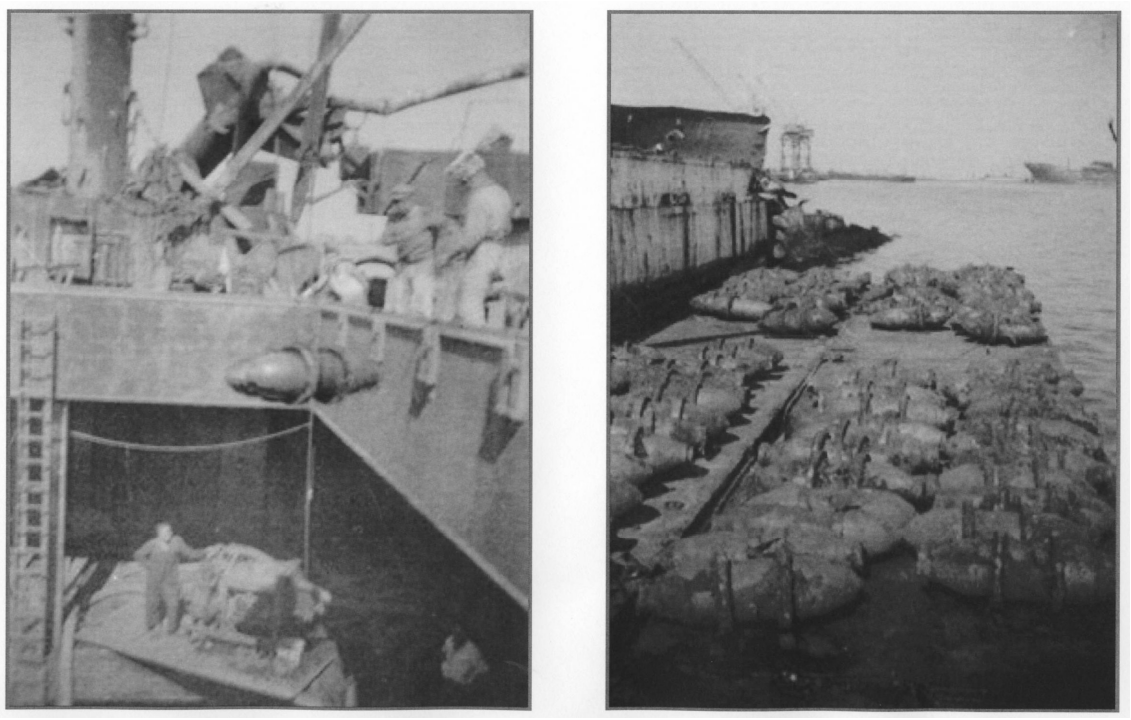

Figure 4.4 *Left: Salvage of mustard gas bombs from the hull of SS Charles Henderson in the port of Bari. Right: Stocking recovered bombs in Bari harbour, ready for dumping (after ICRAM 2006).*

4.3.2 Baltic Sea and Skagerrak

By far the largest part of the CW captured on German territory were dumped in the Baltic Sea and Skagerrak Strait on the orders of the British, Russian and American occupation authorities (Stock 1996) (Figure 4.5). Over 170,000 tons of chemical weapons were dumped in the Skagerrak (BSH 1993, Stock 1996). The main dumpsite is located in the Norwegian trench, south of Arendal (location 1 on Figure 4.5), where two large dumping operations were carried out right after WW2 in water depths ranging roughly from 600 m to over 700 m (Figure 4.6). The first dumping operation was carried out by the British authorities in 1945. In total 30 ships were sunk containing over 120,000 tons of CW, mainly filled with mustard gas, arsenic, nerve agents and blood agents (HELCOM 1993a). The second dumping operation took place in 1945-1946 under orders of the American occupation force. In total 9 ships containing over 30,000 tons of unspecified German CW were sunk in the area, as part of the operation "Davey Jones Locker" (HRRT 2001).

Offshore the Swedish coast a large number of ships filled with CW were sunk after WW2. According to Swedish reports between 1945 and 1947, possibly up to 1948, nine ships were sunk 25 miles west of Måseskaer by the British and American* authorities (location 2 on Figure 4.5) (HELCOM 1994, Granbom 1996). The quantity of CW was estimated to be at least 20,000 tons (according to Laurin (1997) up to 50,000 tons) containing a.o. mustard gas (HELCOM 1993b). According to British reports two additional ships with an unknown quantity of CW on board were sunk in the area by the British authorities in 1946-1947 (HELCOM 1993a).
(American reports only mention one dumping operation. According to HRRT (2001) over 116,000 tons of CW containing mustard gas, phosgene, Sarin, CAP and Adamsite were dumped in 1945)*

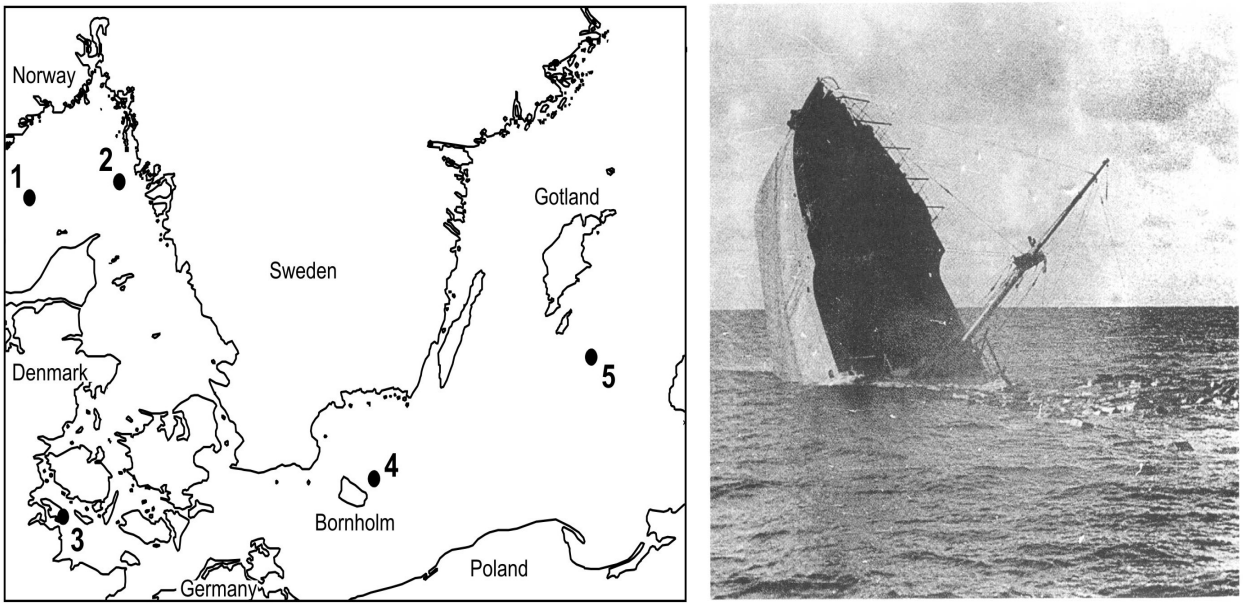

Figure 4.5 *Left: Location of the main chemical munition dumpsites in the Baltic Sea and Skagerrak (red dots). (1) Arendal; (2) Måseskaer; (3) Lille Belt; (4) Bornholm; (5) Gotland (HELCOM 1994, Stock 1996). Right: Sinking of a vessel loaded with chemical weapons off the Norwegian coast (Rapsch & Fischer 2000).*

In the southern Baltic at least 50,000 tons of chemical weapons were dumped (HELCOM 1994). Most of the munition was thrown over the side of the ship. The largest dumpsite is located east of the island of Bornholm (location 4 on Figure 4.5) where over 350,000 tons of CW (containing an estimated 13,000 tons of toxic agents) were dumped by the Soviet authorities. A detailed study of this dumpsite is presented in chapter 6. A second dumpsite is located in the Little Belt (location 3 on Figure 4.5) where 2 ships loaded with 69,000 Tabun shells and 5000 tons of phosgene and nerve gas shells were dumped by the German Wehrmacht in 1945 (in 1959-1960 most of the Tabun shells were recovered and dumped in the Bay of Biscay (BSH 1993)). A third dumpsite is located in the southern Gotland Basin (location 5 on Figure 4.5), where over 2000 tons of CW (total quantity of chemical agents < 500 tons) were dumped by the Soviet authorities (BSH 1993). There are also strong indications that part of the munition was thrown over board during transport to the different Baltic dumpsites (BSH 1993, Schultz-Ohlberg 2001). Witness reports also mention two additional dumping operations southwest of Bornholm in 1946 (4 ships with 15,000 tons of CW) and 1956 (4 ships with 50 tons of CW) (BSH 1993). Unconfirmed reports also claim the dumping of 8,000 tons of CW east of Bornholm (HELCOM 1994). However none of these dumping operations have been confirmed from other sources.

4.3.3 Dumping operations outside Europe

Dumping of CW in the US already started during WW2, when mustard gas shells and bombs were dumped offshore South Carolina and Virginia. Between 1945 and 1970 the US authorities dumped at least 100,000 tons of CW (containing mustard gas, Lewisite, arsenic, phosgene, cyanide and nerve agents) offshore California, Alaska, New Jersey, Virginia, South Carolina, and in the Gulf of Mexico (Figure 4.7) (MEDEA 1997, HRRT 2001, Bearden 2007). Up to 1966

the CW was mainly dumped loose over board. During the last four dumping operations between 1967 and 1970 the CW was sunk in the hull of vessels, as part of the operation "CHASE" (acronym for "Cut Holes And Sink Em") (HRRT 2001, Bearden 2007).

Figure 4.7 *Dumping of mustard gas containers off the coast of New Jersey in 1964 (Photo U.S. Army).*

Official records of dumping operations offshore Canada are very scarce. The existence of two chemical weapons disposal sites and several conventional munition disposal sites have been confirmed by the Canadian Department of National Defence (DND 2004). During one dumping operation in 1946 over 10,000 barrels of mustard gas were dumped roughly 300 km off Halifax.

Around Japan some 4900 tons of CW agents (mainly mustard gas, Lewisite and chlorine) were dumped by the US occupation forces in 1945-1946 (Kurata 1980, HRRT 2001). It is believed that also the Japanese Imperial Army dumped CW on a regular basis (MEDEA 1997). Eight dumping areas have been identified, many of which are located close to the shore. During and after WW2 the US authorities also dumped large quantities of chemical weapons offshore Pakistan (mustard gas bombs, unknown quantity), the Philippines (mustard gas bombs, phosphorus shells), Hawaii (61,000 mustard gas bombs and shells, 1000 mustard gas containers, 190 Lewisite containers, chloride and cyanide bombs, 4200 tons of hydrogen cyanide), and New Caledonia (unidentified CW) (HRRT 2001). In the Bay of Bengal a large amount of CW was dumped by the US in 1945. The dumped war material included 65,000 mustard gas bombs as well as chloride and phosgene bombs, and containers filled with mustard gas and Lewisite (HRRT 2001).

At the end of WW2 at least 21,000 tons of chemical warfare agents (mainly phosgene and mustard gas, contained in aircraft bombs and steel drums) were dumped along Australia's east and south coast by the US Army and the defence forces of Australia (Plunkett 2003). Four different dumping locations have been recorded offshore Sydney, Brisbane, Townsville and Victoria. In 1965 and 1970 two ad-hoc dumping operations were carried out in Australian waters (Plunkett 2003).

4.4 Accidents

Over the last 60 years a large number of accidents related to sea-dumped CW have been reported from different areas including the Baltic Sea, North Sea, Adriatic Sea, and the Sea of Japan. Most accidents involved fishing crews. In some cases complete lumps of mustard gas were fished up, often resulting in serious burning wounds (Figure 4.8). These accidents are partly due to the fact that dumping was often carried out in relatively shallow coastal waters and active fishing areas. But even the deep dumping areas (water depths > 200 m), which were considered as relatively "safe" zones at the time of dumping, are no longer free from human activity, as trawlers nowadays work in depths up to 1500 meters (Plunkett 2003).

Figure 4.8 *Left: Lump of mustard gas caught by fishermen near Gotland. Right: Baltic fisherman with a relatively fresh mustard agent injury.*

Most accidents were reported by Danish fishermen in the Baltic Sea (450 since 1976) (Theobald 2001). This is most likely related to the policy in Denmark that compensates fishermen for each shell that is recovered and brought onshore (HELCOM 1994, Laurin 1997). Table 4.1 gives an overview of the CW caught and registered by Denmark east of Bornholm during the period 1985-1992 (HELCOM 1993c). Between 1995 and 2005 in total 98 incidents were recorded, amounting up to 16,650 kg of chemical warfare agents. During the last decade on average 10 incidents have been reported each year to the Danish Navy (2003 was an exception with 25 catches) amounting to over one ton of toxic agents. The caught war material mostly involves heavily corroded mustard gas shells, the weight of the chemical warfare agent varying from 0.5 kg to 130 kg (HELCOM 2005).

Fishermen from other nations bordering the Helsinki Convention Area are not obliged to notify the authorities of such findings, and therefore only incomplete figures exist on finds by fishermen from other countries (HELCOM 1996). Germany has reported 13 fishing incidents east of Bornholm, without major fatalities (BSF 1993). Since 1980 Sweden has reported six incidents involving mustard gas and Clark from the area east of Bornholm (HELCOM 1993d, HELCOM 2003) and four fishing incidents in the Gotland basin involving mustard gas, Clark and chloroacetophenone (CAP) (HELCOM 1993b).

Year	Number of "catches"	CW mass (kg)	CW agent (kg)
1985	46	2695	585
1986	41	1830	370
1987	14	582	175
1988	19	1044	115
1989	42	1966	120
1990	19	979	182
1991	103	5378	269
1992	58	2597	100
Total	342	17072	1917

Table 4.1 *Total numbers and weight of chemical weapons, and weight of chemical warfare agents, caught east of Bornholm and registered by Denmark in the period 1985-1992 (HELCOM 1993c).*

Lithuania has reported several accidents involving caught chemical munition in the Gotland Basin. In 1986 fishermen were hospitalized after contact with a mustard gas bomb (HELCOM 1993e). Latvia reported several incidents with chemical munitions from the fifties up to the seventies, and occasionally later (HELCOM 1993f). Chemical weapons were also reported by Polish fishermen. Judged from their location it most likely concerns munition that was thrown over board during transport to the dumping area in the Gotland Basin (HELCOM 1993g, Andrulewicz 1996).

In Germany munition is washed ashore more or less regularly, particularly after winter storms, on the beaches of Mecklenburg-Vorpommern along the Baltic Sea. In 1997, 1600 shells and 20 tons of CW agents were washed ashore (HELCOM 1993g). Also along the North Sea coast munition has washed ashore on various occasions, e.g. in Kiel Bay where phosphorus shells were found on the beach (Nehring 2005). In Italy, a large number of CW-related incidents have been recorded in the southern Adriatic Sea since 1946. The largest number of incidents was reported in the period 1951-1955 (67 injuries). Over the years the number of incidents has been steadily decreasing (ICRAM 2006).

In Australia only two accidental recoveries of CW by trawlers have been recorded since WW2 (in 1970 and 1983, each involving 1 ton cylinders of mustard gas). Most likely this low number is due to the fact that the bulk of the war material was dumped away from fishing areas (Plunkett 2003). In Japan this was not the case and many accidents have been recorded from fishing areas around Japan – at one dumping site alone 52 people were wounded in eleven accidents (Kurata 1980, Plunkett 2003). Since 1972, when information was released regarding the Japanese dumping sites, there have been no recorded casualties from accidents in Japanese waters.

Numerous incidents have also been reported related to the washing ashore of shells. In the nineteen nineties thousands of small toxic explosive devices were washed up on the beaches of Northern Ireland and Scotland's west coast (a.o. near Mull, Oban, and Arran) (SOAEFD 1996). The munition had most likely become dislodged as a result of pipe laying activities close to the Beaufort Dyke dumpsite. Some people were badly injured when bombs they picked up on the beach ignited. Seismological investigations in the surrounding area have furthermore revealed a

large number of underwater explosions over the years, possibly due to spontaneous detonation of dumped conventional weapons (Ford et al. 2005, Beddington & Kinloch 2005).

4.5 Past and present dumpsite research

In spite of the often alarming reports, up to now surprisingly few thorough investigations have been carried out at the known chemical munition dumpsites. In the beginning of the nineties expert groups in Denmark, Sweden and Germany prepared several national reports on dumpsites in the Baltic Sea (e.g. HELCOM 1993h & 1993b, BSF 1993, HELCOM 1994). In addition, an ad-hoc working group was set up by the Helcom Commission (HELCOM CHEMU) which deals with the problem of dumped munition in the Baltic countries. The main purpose was to compile the information on the locations, quantities and types of dumped CW in the Baltic Sea and to make recommendations for further action. In recent years an increasing number of dumpsite investigations have been carried out in various countries including the UK, Canada, Norway, Italy, and Hawaii (SOAEFD 1996, Rodacy et al. 2001, Tørnes et al. 2002, ICRAM 2006, Decarlo et al. 2007).

Up to now most of the field research in dumpsite areas has been focused on screening of seabed sediments and water samples for toxic substances. In many cases the sampling sites were more or less picked at random, especially if the munition was buried. Screening was often done for only a few chemical warfare agents, thereby overlooking the possible presence of other toxic warfare agents or explosive-related toxic compounds (e.g. Fonnum 1989, HELCOM 1993b). Toxicity studies have mainly paid attention to the stability of chemical warfare agents under laboratory conditions (e.g. Muribi 1997, Waleij et al. 2001, ICRAM 2006). Still, the marine ecosystem is not comparable with the laboratory environment, due to its varying biological and physico-chemical parameters which will influence the degradability of chemical warfare agents. Furthermore little is known about the dynamic behaviour of sediments and water movements that may affect the fate of toxic compounds, their environmental impact and possible bioaccumulation in fauna and flora.

Over the last years several countries have carried out geophysical and hydrodynamical monitoring investigations (e.g. Emelyanov et al. 2000, Schulz & Ohlberg 2001, Paka & Spridonov 2001, Tørnes et al. 2002). Nevertheless the available information remains very scattered and large gaps remain in our understanding of the dumpsites. Notwithstanding this lack of detailed information most countries conclude that CW dumpsites do pose an immediate danger to the marine environment and recommend that the dumpsites be left undisturbed. These conclusions seem somewhat premature in view of the many uncertainties that still remain. Up to now only a few major recovery operations were carried out in Europe, a.o. in the Lille Belt (HELCOM 1996), in the German Wadden Sea (Rapsch & Fischer 2000), and in the southern Adriatic (ICRAM 2006). Although it is believed that recovery of dumped munition is in some cases technically feasible, there are serious concerns about the high risks involved both for salvage crews and for the marine environment (Missiaen et al. 2001).

4.6 Geophysical dumpsite investigations

One of the major difficulties in managing the risk associated with CW dumpsites is the uncertainty associated with their location. Indeed little is known about the exact location and distribution of the dumped munition. This is partly due to the lack of official records of the dumping operations, which often took place in chaotic circumstances right after the war. Positioning accuracy at the time of dumping was very limited, and crews paid to dispose of

ordnance often ignored instructions to dump it at certain locations because they wanted to return to port as quickly as possible to get the next load. Trawling activities have most likely further spread the dumped war material over large areas.

In many cases the dumped munition is no longer exposed on the seafloor but has become buried under a cover of recent sediments, making "fast" tracking methods such as side-scan sonar or multibeam imaging of little use. As a result a correct estimation of the amount of dumped war material and their exact distribution is still lacking in most cases. Yet this information is crucial in order to carry out a reliable risk assessment of the dumpsite. A first important step in any dumpsite research should therefore focus on mapping the precise location and distribution of the dumped war material including the burial depth. Highly detailed imaging of the internal structure of the dumpsite should furthermore allow to obtain important information on the sedimentary environment (e.g. erosion/deposition processes, features influencing the migration of toxic compounds) and possibly also the type of dumped weapons.

Recent experience in dumpsite research, with a focus on seismic investigations, will be discussed in the light of two case studies from the North Sea and the Baltic Sea. The first study concerns the so-called "Paardenmarkt", an old WW1 dumpsite just off the Belgian coast. An estimated 35,000 tons of munition were dumped here, one third of which is believed to be toxic. Over the years this dumpsite has been the subject of a number of integrated geophysical studies. Although the munition is nowadays completely covered by sediments the close proximity to the coast makes focused research and regular monitoring an absolute necessity.

The second study concerns the Bornholm Basin dumpsite which is the focus of ongoing research in the EC-FP6 project "MERCW". After WW2 over 32,000 tons of chemical weapons were dumped here. Over the years a large number of accidents have been reported in the area when shells and bombs filled with mustard gas were caught in fishing nets. Focused geophysical site investigations should yield a reliable assessment of the dumped weapons and the ecological risks for the marine environment.

CHAPTER 5
THE PAARDENMARKT DUMPSITE CASE STUDY

5.1 Introduction

After WW1 large amounts of war material including chemical munition were dumped on a shallow sand flat called "Paardenmarkt" offshore the Belgian coast, east of the port of Zeebrugge. The dumpsite extends over roughly 3 km^2, its southernmost limit is located one km offshore from the sandy beaches of Knokke-Heist (Figure 5.1). The sand flat forms part of a shoal extending from the harbour of Zeebrugge to the Belgian-Dutch border where the coastline merges into the Westerschelde estuary.

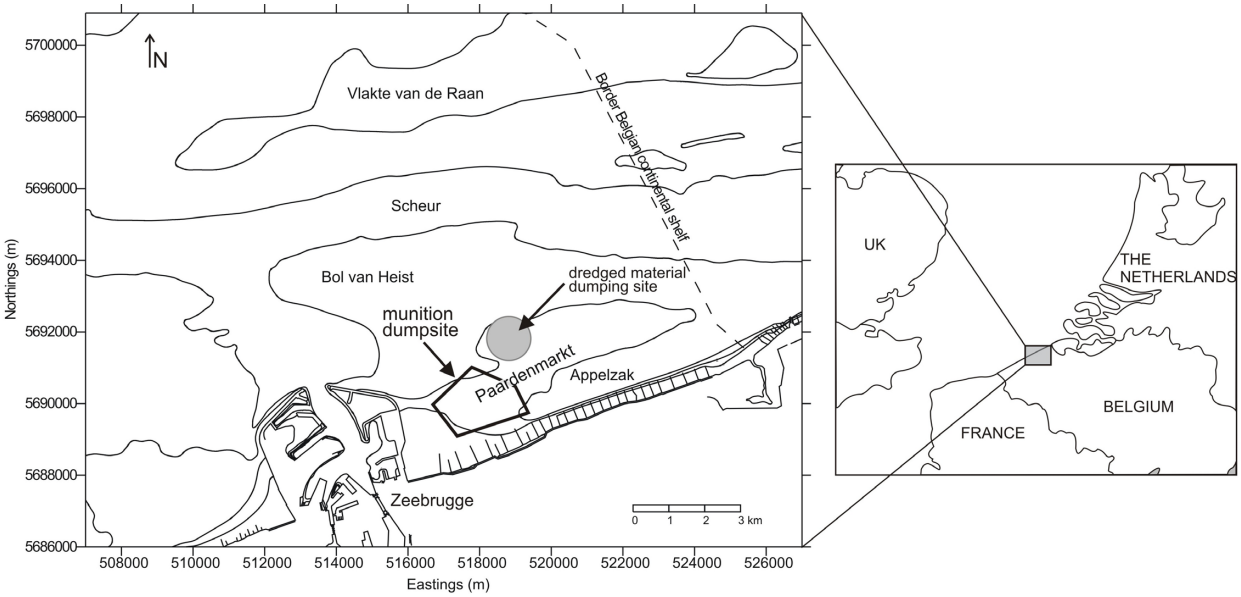

Figure 5.1 *Location of the Paardenmarkt sand flat offshore the Belgian coast. The munition dumpsite is marked by the black pentagon. The grey circle marks the dumping site for dredged material "Zeebrugge East". Coordinates in UTM- ED50.*

Over the years a number of geophysical studies have been carried out at the Paardenmarkt dumpsite (Tijdelijke Vereniging Bergingswerken 1989a/b, Henriet & Winthagen 1996a/b, G-Tec 1996 & 2005, Magelas 1996, Missiaen et al. 2002a/c, Magelas 2003, Henriet & Missiaen 2004 & 2005). This thesis will mainly focus on the seismic investigations. The main goal of these investigations was twofold: (1) to image the shallow internal structure of the dumpsite, and (2) the possible detection of buried munition (or clusters of munition). Detailed information on the shallow geology is crucial with regard to potential sediment displacement (causing resurfacing of the weapons), the possible migration pathways of toxic substances and the behaviour of munition shells (e.g. corrosion, sinking of munition into the sediment).

A first preliminary study, combining reflection seismic and magnetic measurements, was carried out in 1988 (Tijdelijke Vereniging Bergingswerken 1989a/b). Subsequent seismic studies were carried out in 1996 and 1997 (Henriet & Winthagen 1996a/b, Missiaen et al. 2002b). In 1998 a 3D seismic test survey was performed in the framework of the EU project "VHR3D" (Marsset et al. 2001). Between 1999 and 2001 a multi-disciplinary evaluation study was carried out,

focusing on the different geophysical, biological, ecological, geochemical and engineering aspects of the dumpsite. The results of this study were published in the OSTC report "Paardenmarkt site evaluation" (Missiaen et al. 2001). In 2005 combined 2D-3D seismic-electric trials were carried out (Henriet & Missiaen 2005). Most recently ultra-high resolution seismic investigations were carried out using a parametric echosounder.

5.2 Dumped munition

The total amount of dumped war material is estimated to be roughly 35,000 tons, for the most part German munition shells (Missiaen et al. 2001). The shells weigh up to 40 kg and have a length up to 55 cm (DOVO pers. comm.). German production numbers from WW1 suggest that roughly one third of the dumped munition is toxic, i.e. some 12,000 tons (gross weight) (Lheureux 1990). The toxic shells were filled with (di)phosgene, chloropicrin, Clark, and mustard gas (DOVO pers. comm.) According to their content they were referred to as blue, yellow or green cross shells (Figure 5.2). Mustard gas and Clark were widely employed during the later part of the war and it is assumed that these shells form the main part of the dumped toxic munition (Missiaen et al. 2001).

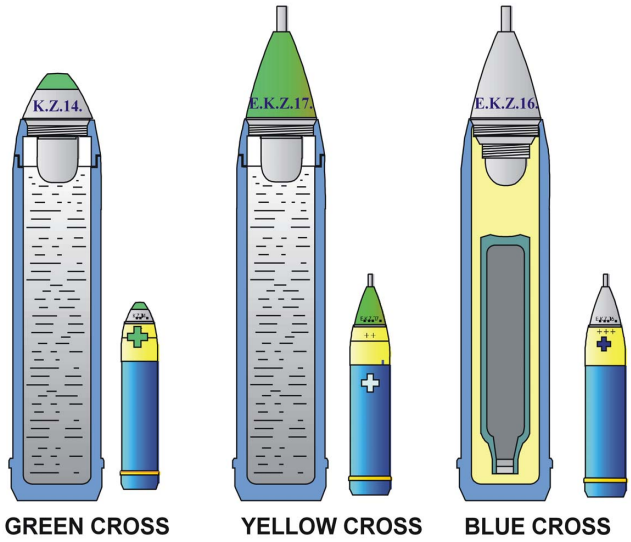

Figure 5.2 *German toxic munition from WW1. Green cross shells contain (di)phosgene or chloropicrin, yellow cross shells contain mustard gas, blue cross shells contain Clark. The latter differ from the other toxic shells in the fact that the toxic agent is stored in a glass bottle.*

Over the years the dumped munition was forgotten. During dredging operations in 1971 a number of large obstacles were encountered on the seafloor. These appeared to be elongated piles of munition (roughly 10 m long, 1-2 m high and up to a few m wide) often encrusted with sediment (Missiaen et al. 2001, 2002c). The shape reflects the storage compartment of the vessels used for dumping (so-called "klepbakschepen"). Diving operations in 1972 revealed the presence of munition shells exposed on the seafloor at 17 different locations (Figure 5.2). Three of these shells were toxic (Lurquin 1972). The dumpsite was subsequently marked on hydrographical maps as a rectangle with a total surface ±1.5 km^2 where anchorage and fishing are prohibited (Missiaen et al. 2001). Later magnetic investigations in 1988 resulted in an extension of the dumpsite area into a pentagon with a total surface of ±3 km^2 (Missiaen et al. 2001, 2002c) (Figure 5.3).

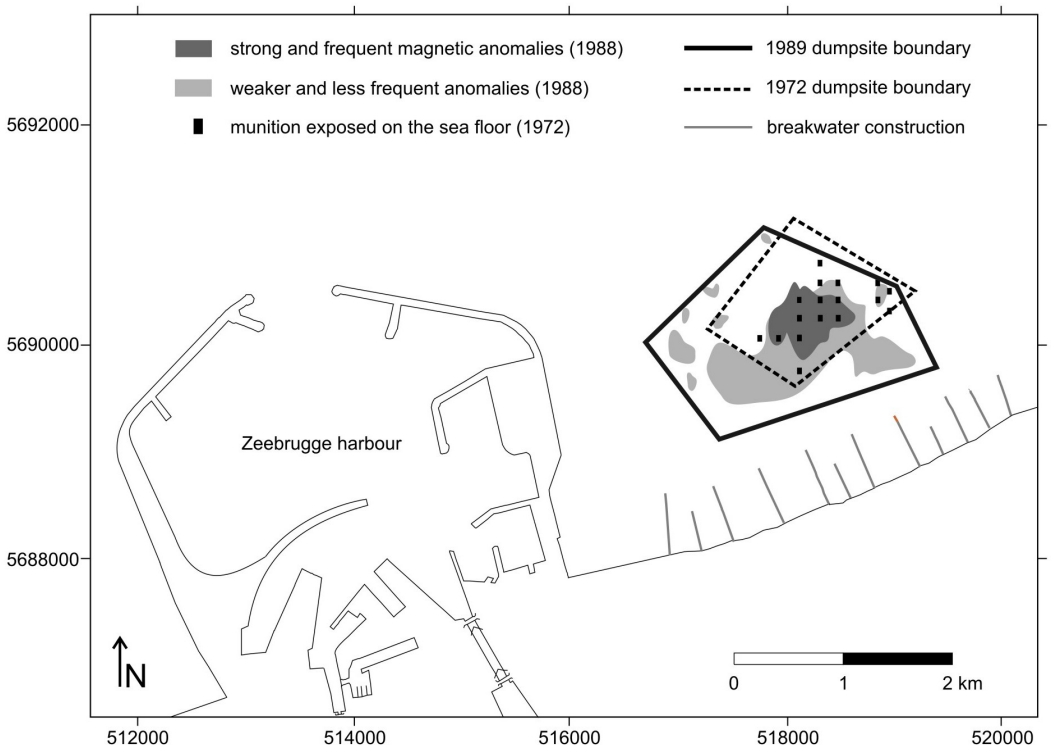

Figure 5.3 *First dumpsite boundary defined in 1972 (dashed rectangle) and final boundary defined in 1989 (full pentagon). Grey areas mark the magnetic anomaly zones observed in 1988. Black squares mark the munition shells found during diving operations in 1972. Coordinates in UTM-ED50 (Missiaen et al. 2001b).*

5.3 Natural setting

The Quaternary sequence in the dumpsite area is made up of reworked sediments resulting from the erosion of outcropping Paleogene clay and sand layers during the Pleistocene and Holocene. The exact thickness of the Quaternary sequence is estimated to be roughly 20 m (Missiaen et al. 2002b). Short vibracores taken near the dumpsite boundaries in the seventies indicate an alternation of fine to very fine sand and clay layers, often with a high mud content (Ministerie van Openbare Werken 1978). The recent hydrodynamic evolution of the area, a result of the harbour extension of Zeebrugge, has most likely altered this sedimentation pattern.

Seafloor sediments mainly consist of fine to very fine sands enriched with mud or clay (Magelas 1996, Charlet 2001). The muddy sediments are often covered with a thin veneer of sand (Magelas 1996). Recent sampling in 2002 and 2003 has shown a predominance of fine sand and sandy silt with increased mud content towards the south, and coarser sandy sediments towards the northeast (Verbeeck 2004). Most likely the surficial sediments are largely influenced by the nearby dumping ground of dredged material "Zeebrugge East" (see Figure 5.1). The dredged material is mainly a mixture of sand and mud (30% clay, 70% silt) (Malherbe 1991).

The seafloor in the dumpsite area gently slopes towards the northeast, ranging from 1.5 m (below MLLWL, mean lowest low water level) in the southwest to 5.5 m in the north (Figure 5.4). The bottom slope is slightly steeper in the southwest (0.15°) and decreases gradually towards the north (0.08°). The shallow area southwest of the dumpsite forms a sediment wedge.

Side-scan sonar data indicate a flat seafloor with local small-scale ripples (10-20 cm amplitude) (Magelas 1996). In the extreme southeast corner of the dumpsite a number of anomalies were observed which are most likely due to rock dumps related to the construction of nearby breakwaters (Magelas 1996).

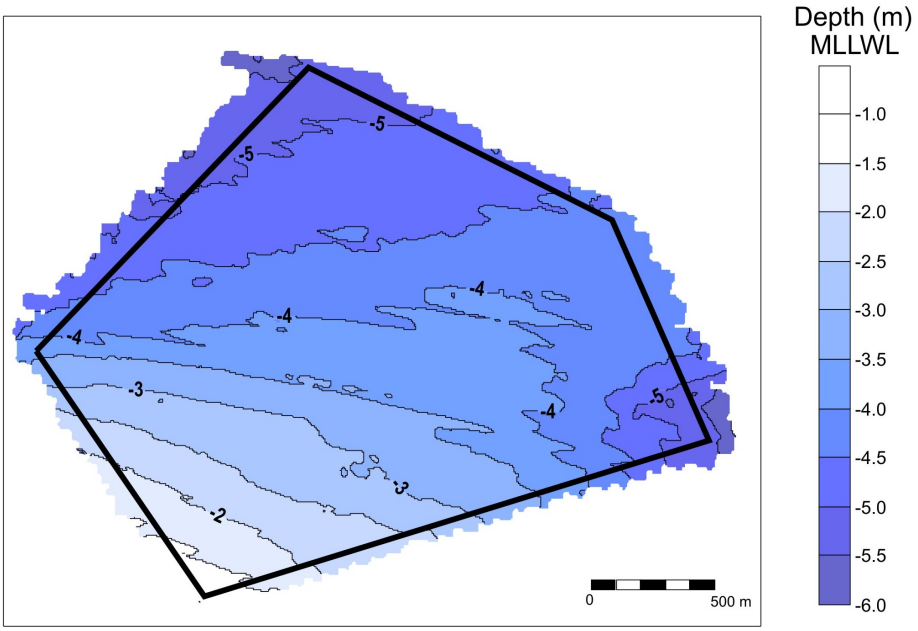

Figure 5.4 *Bathymetry of the dumpsite area based on soundings carried out in 2003 (after Magelas 2003). The black pentagon marks the dumpsite boundary. The seafloor gently slopes towards the northeast, ranging from 1.5 m in the southwest to 5.5 m in the north Depth values are in MLLWL (mean lowest low water level at spring tide).*

Between 1954 and 1976, prior to the extension of Zeebrugge harbour, periods of erosion alternated with accretion phases (Magelas 1996). Most likely this explains the exposed munition shells on the seafloor in 1972. Still the sediment volume in 1976 was nearly similar to that in 1954. Between 1976 and 1982 the area was subject to a pronounced sedimentation induced by the harbour extension (Magelas 1996). This also resulted in an erosion zone northwest of the dumpsite.

Between 1982 and 2003 accretion and erosion phases alternated, but the net thickness of the sediment layer increased. The accretion is most pronounced in the southwest corner (up to 4 m) and decreases gradually towards the north (0.5 m) (Figure 5.5-left) (Magelas 1996, 2003). Between 1996 and 2003 the dumpsite was subject to minor sedimentation, varying between 10 cm in the central and northern part and 70 cm in the southeast (Figure 5.5-right). Two small erosion zones (net erosion ± 10 cm) were observed in the southeast and in the north (Magelas 2003).

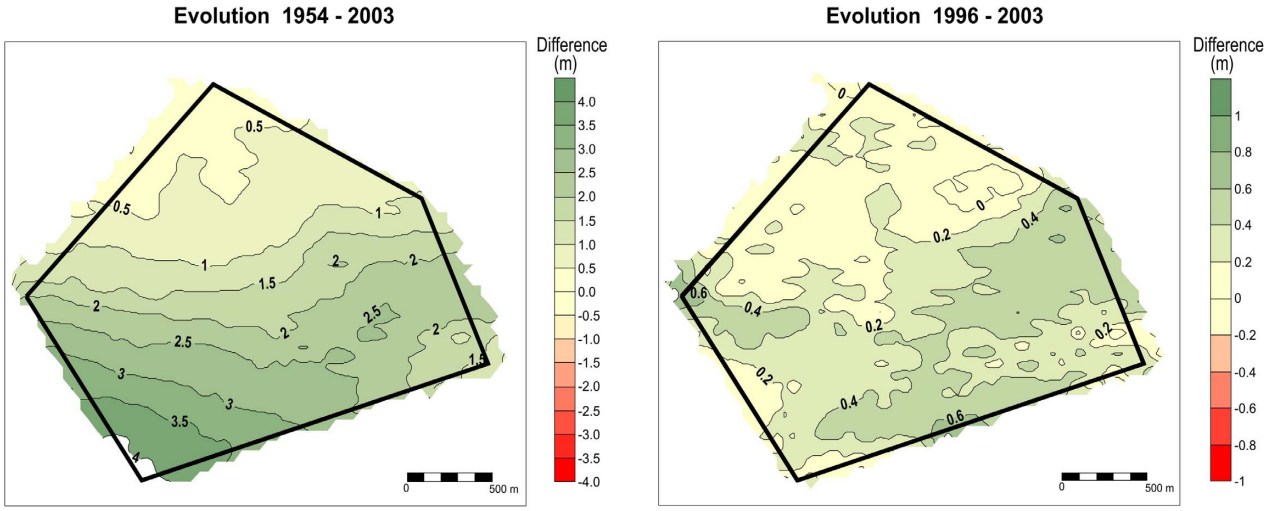

Figure 5.5 *Difference map between soundings carried out in 1954 & 2003 (left) and 1996 & 2003 (right). Green colours indicate accretion, red colours erosion (after Verbeeck 2004). Sediment accumulation is most pronounced in the south-west corner of the dumpsite. Since 1996 little sedimentation is observed.*

5.4 Magnetic investigations

A first magnetic reconnaissance survey was carried out in 1988. In total 100 profiles were recorded with a spacing of ±50 m (positioning accuracy ~18 m) (Tijdelijke Vereniging Bergingswerken 1989a). The results clearly showed two distinct zones: a central zone with numerous strong magnetic anomalies surrounded by a larger zone marked by less frequent and weaker anomalies (Figure 5.3). A second survey took place in 1996. In total 725 profiles were recorded (using a surface-towed system) with a spacing of 10-20 m (positioning accuracy 3-5 m) (G-Tec 1996). Detailed data were obtained from the central zone of the dumped material (Figure 5.6a left). The size of the anomalies suggests that they represent clusters of dumped munition rather than individual munition shells. Outside the central zone a number of smaller but still important anomalies were observed. It is possible that some of these are not related to munition but have a different origin (e.g. related to small ship wrecks or other steel objects). Measuring the magnetic field at two levels allowed to calculate the vertical magnetic gradient which provided more precise information about the exact location and lateral extent of the munition clusters (Figure 5.6a bottom right). These gradient data clearly show that the central dumpzone is marked by large anomaly-free zones. Depth estimations based on the vertical gradient data suggest that in the central zone the munition is buried by a few meters of sediment (G-Tec 1996).

In 2005 a third magnetic survey was carried out. The surveyed area, roughly 1 km x 200 m, largely coincides with the test area for combined seismic and geo-electric measurements (see §5.7). Roughly 30 profiles were recorded with a spacing of 2 to 10 m (G-Tec 2005). The array (consisting of two Caesium vapour magnetometers) was towed ~2 m above the seafloor. Positioning of the array was done using a USBL transducer mounted on the vessel resulting in a horizontal positioning precision of roughly 1 m (G-Tec 2005). The anomalies observed on the vertical magnetic gradient map show a high diversity in shape and form (linear, circular, pointlike, etc) (Figure 4.6b) which probably reflect the size and shape of the munition (individual or in clusters). Linear shaped anomalies can probably be linked to the elongated piles of munition observed by divers in 1971 (see §5.2). Depth estimations based on the new data indicate a burial depth of most objects between 2 and 6 m (G-Tec 2005).

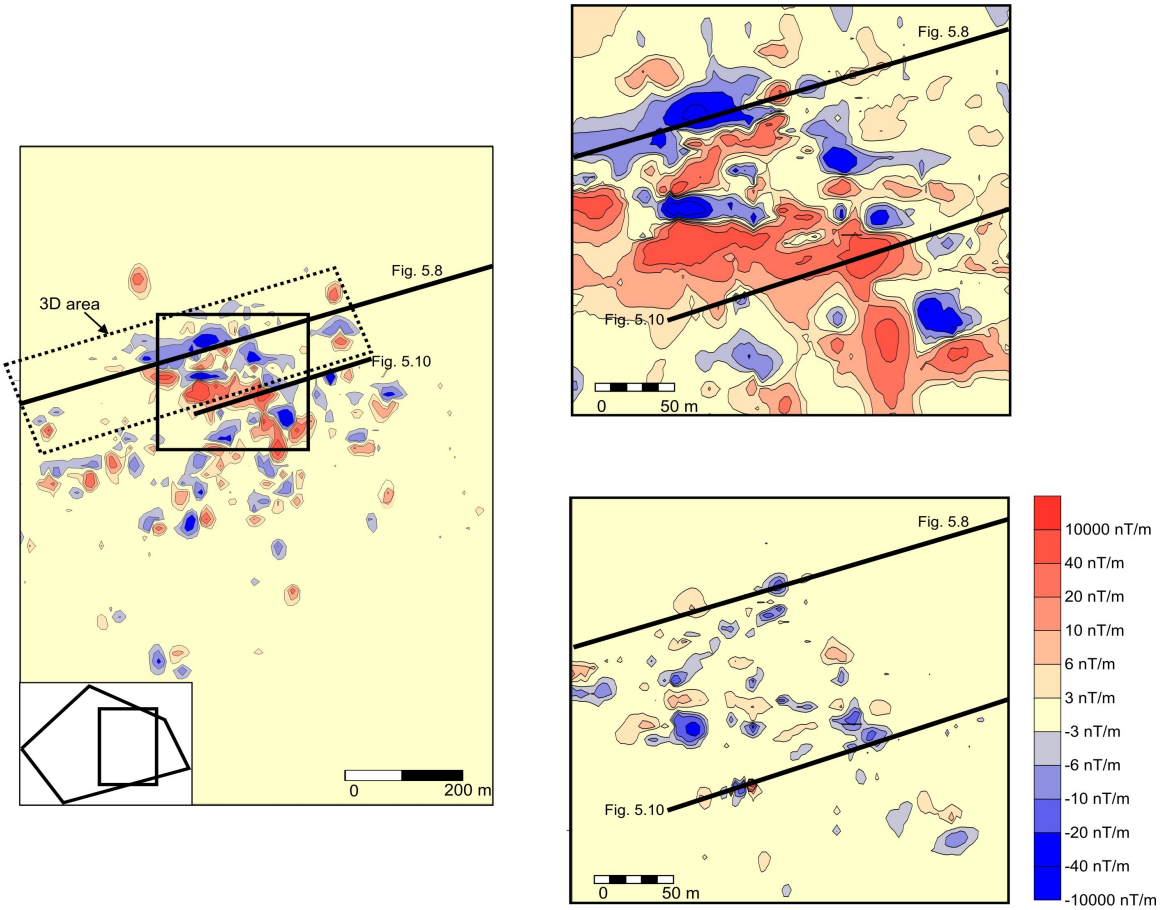

Figure 5.6a *Results of the 1996 magnetic survey in the dumpsite area (nT = nanoTesla) (after G-Tec 1996). Left: Magnetic anomaly map of the central dumpzone (the location is marked in the lower left corner; black pentagon = dumpsite boundary). The black rectangle marks the close-ups shown on the right. Thick black lines mark the seismic profiles shown in Figures 5.8 & 5.10. The dotted rectangle marks the 3D area shown in Figure 5.11. Top right: Close-up of the central part of the magnetic anomaly map. Bottom right: Vertical magnetic gradient map of the same close-up area. The anomalies are now clearly more constricted.*

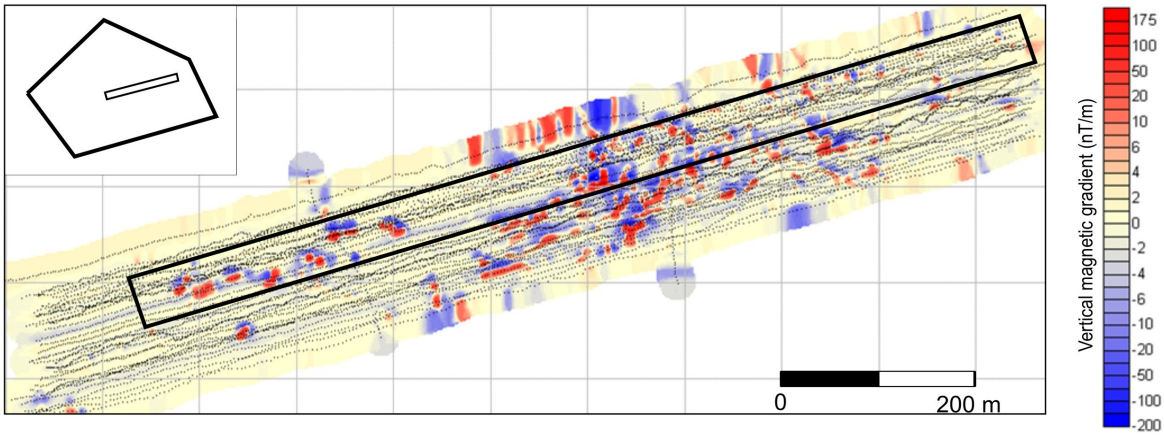

Figure 5.6b *Results of the 2005 magnetic survey in the dumpsite area (nT = nanoTesla) (after G-Tec 2005). Vertical magnetic gradient data were obtained over a small test area of roughly 1 km x 200 m. The location of the test area is shown in the upper left corner (black pentagon = dumpsite boundary). The black rectangle marks the location of the seismic-electric survey (see §5.7).*

5.5 2D seismic investigations

5.5.1 1996 seismic survey

A first extensive seismic survey took place in 1996. In total 70 profiles were recorded (spacing 25 to 200 m) using the Seistec boomer (Figure 5.7). The data were recorded using a Delph2 system (sampling frequency 12 kHz, shot interval 0.25 s). Positioning accuracy was ±5 m (Henriet & Winthagen 1996a). Due to stormy weather the recorded data were not of optimal quality. Data processing (including bandpass filter, agc, spiking deconvolution, swell filter) resulted in data improvement which allowed the identification of a number of shallow reflectors, but penetration remained limited due to the presence of shallow gas (see also chapter 8).

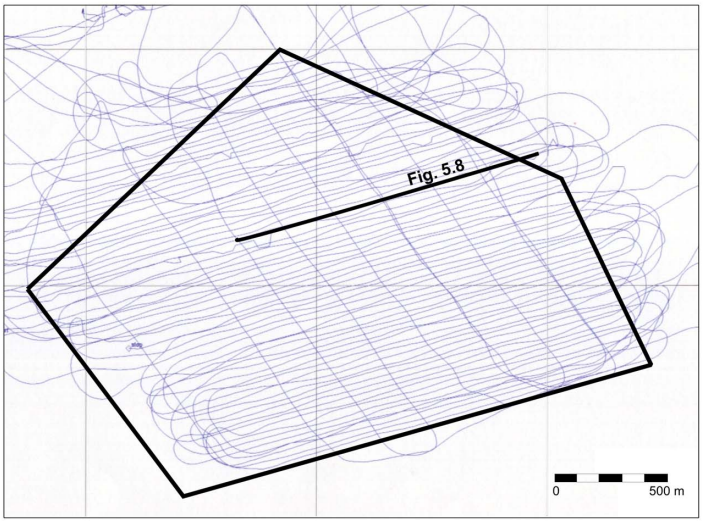

Figure 5.7 *Seismic network recorded at the dumpsite in 1996 (after Henriet & Winthagen 1996a). The black pentagon marks the dumpsite boundary. The thick black line marks the profile shown in Figure 5.8. For comparison with the magnetic/gradiometric data see Figure 5.6a.*

Figure 5.8 shows an example of a processed Seistec profile through the central dumpsite area. The shallowest continuous reflector marks a thin sediment cover with a thickness of ±1.5 m in the southwest and wedging out towards the northeast. Towards the east a deeper reflector is observed which gradually shallows. Both reflectors agree well with the recent sedimentation pattern marked by a pronounced increase in the southwest that gradually decreases towards the north-northeast. In addition to these shallow (semi-)continuous reflectors also a large number of short, discontinuous reflectors were locally observed (Henriet & Winthagen 1996a).

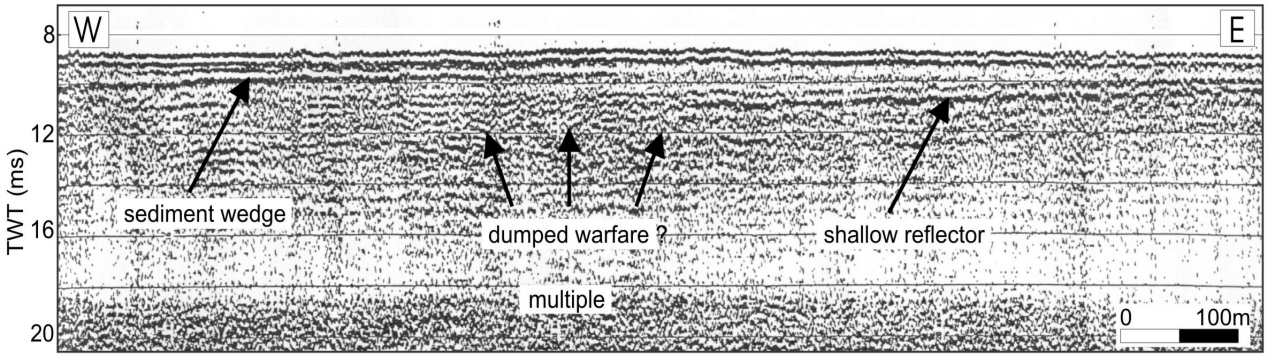

Figure 5.8 *Seistec boomer profile recorded in 1996 (after Henriet & Winthagen 1996a). For location see Figures 5.6a & 5.7. The thin sediment wedge and shallow reflector confirm the recent sedimentation pattern. Locally short discontinuous reflectors are observed. The diffraction clusters in the middle of the profile are possibly related to dumped munition.*

The seismic data are often marked by clusters of diffractions. These can possibly be related to dumped munition, most likely clusters of dumped munition since individual munition shells will probably be too small to allow clear acoustical detection. However, some relation to local gas accumulation or natural features (e.g. shell accumulations) cannot be excluded. As can be seen on the magnetic and gradient maps (see Figure 5.6a) profile 5.8 crosses through the central anomaly zone. The diffraction clusters observed in the middle correlate well with a large vertical gradient anomaly.

5.5.2 1997 seismic survey

A second seismic survey took place in 1997 in the framework of a shallow gas study in the Belgian coastal area (Missiaen et al. 2002b) (see also chapter 7). In total 30 profiles (spacing ±50 m) were recorded over the dumpsite using the Seistec boomer (Figure 5.9). Data recording was done with a Delph2 system (sampling frequency 20 kHz, shot interval 0.25 s). Positioning accuracy was 3-5 m. During the 1997 survey the RV Belgica ran briefly aground at the dumpsite. As a result the seismic network was slightly shifted to the N-NE (see Figure 5.9) to avoid too shallow water depths. Indeed the draught of the vessel (4.4 m) renders survey work in certain parts of the dumpsite very difficult and only feasible during highest water periods.

Similar to the 1996 data, the seismic profiles recorded in 1997 also show a limited penetration, most likely due to the presence of shallow gas. Figure 5.10 shows an example of a Seistec profile through the central dumpsite area. Most profiles were marked by a chaotic facies with discontinuous reflectors. Occasionally some deeper reflectors can be observed, probably due to a local decrease in gas content (Figure 5.10). As can be seen on the magnetic and gradient maps in Figure 5.6a the profile cuts through the central anomaly zone. The chaotic diffraction pattern observed on the west (left corner of the profile) is probably related to the presence of buried objects. Indeed the cluster of diffractions coincides with a large anomaly observed on the vertical magnetic gradient map (Figure 5.6a bottom right).

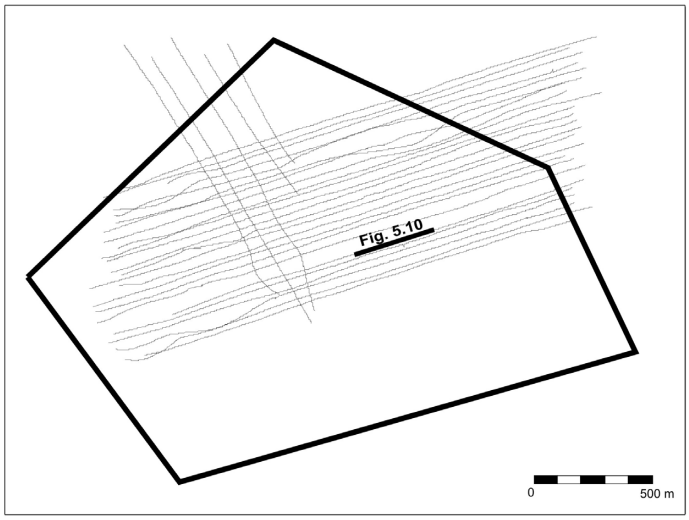

Figure 5.9 *Seismic network recorded at the dumpsite in 1997. The black pentagon marks the dumpsite boundary. The thick black line marks the profile shown in Figure 5.10. For comparison with the magnetic/ gradiometric data see Figure 5.6a.*

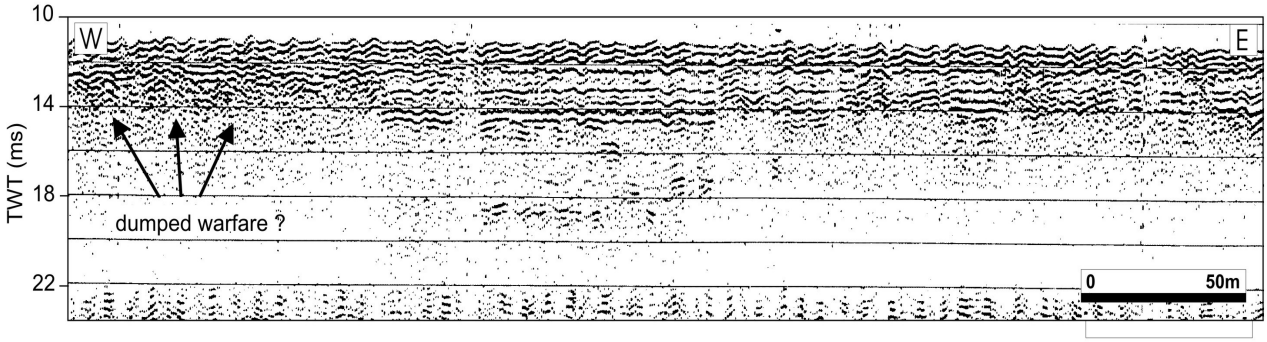

Figure 5.10 *Seistec boomer profile recorded in 1997. For location see Figures 5.6a & 5.9. Limited penetration is due to shallow gas. Locally some deeper short reflectors are observed. The diffraction clusters seen on the left seem to correspond with a large vertical gradient anomaly which suggests a relation to buried munition.*

5.6 3D seismic trials

5.6.1 Seismic acquisition

In 1998 a test survey was carried out on the Paardenmarkt dumpsite using the prototype 3D acquisition array (see chapter 2) (Figure 5.11-top). During the trials the modules were towed roughly 15 m behind the R/V Belgica. Offset between source and nearest receivers was ±7 m. In 1½ days time a network of 45 seismic lines was acquired with an average profile length of 600 m (Figure 5.11-bottom). Theoretical line spacing was set at 7 m, but due to wind, waves and strong currents the achieved line spacing varied between 5 m and 15 m. In order to reduce the noise level the vessel sailed on electrical propulsion.

The survey area was located in the central part of the dumpsite marked by strong magnetic anomalies (see Figure 5.6a). Due to the locally strong currents (especially at high tide) the seismic profiles were sailed along E-W lines roughly parallel to the main current direction. This avoided too strong side currents and helped to keep the 3D array well stretched behind the vessel. In order to avoid large stresses on the inflatable array the vessel was forced to take wide turns in between the profiles.

Positioning during the survey was done using a short-range DGPS system with the reference antenna set up nearby on the eastern harbour dam, theoretically allowing decimeter range accuracy. The positioning antenna was mounted on the rear of the central RIB, as close as possible to both streamers and source. Absolute antenna positions in (x,y) were stored every second. Due to recording difficulties the precision of the positioning data turned out to be very low. Final accuracy was roughly one meter (depending on the profile orientation) which resulted in very irregular and “jumpy” positioning data.

The seismic data were recorded using an Elics Delph24 system (shot interval 0.75 s, sampling rate 16 kHz, record length 50 ms). The total recorded data volume amounted to roughly 2.2 Gbytes. As was the case for the 1996 and 1997 data now the penetration of the seismic profiles was also severely limited due to the presence of shallow gas.

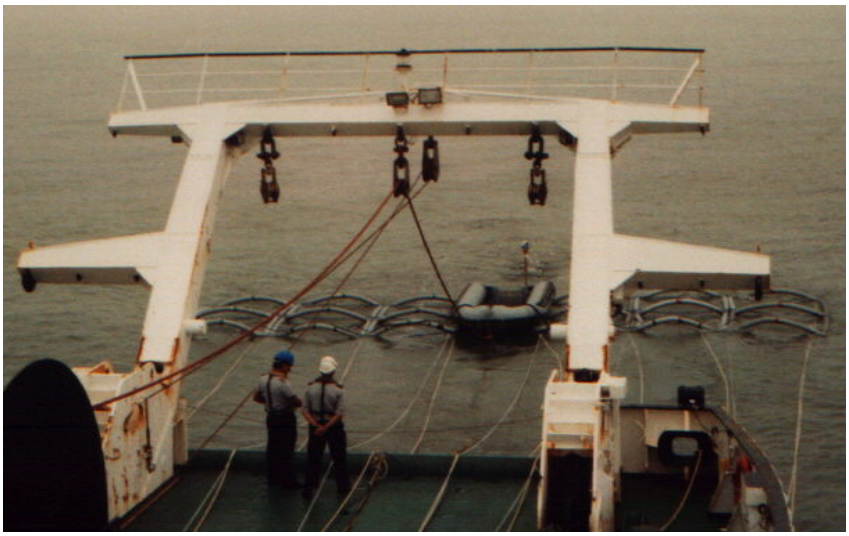

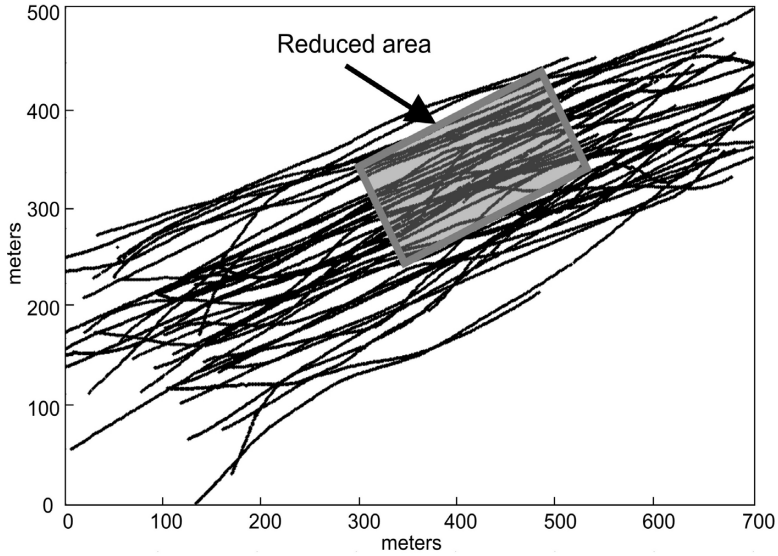

Figure 5.11 *Top: Inflatable acquisition array (prototype) used for the 3D seismic measurements at the Paarden-markt dumpsite. Bottom: 3D seismic network recorded at the munition dumpsite (for location see Figure 5.6a). The grey rectangle marks the reduced area for 3D processing.*

5.6.2 Geometry processing

In a first step corrections were carried out on the raw navigation data. For each shot the positioning data were interpolated and smoothed, taking into account the vessel's heading. Occasional spikes were filtered. The network of antenna positions was rotated and reduced to a 200 x 100 m area covering the central part of the 3D survey area (see Figure 5.11), resulting in a data volume of roughly 0.8 Gbyte. Profiles of inferior data quality were also left out.

Theoretical source and receiver positions were calculated from the antenna positions on the RIB, taking into account the heading and speed, and assuming a rigid array (since the array was well aligned this seemed a reasonable assumption). The distribution of the source and receiver positions in the reduced area is shown in Figure 5.12. The network was finally binned with different grid bin sizes (0.5x0.5 m, 1x1 m, 2x2 m). Due to the irregular navigation pattern (a result of wave action and strong currents) the fold coverage was not uniform over the survey area. The 0.5x0.5 m bin fold coverage was in general very low with a large amount of empty bins, and this bin size was therefore abandoned. Coverage for both the 1x1 m and 2x2 m grid was much higher with only occasional empty bins (Figure 5.13). In order to allow the best possible resolution while still assuring sufficient coverage a bin size of 1x1 m was chosen for the stack procedure.

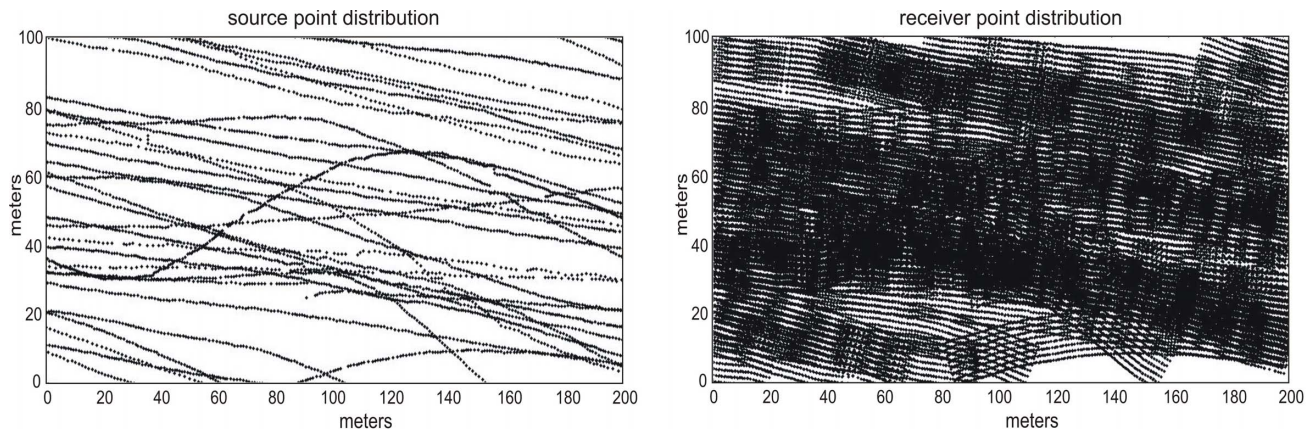

Figure 5.12 *Distribution of source positions (left) and receiver positions (right) in the reduced 3D area, Paardenmarkt dumpsite (for location see Figure 5.11).*

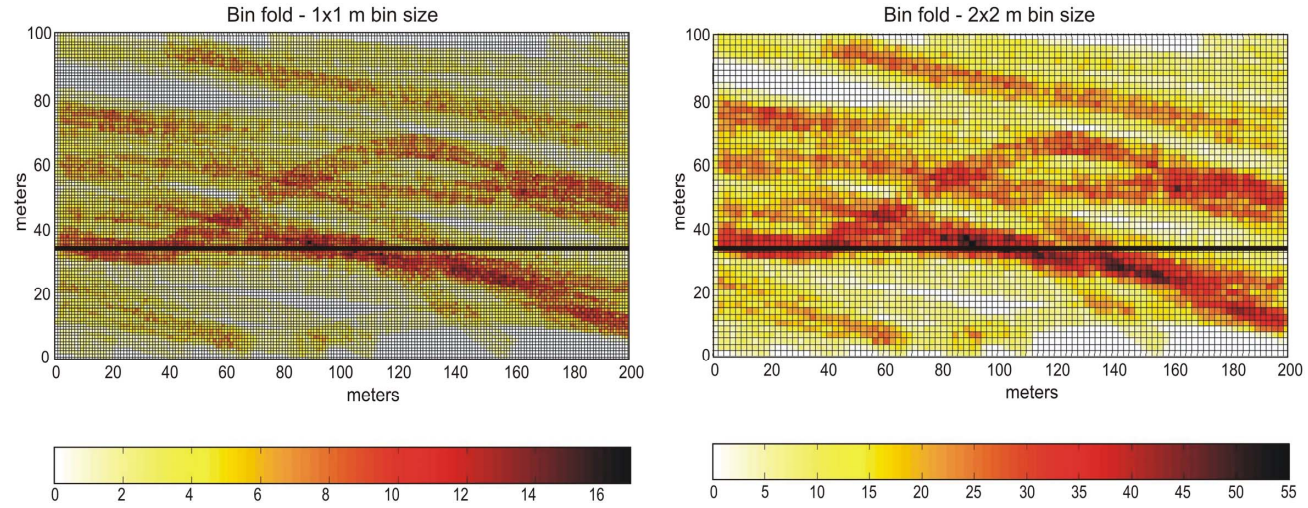

Figure 5.13 *Midpoint fold coverage for 1x1 m bins (left) and 2x2 m bins (right) in the reduced 3D area, Paardenmarkt dumpsite (for location see Figure 5.11). The thick black line marks the inline section shown in Figure 5.18.*

5.6.3 Data processing and imaging

Tidal amplitudes during the 3D survey at the Paardenmarkt dumpsite were very large (>3.5 m) making tidal correction a crucial processing step. The tidal data were deduced from detailed tidal curves for the harbour of Zeebrugge. However these tidal data do not take into account local vertical variations caused by waves and wind. Tidal shifts were carried out on the zero-offset data, after NMO correction, using a velocity of 1550 m/s. Additional preliminary processing included bandpass filtering and agc. Close inspection of the individual bins after NMO and tide correction showed that the traces often do not line up well (Figure 5.14-left). Deviations in arrival times were up to almost 1 ms. This was most likely caused by errors in the relative source and receiver positions (due to swell) and by slight errors in the absolute positions (due to movement of the positioning antenna). In order to minimize these positioning errors a swell filter was applied to the common offset (single channel) 2D data. Comparison of the stack bins

before and after swell correction shows a marked improvement but still the arrival times do not line up entirely (Figure 5.14-right).

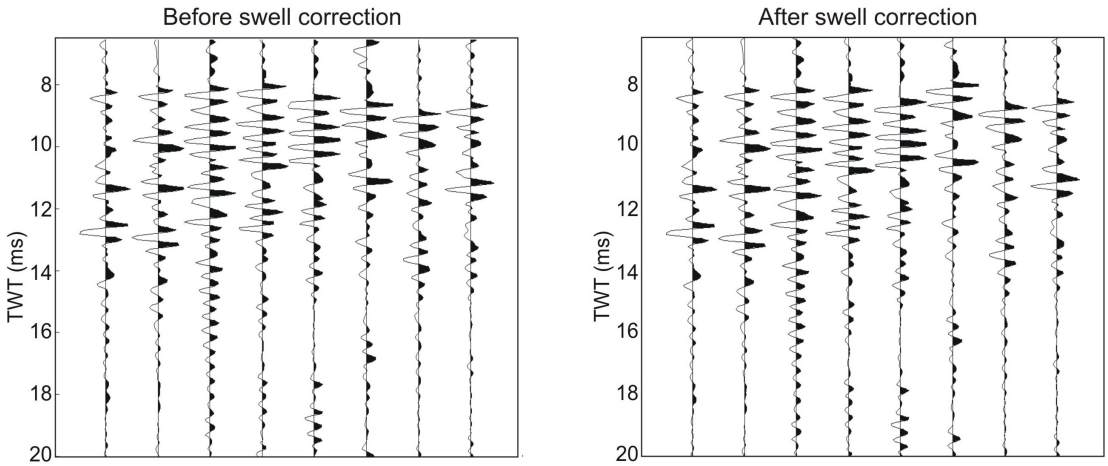

Figure 5.14 *Influence of swell on stack bin traces after NMO and tide correction, Paardenmarkt dumpsite. Left: before swell correction. Right: after swell correction.*

Figure 5.15 illustrates the results after stacking for vertical inline section 37 (for location see Figure 5.13). The upper plot shows the raw unfiltered stack section without any static corrections. The data are very chaotic and marked by an irregular and jumpy water bottom. The effect of swell correction on the stacking process is evident in the middle plot. Stacking of the swell filtered data resulted in a clear increase in resolution (due to improved line-up of the stack bins). The swell filtered data are generally marked by a better defined seafloor and shallow subbottom reflectors. However coherent deeper reflectors are still sparse and penetration remains limited.

To further improve the quality of the stacked data vertical corrections of the seismic traces were carried out in each bin, each trace being shifted to one common first arrival time (i.e. the average arrival time within one bin). Although this is perhaps not entirely accurate (since no exact water depth information was available), the flat seafloor in the area seemed to justified this. The result is shown in the bottom plot of Figure 5.15. An additional improvement in the coherency of the uppermost reflections can be observed, but the deeper reflectors become slightly less coherent. Zones of diffraction clusters can be observed which could possibly correspond with the dumped munition. Comparison with the magnetic vertical gradient data from 1996 indicates that the inline section crosses a large magnetic anomaly. The location of the anomaly (marked by a black arrow) seems to coincide with a small cluster of enhanced chaotic reflections, suggesting some relation to dumped munition. However due to the limited resolution of the data this interpretation remains very preliminary.

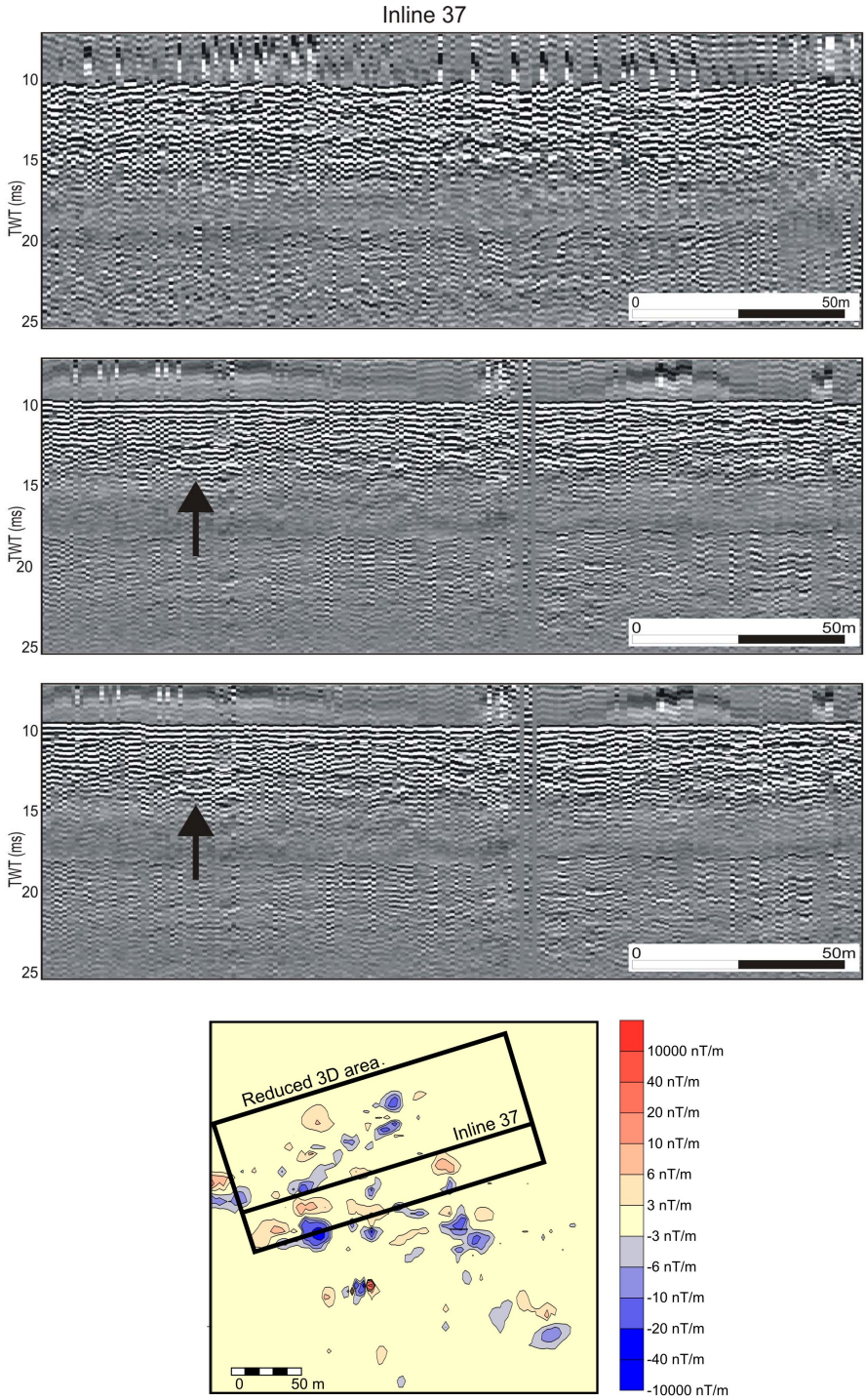

Figure 5.15 *Inline section 37 across the reduced 3D data volume (for location see Figure 5.13). Top: Uncorrected data. The image is chaotic and marked by a jumpy water bottom. Middle: After swell filter. A clear increase in resolution can be seen, marked by a better defined seafloor and shallow reflectors, but coherent deeper reflectors are sparse. Bottom: After swell filter and static correction. There is additional improvement in the coherency of the uppermost reflections but deeper reflectors become slightly less coherent. Thin grey stripes are due to empty bins. At the far bottom the location of the inline section is plotted on a background of the magnetic vertical gradient map from 1996. The inline sections cut through a large magnetic anomaly in the west. The location of the anomaly (black arrow on the profiles) seems to coincide with a small cluster of enhanced chaotic reflections which suggests some relation to dumped munition. However due to the limited resolution of the data this interpretation is very preliminary.*

Finally a number of time slices were obtained from the reduced 3D volume, after swell filtering and static corrections. The results are shown in Figure 5.16. The time slices start at roughly 1.2 m below the seafloor and are separated by 0.4 ms (±30 cm). Similar to the vertical cross sections the time slices did not provide unambiguous evidence of the distribution of the dumped munition. The limited resolution of the 3D data, as compared to the 2D data, is most likely mainly due to the small lateral and vertical positioning errors which caused a misfit in stacked traces. The possible presence of large ripples or other seafloor irregularities (evidenced by the 2007 data, see §5.8) will have caused further misstacks. Combined with the presence of shallow gas, which limited the penetration and severely reduced the overall data quality, this most likely prevented to image the dumped munition on the 3D data.

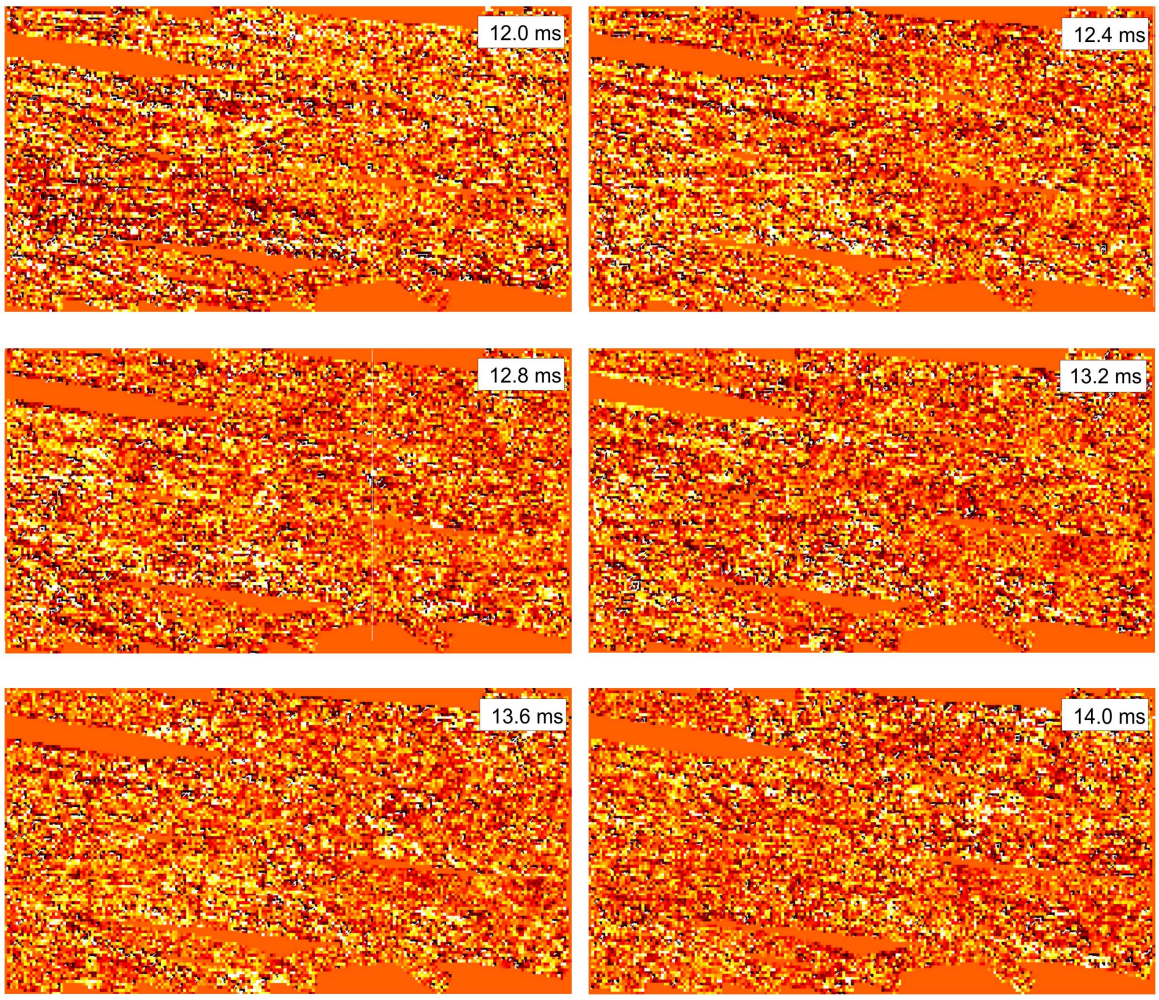

Figure 5.16 *Time sections across the reduced 3D data volume, Paardenmarkt dumpsite. The time slices start at roughly 1.2 m below the seafloor. Interval between consecutive time slices is ± 30 cm. Size of the sections is approx. 200x100 m. The presence of dumped munition or clusters of munition is not evident from the 3D slices.*

5.7 Seismic-electric measurements

Resistivity measurements allow to derive information on the lithology of the shallow subbottom, and correlation between seismic and resistivity data forms a strong interpretation tool (Mosher & Law 1996, Manheim et al. 2001). Resistivity measurements are not influenced by the presence of gas, and in order to better quantify the shallow sediments at the munition dumpsite a combined seismic-electric survey was carried out. Although the presence of individual munition shells is not likely to be sufficient to cause significant resistivity anomalies, it was believed that large clusters of metallic objects may well be detectable.

In resistivity profiling an electric current is injected into the seafloor through two source electrodes. The voltage differences measured at the receiver electrodes are converted into resistivity. The thus calculated "apparent" resistivity is then converted into the "true" resisitivity by inversion processing (Loke 1999). Different source-receiver configurations are possible. In marine resistivity profiling often a dipole-dipole set-up is used. Penetration depth depends on the sediment type, electrode spacing and number of electrodes (wider electrode = deeper penetration). The resolution will decrease rapidly with the vertical distance from the electrodes. Because bottom-towed arrays result in higher penetration and better resolution (a.o. due to the absence of the highly conductive seawater layer) this set-up was used for the Paardenmarkt survey.

In fully saturated marine sediments the porosity can then be estimated as $\phi = (\rho_s / \rho_w)^{-1/m}$ where ρ_s and ρ_w are the resistivity of the sediment and pore fluid and m is the sedimentation factor. The resistivity of sea water is roughly 0.25 Ohm.m. Fine sand will have a cementation factor of ~1.3. Due to the low resistivity of the sea water the electric potentials measured during marine resistivity surveys will be much lower than those for freshwater surveys.

5.7.1 Data acquisition

Seismic-electric trials were carried out in June 2005. Strong winds during the survey did not allow a stand-alone set-up of the OPUS3D system. It was decided to tow the two inner streamers under the catamaran vessel used for the survey (Figure 5.17), thus allowing to reduce the number of inflatable frames as these are very susceptible to wind and waves. The outer streamers were attached to the inflatable frames. The Seistec boomer was towed in the front between the catamaran floaters. Positioning was done using RTK (x,y,z with cm precision) set up on the catamaran.

The bottom-towed resistivity cable was 80 m long. Its design was based on a modified Schlumberger layout using two source electrodes spaced 60 m apart and 10 receiver electrodes (AB/2 values between 0.92 and 45.9 m). This set-up allowed a maximum penetration depth of roughly15 m (Henriet & Missiaen 2005). In total 17 parallel profiles were recorded over a small test area of 1 km x 100 m in the central part of the dumpsite where a lot of magnetic anomalies had been observed (Figures 5.18 & 5.19). A magnetic gradient survey was carried out in this same test area a few months later (see Figure 5.6b). Average spacing between the profiles was 5-10 m. All profiles were sailed against the current to maintain a low vessel speed and to avoid lateral displacement due to waves and side currents. Due to stormy weather only part of the data could be recorded in the 3D set-up in order to avoid damage of the inflatable frames. The remaining profiles were recorded in 2D mode using the Seistec source/receiver system.

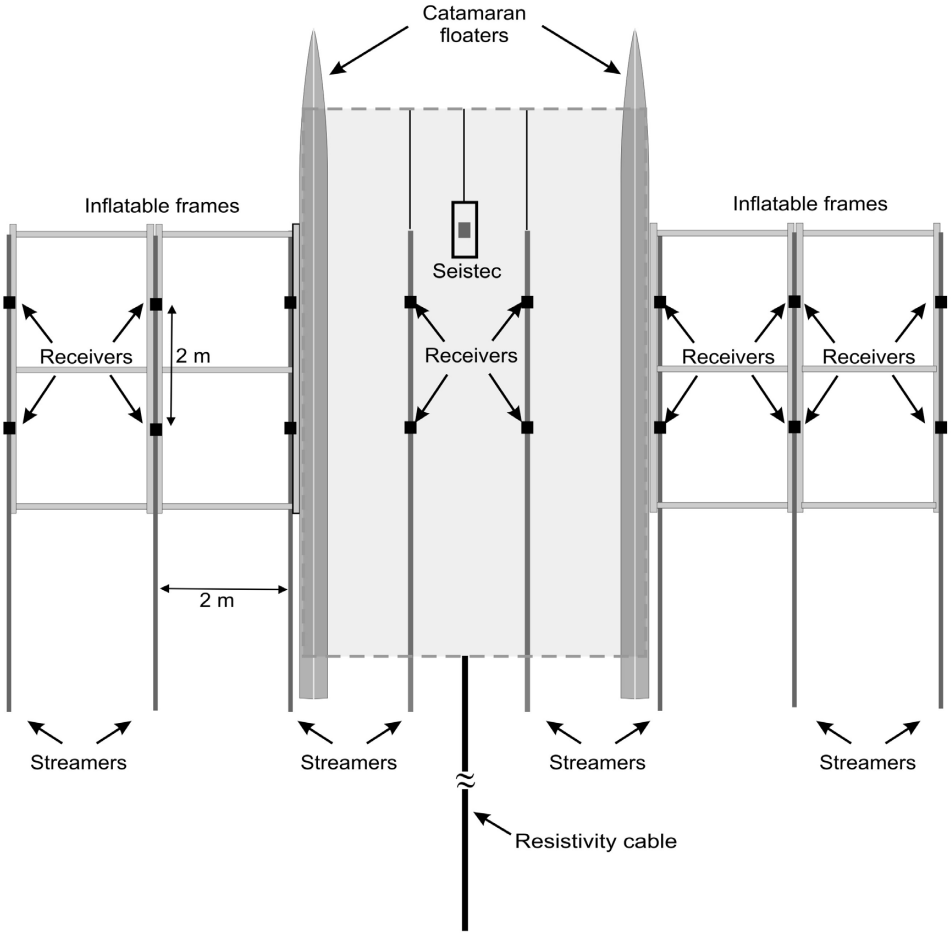

Figure 5.17 *Schematic overview of the acquisition set-up for the seismic-electric survey at the Paardenmarkt dumpsite (after Henriet & Missiaen 2005).*

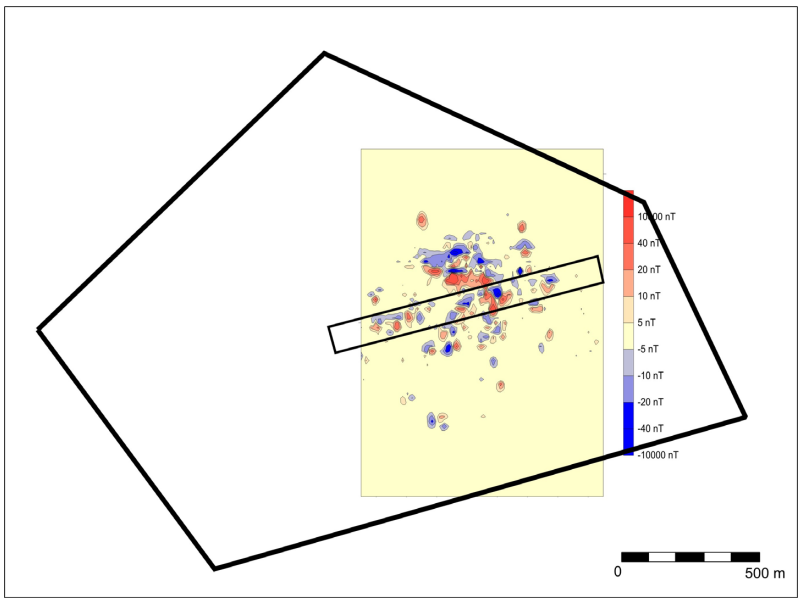

Figure 5.18 *Location of the seismic-electric test area (black rectangle) plot against a background of the 1996 magnetic data. The black pentagon marks the dumpsite boundary. The 2005 vertical gradient map of the test area is shown in Figure 5.6b. The location of individual profiles is shown in Figure 5.19.*

5.7.2 Seismic data

Sampling frequency was 24 kHz for a shot interval of 0.5 ms. Spacing between the shots varied between 0.75 and 1.3 m. Due to the bad weather the noise level on the data was high, and swell filtering was a crucial step. The processed 2D data locally showed some internal stratification, possibly related to thin sandy and silty/muddy layers (Henriet & Missiaen 2005). The thin recent sediment wedge and slightly deeper discontinuous reflector observed on the 1996 data were also clearly identified here, in addition to numerous diffraction clusters.

Detailed analysis of the 3D seismic data revealed a high noise level and irregular signal on the streamers attached to the catamaran floaters (channels 5-6 and 11-12), most likely due to the streamers hitting the vessel's floaters. To determine whether real 3D processing was feasible the midpoint coverage was calculated for a test area of 100x100 m, after filtering out the low quality channels. Fold coverage was calculated for bin sizes of 1x1 m and 2x2 m. In view of the small target larger bin sizes were not considered adequate. The coverage for both bin sizes was very low and highly irregular and did not allow correct 3D processing.

5.7.3 Resistivity data

Before actual inversion processing the apparent (= raw) resistivity data were analysed. Although these do not give the real depth and resistivity values, they may reveal small-scale variations in the resistivity that are easily filtered out during the inversion process. On several of the apparent resistivity profiles small anomalies were observed and in total three different anomaly zones (a1, a2, a3) were identified (Demco 2005). Figure 5.19-top shows an example of a raw resistivity profile. The uppermost curve corresponds with the largest electrode offset, the curves below mark decreasing electrode offsets (i.e. decreasing penetration depth). The anomaly is most prominent on the lower curves suggesting a shallow depth. Comparison with the magnetic vertical gradient data obtained in 2005 shows that the location of the apparent resistivity anomalies generally coincides quite well with major gradient anomalies, confirming a relation to dumped munition (Figure 5.19-bottom).

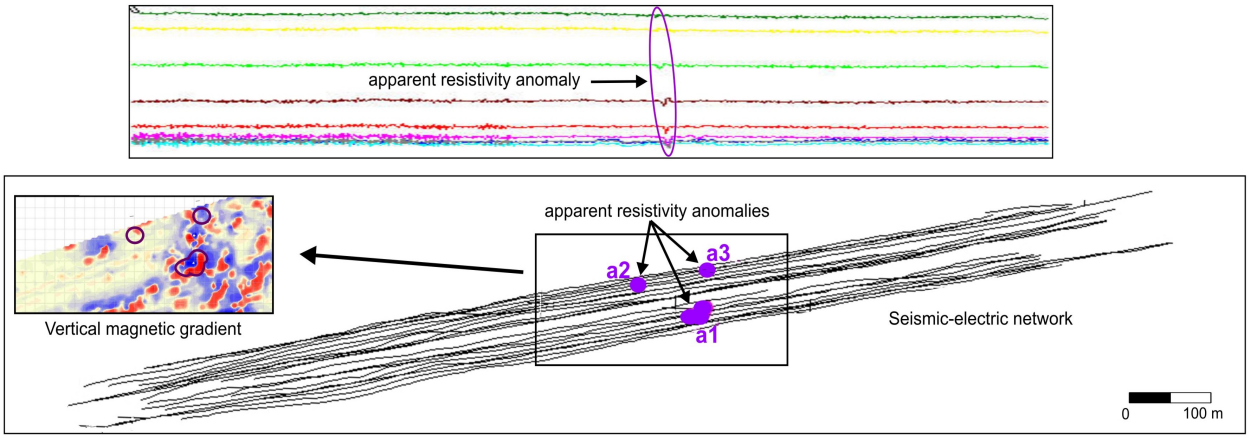

Figure 5.19 *Top: Apparent (raw) resistivity profile showing the presence of a small resistivity anomaly. The lowermost curve (in blue) marks the minimum electrode spacing; the uppermost one (in green) marks the maximum electrode spacing. Bottom: Seismic-electric network and location of the apparent resistivity anomalies (a1, a2, a3). The inset on the left shows the correlation with the magnetic gradient data obtained in 2005. The apparent resistivity anomalies (marked by black circles) generally correlate well with major magnetic gradient anomalies, confirming a relation to the dumped munition.*

Inversion processing resulted in a 3D resistivity volume of the subsurface. Figures 5.20 and 5.21 show examples of vertical cross-sections and horizontal depth slices through the test area (Demco 2005). On the data we can distinguish the following layers (from top to bottom):

- a thin top layer (1 to 1.2 m thick) with intermediate resistivity values between 1.2 and 1.5 Ohm.m (i.e. porosity of 25-30% for m = 1.3);
- a thick layer with low resistivity values between 0.8 and 1.2 Ohm.m (i.e. porosity of 30-45% for m = 1.3). Most likely this layer has a slightly higher clay content;
- a thick layer with high resistivity values of 2 Ohm.m (i.e. porosity of > 20% for m = 1.3). Probably this layer consists of more compacted sandy sediments.

As expected, the small resistivity anomalies identified on the raw resistivity profiles (see Figure 5.24) could not be observed on the inverted resistivity data.

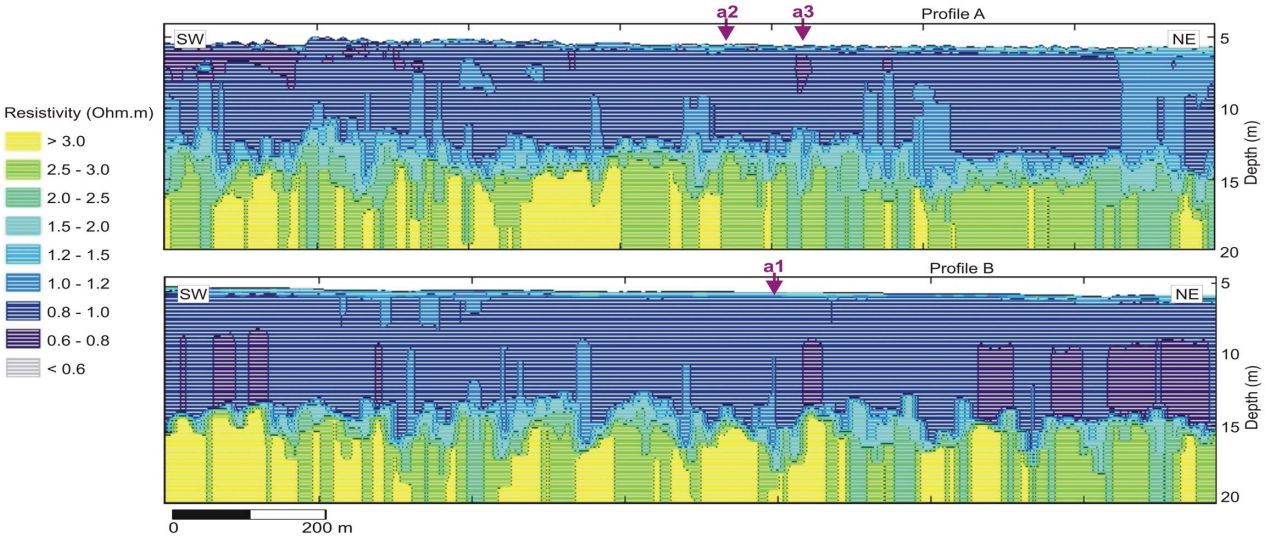

Figure 5.20 *Vertical cross-sections through the 3D resistivity cube (for location see Figure 5.21). A thick low-resistivity layer is overlying high-resistivity deposits. The thin top layer is marked by a higher resistivity. The apparent resistivity anomalies a1, a2, a3 observed on the raw data are no longer clear on the inverted sections.*

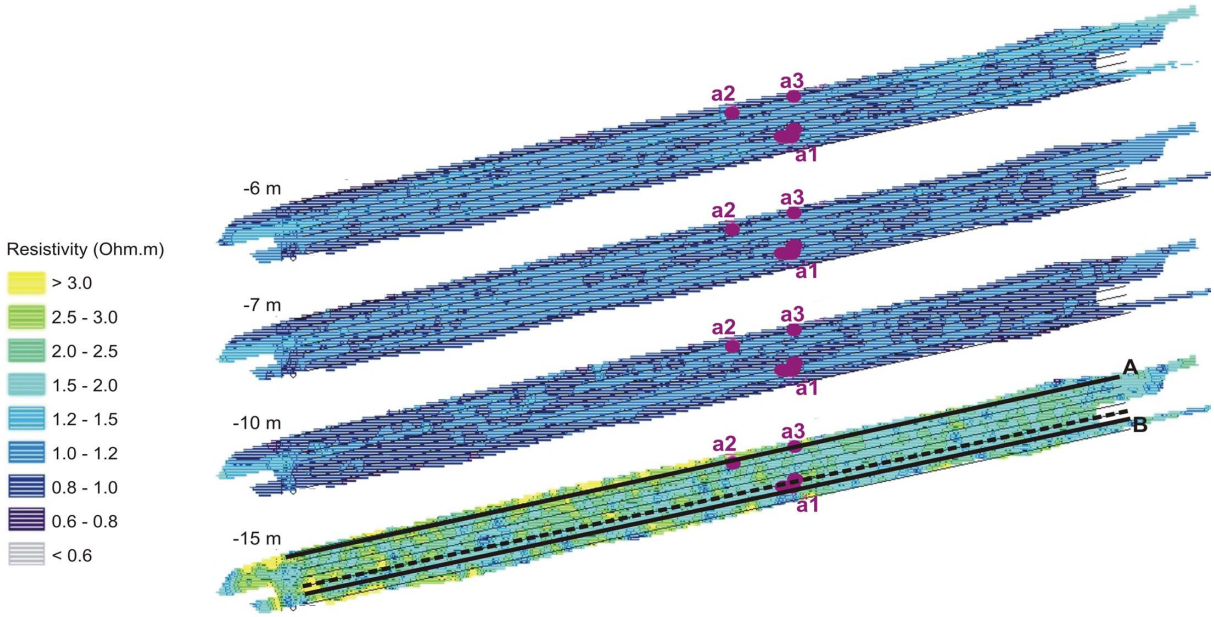

Figure 5.21 Horizontal slices through the 3D resistivity volume at different depths (6 m = seafloor). The full black line marks the profiles shown in Figure 5.20. The dashed black line marks the profile shown in Figure 5.22. Pink dots mark the apparent resistivity anomalies observed on the raw resistivity data.

5.7.4 Data integration

Correlation between the 2D seismic profiles and the resistivity data is illustrated in Figure 5.22. Although the seismic profile does not coincide exactly with the resistivity profile (the latter being a synthetic section through the 3D resistivity volume) the small lateral displacement of less than a few m should allow a reliable comparison. Static corrections were carried out on the seismic data to obtain the same seafloor level (Henriet & Missiaen 2005).

The thin top layer identified on the resistivity data corresponds well with the recent sediment wedge observed on the seismic data. The resistivity values (1.2-1.5 Ohm.m) of this layer suggest an increased sand content compared to the underlying sediments. Deeper resistivity layering could not be linked to the seismic data due to a lack of penetration of the seismic data caused by shallow gas.

As mentioned in the previous paragraph the apparent (raw) resistivity anomalies could not be traced on the inverted resistivity sections. Comparison with the seismic data however showed that the resistivity anomaly coincided with the presence of local disturbances in the shallow stratification caused by small diffraction (see inset Figure 5.22). This suggests that the resistivity anomaly se acoustic disruptions are likely related to the presence of buried munition. Nevertheless some relation to a local increase in gas content cannot be entirely excluded.

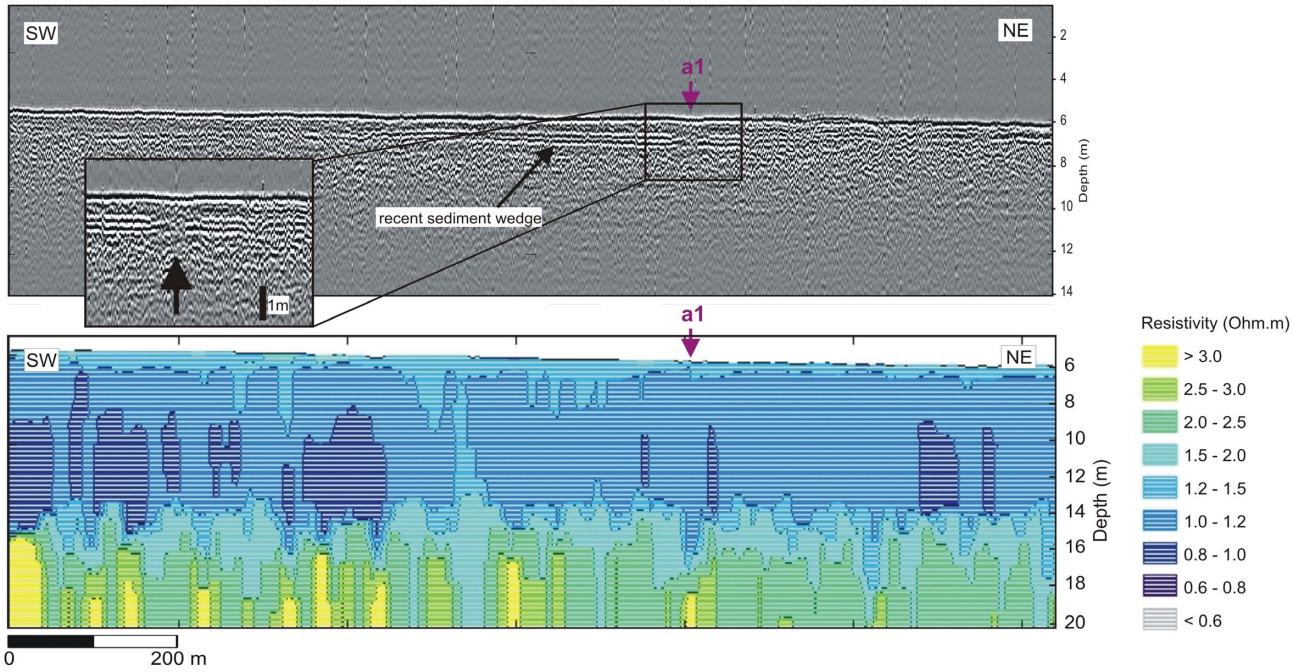

Figure 5.22 *Concurrent 2D seismic profile (top) and resistivity cross-section (bottom) through the test area (for location see Figure 5.21). The thin recent sediment wedge is clearly visible on both data. The deeper resistivity layering is not visible on the seismic data due to the presence of shallow gas. The apparent resistivity anomaly (a1) that was observed on the raw resistivity profiles is no longer visible on the inverted resistivity data. Close inspection of the seismic data however indicates the presence of a small diffraction cluster disrupting the shallow layering (see inset) that roughly coincides with the resistivity anomaly, which suggests a possible relation to dumped munition.*

5.8 2007 seismic data

In 2007 a test survey was carried out with the parametric echosounder. 21 short profiles were recorded over the central dumpzone, with additional long profiles crossing the entire dumpsite (Figure 5.23). To achieve maximum resolution the recording window was set at 6 m, using a secondary frequency of 12 kHz. Positioning accuracy was ±1 m. Swell motion was filtered out using a motion sensor mounted on deck. In view of the high currents in the survey area vessel speed was kept between 3 and 4 knots to allow precise steering. The shallow water depth allowed a high ping rate yielding a shot interval distance on the seafloor of 7-10 cm.

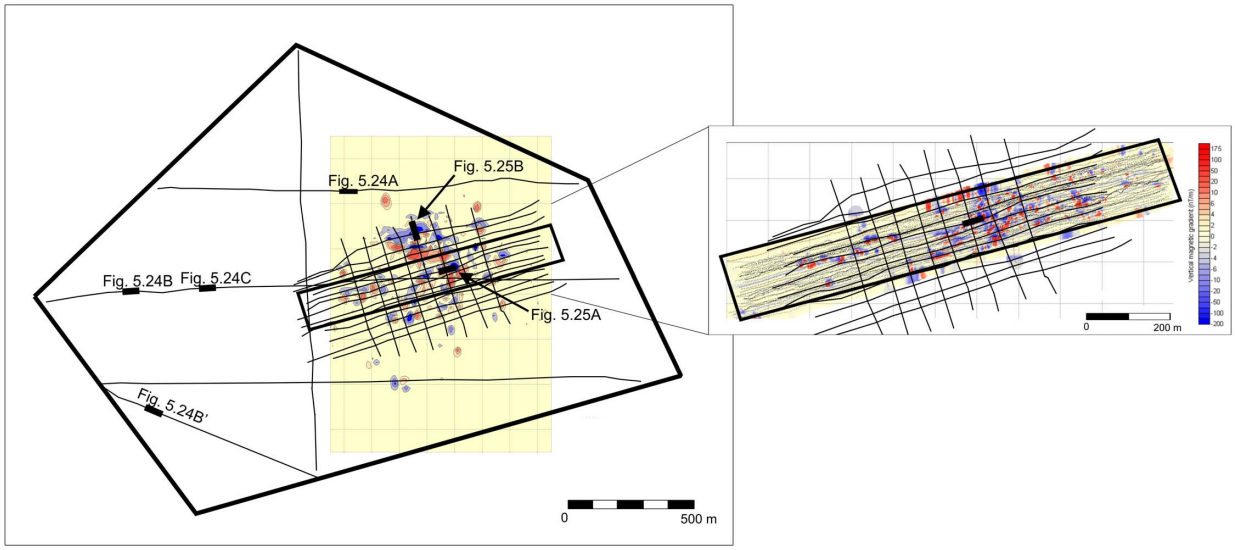

Figure 5.23 *Seismic network recorded in 2007 plotted against a background map of the 1996 magnetic anomalies. The black rectangle marks the magnetic vertical gradient area surveyed in 2005. Thick black lines mark the profiles shown in Figures 5.24-5.25. The inset on the right shows the seismic network against a map of the vertical gradient anomalies (2005 data).*

Although penetration remained limited to a few meter, due to shallow gas, the high resolution of the echosounder data allowed to distinguish several closely-spaced reflectors in the upper sediments (Figure 5.24A), representing a detailed account of the different stages in the recent sedimentation process. The data indicate a higher sediment accumulation towards the south-west which confirms earlier bathymetric studies (see §5.3). Locally the seismic data are marked by deeper penetration, most likely the result of a small decrease in gas content (Figure 5.24C). Small dunes (spacing 5-20 m, average height 0.5 m) were observed in the western and southern part of the dumpsite (Figure 5.24B), reaching a height of 1 m in the extreme south-west. Internal stratification of the dunes (see Figure 5.24B-inset) suggests a movement towards the W-NW. This indicates that notwithstanding the stagnation in the topographical evolution (see §5.3) important sediment displacements still take place at the dumpsite.

The echosounder data were compared with the results from the magnetic/gradiometric surveys. Despite the limited penetration the presence of buried munition is clearly suggested on some of the acoustic data. Indeed there was a striking correlation between a number of strong magnetic/gradiometric anomalies and distinct acoustic disturbances in the sediments marked by large and numerous diffraction hyperbolae (Figure 5.25). It is likely that these acoustic disturbance zones represent very shallow munition clusters which are buried by a relatively thin layer of sediment. Deeper buried munition will probably become acoustically invisible due to the strong turbidity and scattering related to the presence of shallow gas.

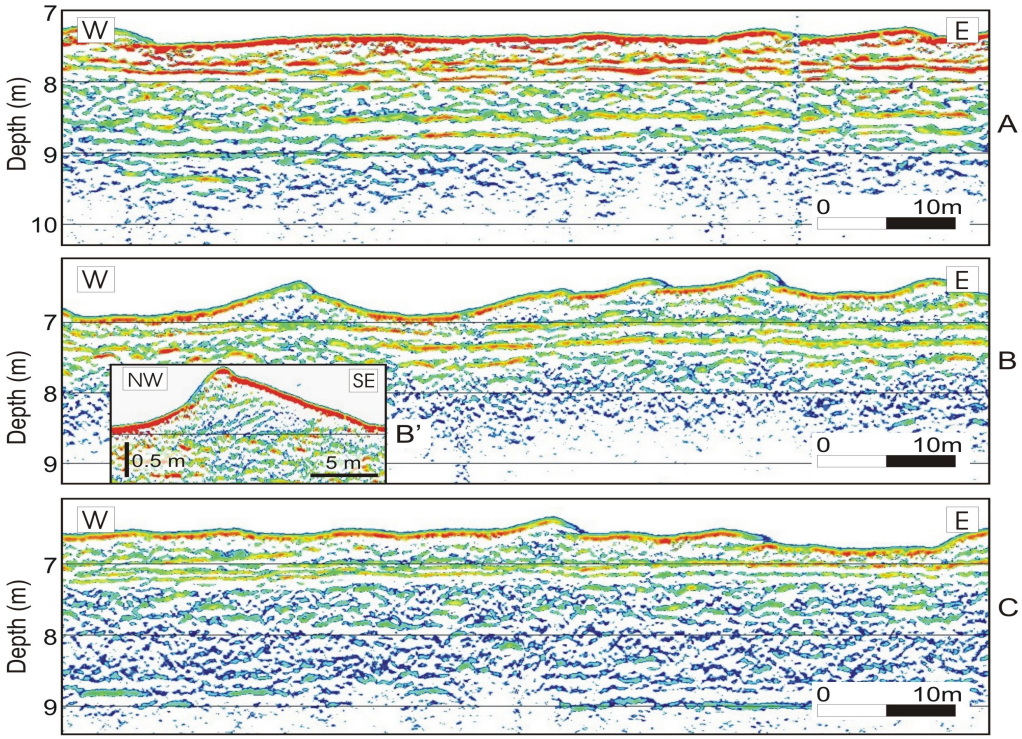

Figure 5.24 *Parametric echosounder profiles (12 kHz) recorded in 2007 (for location see Figure 5.23). The upper sediments are marked by very fine layering related to different stages in the recent sedimentation process (Profile A). Large sand waves occur towards the south-west, often showing internal stratification (Profile B + inset). Some areas show an increased penetration and deeper reflectors, possibly due to a local decrease in gas content (Profile C).*

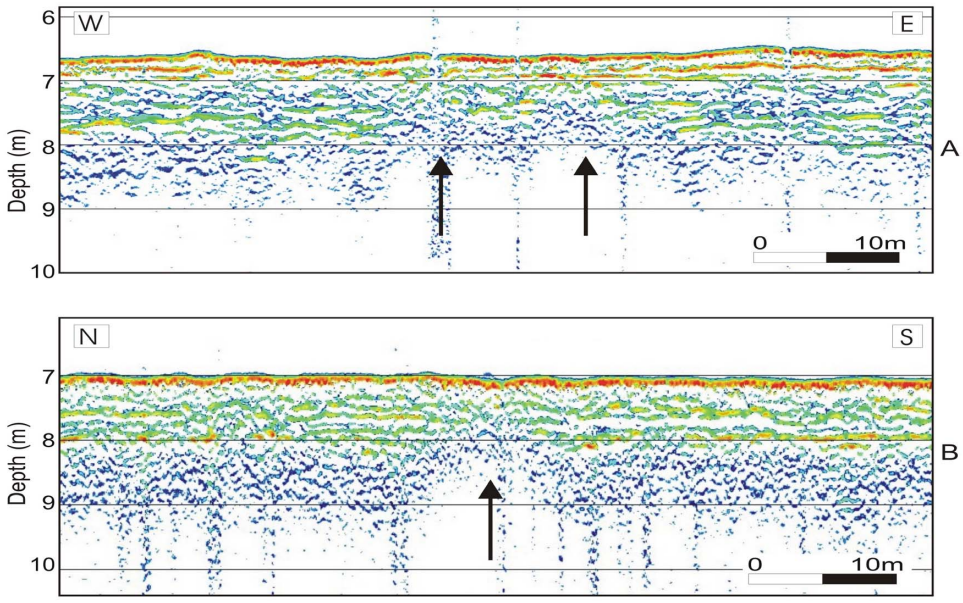

Figure 5.25 *Parametric echosounder profiles (12 kHz) from the central dumpzone (for location see Figure 5.23). Distinct zones of acoustic disturbance, marked by numerous small diffractions, are observed locally (see black arrows). These zones correlate well with some of the large anomalies identified on the magnetic and gradiometric data. Most likely they represent shallow clusters of dumped munition. The width of the acoustic disturbance in profile A suggests we may be dealing with two closely located munition clusters. Vertical disturbances in the data are due to equipment noise.*

5.9 Summary and conclusions

After WW1 an estimated 35,000 tons of war material, including a large amount of chemical munition, were dumped on the "Paardenmarkt", a shallow sand flat just off the Belgian coast. In recent years a number of VHR seismic, magnetic and resistivity studies have been carried out in order to get a better idea of the lateral and vertical distribution of the dumped munition and the internal structure of the dumping site. This is also crucial with regard to the possible migration of the toxic substances and the munition corrosion process. Topographical studies have indicated a marked accumulation of fine-grained sediments since 1976, mainly due to the construction of the outer port of Zeebrugge. As a result the munition is now completely buried. Magnetic investigations have identified a central zone where most of the dumped material seems to be concentrated, and an outer zone marked by scattered dumps. Depth estimates indicate a burial depth of most objects ranging between 2 and 6 m.

Seismic investigations at the dumpsite were severely hampered by the presence of shallow gas, which affected the data quality and limited the penetration depth to a few meters. Nevertheless a number of shallow reflectors could be identified, reflecting different stages in the recent sedimentation process. The data confirm earlier bathymetric studies indicating an increased sediment accumulation towards the south-west. Small dunes up to 1 m high suggest important sediment displacement is still taking place in parts of the dumpsite. Concurrent electrical investigations have identified a thin top layer (~ 1 m thick) of silty/sandy sediments, confirming the seismic observations. Deeper sediments are marked by an increased clay content overlying a layer of more compacted sandy sediments.

Detection of buried munition on the seismic data was not straightforward, not only in view of the shallow gas but also due to the unknown size of the objects (partly too small for acoustic imaging) and the possible advanced state of corrosion (which will decrease the impedance contrast). Burial depth near a layer boundary could further complicate detection. Frequent clusters of diffraction hyperbola were observed on the Seistec data. These are probably linked to clusters of dumped munition, as comparison with magnetic/gradiometric data seems to indicate. 3D seismic trials with the prototype acquisition system did not provide the necessary resolution to allow precise imaging of the dumped munition, yet some correlation between the seismic and magnetic data was observed. Small anomalies on the apparent resistivity data, most likely related to buried munition, seem to correlate well with acoustic disturbances. Recently obtained ultra-high resolution parametric echosounder data locally showed a striking correspondence with the magnetic anomalies. Most likely they represent very shallow munition clusters that are buried by a thin ($\leq$ 2 m) layer of sediment. Deeper buried munition will probably remain acoustically invisible due to the strong acoustic turbidity related to the shallow gas.

The results of the Paardenmarkt surveys clearly demonstrate the importance and added value of combined geophysical methods -in our case acoustic, geo-electric and magnetic/gradiometry- in munition dumpsite research. Increasing the lateral and vertical resolution of the acoustic data will enhance the detection of dumped munition. Nonetheless a large number of factors remain unknown, and monitoring of the dumpsite is crucial to track the evolution of the site and to detect any possible hazards in the future, such as renewed surfacing of shells due to local erosion processes. Regular geochemical sampling should furthermore provide information on possible leakage of the dumped munition. This should finally lead to a correct evaluation of the risks related to the Paardenmarkt munition dumpsite.

CHAPTER 6
BORNHOLM DUMPSITE CASE STUDY

6.1 Introduction

After WW2 approximately 32,000 tons of chemical war material, containing about 11,000 tons of toxic agents, were dumped in the Bornholm Basin, east of the island of Bornholm, in the southern Baltic. The dumping operations were carried out from 1947 till 1948 on the orders of the Soviet military administration in Germany. Estimated quantities of munitions and chemical warfare agents were collected from the Russian report submitted to HELCOM in 1993 (HELCOM 1993h). According to this report the dumped war material in the Bornholm Basin included artillery shells, smoke grenades, aircraft bombs, mines, containers, drums and encasements (Table 6.1). The main chemical agents were mustard gas (63 %), arsenic-containing compounds (such as Clark) (18 %) and Adamsite (31 %), and small amounts of chloroacetophenone (CAP) (Table 6.1). Based on the information from munition recovered along the route towards the dumping grounds it cannot be ruled out that Tabun was also dumped in the Bornholm Basin (Theobald 2001).

Types of CW	Mustard gas	As-cont.	Adamsite	CAP	Others	Total
Aircraft bombs	5920	906	591	479	-	7896
Artillery shells	671	-	61	36	-	768
High-explosive bombs	314	-	-	-	-	314
Mines	42	-	-	-	-	42
Encasements	80	203	693	-	74	1050
Smoke grenades	-	-	65	-	-	65
Containers	-	924	-	-	-	924
Drums	-	-	18	-	-	18
Total	7027	2033	1428	515	74	11,077

Table 6.1 *Types of chemical weapons (CW) and quantities of chemical warfare agents (in tons) dumped in the Bornholm Basin in 1947-1948 (after HELCOM 1993h).*

It is assumed that the war material dumped by the Soviet authorities was mainly cast overboard loose or packed in wooden crates (these were sometimes seen drifting around before sinking to the bottom) (HELCOM 1996h). In contrast to the Skagerrak where most of the dumped weapons were sunk stored in vessels, no official records exist of sunken ships near Bornholm in 1947-1948. HELCOM mentions eight sunken naval vessels and one cargo vessel scuttled in the dumpsite area, but this information is classified as *not verified* (HELCOM 1996). Recent magnetic investigations (see §6.4.2) have indicated the presence of at least four shipwrecks in the dumpsite area, but it is not known when these ships were sunk and if they actually transported chemical war material.

In addition to the 1947-1948 dumping a second dumping operation was carried out between 1953 and 1965. During this period a large amount of CW, discovered after 1952 in the former DDR, was dumped under the orders of the East German authorities. According to classified documents discovered in 1991 in the archives of the Ministry of Internal Affairs of the DDR in total 7 shiploads of CW were dumped in Bornholm Basin. The dumped weapons consisted for

the main part of bombs and small amounts of artillery shells and encasements (Politz 1994). According to the documents the war material was thrown over board except for one dumping operation in 1962 when a barge filled with bombs and drums, all covered in concrete, was sunk (operation "Hanno"). The total amount of dumped chemical compounds has been estimated between 200 and 300 tons, for the larger part mustard gas and phosgene (BSH 1993). If we assume roughly the same ratio between gross weight and toxic compound weight as for the Russian dumping operation, this would amount to a total of 600 to 900 tons of dumped weapons.

6.2 Location of the dumped weapons

The munition dumpsite is located in the southern part of the Bornholm Basin, east of the island of Bornholm, in water depths ranging from 70 m to over 96 m. The primary dumpsite area is marked by a circle with a radius of 3 nautical miles (Figure 6.1), but it is likely that the chemical munitions were spread over a larger area during dumping (HELCOM 1994). The extended dumpsite is marked by a rectangular area roughly ranging between 55°07'N-55°26'N and 15°25'E-15°55'E (Figure 6.1).

When considering the accuracy of the dumpsite location, we should keep in mind that at the time of the dumping operations most vessels were only equipped with strictly necessary navigation equipment (which had very low accuracy). Furthermore it is likely that the dumped weapons were spread over a considerably larger area during dumping, as these operations were often carried out in a hurry. Also it is known that during transport to the dumping sites in the southern Baltic some of the munition was already thrown over board before the dumping area was reached (HELCOM 1996, Schulz-Ohlberg et al. 2001).

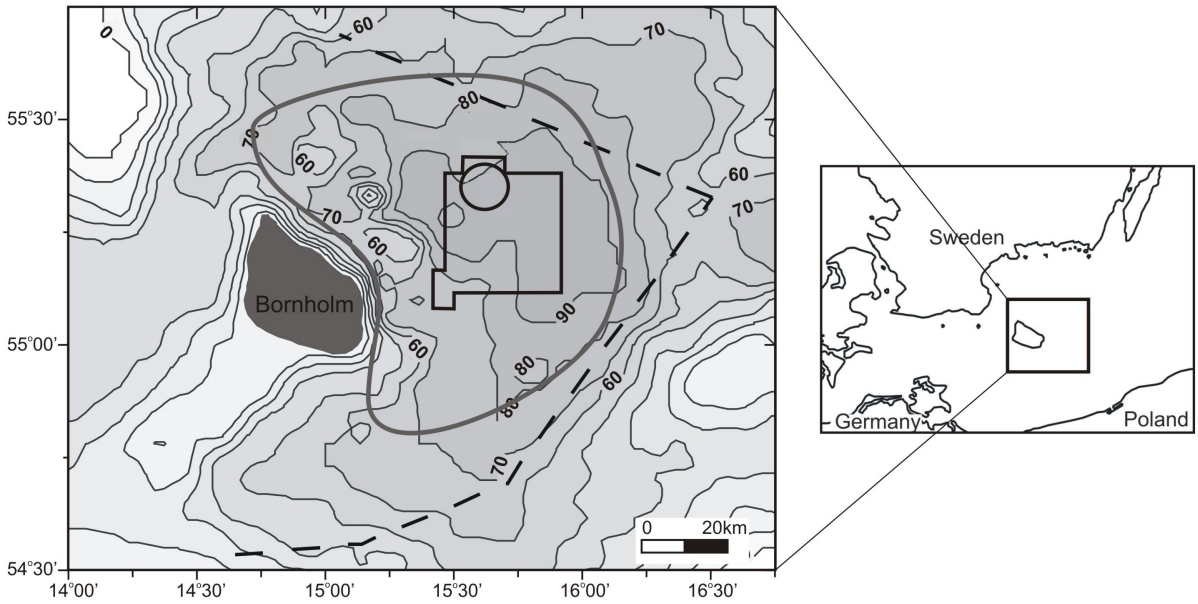

Figure 6.1 *Overview map showing the location of the chemical munition dumpsite in the Bornholm Basin, southern Baltic (depth lines every 10 m). The black circle marks the primary dumpsite area. The black rectangle marks the extended dumpsite boundary. The thick grey line marks the zone where fishing incidents related to chemical weapons have been reported. The dashed line marks the border of the Danish economic zone (modified after HELCOM 2005).*

Additional spreading of the chemical weapons undoubtedly also happened by fishing vessels during trawling*, with munitions being dragged over the seabed over long distances, sometimes without being caught. It can therefore be assumed that the dumped war material is spread over a much larger area than indicated by the official dumpsite boundaries. This is confirmed by the recorded positions where fishermen have caught weapons in their nets, which extends far beyond the actual dumpsite (Figure 6.1) (HELCOM 2006).

(Although the dumping area in Bornholm Basin is marked on nautical charts as "anchoring and fishing not recommended", fishing in these areas is not officially prohibited).*

6.3 Natural setting of the Bornholm dumpsite

6.3.1 Hydrography

The Bornholm Basin is an important buffer and accumulation link on the route of the dense salt-water inflow between the Skagerrak and the Gotland Basin (Figure 6.2), and it is the first deep basin where stagnation effects become apparent. The moderately dense salt-water inflow into the Bornholm Basin is by itself incapable of replacing the near-bottom waters, but nevertheless provides a slow withdrawal of substances accumulated in the near-bottom layer due to turbulent diffusion (Paka & Spiridonov 2001, Paka 2004). Renewal of the bottom water layer in the Bornholm dumpsite due to inflow events takes place every 3 years on average (Zhurbas 2007).

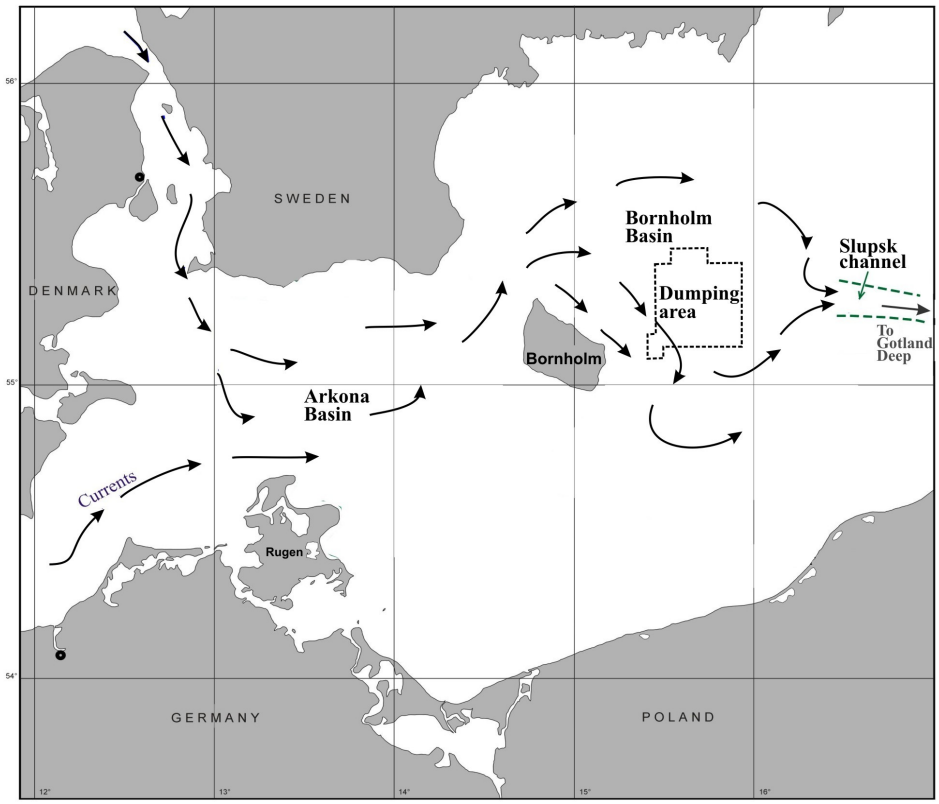

Figure 6.2 *Main currents in the south-western Baltic (modified after Emelyanov & Kravtsov 2004). The dashed line marks the extended dumpsite boundary in the Bornholm Basin.*

The sea water in the Bornholm Basin can be divided into an upper and a lower layer; the halocline is located roughly between 55 and 65 m. The upper layer consists primarily of fresh water (salinity 8‰) flowing in from the Baltic Sea. The lower saline layer originates in the North Sea and on its way to the Bornholm Basin is mixed with water from the upper layer, resulting in a salinity between 9‰ and 23‰. Incoming currents with a salinity of more than 19‰ occur mainly in the fall and winter with a mean frequency of every 4-5 years (HELCOM 1996).

The surface layer is marked by a weak south-westerly current, while in the bottom layer there is a current of 0.05 m/s mainly directed NW-SE (Zhurbas et al. 2004, Zhurbas 2007). Advective and mixing activity in the centre of the Bornholm Basin does not depend only on major inflows. Intermittent turbulence does occur, probably related to the instability of internal waves. This can produce a bottom mixed layer up to 2-3 m in thickness (Zhurbas et al. 2004). Movement of particles over the seabed observed on ROV video images provided further evidence of the presence of local near-bottom currents contributing to the local erosion of bottom deposits (Paka 2004). Detailed analytical/numerical modelling of the flow path and dispersion of possible tracers placed within the near-bottom water layer is carried out within the MERCW project (Zhurbas 2007).

6.3.2 Geological background

The thickness of the Quaternary deposits in the Bornholm Basin ranges between 20 and 50 m, locally up to 80 m. The deposits mainly consist of glacial tills (Pleistocene), clays (Pleistocene and early Holocene) and marine mud (Holocene) (Emelyanov & Kravtsov 2004). In the southern part of the basin the glacial tills reach a thickness of 20-30 m. Varved clays are more abundant in the northern part of the basin, and overlap more with homogeneous clay in the southern part (Voipio 1981).

Large parts of the Bornholm Basin are covered by a thick layer of muddy sediments, locally a few meters thick. Accumulation rates exceed 0.3 mm per year, exceptionally reaching up to 1.0 mm in some places (Emelyanov 1996). The mud is fluid and semi-fluid and contains between 70 and 87 % of < 0.01 mm fraction. The content of sandy fractions (1.0 – 0.1 mm) is usually less than 1%, and that of the 0.1-0.005 mm fraction up to 4.4% (Emelyanov & Kravtsov 2004). The distribution of bottom sediments in the Bornholm Basin depends largely on the halocline. At depths above the halocline mainly clastic sediments occur (sands and coarse silts), whereas below the halocline mainly mud occurs (Emelyanov et al. 1995). In some of the deeper parts of the basin muds are either absent or considerably less thick. This could be due to local strong near-bottom currents preventing accumulation of large masses of muddy material (Emelyanov 1996).

The Holocene clay and mud deposits were deposited during different freshwater and brackish-water stages that have marked the Baltic Sea since the last deglaciation: the freshwater Baltic Ice Lake (*c.* 12 500–10 000 BP), the partly brackish Yoldia Sea (*c.* 10 000–9500 BP), the freshwater Ancylus Lake (*c*. 9500–8000 BP) and the brackish Litorina Sea (*c*. 8000–3000 BP) (Jensen et al. 1999). The last stage, the Present Baltic Sea, is represented by conditions similar to the present.

6.4 Previous dumpsite research in the Bornholm Basin

6.4.1 Sampling and chemical analysis

Previous research carried out at the Bornholm dumpsite was largely focused on sampling of sediment and sea water and chemical analysis of the most common CW agents (mustard gas and Clark) and their by-products. Sampling sites were more or less chosen at random (a result of the fact that the weapons are no longer exposed on the seafloor but completely buried see also §5.4). German and Danish investigations in the late eighties and early nineties generally indicate normal toxic concentrations, but in a few cases increased values were measured (e.g. for arsenic and mustard gas) (BSH 1993, HELCOM 1993c).

Between 1997 and 2006 a number of sampling surveys were undertaken in the Bornholm dumpsite area in the framework of the Russian Federal Programme "World Oceans". Chemical analysis concentrated on arsenic (Clark and Adamsite), phosporus, and mustard gas, and major products of hydrolysis. The presence of mustard gas was not detected, or was below the detection level (Paka 2006). Measured arsenic levels were characterised by a large variability, locally reaching peak values up to 270 ppm (Emelyanov & Kravtsov 2004, Paka 2006). High values were often found in the vicinity of shipwrecks (see §3.2). Although high arsenic concentrations can also be due to natural accumulation processes often related to the presence of Fe-sulphides (Emelyanov 1996), the exceptional high levels and occurrence near the wrecks seems to indicate some relation to CW.

A few samples also showed increased total phosphorus and organic phosphorus concentrations in the near-bottom water. This could indicate the presence of an external source of organic phosphorus, such as from chemical weapons. However anoxic conditions near the bottom may also contribute to an increased level of organic phosphorus (Missiaen & Paka 2007). A number of samples were also subjected to microbiological studies. At different locations the microbiota of near-bottom waters comprised a very large amount of bacteria tolerant to hydrolysis products of mustard gas (Missiaen & Paka 2007). Further screening revealed that these bacteria are able to degrade mustard gas into non-toxic degradation products. This opens new perspectives for self-purification of mustard-contaminated water and sediments by aquatic microorganisms.

6.4.2 Geophysical investigations

Several magnetic surveys were carried out by Russia in 1999 and 2000. Three large magnetic anomalies were observed, most likely related to shipwrecks (Gorodnitski & Filin 2001). In May 2006 a fourth shipwreck was discovered (Paka 2006). In June 2001 a combined multibeam and ROV survey was performed and detailed images were obtained from two of the wrecks (Gorodnitski & Filin 2001). Comparison with recent data indicates that it concerns wrecks 3 and 2 (for location see Figure 6.5). Multibeam data from wreck 3 suggest that it is sticking out roughly 4 m above the seafloor (Figure 6.3). Video images of the same wreck indicate that it is badly destroyed and the hull is covered by trawling nets, often rising up due to the still attached floats (Fig. 6.4-left) (Paka & Spridonov 2001). Most likely the nets have resulted in an exaggeration of the wreck height. A large bomb was observed near the tail of the ship. Video images of wreck 2 show that this wreck seems even more destroyed, and is largely immersed in the bottom sediments. Partly corroded artillery missiles were observed on the deck (Figure 6.4-right).

It is not known if any chemical weapons were stored inside these submerged vessels. The missiles observed on the second wreck seem to suggest a wrecked warship. No living marine

organisms were observed in the near-bottom water and sediments near the shipwrecks, but this could be due to a deficit of oxygen rather than toxicity. As stated earlier in §6.4.1 samples taken near the wrecks showed very high arsenic concentrations which may indicate that some of the sunken vessels actually contain CW.

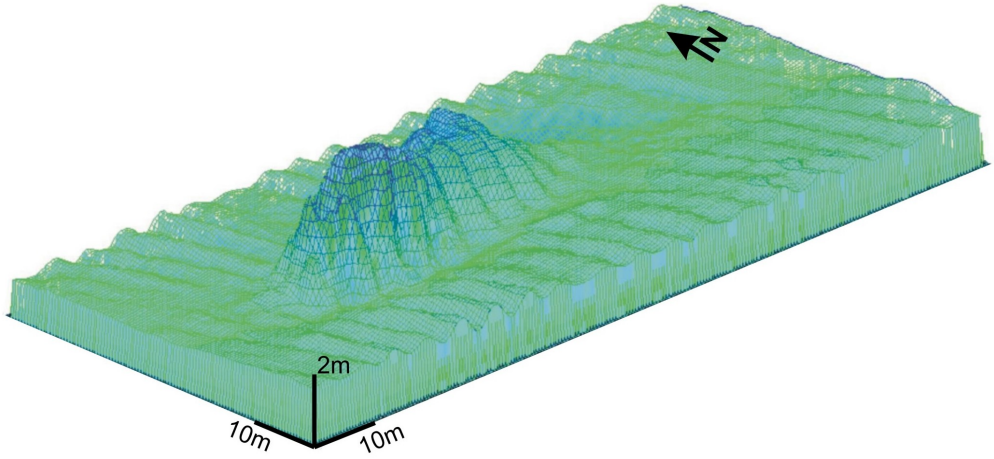

Figure 6.3 *Multibeam image of wreck 3 in the Bornholm dumpsite area (for location see Figure 6.5) (after Gorodnitski & Filin 2001). The wreck height is most likely exaggerated due to floating fishing nets attached to the hull.*

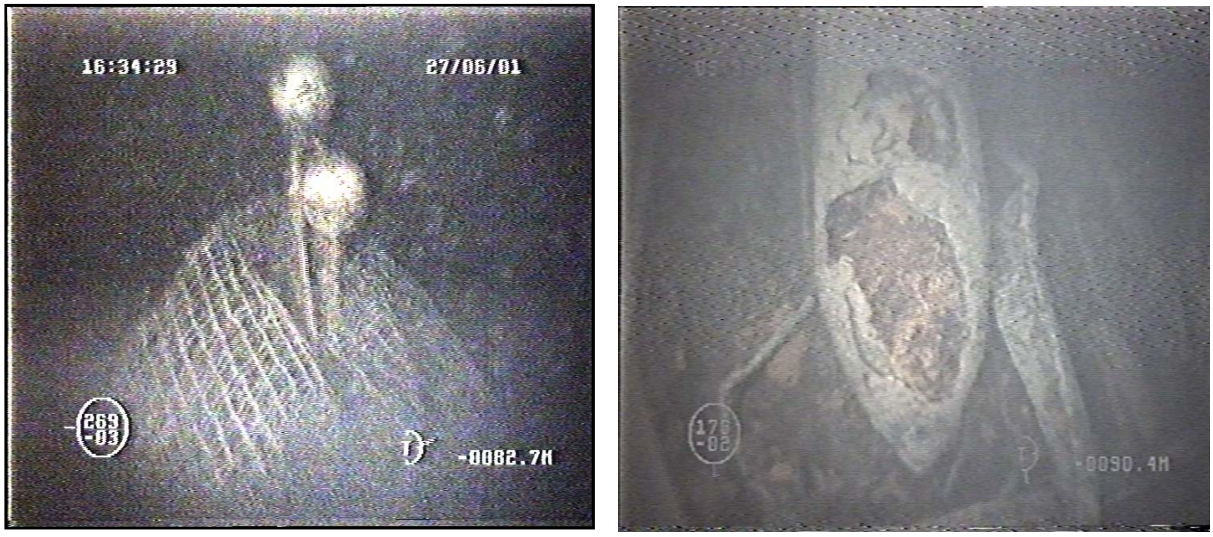

Figure 6.4 *ROV video images of two shipwrecks in the Bornholm dumpsite (after Paka & Spridonov 2001). Left: Wreck 3 covered with fishing nets. The nets are rising up due to the still attached floats. Right: Partly corroded missile found on the deck of wreck 2.*

6.5 Seismic data acquisition

In the summer of 2006 a first seismic survey was carried out in the Bornholm dumpsite area in the framework of the EU FP6 Project "MERCW" (Modelling of Environmental Risks related to sea-dumped Chemical Weapons). A second survey took place in the summer of 2007, combining magnetic and seismic measurements. The main objectives of these surveys included (1) detailed imaging of the internal structure of the munition dumpsite, (2) imaging of the deeper geological framework, (3) detection of possible natural hazards with regards to the dumped weapons, and (4) detection and possible characterisation of buried objects and shipwrecks. Both

surveys largely focused on the primary (circular) dumpsite area. Specific attention was given to areas marked by abnormal arsenic concentrations and the areas where shipwrecks had been identified (see §6.4).

6.5.1 2006 survey

During the 2006 survey on board the Russian vessel "R/V Shelf" three acoustic sources with a distinct frequency range were used (multi-electrode sparker, Seistec boomer, parametric echosounder). The sparker (main frequency 0.6-0.8 kHz) and Seistec (main frequency 3-4 kHz) allowed more penetration and were used to image the deeper geological structure of the dumpsite area. The parametric echosounder has a much higher frequency (8 to 14 kHz) but limited penetration and was used to image the upper meters of sediment in high detail. More information about these acoustic sources was given in chapter 1.

The sparker or Seistec source and the parametric echosounder were deployed simultaneously, the choice for sparker or Seistec mainly depending on the weather conditions (the latter being more sensitive to wave action). Sampling frequency was 6 kHz (sparker) and 10 kHz (Seistec) for a shot interval of 1 s. The echosounder transducer was mounted on a long pole fastened onto the side of the ship. The GPS antenna was mounted on top of the pole. A motion sensor was installed below the antenna. The sparker and Seistec were towed ~30 m behind the vessel to minimise propeller noise. Due to the high vessel speed (5-6 kn on average) the Seistec data were of less quality.

Three different networks were recorded with a total length of roughly 1000 km (Figure 6.5):

(1) Large-scale network covering the primary dumpsite area (33 profiles, line spacing ~750 m), sparker and parametric echosounder recording;
(2) Small-scale network S1 (55 profiles, line spacing 50-100 m), Seistec and parametric echosounder recording, in an area marked by locally high arsenic levels;
(3) Small-scale network S2 (50 profiles, line spacing 50-100 m), sparker and parametric echosounder recording, in an area marked by shipwrecks and increased arsenic levels.

In addition to these three seismic networks a number of long seismic profiles were recorded towards the south of the larger dumpsite area (total length ~130 km).

6.5.2 2007 survey

During the 2007 survey on board the German vessel "Fritz Reuter" two different acoustic sources (C-Boom and parametric echosounder) were used simultaneously with a deep-towed magnetic array. The C-boom has a main frequency of ~2 kHz and penetration of 100 to 150 m, sampling frequency was 12 kHz for a shot interval of 0.5 s. Boomer and streamer were towed ~30 m behind the vessel to minimise propeller noise. The acquisition set-up was similar to the 2006 survey (see previous section §6.5.1). In order to increase the vertical resolution of the shallow seismic data the recording window of the parametric echosounder was reduced to 8-10 m (compared to 20-25 m in 2006).

Two dense seismic-magnetic networks (SM1 & SM2) were recorded with a size of 0.4x1.6 km and 0.5x1.9 km (Figure 6.5). A theoretical line spacing of 10 m was applied which should allow good magnetic coverage. Both networks fall within the boundaries of the small-scale seismic grids recorded in 2006. The southern network (SM1) covers wrecks 1 and 2. The northern network (SM2) covers an area where arsenic anomalies had been observed during previous investigations (see §6.4.1). In addition to these two dense seismic-magnetic networks a number of long seismic profiles were recorded in the northern part of the larger dumpsite area.

The magnetic array consisted of three highly sensitive caesium vapour magnetometers mounted on a triangular-shaped frame which allowed to obtain horizontal and vertical gradients, providing a better horizontal and vertical object localisation. High sampling interval (15-20 cm) was crucial for the mapping of small objects such as shells and bombs. A ballast system holding ballast weight, electronics and sonar altimeter was towed roughly 5 m above the seabed and 150 to 200 m behind the vessel depending on the vessel's speed. The magnetic array was towed 25 m behind the ballast system. This set-up allowed to fine-tune the altitude of the magnetic frame with the help of a depth controller and to avoid the (magnetic) influence of the towing cable and electronics on the magnetic sensors (Missiaen & Feller 2008).

Positioning was done using a DGPS antenna providing 1-2 m accuracy. A second GPS antenna allowed precise calculation of the vessel's heading. Underwater positioning of the magnetic frame was done using a USBL system. The final positioning precision of the magnetic frame is estimated to be around 5 m. Online navigation processing allowed to track the positions of all on-board and towed instruments (including parametric echosounder, boomer, ballast system and magnetometer array) in real time and with reference to the theoretical trackline (Missiaen & Feller 2008)).

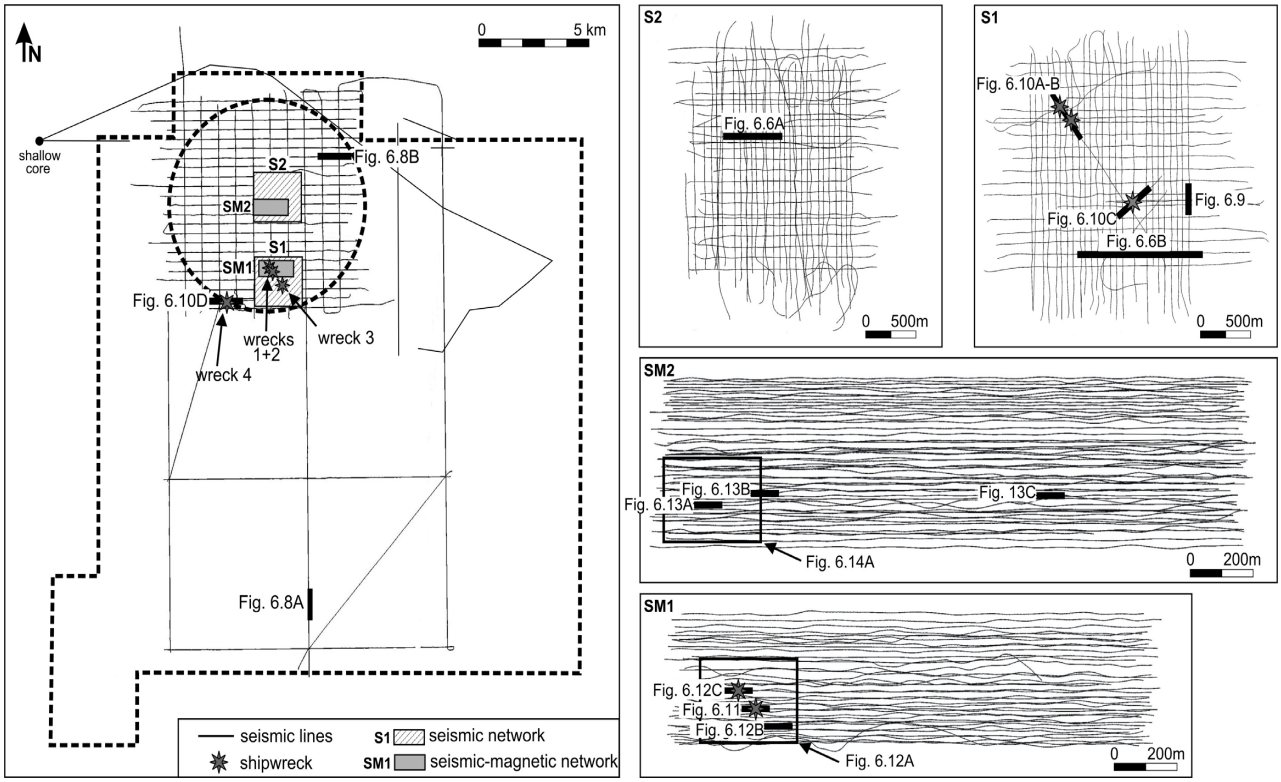

Figure 6.5 *Left: Overview of the seismic and magnetic data acquired at the Bornholm munition dumpsite. The dashed circle and rectangle mark the boundary of the primary and extended dumpsite area. Seismic lines are marked by thin lines. White and grey boxes mark the pseudo-3D seismic (S1,S2) and seismic-magnetic (SM1, SM2) networks. Shipwrecks are marked by stars. Short black lines indicate the profiles shown in Figures 6.8 and 6.10. The black dot marks the location of the shallow piston core described in Andrén et al. (2000) (see Figure 6.7). Right: Close-up of the seismic networks S1 & S2 and the seismic-magnetic networks SM1 & SM2. Short black lines indicate the profiles shown in Figures 6.6 to 6.13. The black rectangles mark the vertical magnetic gradient maps shown in Figures 6.12A & 6.14A.*

6.6 Data interpretation

6.6.1 Shallow stratigraphy

The shallow sediments were observed in high detail on the parametric echosounder data. Penetration was roughly 20-25 m for the secondary frequency signal (10 kHz) and ~10 m for the primary frequency signal (100 kHz). This clearly indicates the presence of very soft upper sediments. The deeper geology was best observed on the sparker and boomer data. Due to their lower resolution these data do not give the same amount of detail as the echosounder data, although often several shallow layers could still be distinguished. The surveyed area was largely free of gassy sediments. Some isolated gassy patches were observed in the southern and western part of the larger dumpsite area but their lateral extent remained very limited.

In general the seafloor topography is quite flat. The water depth in the primary (circular) dumpsite area varies between 92 and 98 m, gradually deepening towards the south-east. The seafloor is marked by a few small pit-like features (≤1 m deep) most likely related to dumped weapons (see §6.6.5). Locally a slight sediment accumulation (~20 cm high) can be observed. This can probably be linked to fluid mud accumulation related to local near-bottom currents, as discussed in §6.3.1. Towards the south of the larger dumpsite area the seafloor becomes more irregular and locally shallows to 70 m.

In total 7 different acoustic units were identified (Figure 6.6). The upper units were observed in high detail on the echosounder data, whereas the lower units were only visible on the sparker and boomer data (Missiaen & Noppe 2008, Noppe 2007):

- Unit 1: transparent seismic facies marked by weak parallel reflectors;
- Unit 2: transparent seismic facies locally marked by discontinuous, parallel reflectors;
- Unit 3: closely spaced, parallel, strong reflectors often exhibiting a wavy structure;
- Unit 4: transparent-chaotic seismic facies;
- Unit 5: facies marked by discontinuous, often parallel and wavy reflectors;
- Unit 6: transparent facies marked by diffractions and locally strong erosional features;
- Unit 7: facies marked by gently dipping parallel reflectors with locally intensive folding where the unit locally outcrops.

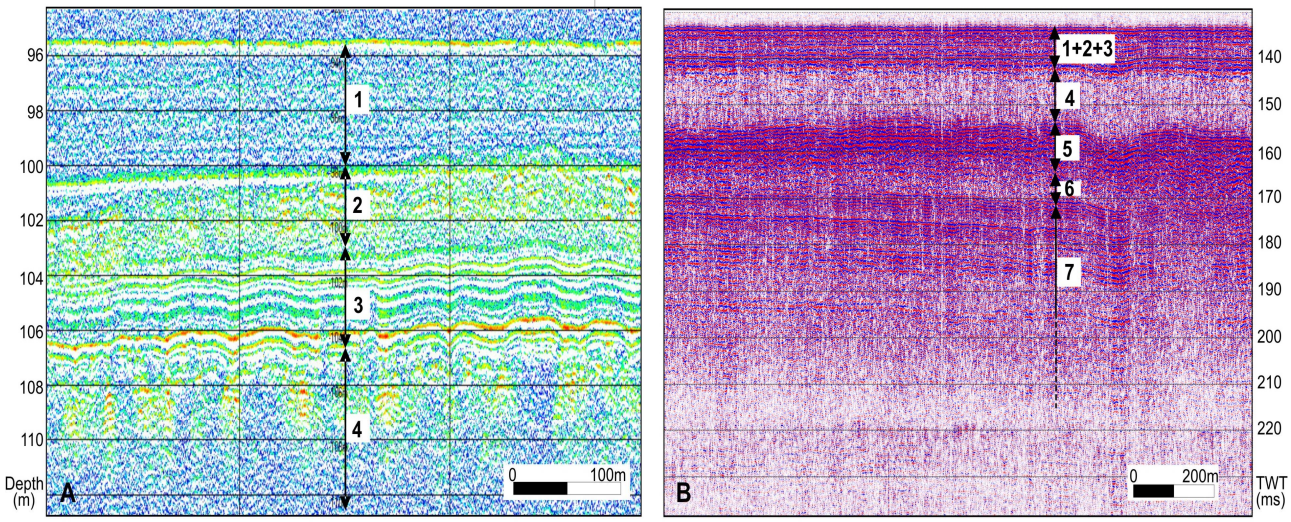

Figure 6.6 *Different seismic-stratigraphic units identified in the Bornholm dumpsite area. Left: Parametric echosounder profile (10 kHz). Right: Sparker profile. The upper units 1 to 4 can be observed in high detail on the echosounder records. The lower units 5 to 7 can only be observed on the sparker records. For location of the profiles see Figure 6.5.*

The lowermost Unit 7 most likely represents pre-Quaternary deposits. The seismic facies shows much resemblance to that described by Perini et al. (1996), who attributed it to Cretacious and Jurassic formations. The irregular morphology at its top seems to indicate glacial erosion. The chaotic seismic facies of the overlying Unit 6 suggests till or till-like features. Most likely this unit contains glacial/fluvioglacial deposits. Some of the thicker accumulations may well be produced by end moraines or eskers. The parallel draping reflectors of Unit 5 indicate a much calmer, lacustrine environment. The unit probably consists of glaciolacustrine deposits, possibly related to the varved clay deposits described by Kögler & Larsen (1979). The facies of Unit 4 suggests glacial till deposits, possibly an early stage of the Baltic Ice Lake. The erosive features at its base may well have been caused by subglacial meltwater channels. The upper Units 3, 2 and 1 most likely represent post-glacial lacustrine and marine deposits (Missiaen & Noppe 2006, 2008).

In 2007 a seismic profile was acquired over a Swedish coring site located slightly west of the primary dumpsite area (Andrén et al. 2000) (see Figure 6.5). The 9 m long piston core contains sediment material from different Baltic Sea stages ranging from the Yoldia Sea to the present (Figure 6.7) (Missiaen & Noppe 2008). Correlation with the echosounder data indicates that Unit 3 can most likely be linked to clay deposits of Yoldia Sea and Ancyclus Lake, possibly including the initial Litorina Sea. Unit 2 seems to correspond with the Gyttja clay of the Litorina Sea stage. The uppermost Unit 1 comprises both Post-Litorina Sea and recent Baltic Sea deposits.

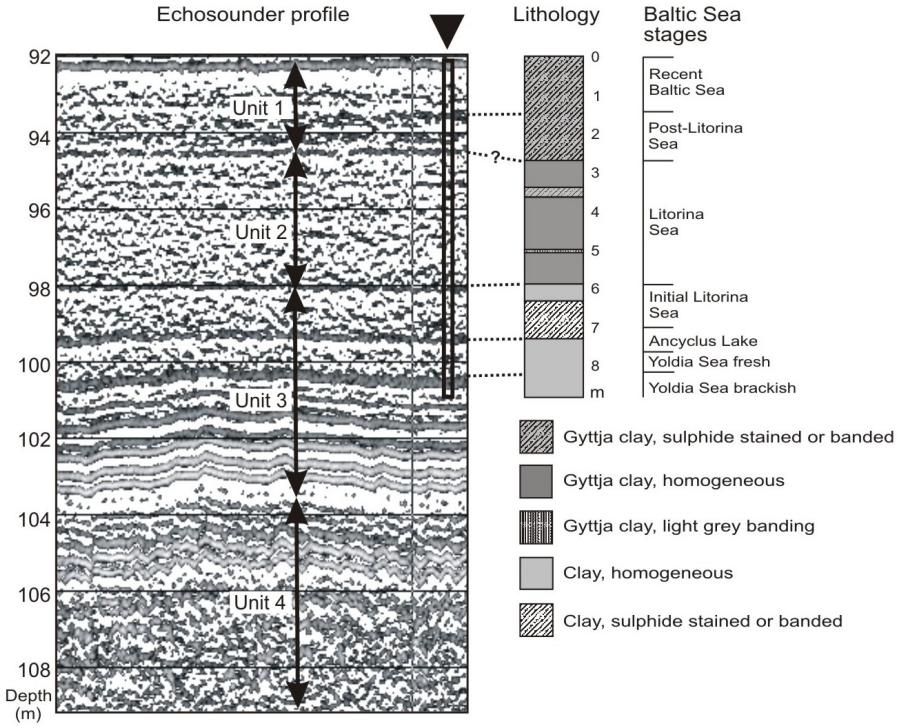

Figure 6.7 *Left: Parametric echosounder profile (10 kHz) with interpreted seismic-stratigraphic units. The location of the piston core is indicated by the black arrow at the top. The core does not reach the lowermost unit 4. Right: Lithology of the shallow piston core (after Andrén et al. 2000) and correlation with different Baltic Sea stages. In general the different layers observed on the seismic data seem to correlate well with the core description. For location of the core see Figure 6.5.*

6.6.2 Sediment mobilisation features

The seismic data were marked by numerous small diapir-like features. They occur throughout the entire larger dumpsite area but were best observed where the upper units are very thin or locally absent (Figure 6.8-left). The acoustically turbid features are roughly between 10 and 30 m wide (locally up to 50 m) and between 4 and 15 m high. They are mostly buried but occasionally reach up to the seafloor. The features seem to originate in the glacial deposits of Unit 6. Most likely they are related to dewatering phenomena related to an increasing sediment load causing overpressure within the pores of the deeper water-saturated sediments which finally leads to an expulsion of fluids, possibly in combination with gas (Missiaen & Noppe 2008, Noppe 2007). Similar features were observed in the Baltic by Winterhalter (2001). These shallow fluid expulsion features may form a possible hazard (be it small) with regards to the dumped weapons as they provide fast upward transport and spreading of the toxic compounds that are leaking from the buried munition.

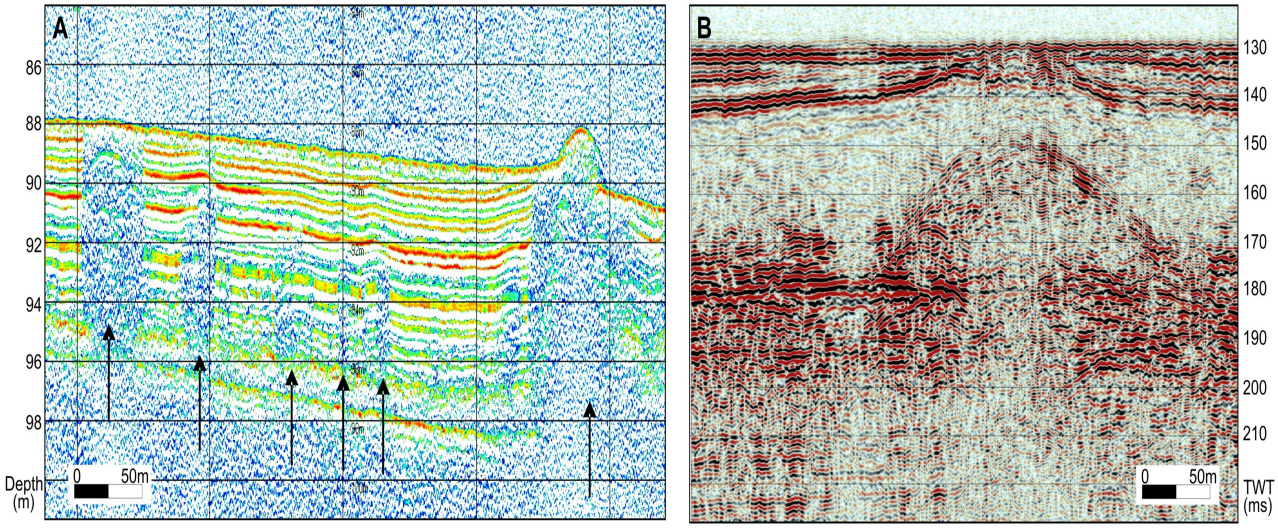

Figure 6.8 *Left: Parametric echosounder profile (10 kHz) showing small-scale sediment mobilisation features (marked by black arrows) presumably related to dewatering phenomena. Right: Sparker profile showing large-scale sediment disruption presumably related to faulting. For location see Figure 6.5.*

In addition to the small-scale fluid expulsion features a number of large sediment disruption features were observed in the north-eastern part of the primary dumpsite area. The dome-like structures are between 200 and 300 m wide and up to 20 m high (Figure 6.8-right). Similar to the dewatering structures discussed above these large dome structures are acoustically turbid and seem to originate in Unit 6 (Missiaen & Noppe 2006, 2008, Noppe 2007). Their linear alignment (along a NW-SE oriented line) suggests a possible relation to tectonic faulting. Indeed the dumpsite area is located near the easternmost edge of the Thornquist fault zone, in the prolongation of a major NW-SE oriented fault. Most likely these large sediment mobilisation structures will have little effect on the dumped weapons and the migration of munition-related toxic compounds.

6.6.3 Acoustic artefacts

During the 2006 survey a large number of 'object-like' features were observed below the seafloor. At first it was believed that these features could be related to buried objects. However their shape (often very large, 10 m or more) and variable depth (between 1 and 15 m bsf) seem to suggest that they are probably the result of an acoustic artefact related to schools of fish. This is most likely caused by the interference of downgoing and upgoing acoustic signals. In order to enhance the resolution of the acoustic image a high ping rate was used (so-called "deep-sea mode") whereby a new signal is sent out before the arrival of the preceding signal. Schools of fish present in the upper part of the water column may thus create an echo in the shallow subsurface data (Figure 6.9). The restricted recording window of the echosounder data (maximum 25-30 m) did not allow to view the entire water column. Close inspection of concurrent sparker data however indicated the presence of schools of fish in the upper part of the water column directly above the presumed object, confirming the above hypothesis related to acoustic artefacts (Missiaen & Feller 2008).

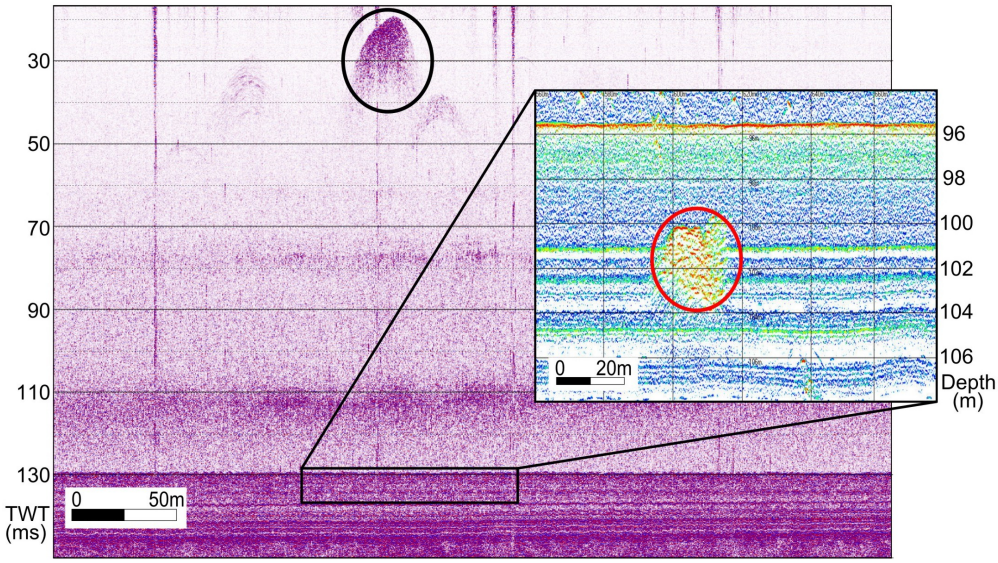

Figure 6.9 *Sparker profile showing the presence of a school of fish in the upper part of the water column (black circle) directly above an object-like feature (the feature is not visible on the sparker data). The inset on the right shows the concurrent parametric echosounder profile; the object-like feature below the seafloor stands out clearly. The presumed object is most likely no more than an acoustic artefact related to the school of fish. For location of the profile see Figure 6.5.*

6.6.4 Submerged wrecks

The presence of four shipwrecks had been indicated by previous magnetic observations (Paka & Spridonov 2001) (see §6.4.2). In 2006 the primary dumpsite area was covered by dense acoustic networks (see Figure 6.5). The wrecks stood out markedly on the parametric echosounder data, in particular the high-frequency records, whereas on the sparker records they were sometimes barely visible (Figure 6.10). Although this is certainly a result of the lower frequencies involved, the lateral offset between sparker and echosounder data may also have affected the acoustic image. The wrecks are all located in the southern part of the primary dumpsite area (see Figure 6.5). The length of the wrecks varies roughly between 20 and 50 m for a width of 5 to 10 m.

Figure 6.10 shows acoustic profiles obtained in 2006 over the different wrecks. Wreck 1, and possibly also wreck 2, seems to be broken up lengthwise (Figure 6.10 top left). Their close proximity (<50 m) suggests that they might represent different pieces of the same ship. Wrecks 3 and 4 seem to be in one piece (Figure 6.10 top and bottom right). The wrecks are marked by strong diffractions, possibly caused by sharp protruding objects (such as the missile observed on the ROV video image of wreck 2, see Figure 6.4) or wreck parts which are not directly below the transducer. Some relation to fish cannot be excluded (this may be the case for the weak 'cloud-like' diffractions (in green) above wrecks 1 and 2) - indeed it is well known that wreck sites attract fish. The large and numerous diffractions observed near wreck 3 may be related to the fishing nets and floaters as observed on the ROV video images (see Figure 6.4).

It is difficult to deduce the exact height of the wrecks from the acoustic data due to the disturbance by indirect reflections. Conservative estimates indicate an average height above the seafloor (not including long protruding parts) of roughly 1-2 m. This confirms the fact that the height of wreck 3 as observed on the multibeam data (Figure 6.3) is probably exaggerated, most likely due to the presence of fishing nets and attached floaters (see §6.4.2).

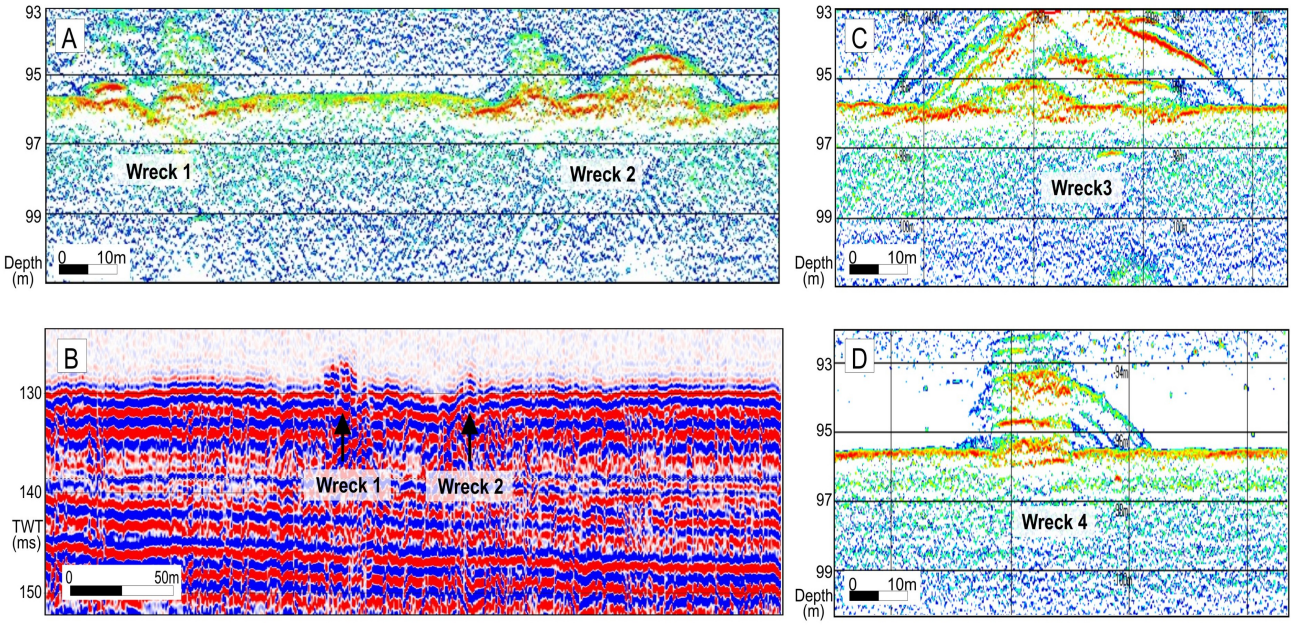

Figure 6.10 *Acoustic images of the shipwrecks obtained in 2006 (for location see Figure 6.5). Top left: Echosounder image (100 kHz) of wrecks 1 and 2. Both wrecks seem to be broken up. Reflections above the wrecks may be caused by small parts sticking out although some relation to fish cannot be excluded. Bottom left: Concurrent sparker image. The wrecks are sometimes barely visible. Wreck 2 is less pronounced, possibly this is due to the lateral offset between the sparker and echosounder data. Right top and bottom: Echosounder images (100 kHz) of wrecks 3 and 4. The wrecks seem to be in one piece. The large diffractions above wreck 3 are possibly caused by fishing nets and attached floaters. (after Missiaen & Feller 2008)*

In most cases no marked scouring features were observed near the wrecks on the acoustic data, which seems to confirm the relatively weak bottom currents in the Bornholm Basin (see §6.3.1). Some weak scouring was observed near wreck 3. The location of the scour features, along the eastern edge of the wreck, agrees well with the scouring observed on the multibeam data (Figure 6.3) and indicates a flow direction roughly parallel to the wreck orientation (WNW-ESE). This

confirms the main current direction in the bottom layer. However some local effects related to periodic turbulence in the near-bottom water cannot be ruled out.

Wrecks 1 and 2 were also covered by the dense seismic-magnetic grid in 2007 (see Figure 6.6). Reducing the recording window of the echosounder data allowed to resolve the shipwrecks in much higher detail. Figures 6.11 and 6.12 (bottom) show different echosounder profiles (100 kHz) over the two wrecks. The three successive profiles across wreck 2 have a line spacing of roughly 10 m. The images indicate that the wrecks are only partly covered by a thin layer of sediments. Towards the edges the sediment cover increases and lower parts of the wrecks are largely filled with soft sediments. No clear scouring features are observed around the wrecks. The strong reflections observed in the water column above the wrecks are most likely caused by different reflections from the irregular surface and various protruding parts, possibly also from wreck parts that are not exactly below the transducer. The exact depth of the wrecks below the seafloor cannot be deduced from the acoustic data. Several small diffractions show up below the seafloor near wreck 1 (Figure 6.12 bottom) but these are likely due to multiple reflections from different submerged wreck parts. The shallow reflectors observed to the right of wreck 1 may be related to small detached pieces of the wreck.

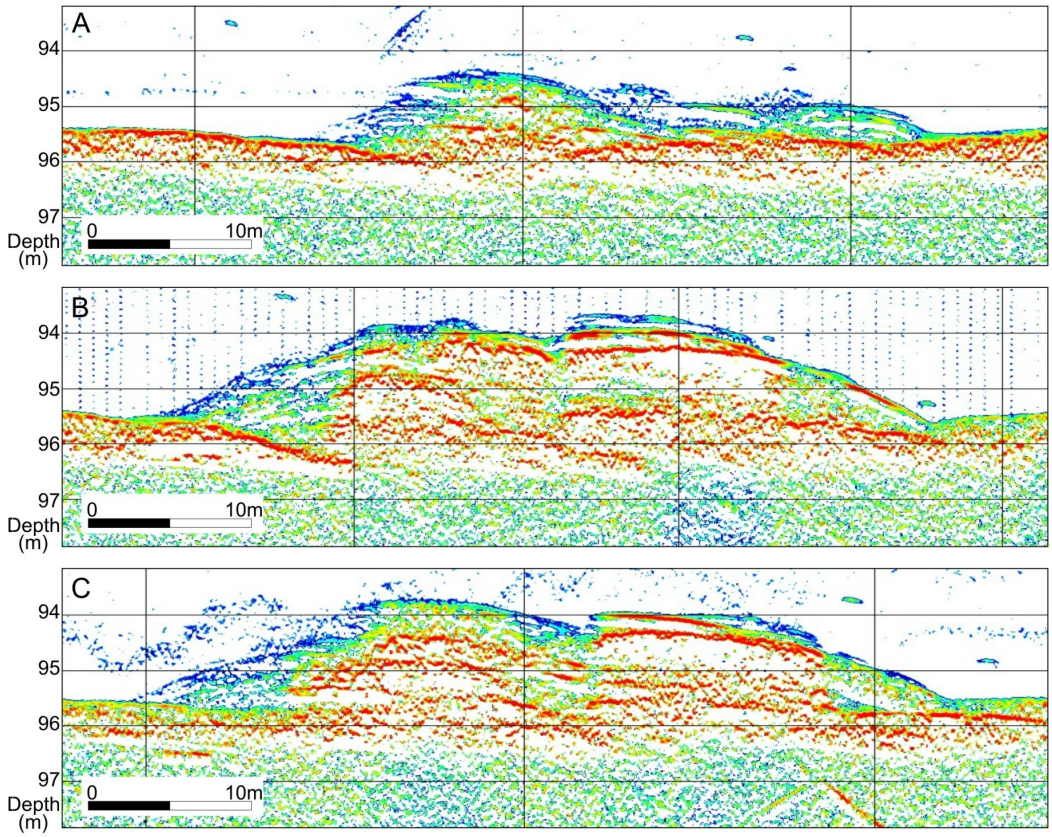

Figure 6.11 *Parametric echosounder profiles (100 kHz) over wreck 2 with 10 m spacing (2007 data). For location see Figures 6.5 & 6.12. The wreck is partly covered by soft sediments (marked by blue-green colour), increasing in thickness near the edges and in the lower parts. The height of the wreck above the seafloor most likely does not exceed 2 m. The numerous strong reflections and diffractions are probably related to the irregular form of the wreck and various protruding parts. The 'wave-like' features in the water column of profile C are likely caused by fish. The vertical disturbances in the water column of profile B are due to acoustic noise related to the equipment. The steep reflector below the wreck on profile C is most likely caused by multiple reflection rather than a buried object (after Missiaen & Feller 2008).*

The vertical gradient magnetic data confirm the presence of two submerged shipwrecks (Figure 6.12A). The anomalies seem to agree well with the observations from the acoustic data regarding size, shape and orientation of the wrecks. The magnetic data also indicate the presence of a number of relatively large objects scattered around the shipwrecks, most likely detached wreck pieces. The objects were clearly visible on the parametric echosounder data (Figure 6.12 B).

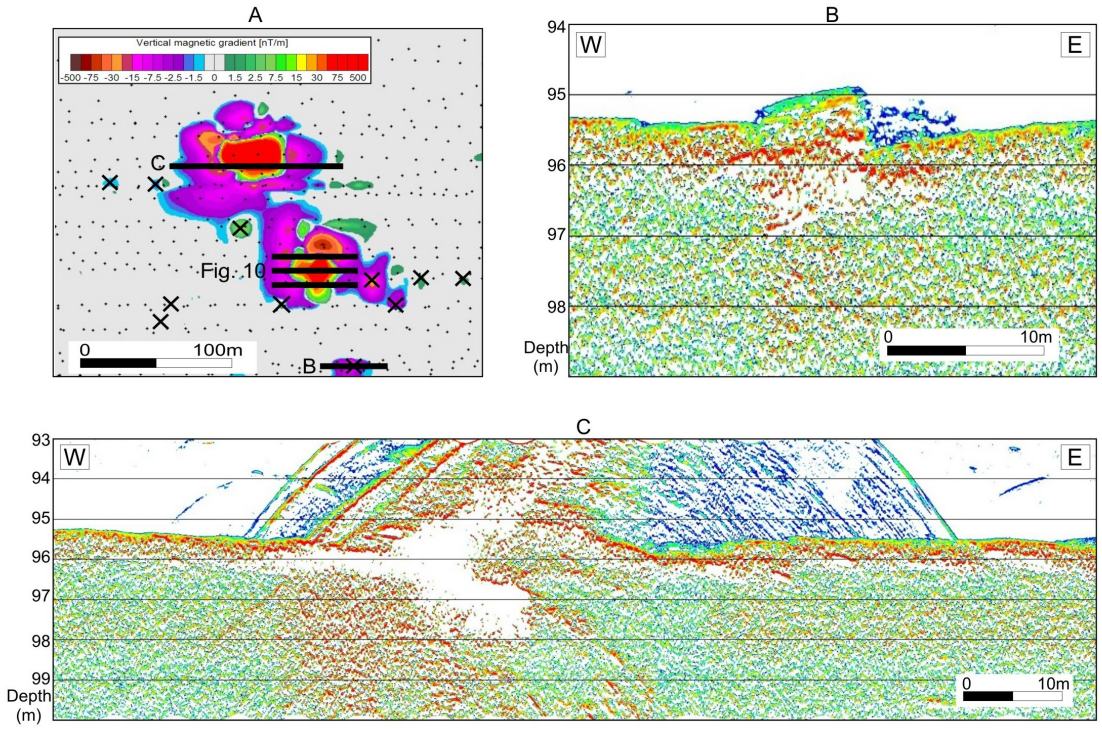

Figure 6.12 *A: Vertical magnetic gradient map from the southern network SM1 covering the immediate wreck area (for location see Figure 6.5). Green and red indicate positive anomalies, purple and blue indicate negative anomalies (unit = nanoTesla per meter). Black crosses mark the locations of detected objects. Thin dotted lines mark the magnetic tracklines. Thick black lines mark the acoustic profiles shown in this figure and in Figure 6.11. B: Parametric echosounder profile (100 kHz) across an object south of wreck 2, possibly a detached wreck piece. The small elevation in the seabed is likely due to local sediment accumulation around the object. Very soft sediments (marked in blue) have filled the small depression on the right. C: Parametric echosounder profile (100 kHz) across wreck 1. The large diffractions are probably due to protruding wreck parts or pieces of the wreck that are not directly below the transducer. The reflectors observed just below the seabed to the right may be related to small detached pieces of the wreck. The average height of the wreck is estimated to be no more than 2 m. (after Missiaen & Feller 2008).*

6.6.5 Buried objects

Reducing the recording window of the echosounder data during the 2007 survey allowed to image the uppermost sediments with the highest detail. On the high-frequency data (100 kHz) the presence of a large number of object-like features was clearly observed in the upper sediments (Figure 6.13). The absence in many cases of clear hyperbolic diffractions is most likely due to the inclination and lateral extent of the object. The objects are generally buried no more than 1 to 2 m below the seafloor. The size of the objects varies generally between 1.5 and 5 m, occasionally up to 10 m or more. Large objects are often accompanied by an irregular seafloor directly above the object.

Although there is no absolute certainty about the origin of the buried objects it seems reasonable to assume that we are dealing here with dumped weapons. The low sedimentation rates in the Bornholm Basin (see §6.3.2) can probably not account for the observed sediment cover. Most likely the recent burial depth is largely due to a gradual sinking of the weapons into the very soft muddy sediments (Missiaen & Feller 2008). In most cases the buried objects appear scattered, although locally clusters of smaller objects can be observed (Figure 6.13C). The seafloor above some of the larger objects is often deformed, showing pit-like structures (Figure 6.13A) and an irregular morphology (Figure 6.13B). These are probably caused by the impact of the dumped material upon hitting the seafloor. The shallow pits are often filled with a layer of very soft or semi-liquid sediments, as suggested by the low amplitude of the infill material.

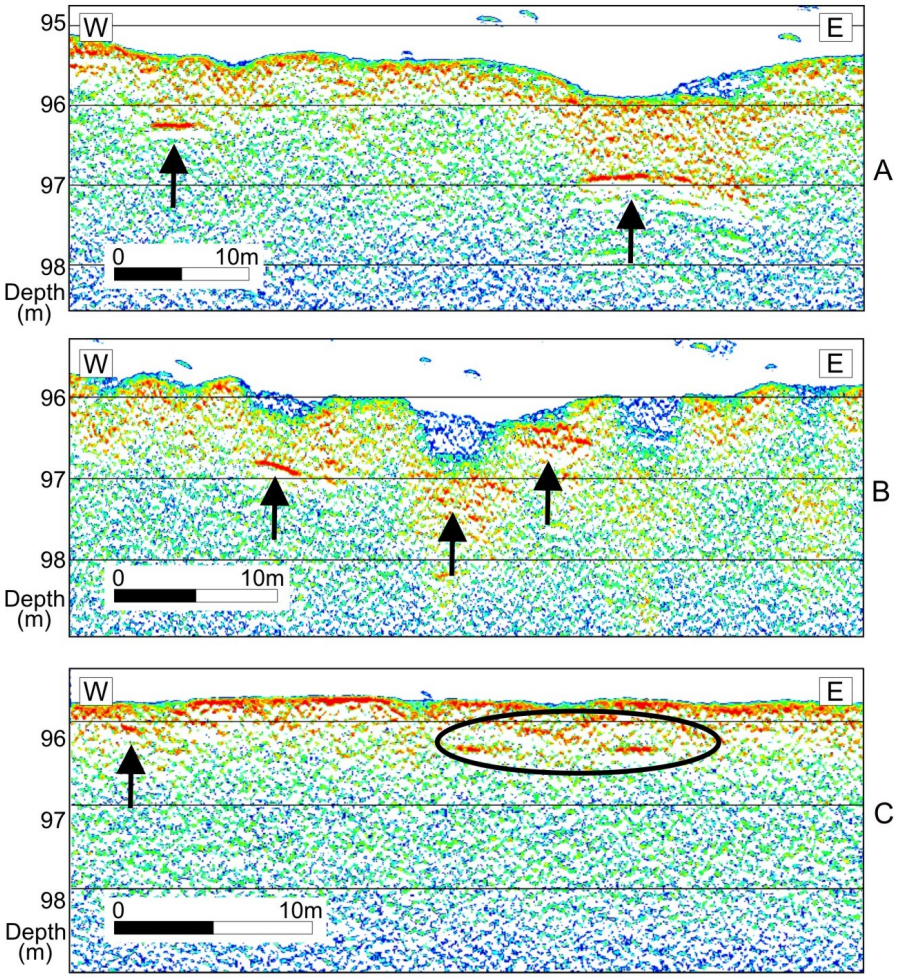

Figure 6.13 *Parametric echosounder profiles (100 kHz) indicating the presence of buried objects (marked by black arrows) (2007 data). For location of the profiles see Figure 6.5. A: Buried objects coinciding with large pit-like structures in the seafloor. This is probably a result of the dumping impact. B: Irregular seafloor morphology above various buried objects. The small pits have become filled with soft sediments (marked in blue). C: Singular shallow object (arrow on the left) and a cluster of shallow objects (ellipse) (after Missiaen & Feller 2008).*

The magnetic data confirm the presence of a large number of iron-containing objects. In many cases the anomalies observed on the magnetic gradient data could also be traced on the echosounder data (Figure 6.14). In some cases however no match was found with the acoustic data. This may be due to different reasons: (1) the object was too small for acoustical detection,

(2) the object orientation was perpendicular to the trackline resulting in a small cross-section, (3) the object was located at a short lateral offset from the trackline and therefore 'missed' by the acoustic signal*, or (4) a local mismatch between the seismic and magnetic data related to the positioning accuracy of the magnetic array (~5 m) (Missiaen & Feller 2008). An advanced corrosion state may also have affected the acoustic visibility. Even closely located objects can be seen to show up as separate magnetic anomalies (Figure 14A&B). However when the objects were too closely located (< 5 m) they generally appeared as one single anomaly (Figure 14A&D).
(The acoustic footprint of the parametric echosounder being very small, roughly 2-3 m for the encountered water depth)*

Comparison of the acoustic data with the magnetic results has revealed that the burial depth calculated from the vertical gradient magnetic data is generally over-estimated. This is mainly due to the fact that most objects are only observed along one single profile (line spacing being roughly 10 m). During data inversion the assumption is made that the object is located exactly below the trackline (since there is no other information from parallel tracks regarding the lateral trend of the object). An object at a few m offset from the profile will yield a lower magnetic gradient than the same object located directly below the trackline, thus resulting in a greater burial depth (the amplitude of the magnetic anomaly decreases with the 3rd power of the distance). The only way to overcome this problem is to apply a closer line spacing (e.g. 5 m) but due to a lack of time this was not possible during the survey (Missiaen & Feller 2008). In practice such precise line spacing is not easily achieved taking into account the long cable length (200 m) involved.

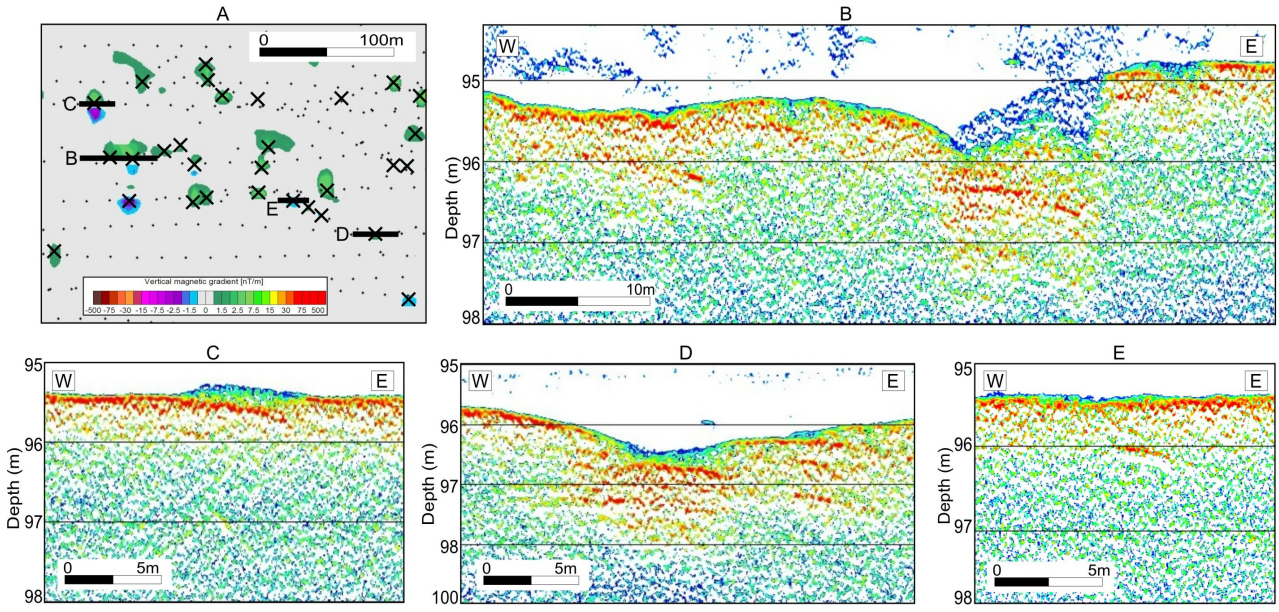

Figure 6.14 *Top: Vertical magnetic gradient data from the northern network SM2 (for location see Figure 6.5). Green and red indicate positive anomalies, purple and blue indicate negative anomalies (unit = nanoTesla/meter). Black crosses mark the locations of detected objects. Thick black lines mark the acoustic profiles shown in this figure. Thin dotted lines mark the magnetic tracklines. B to E: Parametric echosounder profiles (100 kHz) across different buried objects. Fish are occasionally observed in the water column (profiles B, D). Very soft sediments have locally filled shallow pits in the seafloor (profile B). The objects in profile B show up as separate anomalies on the magnetic data. This is not the case for profile D, where the objects are too close and therefore show up as one single magnetic anomaly (after Missiaen & Feller 2008).*

Preliminary estimates from the vertical gradient magnetic data indicate that the mass of the buried objects ranges from 10 kg to over one ton, with the majority of the objects having a mass between 100 and 500 kg. However we should keep in mind that any over-estimation of the vertical distance, as discussed in the previous paragraph, will also lead to over-estimation of the magnetic moment hence mass. Moreover, due to the 3rd power law a small error in computed depth may induce quite large errors in the computation of the magnetic moment. Additional errors in the mass estimation can also be induced by the susceptibility value which was assumed to be 3 in this case (Missiaen & Feller 2008).

6.6.6 Size and distribution of the buried objects

The high diversity, both in shape and in size, of the acoustic features and magnetic anomalies suggests that we are dealing with objects greatly varying in size, weight and shape. This confirms the existing information that a wide variety of war material was dumped in Bornholm Basin, ranging from shells and bombs to large encasements and containers (see Table 6.1). Aircraft bombs have a gross weight between roughly 150 and 330 kg, depending on the type (S. Nehring, personal communication). This gross weight however also includes the chemical content - the real (net) weight of the metal casing ranges between 50 and 120 kg (Fleischer 2003). This is much lower than the average mass estimations from the magnetic data (between 100 and 500 kg). However, as we discussed previously these mass values are in many cases very likely over-estimated.

The size of the aircraft bombs generally does not exceed 1.6 m x 50 cm (S. Nehring, personal communication). Yet most of the objects identified on the acoustic data have a size between 1.5 and 5 m. This disagreement could be due to the fact that small objects are not easily detected and may be overlooked on the acoustic data. The acoustic "visibility" of the object will furthermore depend on the position and orientation of the object with respect to the profile. Objects oriented parallel to the trackline will appear larger (and are therefore easier detected) than objects oriented perpendicular to the trackline. Another possible explanation is that we are often dealing with small clusters of closely packed bombs (and/or shells), possibly cemented together. This could also help to explain the high mass estimations of the detected objects.

Individual artillery shells and mines, with a length around 40 cm and a net weight (= metal casing) between 6 and 13 kg (S. Nehring, personal communication), may be too small to allow unambiguous acoustical detection. In many cases however they should allow magnetic detection (theoretically, an array towed 5 m above the seabed will detect objects with a mass less than 10 kg and buried 0-1 m below the seabed) (Missiaen & Feller 2007). Large objects on the acoustic data (well over 2 m) are likely related to large encasements and containers. These can have a gross weight up to 1.5 tons (Politz 1994). Their metal casing is relatively thin compared to the amount of stored toxic compounds which make up the largest part of the gross weight (HELCOM 1993h). This difference between gross and net weight may explain why large objects identified on the acoustic data do not always coincide with large magnetic gradients and mass estimates (Missiaen & Feller 2008).

The object density differs a lot between the two seismic-magnetic networks. Over 440 buried objects were identified in the northern network SM2 (density of 460 objects/km^2) in contrast to the southern network SM1, covering the wrecks, where just over 40 objects were identified (density of 60 objects/km^2). According to the Russian report submitted to HELCOM in 1993 the total amount of war material dumped in the Bornholm Basin by the Soviet Union amounts to over 560,000 objects (HELCOM 1993h). The main part involves artillery shells (over 380,000) and bombs (over 100,000). If we assume that the majority of the war material (e.g. 80%) is

located in the primary dumpsite area we obtain a mean distribution of roughly 4400 objects per km^2. This is almost 10 times the object density observed for network SM2. This would suggest that large parts of the dumpsite have an even much higher object density than our data suggest.

However there are a number of reasons that could explain at least part of this disagreement between the observed and assumed object density: (1) very small objects (mass well below 10 kg) are likely not detected whereas these objects make up a substantial part of the dumped material, (2) small objects (mass 10-20 kg) located in the middle between two tracklines (± 1 m) will not be detected, (3) objects that are cemented together or located too close (less than a few m, depending on the mass) will show up as one single magnetic anomaly, and (4) the amount of war material located outside the primary dumpsite area is much larger than assumed (Missiaen & Feller 2008). As we have seen in chapter 4 most of the munition caught by fishermen near Bornholm was heavily corroded (§4.4). An advanced state of corrosion will reduce the detectability of the object (as it changes the magnetic susceptibility), but this effect is believed to be rather limited - although it may hinder the detection of small objects. Still all this does not alter the fact that the distribution of war material in the Bornholm dumpsite area is very heterogeneous, most likely marked by areas of high object density alternating with zones where the objects are spread very thinly.

6.7 Summary and conclusions

After WW2 over 32,000 tons of chemical weapons were dumped east of Bornholm in the southern Baltic. The dumping operation took place primarily inside a circular area with a radius of 3 nautical miles but it is likely that the dumped war material is spread over a considerably larger area. Chemical analysis of water and sediment samples has revealed locally high arsenic levels, also in the vicinity of the shipwrecks, suggesting that some wrecks may contain CW. In 2006 and 2007 high-resolution seismic surveys, combined with magnetic investigations, were carried out. Simultaneous deployment of different acoustic sources resulted in detailed information on the internal structure of the dumpsite. Seven seismic stratigraphic units were identified related to different stages in the Holocene and late-glacial history. A large number of diapir-like features were observed which are most likely related to dewatering phenomena. These could pose a possible hazard with regards to the migration of munition-related toxic compounds.

Four shipwrecks were identified in the area. All wrecks stood out clearly on the parametric echosounder data, their length ranging between 20 and 50 m (width 5 to 10 m) with a height above the seafloor of roughly 1 to 2 m. Two wrecks seem to have broken apart. Clear scouring features were mostly absent, probably a result of the weak bottom currents. The wrecks are partly covered by a thin layer of soft sediments. The acoustic data indicate that the wreck surfaces are highly irregular. The precise outline of the wrecks is obscured by reflections from various protruding parts or wreck parts that are not exactly below the transducer. Objects identified in the vicinity of the wrecks most likely represent wreck pieces that have become detached.

A large number of buried objects were observed on the acoustic data. The objects are generally buried no more than 1 to 2 m below the seafloor, their size varies roughly between 1.5 and 5 m, occasionally up to 10 m. Shallow pits in the seabed above some of the objects are probably due to the impact of dumping. The magnetic vertical gradient data confirm the presence of numerous metal objects. In many cases the anomalies could be traced on the acoustic data. Local discrepancies were probably due to the limited size of some objects or a small mismatch in positions. Large objects identified on the acoustic data did not always coincide with large

magnetic anomalies. This was most likely due to the fact that toxic agents make up a large part of the gross weight of these objects.

The distribution of dumped warfare seems to be very heterogeneous, with locally high object concentrations surrounded by areas with relatively few objects. The acoustic and magnetic data furthermore confirm the wide variety of dumped war material ranging from shells and bombs to encasements and containers. Individual shells or mines were most likely too small to allow unambiguous acoustic detection.

The results of this case study clearly illustrate once more the benefit of complementary geophysical investigations for munition dumpsite research. Ultra-high resolution seismic profiling and concurrent magnetic acquisition at the Bornholm munition dumpsite has not only allowed to map the exact location, distribution and burial depth of the scattered war material (in two designated areas), but it has also allowed to gain more insight into the diversity and type of dumped weapons. Combined with the detailed information on the internal geological structure, including potential natural hazards, that was obtained from acoustic imaging this will yield a better assessment of the current status of the dumpsite and the possible ecological risks related to the dumped war material.

CHAPTER 7
ARCHAEOLOGICAL SITE INVESTIGATIONS

7.1 Introduction

Over the last decades marine geophysical techniques have been used in the investigation of archaeological sites (e.g. Rao 1988, Hobbs et al. 1994, Quinn et al. 1997a/b, Quinn et al. 2002). The most commonly applied techniques include side-scan sonar and echosounder systems to identify archaeological artefacts lying on the seabed. Often the technology behind this instrumentation was primarily developed for military and commercial purposes, but the techniques have been increasingly adopted in site-specific archaeological surveys. Yet their main disadvantage is that they cannot penetrate the subsurface and are unable to image buried objects.

The application of marine reflection seismic profiling for the detection of buried archaeological artefacts (in particular wooden shipwrecks) was long restricted by poor resolution and the difficulties to image the seabed and shallow subsurface in very shallow water depths. The recent advances in VHR subbottom imaging in shallow water environments, however, make this technique an ideal tool for rapid site assessment and site delineation prior to more detailed in-situ surveys. The rapidly increasing development of coastal areas and continental shelves forms a potential threat for these archaeological wreck sites. Since the late eighties there has been a sharp increase in research into the location and identification of archaeological shipwrecks using seismic techniques (a.o. Quinn et al. 1997a, Bull et al. 1998, Quinn et al. 2000).

In this thesis the results of two seismic surveys over buried wooden shipwreck sites will be discussed, using both 2D and 3D techniques. The 2D survey was carried out on the river Schelde using a Seistec boomer system. The 3D survey took place in the Dutch Wadden Sea, using the inflatable 3D acquisition system (described in chapter 2) and a 3.5 kHz echosounder. The use of 3D techniques for offshore archaeological site surveys is quite novel. In the past, pseudo 3D investigations have been carried out over a few wreck sites (e.g. Quinn et al. 1997b). Very recently 3D seismic studies were conducted in Germany and Turkey to investigate ancient settlement structures, but the results so far are not conclusive (Müller et al. 2006, Müller et al. 2007).

The latest developments in archaeological studies increasingly focus on pre-historic archaeology, in particular the impact of human activities on submerged terrestrial landscapes (Westley et al. 2004, Lafferty et al. 2006). The reconstruction of paleo-landscapes is not only an important requirement to help understand their archaeological potential (such as submerged or re-worked material) but it may also provide key information on the human evolution. Sea-levels were generally much lower in late Pleistocene and early Holocene times and only reached near-present levels during the later part of the Holocene. Recently seismic studies haven been carried out offshore the Belgian coast, between Oostende and Nieuwpoort, to study the possible remains of Roman dykes and salt/peat exploitation, and the distribution of the pre-Roman tidal gully system (Missiaen et al. 2008b). This should lead to a better understanding of the complex late Holocene evolution of the coastal area and the human impact on this region.

7.2 Acoustic detection of archaeological wood

The ability to image wooden objects in the seafloor will largely depend upon the acoustic impedance contrast between the object and the surrounding sediment, which in turn will determine the reflection strength. The latter is defined by the reflection coefficient $R = (V_2\rho_2 - V_1\rho_1)/(V_2\rho_2 + V_1\rho_1)$ where ρ_1,ρ_2 and V_1,V_2 refer to the density and compressional velocity of wood and sediment respectively (the product of density and compressional velocity is called impedance). Typical subsurface values of R are generally in the range of ±0.1 (Anstey 1981). In marine archaeological situations, values of R may have a broader range due to possible higher acoustic impedance contrasts between wooden artefacts and the surrounding sediments (Quinn et al. 1997a). Typical values for density, compressional sound speed and impedance are given in Table 7.1 (Anderson & Hampton 1980, Quinn et al. 1997a). The sediments are unconsolidated and gas-free. Mud consists of various components (sand, silt, clay) with a different composition, and it can therefore exhibit a large variation in acoustic characteristics. As a result the impedance contrast with buried wooden objects will be able to vary strongly.

	density (kg/m^3)	velocity (m/s)	impedance ($10^3 kg/m^2s$)
oak	660	1230-3120	810-2050
water	1000	1450	1450
mud	1200	1500	1800
clay	1450	1500	2200
sand	2000	1700	3400

Table 7.1 *Acoustic characteristics of different media (at 10 kHz). The sediments are unconsolidated and considered gas-free (Anderson & Hampton 1980, Quinn et al. 1997a.)*

Theoretical and experimental studies have indicated that reflection coefficients from wood buried in unconsolidated marine sediments are often large and negative, their exact magnitude depending upon the wood species, sediment type, and exposure histories (Quinn et al. 1997a/b, Bull et al. 1998). The impedance contrast will also depend on the orientation of the incident acoustic wave. Compressional wave velocities parallel to the trunk of the tree (V_L) are consistently higher than wave velocities perpendicular to the growth of the rings (V_R) and parallel to the rings (V_T) (Figure 7.1) (Quinn et al. 1997b). Tests on dried oak wood samples from the *Mary Rose* wreck site in the East Solent indicate that $V_L >> V_R > V_T$ (Arnott et al. 2005). Since the dominant ship-building timbers are plain wooden boards, it is likely that the radial and tangential directions will be insonified during subbottom profiling (presuming the wreck is relatively undisturbed) (Arnott et al. 2005).

The above results apply to air-dried samples, whereas submerged wood is fully saturated and most likely degraded. This degradation is caused by fungi and bacteria and often requires a minimum oxygen level, although some bacteria are known to have a high tolerance to low oxygen (Blanchette 2000). In oxygen-rich marine environments soft rot fungi will often be the dominant wood degrading mechanism; when oxygen becomes scarce the degradation will mainly be due to erosion and tunnelling bacteria (Figure 7.2-left) (Jurgens et al. 2003). Burial in marine sediments will severely restrict the oxygen supply, which is expected to limit the progression of degradation (Figure 7.2-right). Studies of the *Uluburun* shipwreck, a late Bronze Age ship thank sunk off the Turkish coast approximately 1400 BC, have indicated that sections of the hull that were buried in sediment survived for several thousand years (Blanchette 2000). In addition, the presence of copper and other metals products may have an inhibitory effect on microbial growth and help in the preservation of the wood (Jurgens et al. 2003).

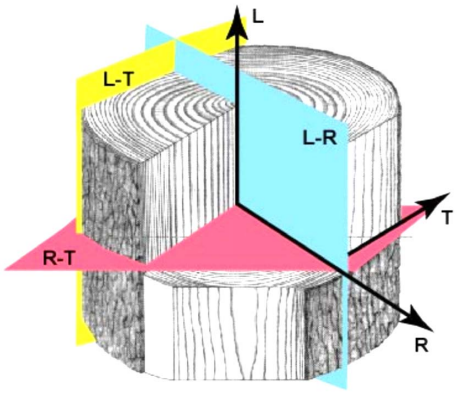

Figure 7.1 *Acoustic transmission directions in wood. L = longitudinal, R = radial, T = tangential. Acoustic measurements on dried samples suggest $V_L >> V_R > V_T$ (Arnott et al. 2005).*

In order to predict the reflection coefficients of wood in a variety of states of degradation, measurements of compressional wave speed and density have been carried out on oak and pine samples (Arnott et al. 2005). Historically, oak and pine were the prime choices for construction material for pre-nineteenth century wooden ships in Europe (McGrail 1998). Although the experiments involved a central frequency of 800 kHz, the results are likely to be a good indication of what can be expected in the field using typical sub-bottom profiling systems (Arnott et al. 2005).

The results of the experiments indicate that oak and pine are mostly detectable when buried in a variety of marine sediments, with sandy sediments generally giving rise to stronger negative reflections than sand-silt-clay mixtures and clay and the reflection coefficients becoming more negative with increasingly degraded samples (Arnott et al. 2005). Pine generally has lower reflection coefficients than oak owing to its lower bulk density. In some cases, for example moderately degraded oak buried in clay, the reflection coefficients are very small and impedance contrast is likely insufficient for detection. Wood exposed on the seafloor usually has sufficient impedance contrast for detection, unless it is heavily degraded in which case the reflection coefficient decreases almost to zero (Arnott et al. 2005).

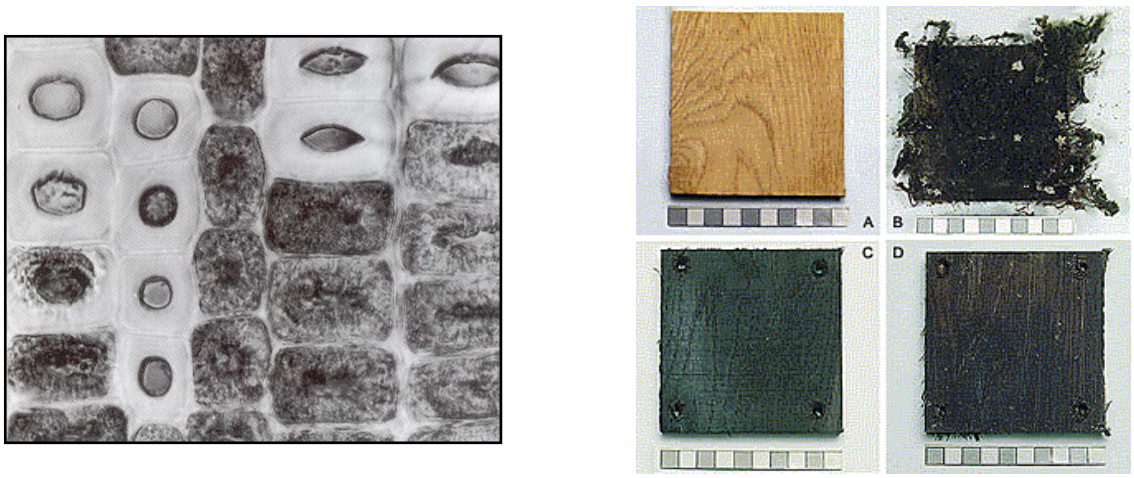

Figure 7.2 *Left: Wood cells degraded by erosion bacteria. Advanced levels of decay create a typical pattern of heavily degraded cells adjacent to apparently sound tracheids (after Björdal et al. 2003). Right: Series of photographs showing wood samples after exposure to various environments: A) Control wood sample, B) Wood sample exposed to seawater for 32 weeks, C) Wood sample buried 1 cm below the seabed for 52 weeks, D) Wood sample buried 50 cm below the seabed for 52 weeks (after Gregory 1999).*

The ability to image buried wooden artefacts will not only depend on the impedance contrast, but also on the size of the object. Acoustic reflections from a shipwreck will mainly be caused by long boards. To allow detection the wavelength of the seismic signal should therefore not be much bigger than the thickness of the boards, i.e. of the order of decimeters. In our case, working with main frequencies >2 kHz this will most likely not be a problem. Furthermore the growth of algae or shells on the wooden boards may increase the impedance contrast.

It is possible that the sediment nearby the wreck differs from the surroundings due to eroded and decayed wood fragments. Caston (1979) identified longitudinal scour pits around wreck obstacles; the scour pits are shallow (1-2 m) relative to their widths and lengths and depending on the peak tidal flow and the orientation of the shipwreck single or double scour marks may occur. In time these scour features may become filled in and buried. Paleo-scour features observed at the *Mary Rose* wreck site were thought to be due to fill material including wreck fragments and coarse grained sediment (Quinn et al. 1997b). The dimensions of the scour features (often much larger than the wreck itself) may make them more easily recognized on sub-bottom profiles. In the extreme case of a completely degraded wreck, no longer detectable by reflection profiling, or excavation of the wreck, the scour pits may form the only remaining evidence of the wreck site (Quinn et al. 1997b).

7.3 2D case study – Schelde river, Antwerpen

7.3.1 Introduction

In October 2004 a geophysical survey was carried out on the river Schelde, north of Antwerpen (Figure 7.3). Target of the survey was a small wooden shipwreck (15-20 m long), presumably of the 17th century. In the recent past the wreck had been damaged by dredging operations and was most likely broken up in pieces (Missiaen et al. 2004). Multibeam investigations in the area indicate that the wreck is now completely buried. Water depths in the area vary between 8 and 12 m, depending on the tide.

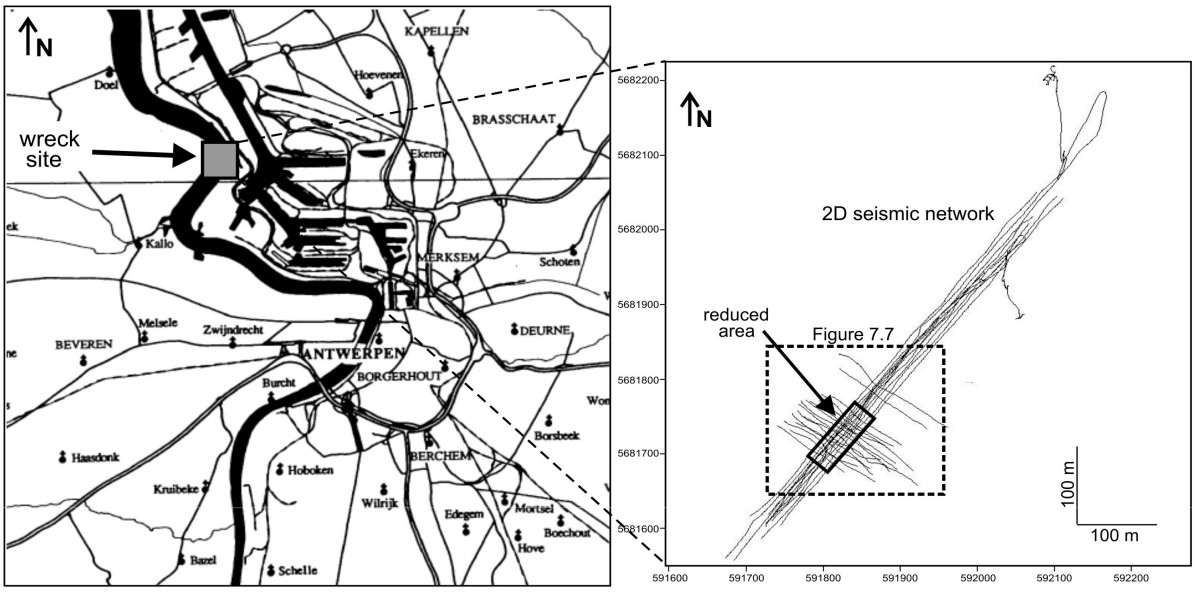

Figure 7.3 *Location of the wooden shipwreck site on the river Schelde (left) and 2D seismic network acquired over the wreck area (right). The full black rectangle marks the reduced area for pseudo-3D processing. The dashed black rectangle marks the area shown in Figure 7.7. Coordinates in UTM-ED50.*

7.3.2 Data acquisition

The seismic measurements were carried out using the Seistec boomer (shot interval 0.75 s, record length 50 ms, sampling frequency 20 kHz). In total 31 seismic profiles were recorded over the wreck site (Figure 7.3). During the survey the source was attached to the side of the boat to reduce engine noise. Average profile spacing ranged between 5 and 10 m. Average profile length was ~600 m for the longitudinal lines and ~100 m for the cross lines. Due to the high current and low vessel speed regular profile spacing could not always be achieved. The longitudinal profiles were recorded sailing against the current in order to assure a low enough velocity (max. 3 knots). Strong side currents forced the lateral profiles to be recorded with a higher vessel speed in order to allow correct steering, and as a result these profiles have a reduced lateral resolution.

Seismic penetration in the surveyed area was very limited. Northeast of the wreck area a thin upper layer of sediments (< 2 m thick) is observed, most likely soft mud-rich sediments, which wedges out towards the actual wreck site (Figure 7.4). In this layer several shallow reflectors are visible, possibly related to thin layers of sandy or silty material (Missiaen et al. 2004, Missiaen & Versteeg 2006). Further down the seismic facies becomes more chaotic, with locally some weak discontinuous reflectors. The wreck area itself is marked by large ripple-like features on the river bottom, with amplitudes of roughly 20-25 cm and wavelengths up to 10-20 m (Figure 7.4). This seems to suggest that the poor penetration is also related to an increase in sandy material.

On several profiles a number of short, strong reflectors can be seen which do not follow the bottom morphology (Figure 7.4). Below these reflectors the seismic signal is attenuated, which seems to indicate the presence of an object. The reflectors are marked by a clear phase inversion. As we have seen in the previous section (§7.2) a large negative reflection coefficient is typical for wooden objects (in particular oak) buried in sandy sediments. Still, phase reversal could also be a sign of local gas accumulation (see chapter 8), but the size and appearance of the reflectors and their shallow depth suggest that we are most likely dealing with buried wood. The high amplitudes seem to indicate that the wood is heavily degraded, which is not surprising considering the age of the wreck. The wooden wreck parts are buried under a thin (~0.5 m) sediment cover. In total six different wreck parts were identified in the surveyed area (Figure 7.5) (Missiaen et al. 2004).

7.3.3 Pseudo-3D processing

In order to see if pseudo-3D processing of the single-channel data was feasible we focused on the central part of the surveyed area (approx. 80 x 40 m) where line coverage was dense (see Figure 7.3) (we rather refer to ‘pseudo-3D’ instead of ‘3D’ because no real 3D data were recorded). The distribution of shotpoints in this reduced area is shown in Figure 7.6-left. Different coverage maps were calculated for bin sizes of resp. 1x1 m, 2x2 m, and 3x3 m. Due to the large difference in shotpoint spacing between the inline and crossline direction (resp. 0.5-1 m and 5-10 m) the coverage was very heterogeneous. The smallest bin size of 1x1 m resulted in extremely low coverage marked by numerous empty bins. The larger bin size of 2x2 m showed better coverage although still with some empty bins (Figure 7.6-right). The 3x3 m bin size resulted in the highest coverage, but the large size of the bin cells ($9m^2$) was considered not suitable in view of the size of the wreck pieces (varying between 5 m and 25 m in length) and the high vertical resolution causing an easy mismatch between the bin traces. It was therefore decided to use the 2x2 m bin size for further processing.

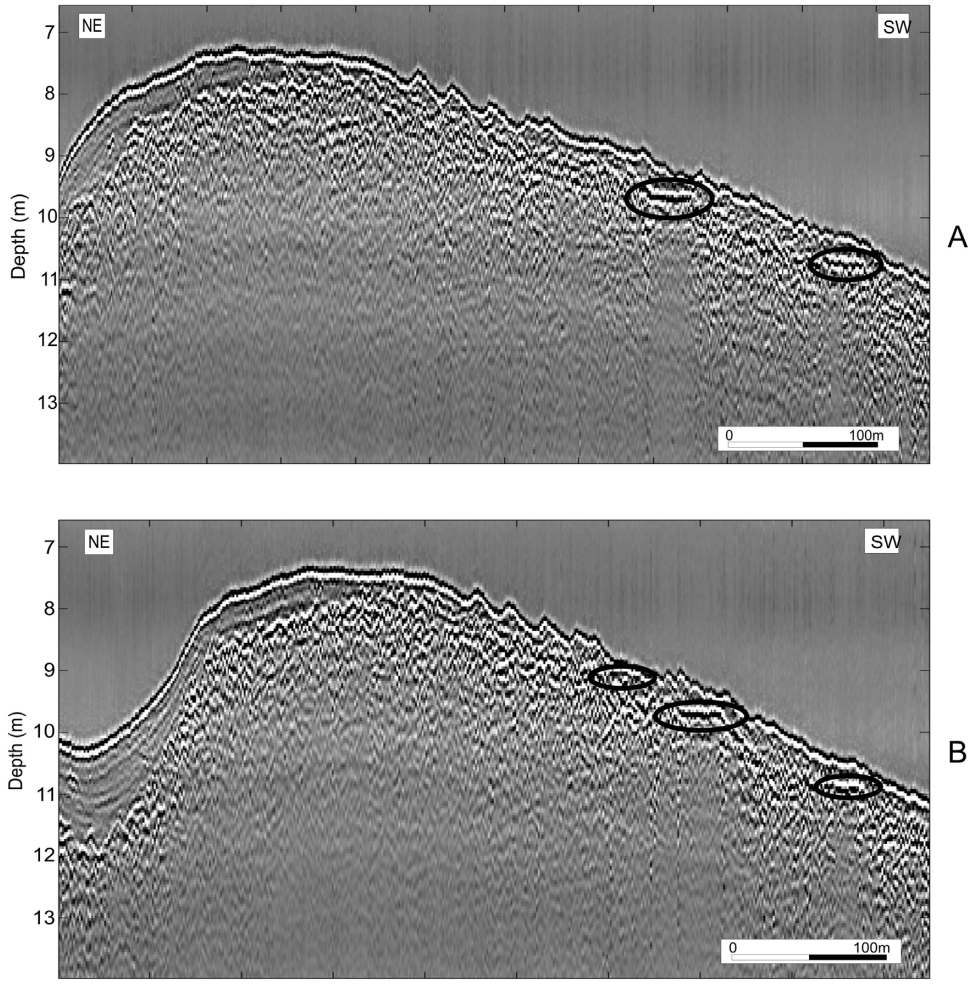

Figure 7.4 *Seismic profiles across the wreck site showing evidence of buried objects (marked by ovals), most likely wooden wreck parts (for location of the profiles see Figure 7.5). Notice the marked phase inversion of the wreck reflectors. Depth conversion was carried out using a sound velocity of 1500 m/s.*

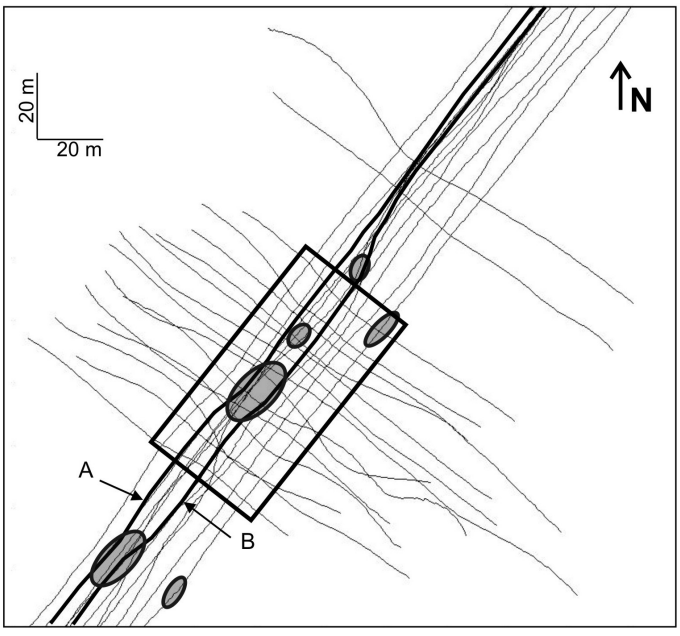

Figure 7.5 *Distribution of wreck parts in the survey area (black ovals). Thick black lines mark the profiles shown in Figure 7.4. The rectangle marks the reduced area for pseudo-3D processing.*

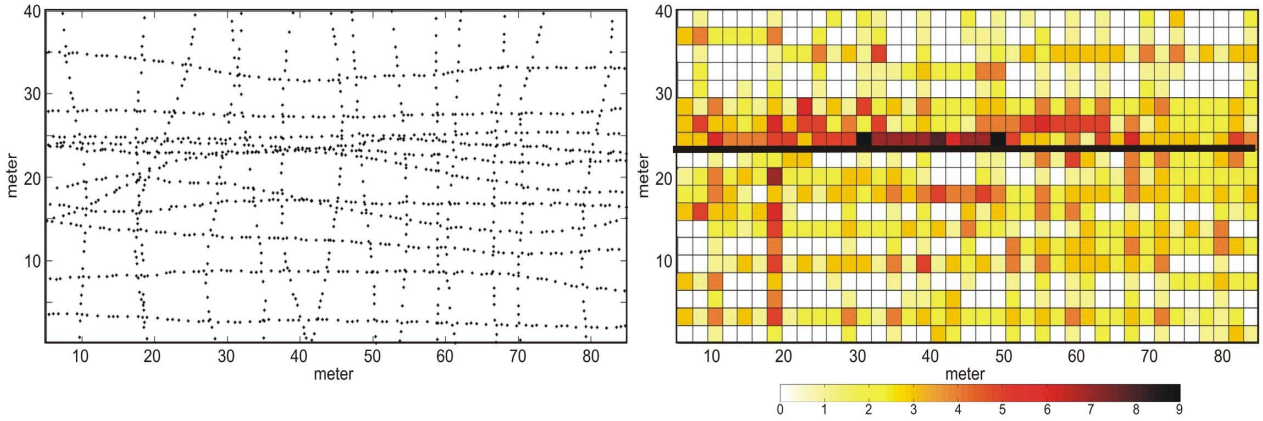

Figure 7.6 *Shotpoint distribution (left) and stack fold coverage for 2x2 m bin size (right) over the reduced wreck area (for location see Figure 7.5). Due to the large crossline spacing the coverage is very heterogeneous. The thick black line indicates the vertical cross-section shown in Figure 7.8.*

Preliminary data processing included bandpass filtering, agc and deconvolution. No swell filtering was needed due to the calm river environment. Still small positioning errors were possible due bottom ripples and minor wave action caused by ship traffic. Multibeam data, recorded simultaneously during the survey, were used to carry out vertical corrections to the 2D seismic data (each trace being shifted so as to overlap the seismic first arrival with the multibeam first arrival). Figure 7.7 compares river bottom data obtained from the seismic data and the multibeam data. Differences could locally mount up to as much as 20 cm (~0.3 ms).

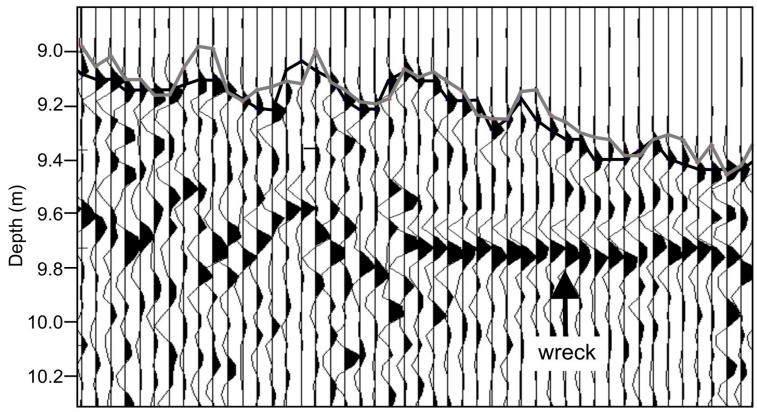

Figure 7.7 *Picking of first break arrivals. Black line = picks from the seismic data. Grey line = picks from the multibeam data. The horizontal reflector on the right marks a wreck piece.*

The data were stacked with a bin grid of 2x2 m. The results after stacking are shown in Figures 7.8 & 7.9. Due to the relatively large bin size the resolution is rather low. The effect of static corrections is evident on the vertical cross-sections (Figure 7.8). Whereas the raw stacked data are very chaotic and marked by a highly irregular seafloor reflector, the corrected data show a better line-up and more continuous seafloor. Still adjacent traces are often marked by small vertical offsets. The presence of a buried wreck part (marked in red) is suggested but remains rather ambiguous. Figure 7.9 shows a series of depth slices at ~20 cm interval. Again the presence of a buried wreck part (marked in red) is suggested but the image is lacks coherence. Most likely the combination of low data coverage and large bin size, causing vertical and horizontal positioning inaccuracies, has prevented correct imaging of the buried wreck parts.

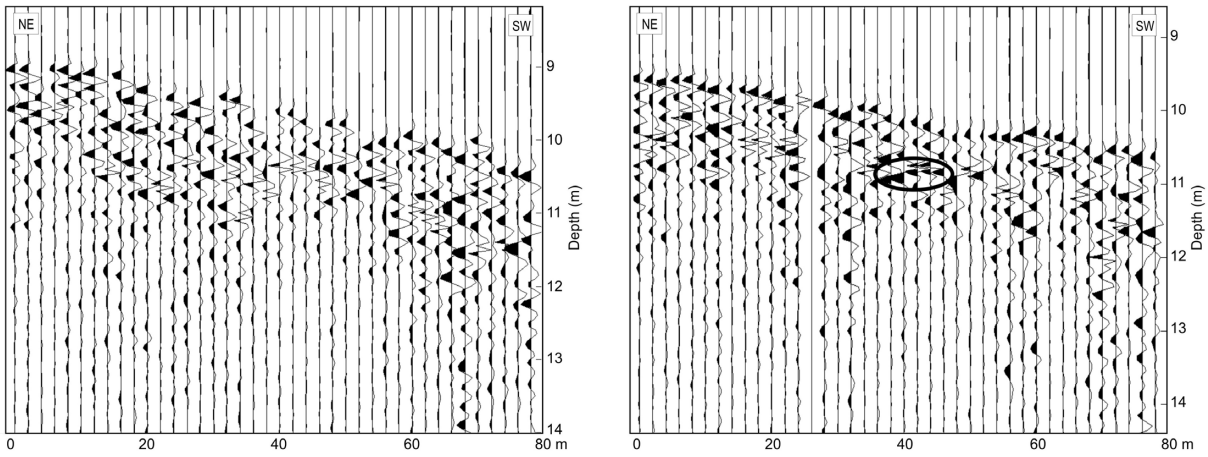

Figure 7.8 *Post-stack vertical cross-section through the 3D volume (for location see Figure 7.6). Left: raw data. Right: after static corrections. The presence of a buried wreck part (marked by the black oval) is indicated but its outline is not sharply defined.*

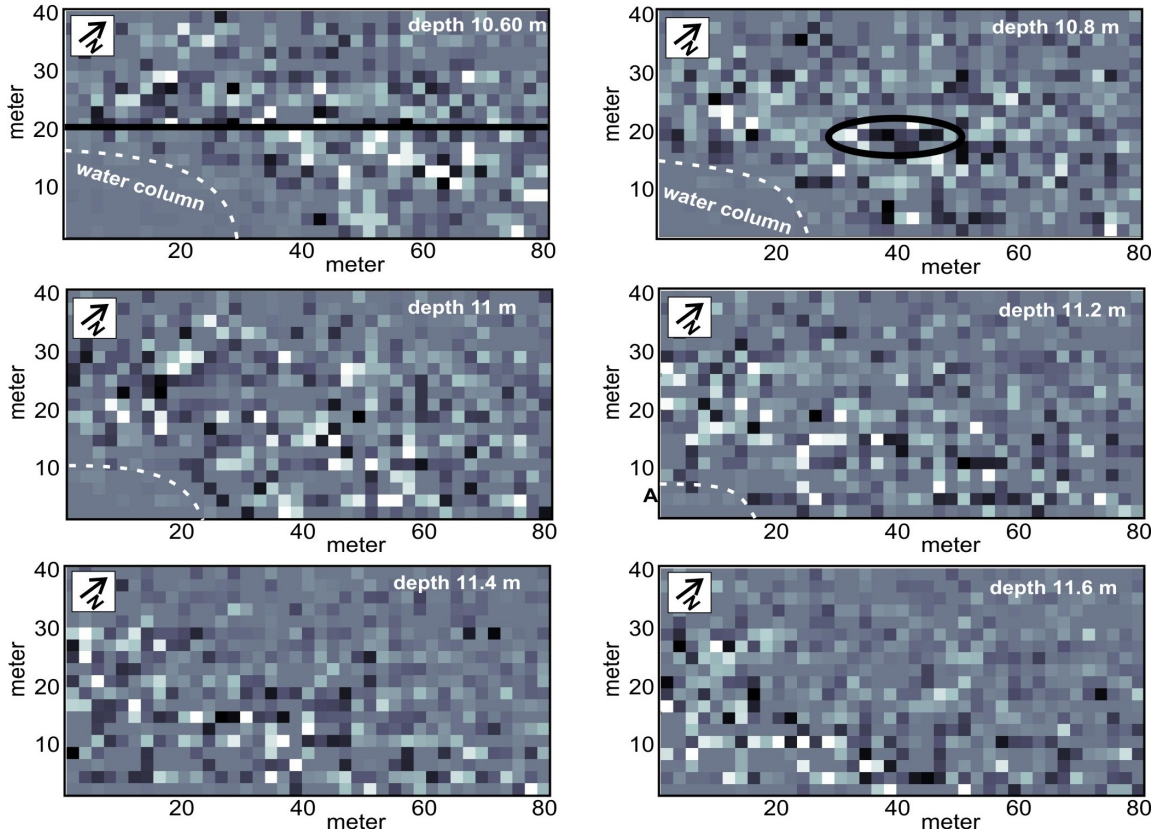

Figure 7.9 *Series of depth slices (20 cm interval) across the 3D volume. The black line in the upper left slice marks the vertical cross section shown in Figure 7.8. The presence of a buried wreck part (marked by the black oval) is suggested in the second depth slice.*

7.4 3D case study – Wadden Sea, The Netherlands

7.4.1 Introduction

In 2001 the Dutch Directorate-General for Public Works and Water Management (Rijkswaterstaat) initiated the IMAGO project ("Innovatief Meten aan Gezonken Objecten"), which focused on measurement techniques for the detection of buried objects in the water bottom (van de Brenk et al. 2003). Timely detection of these objects can have a significant impact on the maintenance operations of the shallow waterways, minimizing time delays and saving costs, and helps to avoid possible damage of valuable archaeological relics during dredging.

In July 2003 a 3D seismic survey was carried out in collaboration with TNO-TPD (The Netherlands) over a buried wooden shipwreck using the inflatable acquisition array. The aim of this survey was to test the suitability of very high resolution 2D and 3D seismic techniques for the detection and identification of buried wooden objects. The wreck ('Scheurrak SO1') is located in the southern part of the Dutch Wadden Sea, some 25 km NE of Den Helder, on the transition of the Texel and Scheurrak tidal channels (Figure 7.10). The area is marked by very strong tidal currents, and water depth varies roughly between 6.5 and 8 m below MLLWL (mean lowest low water level at spring tide). Surficial sediments mainly consist of fine sandy silt marked by asymmetric megaripples (~5 m wavelength) with superimposed microripples (10-20 cm wavelength) (Rijkswaterstaat 2003).

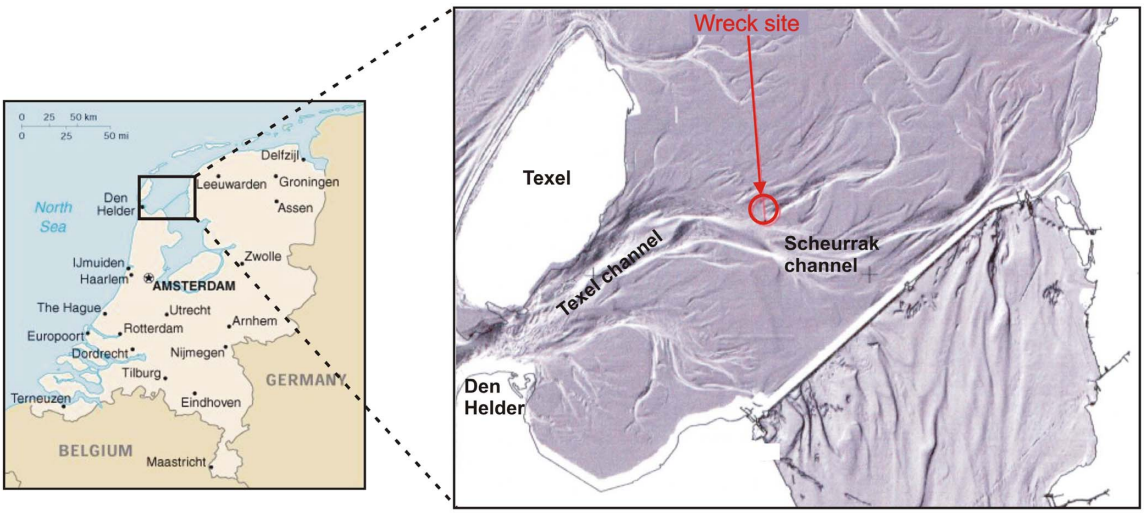

Figure 7.10 *Location of the wreck site 'Scheurrak SO1' in the Scheurrak tidal channel, Dutch Wadden Sea (after Rijkswaterstaat 2003).*

The wreck is roughly 25 m long and dates presumably from the late 16th to early 17th century. In the early nineteen nineties the wreck site was surveyed by divers - at that time the wreck was largely exposed on the seafloor (Rijkswaterstaat 2003). The results showed that the wreck had been broken lengthwise in two main parts (Figure 7.11). Because accurate positioning was not available during the diving operations the site was marked by a number of short poles (Rijkswaterstaat 2003). Recent sedimentation has resulted in complete burial of the wreck under a thin layer of fine sandy sediments. Side-scan sonar investigations were carried out over the wreck site in May 2003. The results confirmed that the wreck is completely buried. The seafloor is relatively flat and locally marked by large ripple features (van de Brenk et al. 2003). In the wreck area a slightly disturbed seafloor is observed but it is not clear whether this is related to the shipwreck or not.

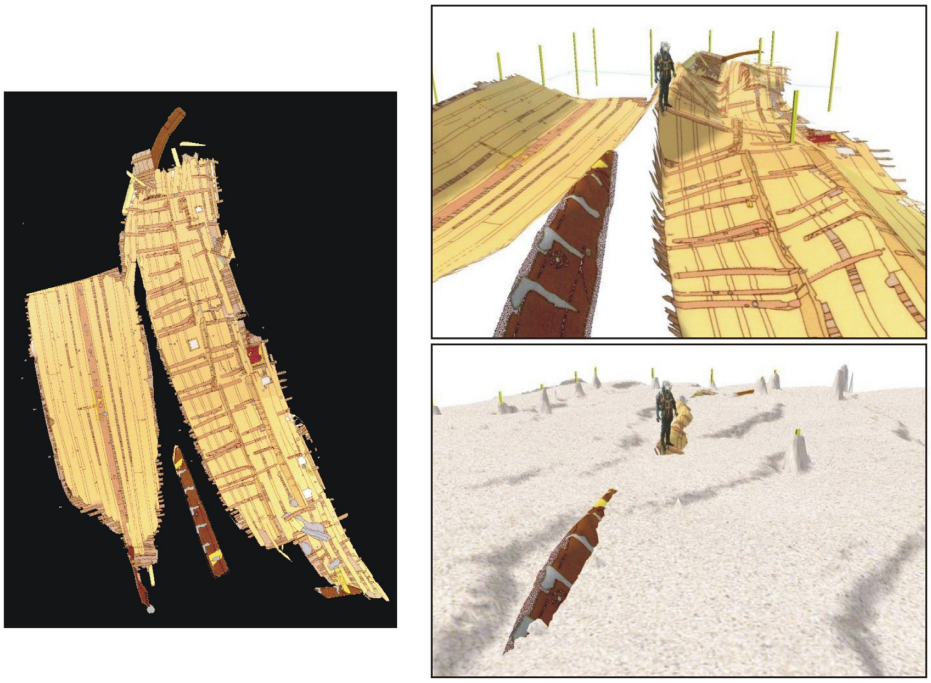

Figure 7.11 *Schematic views of the shipwreck 'Scheurrak SO1' in the Dutch Wadden Sea, based on diving observations in the early nineteen nineties. Left: Top view of the wreck that has been broken in two large pieces. Right top: 3D model of the wreck. The poles were put in by divers to mark the wreck area (the diver marks the scale). Right bottom: 3D model of the seafloor based on multibeam data. The partly exposed keel can be seen on the foreground. Spikes are due to the partly exposed poles.*

7.4.2 Data acquisition

Seismic acquisition on the Wadden Sea took place on board the R/V Westergat from 7 to 10 July 2003. A dense network of perpendicular E-W and N-S profiles was recorded with some additional oblique NW-SE lines. Different sail directions also assured targeting at a wide range of angles, which should increase the image quality. Weather conditions during the survey were generally good. Occasionally strong winds made deployment of the 3D system too hazardous and measurements had to be stopped. During the survey concurrent multibeam data were recorded together with the seismic data. On these multibeam data we can clearly observe the short poles placed by divers to mark the wreck area (Figure 7.12).

The acquisition system (RIB + inflatable array) was towed 25 m behind the vessel to minimise possible engine noise (Figure 7.13). As the Seistec boomer was not available at the time of the survey a 3.5kHz echosounder was used that was towed close behind the RIB. The streamers were towed underneath the inflatable frames (at 15-20 cm depth), which helped to reduce lateral positioning errors. Offset between the source and nearest receivers was roughly 5 m. Tidal currents in the wreck area are fairly strong (max. 1 m/s), with a very short slack water period (often < 15 minutes). The survey was to a large extent marked by strong side currents, resulting in an inclined position of the acquisition array behind the tow vessel. In order to avoid large stresses on the array the vessel took wide turns in between the profiles. The tow-ropes were attached to side booms which assured good stability of the outer frames, even during turning (Figure 7.13).

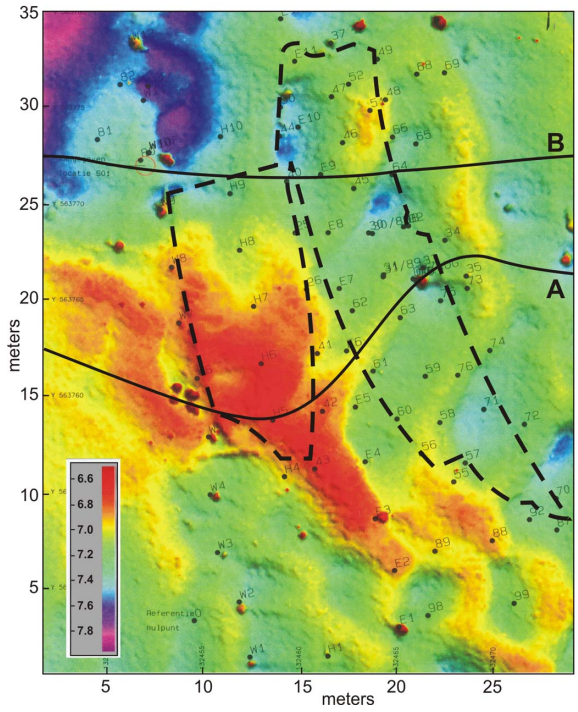

Figure 7.12 *Multibeam recording over the wreck area (modified after RWS 2003). Red dots mark the short poles that were used to delineate the wreck site. The dashed black line marks the contour of the shipwreck observed by divers in the early nineteen nineties (see Figure 7.11). The full black lines mark the profiles shown in Figure 7.15.*

Figure 7.13 *3D acquisition system on the Wadden Sea during turning. The side boom (in white) assures good stability of the outer inflatable frames*

In total 62 profiles were acquired with an average profile length of 200-250 m and profile spacing of roughly 7 m (Figure 7.14). Strong side currents made it not always possible to steer exactly along the planned profiles. The westernmost part of the network is marked by poor coverage due to the presence of a surface buoy. The seismic data were recorded using an Elics Delph18 multichannel seismograph, with a shot interval of 0.5 s. and record length of 100 ms. Due to problems with the recording system the sampling rate was limited to 12 kHz. The total recorded data volume amounted to roughly 1.5 Gbytes.

Positioning was done using a short-range DGPS system based on RTK positioning. Real-time (x,y,z) positions were acquired each second with cm accuracy. The positioning antenna was installed on the echosounder frame in order to minimise relative positioning errors. A second RTK positioning antenna was installed on the bow of the tow vessel, and allowed to track the ship's direction with high precision (van de Brenk et al. 2003).

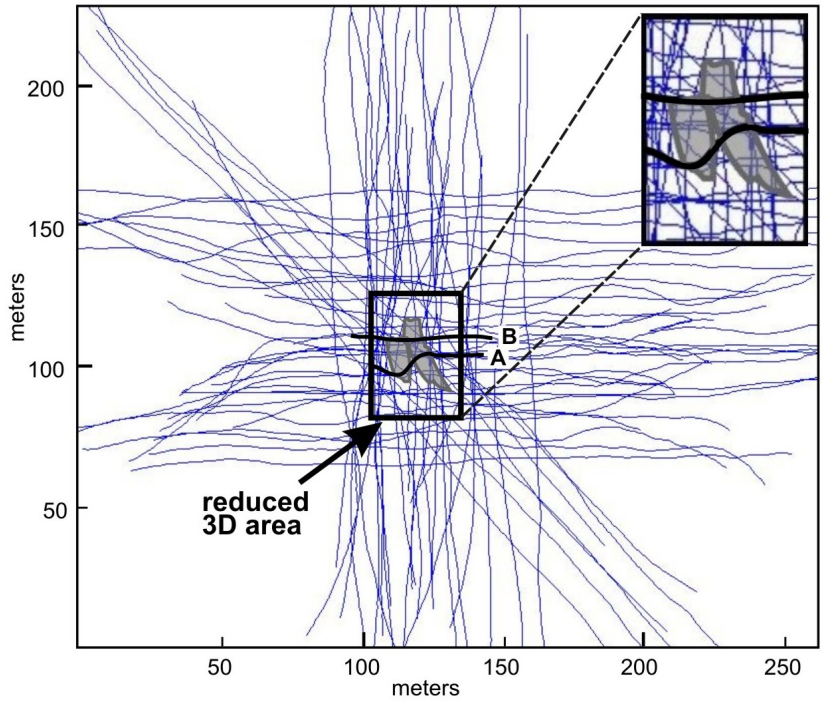

Figure 7.14 *Seismic network recorded over the wreck site in the Wadden Sea. The black rectangle marks the reduced area used for 3D processing. The wreck outline is marked in grey (see also Figure 7.12). Thick black lines mark the profiles shown in Figure 7.15.*

Figure 7.15 shows two examples of 2D profiles and interpreted line-drawings across the wreck site (for location see Figures 7.12 and 7.14). Applied processing included bandpass filter, predictive deconvolution and agc. The seismic data were marked by relatively poor penetration which is most likely due to the presence of shallow gas and/or a high sand content of the seafloor sediments. The data indicate that the deepest part of the wreck is covered by roughly 1.5-2 m of sediment. The wreck-related reflectors are marked by phase inversion, although less pronounced than the Schelde data (see Figure 7.4). This could be due to a less advanced state of decay of the wood or to the presence of gas which will lower the acoustic velocity of the sediments resulting in a decreased impedance contrast.

Profile A crosses the wreck more or less obliquely. The wreck stands out clearly on the data. The irregular shape of the western wreck piece (in particular its southern edge, see Figure 7.11) most likely caused multiple reflections. The large diffraction in the middle at 12 ms may be related to the ship's keel (see Figure 7.11). Profile B is located more to the north and crosses the wreck (mainly the right wreck piece) at a right angle. Shallow gas cuts through the stratification. Multiple reflections from the curved wreck edges conceal the exact wreck outline. The deeper, horizontal reflector possibly represents a paleo-scour feature.

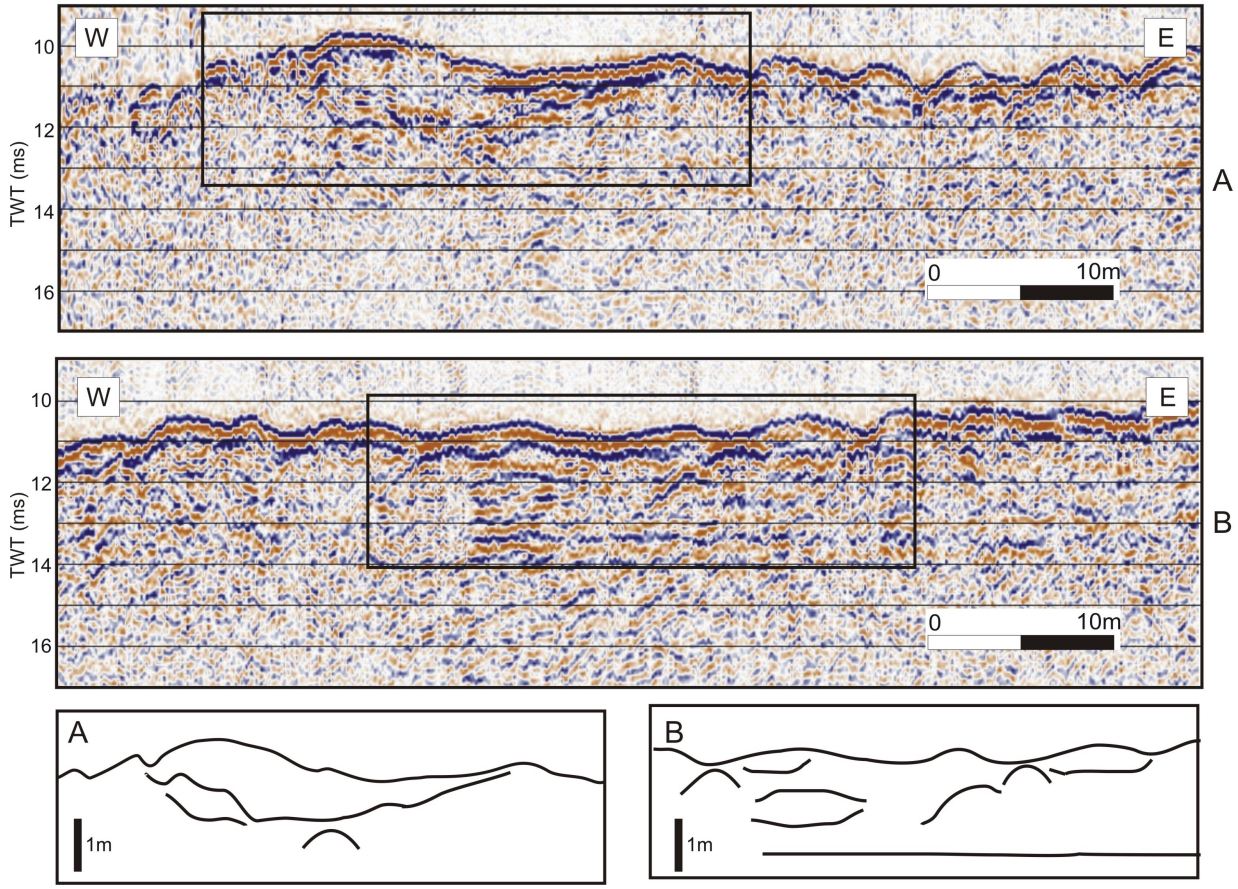

Figure 7.15 *Examples of processed 2D profiles and interpreted line-drawings across the wreck site (for location see Figures 7.12 and 7.14). The buried wreck parts are marked by polarity inversion. Profile A crosses the wreck more or less obliquely; the wreck outline is clearly observed. The large diffraction in the middle may be related to the ship's keel. Profile B crosses the wreck (mainly the right wreck piece) at a right angle. Multiple reflections from the curved wreck edges conceal the exact wreck outline. The deeper, horizontal reflector possibly represents a paleo-scour feature.*

7.4.3 Geometry processing

Source and receiver positions were calculated from the positioning antenna on the source, taking into account the position of the tow vessel. This was necessary in order to correct for the deviation between the course of the vessel and the course of the inflatable array which showed an inclination due to strong side currents. Profiles of inferior data quality were left out. The distribution of the source and receiver points in the wreck area (approx. 30x40 m) is shown in Figure 7.16.

Binning was carried out using two different grids of resp. 0.5x0.5 m and 1x1 m bin size. The resulting stack fold over the reduced area is shown in Figure 7.17. Coverage for the smaller bin size of 0.5x0.5 m was rather heterogeneous but still sufficiently high, with few empty bins. In order to obtain optimal resolution it was decided to use this small grid size for further 3D processing.

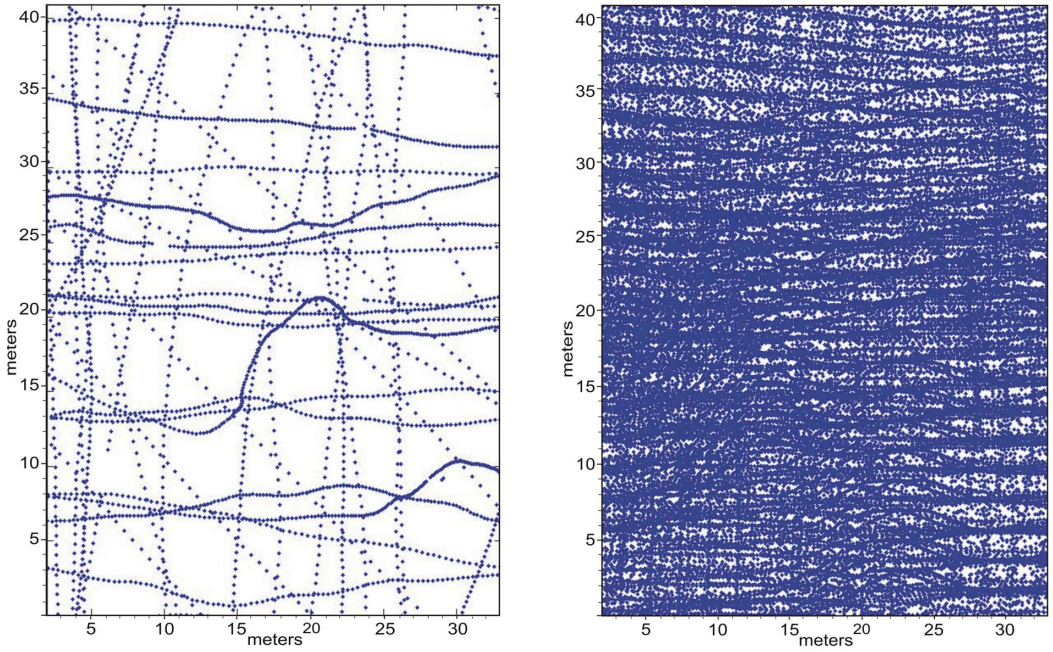

Figure 7.16 *Calculated shot positions (left) and receiver positions (right) over the reduced wreck area in the Wadden Sea (for location see Figure 7.14).*

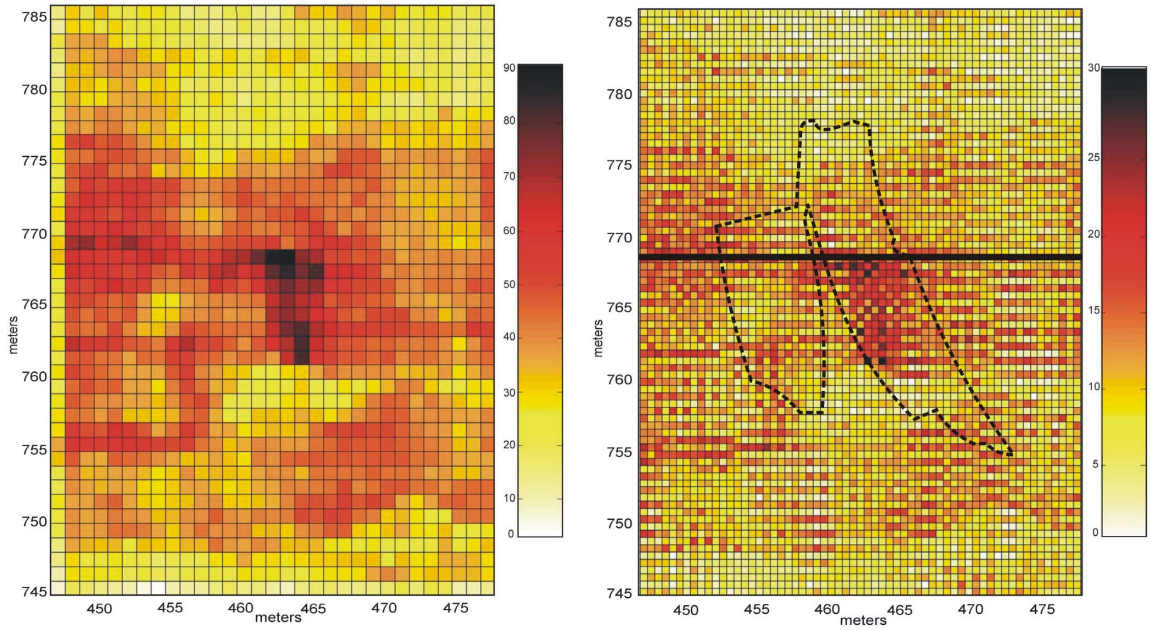

Figure 7.17 *Calculated fold coverage for 1x1 m bin size (left) and 0.5x0.5 m bin size (right) over the reduced wreck area in the Wadden Sea (for location see Figure 7.14). To allow optimum resolution the smaller bin size was used for further 3D data processing. The dashed black line marks the position of the wreck (see Figure 7.11). The full black line marks the location of the vertical section shown in Figure 7.19.*

7.4.4 Data processing and imaging

Tidal amplitudes during the Wadden Sea survey were up to 2 m, making tidal correction essential. The vertical positions were marked by high-frequency variations (as the antenna was mounted on the source frame), but their limited size (< 5 cm) did not require any filtering. Tidal shifts were carried out on the zero-offset data, after NMO correction, using a velocity of 1500 m/s. Additional preliminary processing included bandpass filtering and agc.

Seafloor data derived from the multibeam records were compared to the first break arrival times from the 3D seismic data. At first sight both surfaces are highly comparable, but as expected the seismic data show less resolution due to lower spatial coverage (Figure 7.18) (in general seismic spatial resolution is inferior to multibeam in water depths < 500 m, see Mosher et al. 2002). Subsequently the multibeam data were gridded to the same grid used for the 3D binning operation (0.5x0.5 m bin size) (TNO-TPD 2003). Close inspection of the seafloor arrival times showed that differences could mount up to as much as 0.4 ms. Taking into account the importance of accurate vertical positioning in the stacking process, it was decided to use the multibeam data to carry out static (vertical) corrections of the seismic traces, each trace being shifted so as to overlap the seismic first arrivals with the calculated (multibeam) first arrivals.

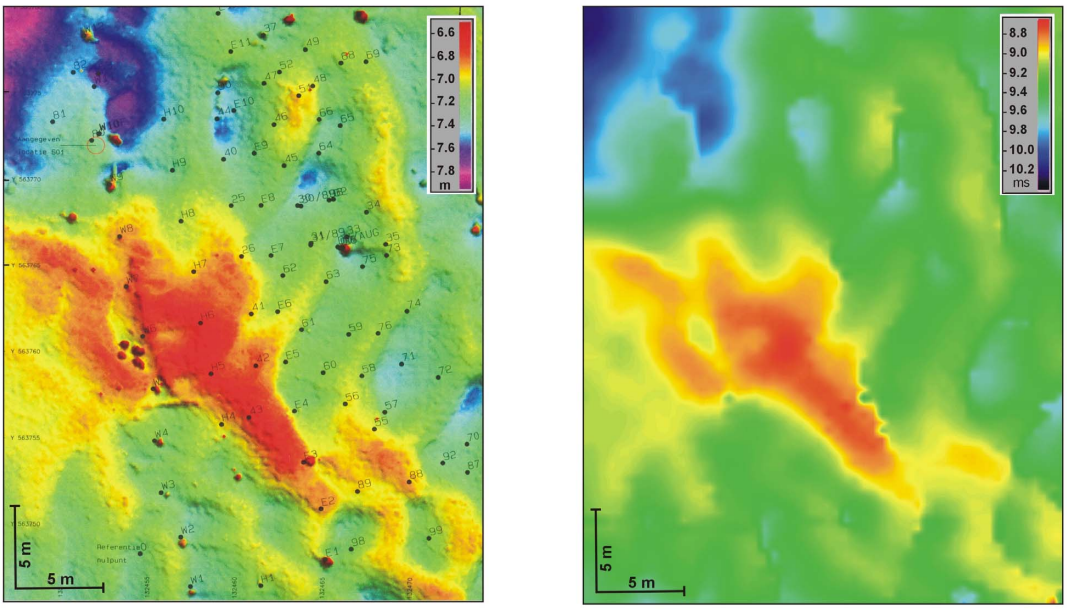

Figure 7.18 *Detailed seafloor depth maps of the wreck area obtained from multibeam data (left) and 3D seismic data (right). The maps compare well, but as expected the seismic depth map shows less resolution.*

The static corrections had a pronounced effect on the stacking process. Whereas uncorrected stack sections were often marked by an irregular water bottom (Figure 7.19 top), corrected stack data showed more coherence due to improved line-up of the stack bins (Figure 7.19 middle). This resulted in an improved image of the water bottom and the shallow reflectors, and the presence of a buried object (most likely the right wreck part) can now be observed. In order to further improve the data quality fxy deconvolution processing was applied (TNO-TPD 2003). This is a prediction error filter which attenuates the incoherent noise in the post-stack data resulting in data enhancement. The results after fxy deconvolution show an additional improvement in the coherency of the shallow reflections and further noise suppression (Figure

7.19 bottom). A second shallow reflector is now observed, more to the left, possibly related to the second wreck part.

Figure 7.20 shows a series of consecutive time slices at 0.5 ms interval (~40 cm) through the final stacked 3D data volume (after static corrections + fxy filtering). The uppermost time slice roughly corresponds to the seafloor. The large amplitude pattern observed in the west and south agrees well with the seafloor morphology observed on the multibeam data (see Figure 7.18). The location of the buried wreck is suggested in time slices 4 and 5 (marked by black circles), taken at 1.5 and 2 ms below the seafloor (~1 m and 1.5 m). However the interpretation of the time slices is not straightforward, and the exact size and form of two wreck parts remain unclear.

Although the presence of the buried shipwreck is quite apparent on the 3D data, in particular the vertical cross-sections, the exact shape and dimension of the wreck (pieces) could not be precisely defined as was the case for the single-channel data. This is due to the lower resolution of the 3D data which is most likely caused by a combination of factors:

- highly heterogeneous midpoint coverage;
- small lateral and vertical positioning errors (causing a misfit in stacked traces);
- multiple reflections due to locally high curvature of the wreck parts.

The availability of concurrent multibeam data however proved to be a crucial factor, as this allowed a marked improvement of the data quality due to precise static corrections.

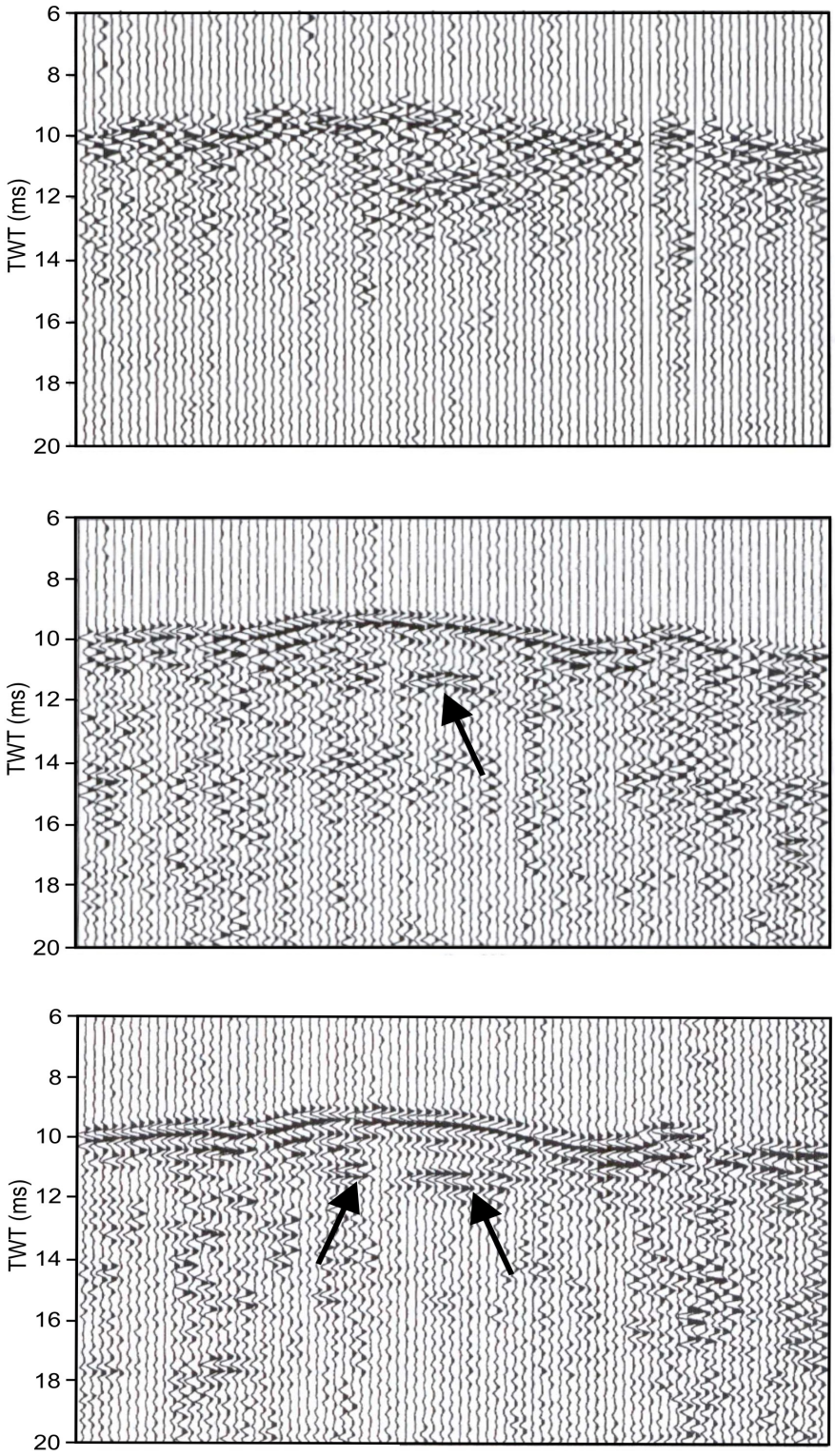

Figure 7.19 *Examples of stack sections from the 3D volume at the wreck area (for location see Figure 7.17). Top: Stack section after raw stack; the results of destructive stacking are evident. Middle: After static corrections based on multibeam data. The seafloor clearly lines up. The shallow reflector in the middle (marked by the arrow) is related to the wreck. Bottom: After additional post-stack fxy deconvolution. The image shows an overall improved coherency. A second, smaller wreck piece can now be identified (arrow on the left). This seems to confirm the presence of two large wreck parts (see Figure 7.11).*

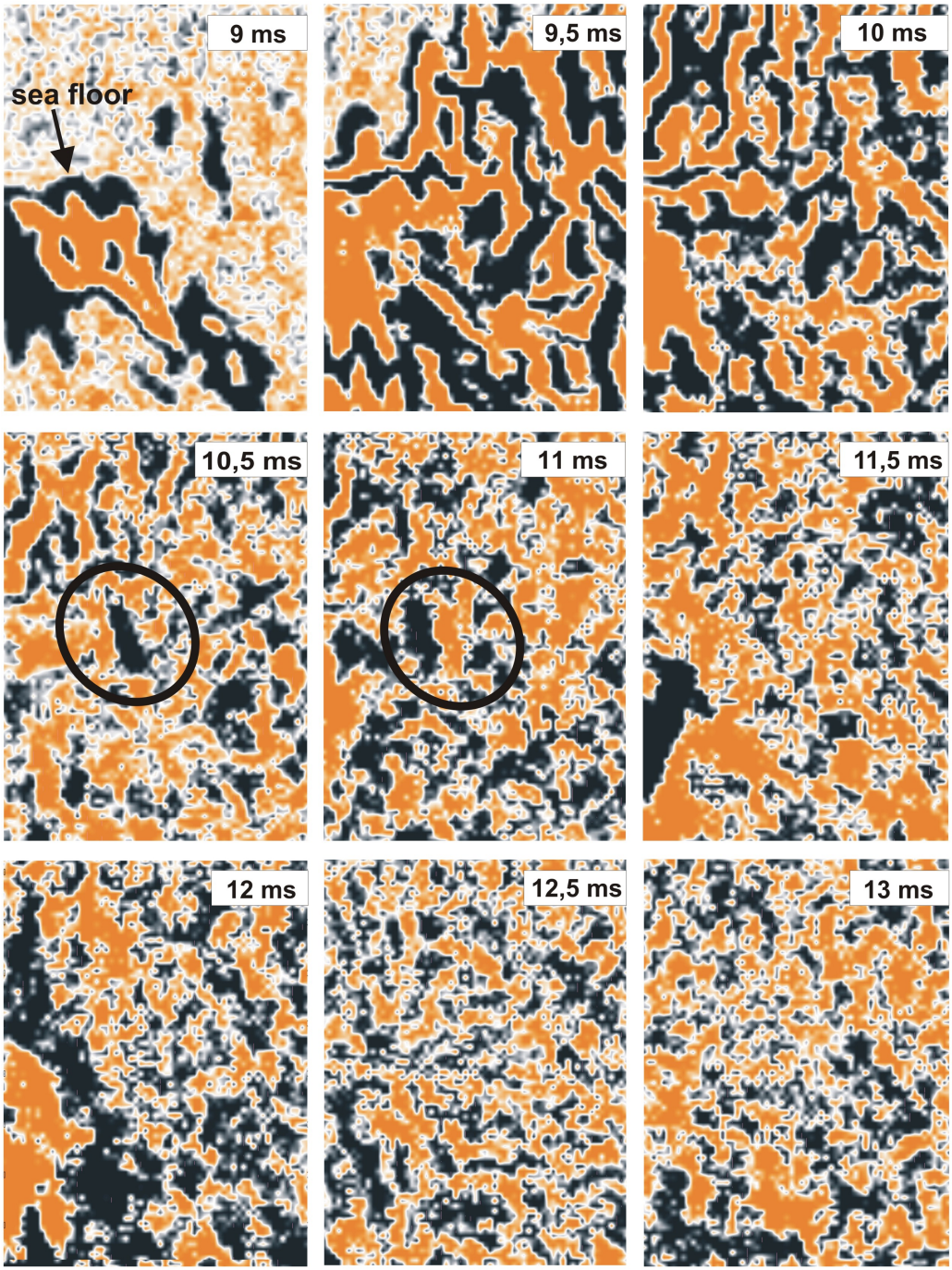

Figure 7.20 *Series of consecutive time slices at 0.5 ms (~40 cm) interval through the 3D volume at the wreck area. The uppermost time slice marks the seafloor. The reflection pattern showing up in the time slices at 10.5 and 11 ms (see black ovals) is most likely related to the buried shipwreck.*

7.5 Summary and conclusions

The application of marine reflection seismic profiling methods for archaeological site investigations, such as buried wooden shipwrecks, has been growing steadily over the last years. The ability to image wooden objects will highly depend on the type of wood, the level of decay, and the surrounding sediment. On the whole, oak and pine artefacts are detectable in a wide range of marine sediments. Increasing wood degradation will generally yield more negative reflection coefficients. The size of the object and its orientation will also affect the imaging potential.

In recent years two surveys were carried out over buried wooden shipwrecks. A first 2D seismic survey took place on the river Schelde near Antwerpen. The target was a small 17th century wooden shipwreck, almost certainly severely damaged by dredging operations. The wreck pieces stand out clearly on the 2D data as strong negative reflections, suggesting that the wood is heavily degraded. Six wreck parts were identified, spread over a distance of ~150 m. Contrary to the general practice, pseudo-3D processing was applied to the network of single-channel data. The resulting vertical and horizontal sections indicate the presence of buried wreck parts, but the exact size and shape of the wreck were not sharply defined. Most likely this was due to the irregular fold coverage and relatively large bin size (2x2 m) which affected the resolution of the stack data.

A second seismic survey was carried out over a buried 17th century wreck in the Dutch Wadden Sea using the inflatable 3D acquisition array. Although the seismic data have limited penetration (most likely due to shallow gas) the wreck stands out clearly on the 2D data. The images confirm the existing information regarding shape and setting of the wreck. The wreck is covered by maximum 2 m of sediment. The weak phase inversion suggests less degraded wood compared to the Schelde wreck. 3D data processing was carried out using a 0.5x0.5 m bin size. The application of precise static corrections (using concurrent multibeam data) and predictive noise filtering resulted in a marked improvement of the stacked data quality. The two main wreck pieces were identified on the vertical cross sections. Time slices at 40 cm interval suggest the location of a large buried wreck piece but the features are not sharply defined. This was partly due to the heterogeneous coverage and small positioning inaccuracies related to source and streamer movement. Most likely the multiple reflections related to the curvature of the wreck pieces have also affected the 3D image quality.

The results from these two case studies clearly demonstrate the suitability of very high resolution acoustic imaging for marine archaeological site investigations. The acoustic ‘visibility’ of buried wooden artefacts will depend on various factors, most importantly sufficient impedance contrast between the wood and the sediment. If this condition is fulfilled detection of the wooden object is possible, not only in 2D but also in 3D, provided that the positioning precision and coverage is high enough. The application of 3D techniques in archaeological studies is quite novel, and we have shown that concurrent multibeam data can greatly improve the quality of the 3D image. This opens new perspectives for the use of acoustic profiling in marine archaeological site surveys.

CHAPTER 8
SHALLOW GAS, A MAJOR PROBLEM

8.1 Introduction

As we have seen in the previous chapters, much of the seismic data from shallow coastal areas and river estuaries is affected by the presence of shallow gas. Extensive seismic investigations on the Belgian Continental Shelf have revealed the widespread occurrence of shallow gas in the nearshore area (Liu et al. 1992, Missiaen et al. 2002b). The gas is commonly regarded as a nuisance because it reduces the data quality and limits the seismic penetration, and for a long time no serious attempt was made to quantify and describe the shallow gas zones. Yet the growing concern about their potential impact on the marine environment and on human activities, bearing in mind the industrial and economical importance of the nearshore area, demands a better knowledge of these gassy sediments.

Shallow gas can significantly alter the geotechnical properties and behaviour of seafloor sediments (e.g. Wheeler 1990, Sills et al. 1991). This can be of crucial importance for geoacoustical modeling studies and engineering applications, such as foundation design for offshore structures. Over the years shallow gas has become the subject of various studies, mostly focused on a more qualitative description of the acoustic characteristics (e.g. Anderson & Bryant 1990, Hart & Hamilton 1993, Figueiredo et al. 1996). Detailed studies of the behaviour of fine-grained soils containing gas have been carried out in laboratories (e.g. Wheeler 1990, Sills et al. 1991). Recently more quantitative studies of the in-situ acoustic characteristics of shallow gas-bearing sediments based on seismic investigations have been performed (e.g. Best et al. 2004, Kogan & Paull 2004, Robb et al. 2006).

This chapter presents the results of a study of the shallow gassy sediments offshore the Belgian coast based on very high resolution reflection seismic data (Missiaen et al. 2002b). The study focuses on the eastern part of the nearshore zone, roughly between Oostende and the Schelde estuary, where most of the shallow gas is observed. The different sections focus on various aspects of the gas such as seismic evidence, origin, distribution, quantification and bubble resonance effects. The understanding of shallow gas-bearing sediments is constantly progressing and this study is by no means complete. In order to tackle all aspects of shallow gas in depth a multi-disciplinary approach is necessary in which geophysical, geotechnical, geochemical and biological techniques are combined.

8.2 Seismic data base

The seismic data base used for the shallow gas study in the eastern part of the Belgian nearshore zone involved two main data sets (Figure 8.1):

- A set of older, mainly analogue sparker and Uniboom profiles (main frequency <1 kHz, penetration ≥100 m). Part of these data was acquired in the framework of a site study for the expansion of the Zeebrugge harbour, which did not only cover the harbour area but reached as far as 30 km offshore (Henriet et al. 1978). Although these sparker and boomer records were quite ‘dated’ (1977-1985) their quality was often remarkably good.
- A set of digital Seistec boomer records (main frequency ~4 kHz, penetration ≤50 m) for the larger part acquired in the framework of a study of the Paardenmarkt dumpsite (see chapter 5).

The Seistec boomer data allowed a detailed study of the shallow subsurface features, thus forming a complementary data base to the analogue sparker and boomer records which focused on the deeper reflectors and gas zones. Some additional refraction seismic data were also obtained in the Paardenmarkt area in 1996.

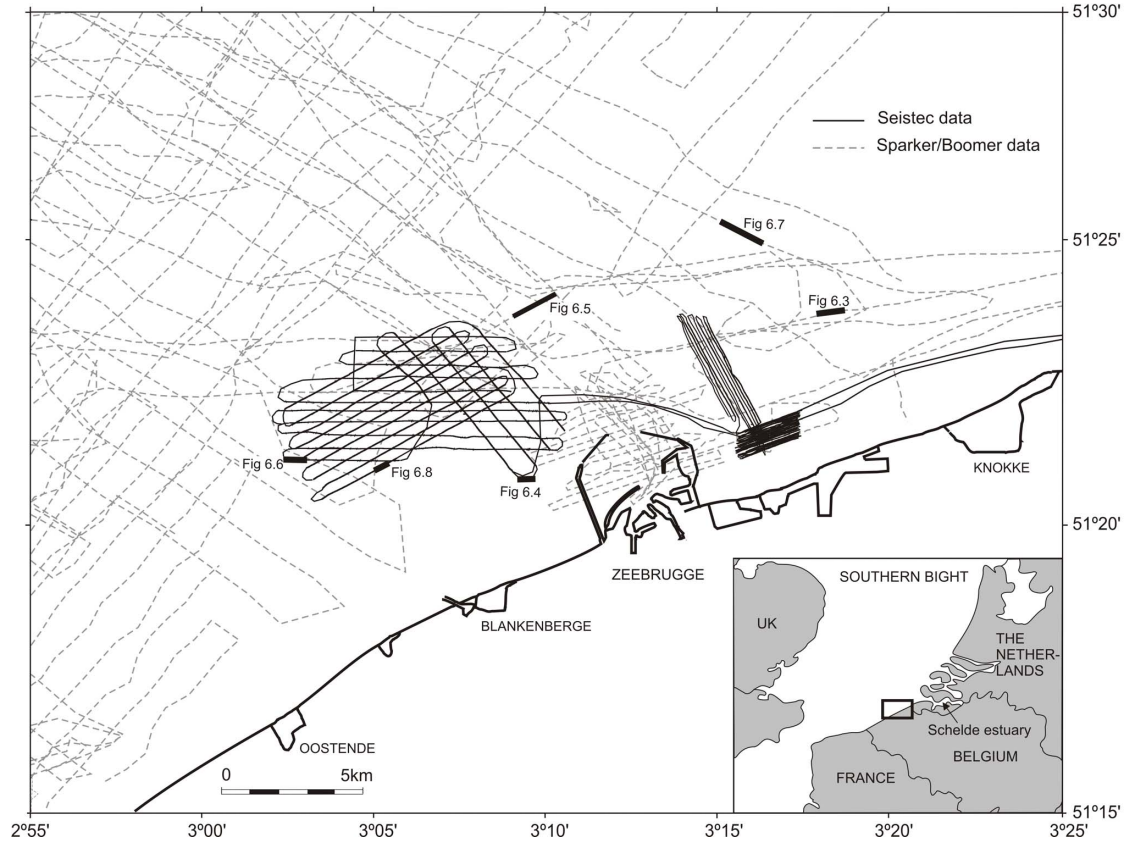

Figure 8.1 *Overview of the seismic network used for shallow gas study in the eastern part of the Belgian nearshore area (after Missiaen et al. 2002b). Thick black lines mark the location of profiles shown in Figures 8.3 to 8.8.*

8.3 Natural setting

The Quaternary deposits in the coastal zone are characterized by strong lateral variations in lithology and stratigraphical build-up, reflecting the rapid succession of glacial and interglacial phases, and with an overall thickness ranging from a few m up to 30 m locally (Liu 1990). The Pleistocene deposits mainly consist of reworked Tertiary clays and sands, with an increasing content of aeolian and fluviatile deposits towards the top (Libbrecht 1980). The rapid sealevel rise at the onset of the Holocene induced strong tidal currents which caused serious reworking of the outcropping Pleistocene and Tertiary deposits. During the later part of the Holocene a repeated reworking and removing of the fine-grained material took place which led to the deposition of the present seabed sediments (Liu 1990).

The seabed mainly consists of fine to very fine sands with a high content of mud (70 % silt, 30% clay) taking the form of an elongated mud belt, whereas further offshore the sediments become more sandy (Figure 8.2) (Ministerie van Openbare Werken 1993). The muddy sediments are most likely related to local erosion of outcropping Paleogene clay layers. The present sedimentation in the shallow coastal zone is mainly due to reworking related to local flow conditions. This has resulted in a high residual sediment transport marked by a turbidity

maximum near Zeebrugge, which acted as a 'hydrodynamical trap' for the suspended mud sediments (Ministerie van Openbare Werken 1993).

The extension of the outer harbour of Zeebrugge and recent dredging and dumping activities have influenced the local transport pattern (see also chapter 5), causing sediment displacements often greater than those due to natural processes. The mud-rich sediments in the eastern coastal area are highly anoxic, and marked by a high amount of organic matter (2-8%) and carbonates (20%) (Malherbe 1989).

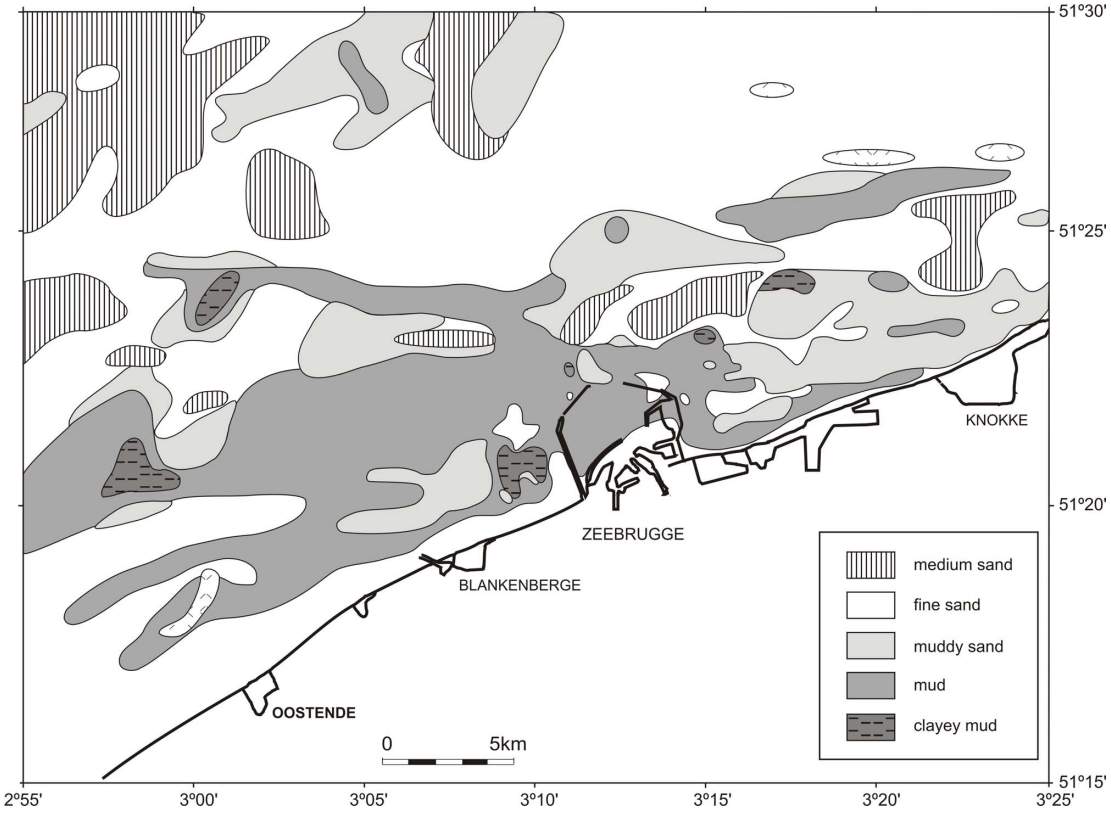

Figure 8.2 *Distribution of seabed sediments in the eastern Belgian nearshore zone (after Ministerie van Openbare Werken 1993).*

8.4 Seismic evidence of gas

The most evident gas-related feature is acoustic turbidity which appears as a diffuse and chaotic seismic facies masking nearly all other reflections. It most likely results from scattering of the acoustic energy by interstitial gas bubbles in the sediment (Schubel 1974). The acoustic turbidity was observed in the upper sequence, sharply cutting across the stratification and occasionally reaching up to the seafloor (Figure 8.3). No clear velocity effects (e.g. pull-down) could be observed at the edge of the gassy zones. The top of the turbid zone could not always be clearly resolved, possibly due to minor gas diffusion (Missiaen et al. 2002b).

The gassy zones were occasionally marked by reflection-free patches (Figure 8.4). This is most likely due to acoustic blanking caused by absorption of the seismic signal in the gas-charged sediments (due to bubble damping losses) (Schubel 1974). However, it could also be related to the local absence of sediment layering (possibly due to the migration of gas) (Missiaen et al. 2002b). The presence of a hard layer may also produce a similar effect, disrupting the deeper sediment layering due to a sudden reduction in penetrating energy. This was the case for some

buried shell-rich sand layers observed in the Schelde estuary (Henriet et al. 1986), and the presence of similar layers in the nearshore area cannot be excluded. Still, the particular effect of sharply cutting across the stratification is a strong indication of gassy sediments.

The acoustic turbidity often started at a few meters below the seafloor. The overlying sediment layer was locally marked by a large number of (sub-)parallel reflectors (Figure 8.5) indicating different phases of deposition and erosion, most likely related to tidal and storm sequences, as indicated by the alternating thin sand and mud layers in shallow cores near Zeebrugge (Ministerie van Openbare Werken 1993). Similar thin layering has also been reported along the Dutch coast, where temporary mud was deposited during slack tide or during prolonged periods of calm weather and eroded again with increasing wave action, some mud being buried under sand (Eisma 1981). Some of the thin mud beds probably acted as traps for the upward migrating gas, giving rise to different levels of upward gas penetration (Figure 8.5).

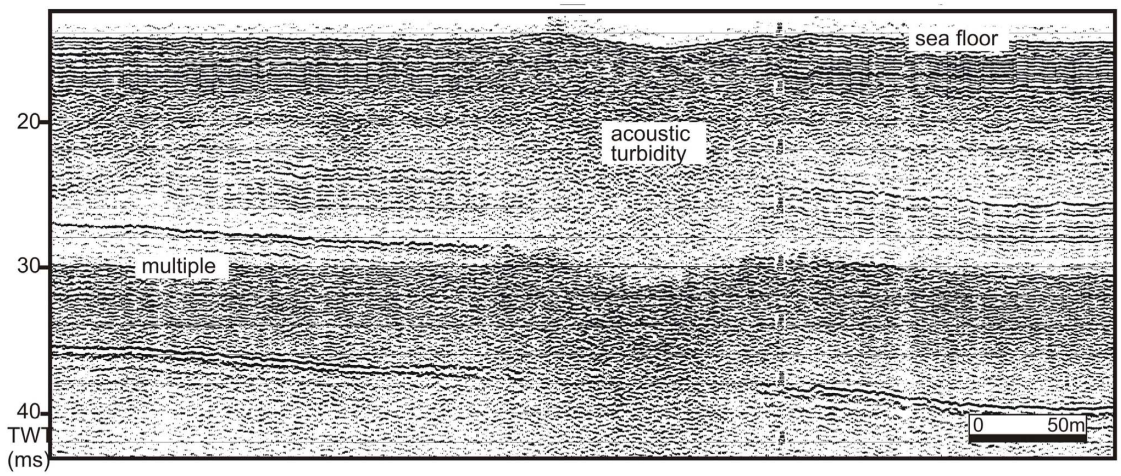

Figure 8.3 *Seistec profile showing acoustic turbidity cutting across the layering. The turbidity reaches up to the seafloor. It is uncertain whether the shallow depression in the seafloor is due to the presence of gas or related to human interference.*

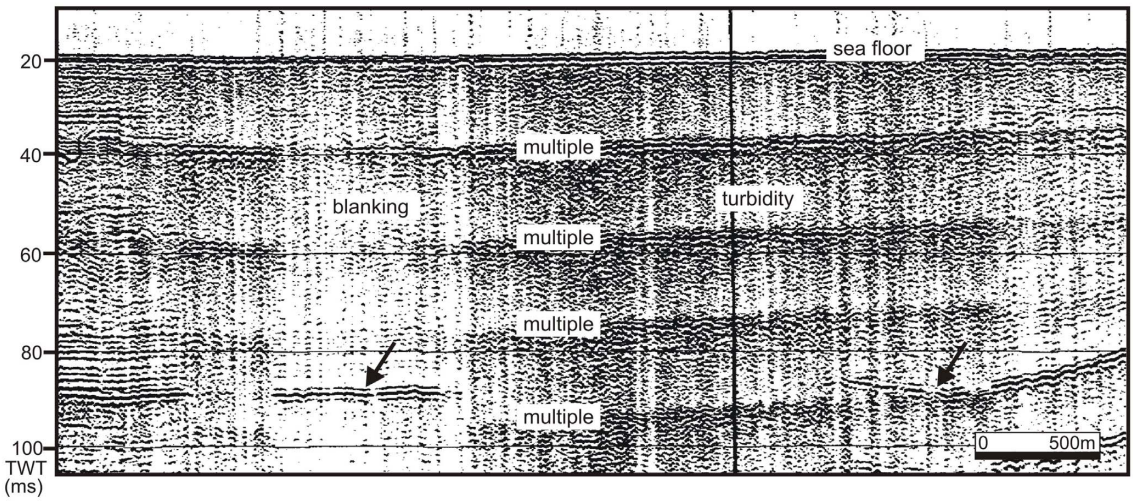

Figure 8.4 *Analogue sparker profile showing acoustic blanking and turbidity due to shallow gas. The arrows mark reflectors locally showing up in gas-rich zones. The noise in the water column is most likely related to the seismic equipment and/or the vessel.*

Some of the seismic records are locally marked by diffraction hyperbolas, mainly concentrated in the uppermost part of the sediment column or at the seafloor. The diffractions are often related to gas horizons, and possibly caused by an irregular morphology due to the presence of gassy sediments. Still, some relation to local gravel or shell layers, small sand waves, boulders or dumped debris cannot be ruled out. At the Paardenmarkt dumpsite the seismic diffractions are also possibly caused by clusters of dumped weapons, as discussed in chapter 5.

Enhanced reflectors were occasionally observed, probably due to a local increase in gas concentration. On some profiles a polarity inversion could be observed at the seabed indicating a large mismatch in acoustic impedance (Figure 8.6). This effect of phase inversion is best observed on the sparker records and can possibly be related to the effect of a lower sound speed (associated with lower source frequencies) which will increase the impedance anomaly and the chance to generate a negative reflection coefficient (Missiaen et al. 2002b).

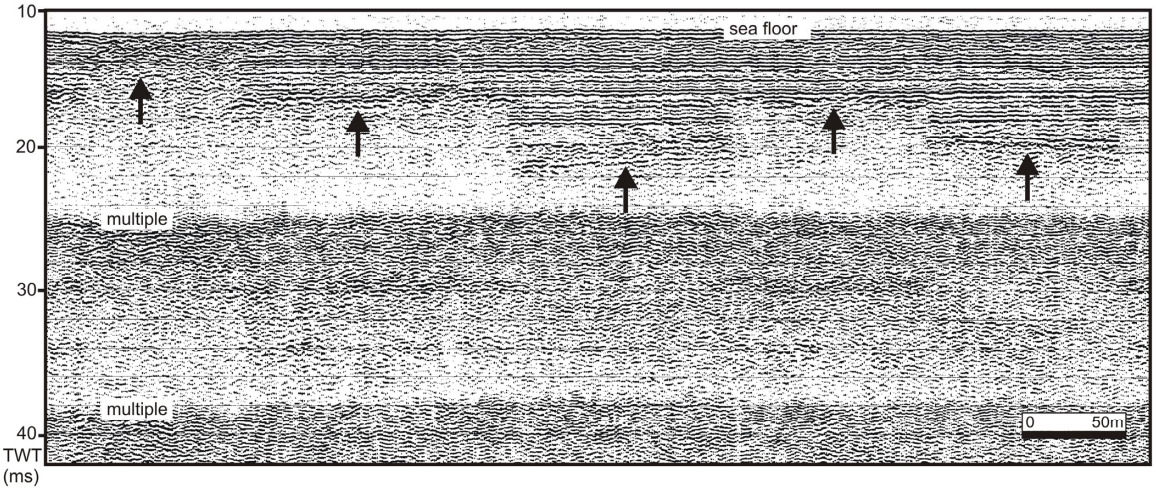

Figure 8.5 *Seistec profile showing different levels of acoustic turbidity (marked by black arrows) attributed to upward gas migration.*

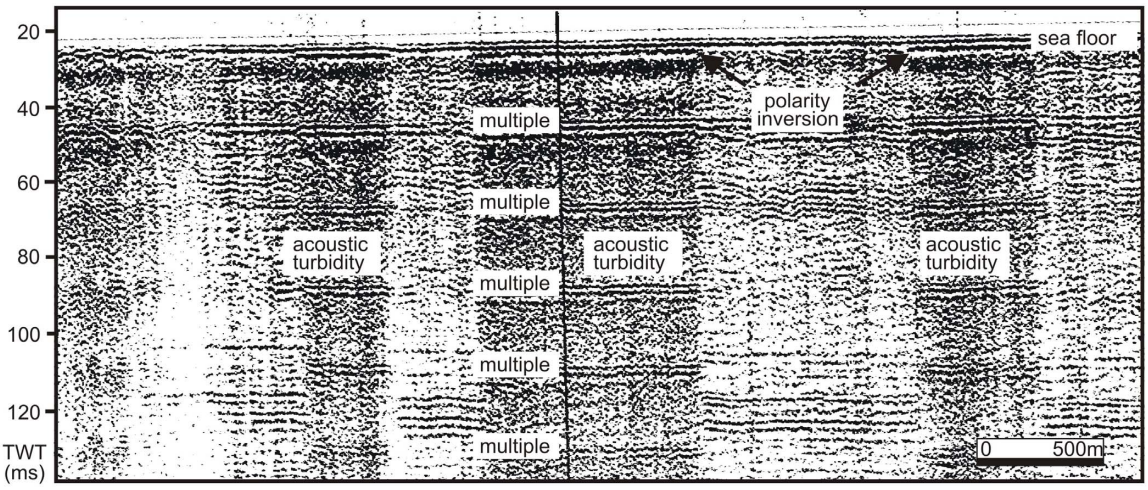

Figure 8.6 *Analogue sparker profile showing acoustic turbidity and strong multiple sequence marked by phase reversal at the seafloor.*

The gassy zones were often marked by strong series of seafloor multiples (Figures 8.4 & 8.6). This is a result of the fact that most of the acoustic energy will be reflected by the gassy surface and re-reflected at the sea surface, resulting in many repetitions of these low-loss reflections. Strong seafloor multiples may however also be related to an affluent of waste material, a phenomenon often observed in industrial areas subject to human activity. Due to the proximity of the Schelde estuary and the Zeebrugge harbour this effect cannot be ruled out completely (Missiaen et al. 2002b).

In the case of buried gassy sediments internal multiples between the seafloor and the top of the gas (so-called 'peg-legs') are locally observed (Figure 8.7). This could be due to the constructive interference of equivalent paths of propagation which are spatially different but equivalent in travel time (McGee 1991).

Although the acoustic turbidity locally reaches the surface, the seafloor morphology does not reveal any marked gas-related features. The small depression on Figure 8.3 seems to be related to the local presence of gas. Indeed gas can affect the sediment strength, eventually resulting in local collapse. However this effect is expected to be small in fine-grained sediments (see §8.8) (Wheeler et al. 1990). Close inspection of the seismic data revealed less distinct but similar seafloor features on a few adjacent profiles, indicating some lateral extension (e.g. shallow gully) rather than an isolated depression. The proximity of the Zeebrugge harbour may suggest a possible relation to dredging operations, but the location of the seafloor feature (due west of the harbour entrance) and its limited depth (< 60 cm) make this rather unlikely. Still some human interference (e.g. related to cable or pipeline works) cannot be ruled out (Missiaen et al. 2002b).

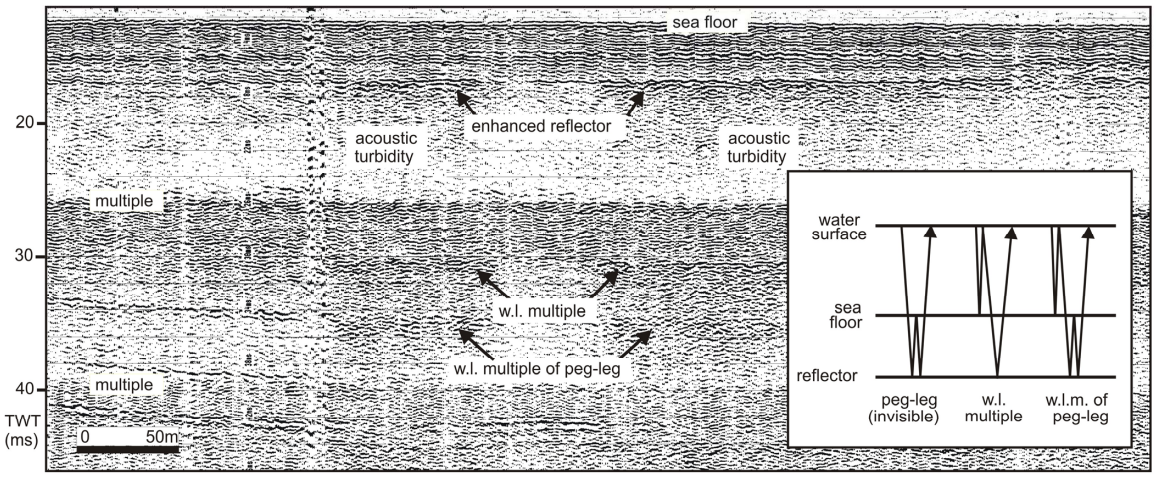

Figure 8.7 *Seistec profile showing different types of multiples related to a gas horizon (w.l.= water layer). The vertical disturbances observed on the left are most likely due to acoustic noise.*

The reflection seismic data do not provide any clear evidence of gas escape from the seabed, such as pockmarks or gas plumes in the water column. The small vertical disturbances occasionally observed in the water column (see Figure 8.4) could suggest the presence of small gas seeps. However, these features are also observed in gas-free areas, indicating that they are most likely due to acoustic noise related to the seismic equipment and/or the vessel itself, or possibly fish (Missiaen et al. 2002b). Nevertheless some minor local seepage of small bubbles or dissolved gas through the seabed cannot be excluded.

8.5 Seismic refraction data

In 1996 a number of refraction seismic measurements were carried out at the Paardenmarkt dumpsite area using a 32 m long 16-channel bottom streamer (hydrophone spacing 2 m) and a small borehole sparker resting on the seafloor (Winthagen 1996). The bottom streamer was positioned 35 m behind the vessel; offset between sparker source and first hydrophone was 2 m. Measurements were carried out along several transects across the dumpsite and in the surrounding area (Henriet & Winthagen 1996b).

Refracted seismic waves travel along an impedance boundary. Their refraction angle is defined by Snell's law $sin(\alpha_1)/V_1 = sin(\alpha_2)/V_2$ where V_1 and V_2 denote the velocity in the upper and lower layer, α_1 is the angle of the incident ray path with respect to the vertical, and α_2 is the angle of transmission of the refracted ray path with respect to the vertical (Sheriff & Geldart 1982). For a certain critical angle α_c the refracted wave will run along the interface in the lower layer. This critical angle is given by $\alpha_c = sin^{-1} (V_1 / V_2)$ (Sheriff & Geldart 1982). The passage of the refracted wave along the interface will generate a plane wave travelling upward in the upper layer at the same angle α_c.

NMO analysis of the refraction data yielded interval velocities as low as 850 m/s (Henriet & Winthaegen 1996b). The latter are most likely related to an increased gas concentration. The results also indicated a maximum depth of roughly 18 m for the gas-bearing sediments. Direct wave velocities ranged between 1350 and 1505 m/s. The lowest values were observed in areas marked by low seismic penetration suggesting a relation to the shallow gas. If the direct wave travelled through the water column the velocity changes could be related to small gas bubbles leaking into the water. However it is not unlikely that locally the source and receivers were sagging slightly into the sediments, in which case the changes in direct wave velocity may be related to differences in gas concentration in the sediments (Henriet & Winthaegen 1996b).

The refraction experiments also generated surface (Stoneley) waves. These waves propagate along the water-sediment boundary and are marked by high amplitude and low frequency. The amplitude decreases away from the boundary. For the given frequency range (65-75 Hz) the maximum depth of the surface waves was roughly 4 m (Henriet & Winthaegen 1996b). The observed velocity changes were probably caused by lateral and vertical variations in gas concentration of the shallow sediments.

8.6 Origin and distribution of the shallow gas

Gas in shallow marine sediments has two main potential sources: (1) biogenic gas produced by bacterial degradation of organic matter at low temperatures, and (2) thermogenic gas produced by high-temperature degradation and cracking of organic compounds at considerable burial depths. The geology of the study area does not suggest any possible deep thermogenic sources, and it seems more likely that the gas has accumulated *in situ* in the shallow organic-rich sediments. Geological studies, both offshore and onshore Zeebrugge, have revealed the presence of a thin (1-2 m) peat-rich layer containing methane gas that can most likely be linked to the Late Pleistocene/Early Holocene formation of Wenduine (Ministerie van Openbare Werken 1978; Libbrecht 1980). The layer is located at a depth between 6 and 9 m below the seafloor, dipping deeper further offshore. It most likely represents the widespread 'basal peat' which developed on the Pleistocene surface due to the rise in ground water level caused by the postglacial sea-level rise (Köhn 1988). This peaty layer, perhaps in combination with remnants

from other peat-rich layers related to regressive phases, could well be a major cause for the acoustic turbidity observed in the nearshore area.
The geographical extent of the gas-bearing sediments in the nearshore area is shown in Figure 8.8. The gassy zone is bound to a wide band oriented more or less parallel to the coast, possibly reflecting the boundary of the marsh area where peat-growth was induced. The top of the gas is generally less than 10 ms (~7.5 m) below the seafloor. The depth may to some extent be controlled by the lithology of the overlying sediments (a higher permeability allows the gas to migrate upward more freely) and the amount of gas trapped in the sediments (a higher concentration will favour gas escape) (Missiaen et al. 2002b). In addition, the abundant presence of fine-grained muddy sediments and the high sedimentation rates (resulting in fast burial of the organic matter) most likely also formed an ideal basis for the generation of biogenic gas. Furthermore the extensive human activity in the Zeebrugge area possibly caused some minor organic contamination that may have induced a limited degree of gas formation in the uppermost sediments (Missiaen et al. 2002b).

The thickness of the gas-rich layer is rather uncertain. The maximum depth of 18 m as suggested by the refraction data is most likely a rough approximation. It is difficult to determine the exact thickness from the single-channel reflection seismic profiles due to the masking effect. According to Schubel (1974) complete masking may already result from a thin gassy layer of 1 to 2 m. This seems to be supported by the NMO analysis on refraction data from the Paardenmarkt dumpsite which suggest the presence of thin low-velocity layers with a maximum thickness of ~2 m (Henriet & Winthagen 1996b) most likely related to gassy sediments.

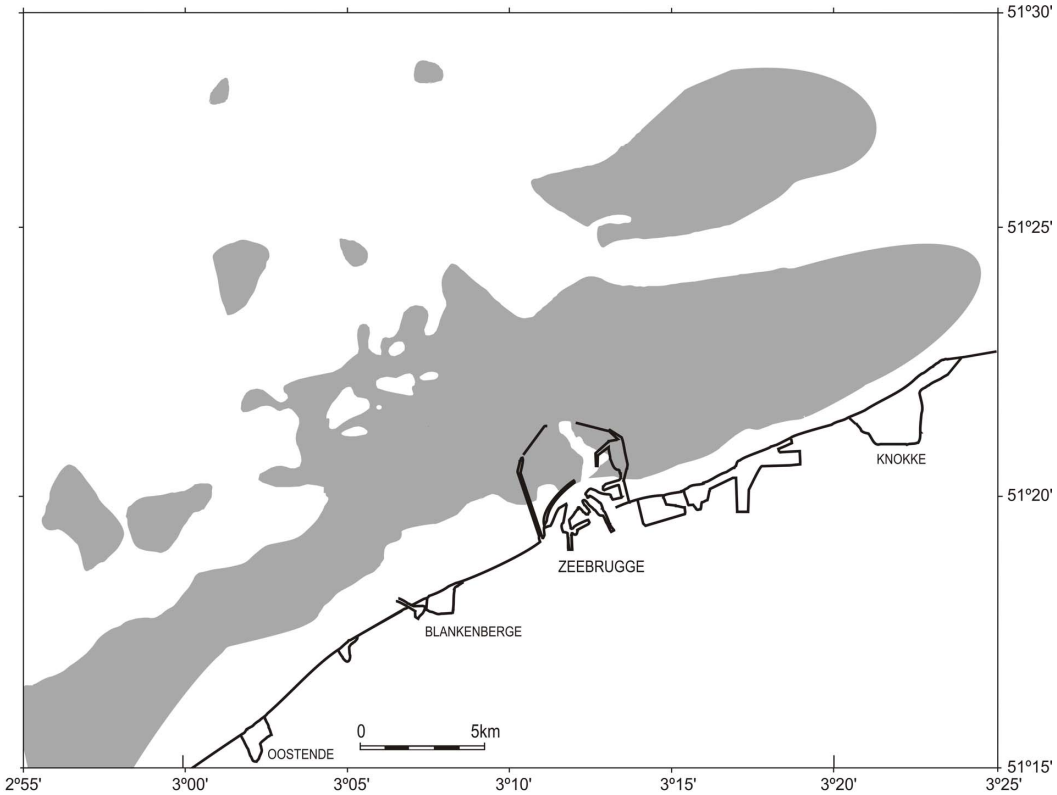

Figure 8.8 *Geographical distribution of the gas-bearing sediments (marked in grey) in the nearshore area (after Missiaen et al. 2002b).*

8.7 Quantification of the gas

A quantification of the gas based on seismic data is difficult since a small amount of gas as well as high gas saturation both may produce a similar response (Hovland & Judd 1988). It is generally believed that gas in shallow fine-grained sediments normally occurs in relatively low concentrations of discrete gas voids that are characterized by zones of acoustic turbidity, whereas interconnected gas-filled pore spaces may lead to much higher concentrations in coarse-grained sediments, giving rise to enhanced reflections and bright spots (Hovland & Judd, 1988). The scarce presence of the latter seems to indicate a low gas concentration, allowing the attenuation and diffusion of the seismic energy but generally insufficient to form strong enhanced reflections. The lack of clear velocity pull-down effects also seems to confirm this. Studies of shallow gas-rich muddy sediments in the Western Baltic have shown that acoustic turbidity may already occur with less than 0.5 % gas present (Abegg & Anderson 1997). Analogy with the mud-rich deposits observed in the nearshore area suggests equally low values here.

The sound velocity may give an indication of the overall gas volume of the sediment. Because the bulk modulus of a gassy soil is much lower than that of a saturated soil, the velocity will rapidly decrease with increasing gas content (this is true for frequencies below the bubble resonance frequency – see §8.7) (Anderson & Hampton, 1980). Refraction and borehole measurements on land in the Zeebrugge area have revealed P-wave velocities of 1050 m/s, locally even down to 700 m/s, for the methane-containing peaty sediments* (Cherlet 1978, Libbrecht 1980). Refraction data from the dumpsite yielded velocity estimates as low as 850 m/s (see §8.5). These velocity values are well in agreement with the theoretical and experimental curves presented by Anderson & Hampton (1980) and Sills et al. (1991) and suggest a gas concentration of less than one percent.
(It is known that the presence of peat-rich sediments, even without gas, can in itself lower the acoustic velocity. This is due to the increased compressibility, as organic matter absorbs water and causes clay particles to aggregate, creating an open structure that is weak and easy to deform (Silva & Brandes 1998). Still the extreme low velocities encountered here, together with the evidence displayed in the seismic data, strongly support the presence of gas.)*

Gas bubbles in fine-grained sediments are generally larger than the soil particles and the pore spaces, making it difficult for them to displace the soil while maintaining their structure (Richardson & Davis 1998). In the case of weak sediments, and if the bubbles are large enough, the buoyancy effect may allow them to move upward. Under static loading conditions bubbles of a realistic size can only move upward in very weak sediments (Wheeler 1990). Cyclic loading (e.g. due to wave action or tides), however, can reduce the critical bubble radius, but even then bubble movement is only expected in fairly weak sediments (Wheeler 1990). It seems realistic that the shallow mud-rich sediments in the study area are (locally) sufficiently weak to allow upward gas migration. Pockmarks require a large upward movement of gas bubbles, and their absence on the seismic data is therefore more likely due to low gas concentration rather than a lack of bubble movement.

8.8 Gas bubble effects

Shallow gas is present both in solution in the interstitial water and, when the dissolved gas becomes saturated, in the form of free gas bubbles (Richardson & Davis 1998). It is these free gas bubbles that are responsible for the acoustic disturbance observed on the seismic profiles, as they are excited into pulsation by incident acoustic waves. Anderson & Hampton (1980) developed a theoretical model that predicts the effect of free gas on the velocity and attenuation

of acoustic waves in marine sediments. The model predicts strong, frequency-dependent resonance effects. Bubble size plays an important role, each bubble diameter having its own specific resonance frequency when the bubble will vibrate and most of the acoustic energy will be attenuated and scattered (Anderson & Hampton 1980).

The resonance frequency of the gas bubble depends on the bubble radius, the thermal properties of the gas, the dynamic bulk and shear moduli of the sediment, the sediment bulk density, and the ambient hydrostatic pressure (Anderson & Hampton 1980). For example, for surficial gassy mud at 10 m water depth and with an average bubble size of 2.5 mm the resonance frequency is around 4 kHz. For a bubble size of 1 mm the resonance frequency will increase to roughly 10 kHz (Wilkens & Richardson 1998, Anderson et al. 1998). The Anderson & Hampton model furthermore shows that there is a significant difference between the acoustical responses below, above or near the resonance frequency of the gas bubble (Figure 8.9). If the insonifying frequency is lower than the bubble resonance frequency the sound velocity V of the gassy sediment is less than that of the non-gassy sediment V_o. Near resonance frequency the velocity increases rapidly to values much greater than for gas-free sediments, and then gradually decreases to V_o at frequencies above the resonance frequency.

Attenuation is also strongly affected by the presence of gas bubbles, increasing dramatically near the bubble resonance frequency. Above resonance the attenuation coefficient will remain high. The dramatic increase near the resonance frequency is due to the fact that at resonance the apparent cross-sectional area of the gas bubble becomes much larger than its actual physical size, leading to strong scattering and high signal attenuation (Best et al. 2004). In reality most gassy sediments will exhibit a wide range of bubble sizes, and the effects due to the bubble resonance frequency can therefore be detected across a range of frequencies. Typical fine-grained sediments contain gas bubbles ranging in size from 0.1 mm to over 10 mm. The resonance frequency for these bubbles will roughly vary between 100 kHz and 1 kHz. Investigations of shallow mud-rich sediments in the Western Baltic indicate a bubble resonance frequency in the range of 2-5 kHz (Mathys et al. 2005). Experiments at an intertidal site near Dibden Bay, Southampton (UK), show an attenuation maximum around 1-1.2 kHz (Best et al. 2004).

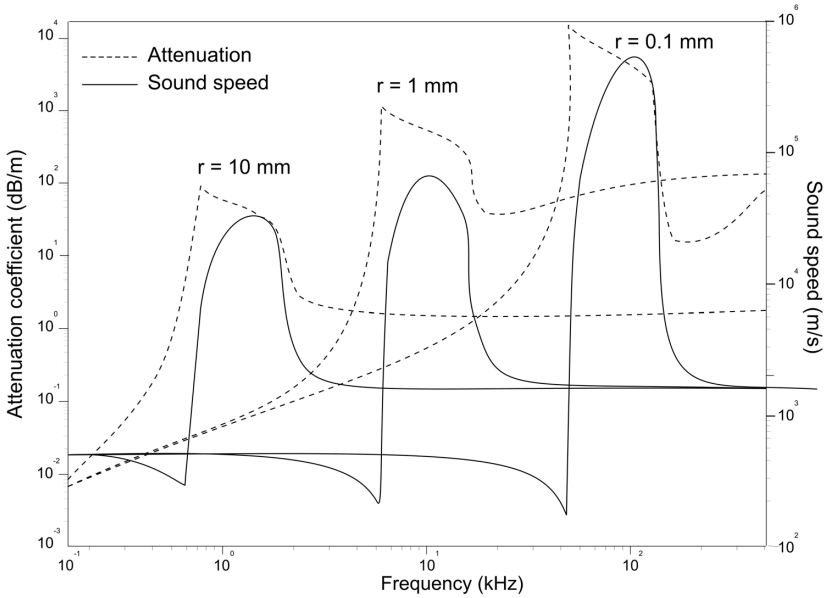

Figure 8.9 *Variation in sound speed and attenuation coefficient with frequency for different bubble sizes (0.1-1-10 mm) according to the model of Anderson & Hampton (1980). Gas content is 0.001. (after Best et al. 2004)*

In practice however not all bubble sizes will be equally distributed. The acoustic scattering strength will generally be dominated by the larger bubbles, although the relative importance of smaller bubbles may be increased by their increasing number (Anderson et al. 1998). The relation between bubble size and number of bubbles is given by $N = 10^a r^{-b}$, where N is the number of bubbles per m^3 at each radii r, and the parameters a and b control the void fraction and gradient of the distribution respectively (Anderson et al. 1998).

The bubble resonance frequency may explain the sometimes different appearance of sparker and Seistec records in gassy areas. Sparker sources are marked by a low frequency range (200-800 Hz) which is generally below the bubble resonance frequency, whereas the frequency range of the Seistec (1-8 kHz with peak frequency around 3-4 kHz) may partly overlap with the bubble resonance frequency. As a result acoustic masking (due to attenuation) is likely to be more complete on the Seistec data than on the sparker data where weak reflectors locally show up in gassy zones. The same effect was observed on data from the Schelde river (Missiaen et al. 2004). The fact that phase inversion is better observed on the sparker records is also probably due to the low frequencies (below the bubble resonance frequency) inducing a lower sound speed, thereby increasing the impedance anomaly and the chance to generate a negative reflection coefficient. Low source frequency most likely also explains the low sound velocities observed onshore near Zeebrugge and at the Paardenmarkt dumpsite (see §8.7). Still some relation to a local increase or decrease in gas content cannot be excluded.

The presence of gas bubbles will not only change the acoustical behaviour of marine sediments, it will also affect the physical properties. Theoretical and experimental results have shown that the undrained shear strength can be either increased or reduced depending upon the consolidation pressure and the initial pore water pressure; the effects will be most detrimental for deep water locations (Wheeler 1988). The undrained strength and consolidation component of settlement in fine-grained shallow sediments are not significantly altered by gas bubbles (Wheeler et al. 1990). This was confirmed by in-situ observations in fine-grained gassy sediments in the Baltic Sea (Wilkens & Richardson 1998). It is therefore not expected that the presence of shallow gas at the Paardenmarkt dumpsite will have caused (further) sinking of the dumped weapons into the sediments.

In shallow gassy sediments the effect of cyclic loading due to tides or storms can have a marked effect on the dominant resonance frequency. This is due to changes in hydrostatic pressure which will affect the internal bubble pressure (Wheeler et al. 1990). In-situ data obtained offshore Southampton (UK) have indicated shifts in the attenuation maximum (up to -32 dB/m) ranging in frequency from 1050 Hz at low tide to 1250 Hz at high tide (Best et al. 2004). It is possible that such cyclic loading effects also play a role in the shallow gas sediments off the Belgian coast. However it is as yet not fully known what the precise effect of such cyclic loading will be on the sediment strength.

The shape of the gas bubbles may also influence the possible frequency effects. Both spherical and non-spherical bubbles have been observed in sediments (Anderson et al. 1998, Best et al. 2004). Spherical bubbles are more common in sands and silts, whereas elongated bubbles are observed more in fine-grained muds, with bubbles becoming more elongated as bubble size increases. The presence of non-spherical bubbles could explain the more pronounced tide-induced shift in frequency and attenuation observed by Best et al. (2004) compared to the model predictions by Anderson and Hampton (1980).

8.9 Summary and conclusions

Detailed very high resolution reflection seismic investigations off the Belgian coast have revealed an extensive area marked by acoustic turbidity and poor seismic penetration likely due to the presence of shallow gas. The gas is believed to be of biogenic origin, and its geographical distribution is roughly bound to a wide band oriented more or less parallel to the coast. The origin of the gas is probably related to the presence of a thin peat-rich layer of Late Pleistocene/Early Holocene age, possibly in combination with minor gas formation in the fine-grained mud-rich Holocene sediments.

Gas-related features on the seismic data include acoustic turbidity and blanking, strong multiple reflections, and occasional enhanced reflections and phase reversal, as well as internal multiples. The acoustic turbidity often cuts sharply through the stratigraphy, and is frequently marked by varying offsets indicating different levels of upward gas penetration related to interbedded deposits of fine sand and mud. The top of the gassy sediments is less than 8 m below the seafloor, occasionally reaching up to the seafloor. Velocity effects at the edge of the gassy zones seem to be absent, and no clear gas-escape features are observed from the seabed, although minor seepage cannot be ruled out. Refraction studies at the Paardenmarkt suggest the presence of thin gassy layers (thickness $\leq$ 2 m) and indicate a maximum depth of 18 m for the gassy sediments.

The seismic characteristics (scarce presence of enhanced reflections and bright spots, absence of velocity pull down or gas escape features) and velocity data from refraction and borehole measurements both on land and at sea suggest a low gas concentration of less than 1%. Cyclic loading, due to storms and waves, may have affected the upward bubble migration in shallow water areas. Bubble resonance effects most likely explain the different appearance of gassy sediments on sparker and Seistec records. The high frequency of the latter partly overlaps with the bubble resonance frequency and as a result acoustic masking is more complete. The presence of gas bubbles most likely does not have a marked impact on the physical properties of the shallow fine-grained sediments, and it is therefore not expected that shallow gas will cause further sinking of the dumped munition into the sediments at the Paardenmarkt dumpsite.

CHAPTER 9
CONCLUSIONS AND SUMMARY

This thesis focuses on the applications of shallow marine acoustic imaging for environmental, geotechnical and archaeological site investigations. The benefit of true 3D seismic acquisition for small-scale site geotechnical investigations is demonstrated with the study of a small clay diapir on the river Schelde. Very high resolution acoustic imaging techniques, both 2D and 3D, are also becoming increasingly important in munition dumpsite research and archaeological site investigations such as buried wooden shipwrecks. Different case studies are presented from a variety of settings, ranging from fluvial and nearshore environments to the open sea. The acquisition of seismic images is often rendered difficult due to shallow gas. Its potential impact on the marine environment and on human activities demands a better knowledge, and recently a study was carried out focusing on gassy sediments in the Belgian nearshore area.

3D site investigations

The design of VHR 3D seismic surveys requires specific strategies, and the optimum approach will necessarily be a compromise between the need for high resolution and the constraints of physical laws. A new flexible array (OPUS3D) was developed at RCMG for small-scale surveys in shallow water. The array consists of 8 dual-channel streamers attached to 6 inflatable frames centered around a semi-rigid platform (RIB). Streamer and channel spacing are 2 m. The modular set-up is adaptable to specific site characteristics and allows convenient deployment and recovery from small vessels. The central RIB furthermore permits to use the system on a stand-alone mode in sheltered areas.

Accurate positioning is crucial because small movements of the array can easily lead to a degradation of the seismic signal. In view of the required resolution (< 1 m) the geometry of the source-receiver positions should be known with decimeter precision. Short streamers and offsets will reduce the positioning uncertainty. In sheltered areas the movements will be very small and can be reasonably neglected. In offshore areas waves and currents can reduce the array stability and geometry corrections may be needed.To avoid spatial undersampling a compromise between the sampling interval, reflector dip and signal frequency is needed. A source frequency of 2 kHz allows correct imaging of dips up to 24 degrees. In order to prevent aliasing of the high frequencies the hydrophone array must be kept short (spacing 25 cm). This assures good results for frequencies of 2-3 kHz in shallow water (<20 m) and using short offsets (≤ 15 m). The optimal bin dimension will depend on the frequency and the target depth. Steeper target dips will require a reduction in bin size.

A 3D survey was carried out over a small clay diapir on the river Schelde near Antwerpen. The diapir had been the subject of previous investigations and formed a well-documented test ground. The inflatable array was easily deployed and due to the relatively sheltered environment the source and receiver movement array was minimal. Stacked data (using a 1x1 m bin size) showed great detail with a large number of sharp reflectors and time slices revealed a sharply defined concentric reflector pattern growing towards the base of the diapir. The upper part of the clay diapir remained largely disturbed with some weak internal reflectors, most likely a result of gravitational collapse. The clay sequence is marked by calcareous-rich horizons containing carbonate concretions (so-called “septaria”). These can pose a problem for geotechnical construction works, and it was a challenge whether the 3D set-up would provide information on

their spatial distribution. Vertical stack sections showed the presence of numerous diffraction hyperbolae which can most likely be linked to the septaria. A number of horizons were picked and series of corresponding horizon slices were made at very small intervals. The slices revealed a slowly appearing and disappearing pattern that probably reflects the local distribution of the septaria.

The results of this survey illustrate the importance of VHR 3D shallow seismic investigations for engineering geophysics and geological and geotechnical site investigations. The study also shows that it is feasible to acquire high-quality VHR marine 3D data in a modest and cost-effective way, without requiring complex field procedures. The inflatable acquisition system OPUS3D allowed to improve the imaging resolution, even when based on relatively simple processing, and so further scale down the shallow 3D method to ultra-high resolutions and dm scale.

Munition dumpsite investigations

Dumped weapons, and in particular chemical weapons, are the subject of growing concern. The amount of these weapons dumped in the North European seas alone runs into hundreds of thousand of tons at least. The toxic war material was often dumped in relatively shallow waters and areas of active fishing, and represents a serious threat to the marine environment and the densely populated coastlines. Over the last decades a large number of accidents have been reported from different areas, mostly involving fishing crews. Up to this day little is known about the exact location and distribution of the munition in most dumpsites. The dumped weapons are nowadays often buried under a layer of recent sediments. Detailed imaging of the internal structure of the dumpsite, not only regarding the buried weapons but also with respect to possible natural hazards, is crucial for a reliable risk assessment.

The “Paardenmarkt” is an old dumpsite offshore Knokke-Heist. After WW1 an estimated 35,000 tons of German munition were dumped here, including toxic shells. Over the years the dumpsite has been the subject of a number of integrated geophysical studies. Magnetic investigations have indicated that the munition is nowadays covered by a few m of sediments, a direct result of the construction of the outer harbour of Zeebrugge. Acoustic investigations were severely hampered by the presence of shallow gas, limiting the penetration depth to a few meters. Shallow reflectors reflect the different stages in the recent sedimentation process and confirm an increased sediment accumulation towards the south-west. Small dunes up to 1 m high suggest important sediment displacement is still taking place in parts of the dumpsite. Detection of buried munition on the seismic data was not straightforward, not only in view of the shallow gas but also due to the unknown size of the objects and the possible advanced state of corrosion. Frequent clusters of diffraction hyperbola were observed on the seismic data. These can probably be linked to small groups of dumped weapons (individual shells are likely too small to allow clear acoustic detection). Correlation with electric and magnetic/gradiometric data confirms the relation to buried munition clusters. Most likely they represent very shallow war material that is buried by a thin ($\leq$ 2 m) layer of sediment. Deeper buried weapons will probably largely remain acoustically invisible due to the strong acoustic turbidity related to the shallow gas.

A second case study focused on the chemical munition dumpsite east of the island of Bornholm in the southern Baltic Sea. After WW2 over 32,000 tons of chemical weapons were dumped here. Previous research indicated the presence of four shipwrecks in the area and locally increased arsenic levels in the shallow sediments. Two detailed seismic surveys, combined with high resolution magnetic investigations, were carried out at the dumpsite. Simultaneous deployment of different acoustic sources (parametric echosounder, sparker, boomer) resulted in

a detailed image of the shallow stratification of the dumpsite and the deeper structure. Seven seismic stratigraphic units were identified, related to different stages in the Holocene and late-glacial history. Numerous diapir-like features were observed which most likely represent dewatering phenomena related to overpressure. The wrecks were observed in high detail on the acoustic data. Their length ranges from 20 to 50 m height above the seafloor is roughly 1 to 2 m. The wrecks are partly covered by a thin layer of soft sediments. Strong and frequent seismic diffractions indicate a highly irregular surface with many protruding parts. Objects identified in the vicinity of the wrecks most likely represent wreck pieces that have become detached.

A large number of buried objects were observed on the high-frequency data. The objects are generally buried no more than 1 to 2 m below the seafloor and their size varies roughly between 1.5 and 5 m, occasionally 10 m. Shallow pits in the seabed are probably due to the impact of dumping. The magnetic gradient data confirm the presence of buried objects, and in many cases a good correlation was found with the acoustic data. Large objects identified on the acoustic data did not always coincide with large magnetic anomalies. This was most likely due to the fact that toxic agents make up a large part of the gross weight of these objects. The distribution of dumped weapons seems to be very heterogeneous, with locally high object concentrations surrounded by larger areas of lower object density. The data confirm the wide variety of dumped war material ranging from bombs and shells to encasements and containers.

The results of these case studies illustrate the importance of very high resolution seismic measurements in munition dumpsite research and the benefit of complementary geophysical investigations. Increasing the lateral and vertical resolution of the acoustic data will enhance the detection of dumped weapons. Concurrent ultra-high resolution seismic and magnetic acquisition may not only allow to map the exact location, distribution and burial depth of the scattered munition, but may also provide information on the diversity and type of dumped weapons. Combined with detailed information on the internal geological structure and potential natural hazards obtained from acoustic imaging (and possibly also electrical measurements) this will finally yield a better assessment of the current status of the dumpsites and the possible ecological risks related to the dumped weapons. In the meantime regular monitoring is crucial to track the evolution of the site and to detect possible future hazards, such as renewed surfacing of munition due to local erosion processes.

Archaeological site investigations

The application of marine reflection seismic profiling methods for archaeological site investigations, in particular buried wooden shipwrecks, is becoming increasingly important. The ability to image buried wooden objects will highly depend on the type of wood, the level of decay, and the surrounding sediment. On the whole, oak and pine artefacts are detectable in a wide range of marine sediments, and increasing wood degradation will generally yield more negative reflection coefficients. The size of the object and its orientation will also affect the imaging potential. The suitability of 2D and 3D acoustic techniques in submerged archaeological studies was tested with two different surveys over buried wooden shipwrecks.

A first 2D seismic survey took place on the river Schelde near Antwerpen. The target was a small 17th century wooden shipwreck severely damaged by dredging operations. The wreck pieces stood out clearly on the acoustic data as strong negative reflections, which suggests that the wood is heavily degraded. Six buried wreck parts, covered by 0.5-1 m of sediment, were identified spread over a distance of roughly 150 m. Pseudo-3D processing was applied to the single-channel network. Vertical and horizontal sections indicated the presence of buried wreck parts but the exact size and shape were not sharply defined. Most likely this was due to the

irregular fold coverage and relatively large bin size (2x2 m) which affected the resolution of the 3D data volume.

A second seismic survey was carried out over a buried 17th century shipwreck in the Dutch Wadden Sea using the inflatable 3D acquisition array. Although seismic penetration was limited (probably due to shallow gas) the wreck stands out clearly on the 2D data. The images confirm the existing information regarding shape and setting of the wreck (which has broken apart in two large pieces). The wreck is covered by maximum 2 m of sediment, and possible paleo-scour features are observed at its base. Weak phase inversion suggests a less advanced state of wood degradation. 3D data processing was carried out using a 0.5x0.5 m bin size. The application of precise static corrections and predictive noise filtering resulted in a marked improvement of the stacked data quality. The two main wreck pieces were identified on the vertical 3D cross sections. Time slices at 40 cm interval suggest the location of a large buried wreck piece but the features are not sharply defined. Most likely the data quality was influenced by the heterogeneous coverage (due to strong side currents) and small positioning inaccuracies related to source and streamer movement. Multiple reflections from the curved wreck pieces have probably also affected the 3D image quality.

The results from these two case studies clearly demonstrate the suitability of very high resolution acoustic imaging for detailed marine archaeological site investigations. The acoustic 'visibility' of buried wooden artefacts will depend on various factors, most importantly sufficient impedance contrast between the wood and the sediment. If this condition is fulfilled detection of the wooden object is possible, not only in 2D but also in 3D, provided that the positioning precision and coverage is high enough. The application of 3D techniques in archaeological studies is quite novel, and we have shown that concurrent multibeam data can greatly improve the quality of the 3D image. This opens new perspectives for the use of acoustic profiling in marine archaeological site surveys.

Shallow gas study

Shallow gas renders the acquisition of seismic images particularly difficult. The potential impact on the marine environment and on human activities stresses the need for a better knowledge of shallow gassy sediments. Detailed very high resolution reflection seismic investigations off the Belgian coast have revealed an extensive area marked by acoustic turbidity and poor seismic penetration likely due to the presence of shallow gas. The gas is believed to be of biogenic origin, and its geographical distribution is roughly bound to a wide band oriented more or less parallel to the coast. The origin of the gas is probably related to the presence of a thin peat-rich layer of Late Pleistocene/Early Holocene age, possibly in combination with minor gas formation in the fine-grained mud-rich Holocene sediments.

Gas-related features on the seismic data include acoustic turbidity and blanking, strong multiple reflections, and occasional enhanced reflections and phase reversal, as well as internal multiples. The acoustic turbidity often cuts sharply through the stratigraphy, and is frequently marked by varying offsets indicating different levels of upward gas penetration related to interbedded deposits of fine sand and mud. The gas occasionally reaches up to the seafloor. Velocity effects at the edge of the gassy zones seem to be absent, and no clear gas-escape features are observed from the seabed, although minor seepage cannot be ruled out. Refraction studies at the Paardenmarkt suggest the presence of thin gassy layers (thickness $\leq$ 2 m) and indicate a maximum depth of 18 m for the gassy sediments.

The seismic characteristics (scarce presence of enhanced reflections and bright spots, absence of velocity pull down or gas escape features) and velocity data from refraction and borehole measurements both on land and at sea suggest a low gas concentration of less than 1%. Cyclic loading, due to storms and waves, may have affected the upward bubble migration in shallow water areas. Bubble resonance effects most likely explain the different appearance of gassy sediments on sparker and Seistec records. The high frequency of the Seistec partly overlaps with the bubble resonance frequency and as a result acoustic masking is more complete. The presence of gas bubbles most likely does not have a marked impact on the physical properties of the shallow fine-grained sediments, and it is therefore not expected that shallow gas will cause further sinking of the dumped munition into the sediments at the Paardenmarkt dumpsite.

Ongoing work and future approach

The estuarine environment, at the boundary between land and sea, is an important focus in ongoing work. Minor changes in sea level have a direct impact on the hydrodynamic processes, sediment supply, morphology and preservation potential. The extreme shallow water depth of these transition environments, in particular intertidal flat areas, demands an adapted strategy. Specific operational techniques are needed to achieve sea-land data continuity without loss of coverage. This can optimally be done by using both land and marine sources. A recent study was carried out in the Verdronken Land van Saeftinge in the Westerschelde estuary, where high tidal amplitudes enabled the application of different techniques on land and on water (seismic, geo-electric, electromagnetic, CPT, coring). The results of this study indicate that no single technique can provide all the answers, and only an integrated use of complementary methods will allow getting a better grip on the sedimentary architecture. The simultaneous application of ocean-bottom cables and land cables may further decrease the gap between land and marine profiles by the acquisition of marine-marine, marine-land, land-marine and land-land data. Finally such integrated approach will help to improve our understanding of these highly complex sedimentary environments and allow the development of high-resolution predictive models for the dynamics of sediment redistribution at the land-sea interface. This is the key to understanding the response of coastal areas to a future sea level rise.

The study of submerged prehistoric landscapes forms an important new challenge in marine archaeological research. The reconstruction of submerged terrestrial landscapes and the possible impact of human activities on these landscapes are important requirements to help understand their archaeological potential (in the form of both submerged and re-worked material), but it may also provide key information on the human evolution (Westley et al. 2004). Sea-levels were generally much lower in late Pleistocene and early Holocene times and only reached near-present levels during the later part of the Holocene. Local sea-level fluctuations due to sedimentation or man-made interventions may have resulted in further submergence in certain areas. Although undoubtedly many sites may have been eroded or destroyed by rising sea levels, the existence - and importance - of submerged landscapes is nowadays generally accepted. In Belgium recent surveys have been undertaken to assess the potential of highly detailed acoustic imaging in the study of inundated terrestrial sites on the continental shelf. A first study focuses on the possible remains of Roman dykes and salt and/or peat exploitation offshore Raversijde, west of Oostende, and the distribution of pre-Roman tidal gullies. This should lead to a better understanding of the complex late Holocene evolution of the coastal area and the human impact on this region.

The geophysical challenge of shallow marine environments calls on advances in technology, combined with a certain pragmatism and creativity. The added value of integrated multi-parameter surveys, merging seismic acquisition with electrical, electromagnetic and

magnetic/gradiometric measurements, has clearly been demonstrated in this thesis. Potential future strategies include a.o. the combined deployment of surface-towed and seabed sources and sensors, and the simultaneous acquisition of land and marine data. The merging of different data sets into intelligible images is a challenge, which may find solutions in the advanced geostatistical tools and the developments in reservoir imaging in the hydrocarbon industry.

SAMENVATTING

Het hier voorgestelde onderzoek is gericht op de toepassing van ondiepe mariene akoestische beeldvorming voor milieu-, geotechnische en archeologische studies. Het nut van 3D seismische opnames voor kleinschalige studies van de ondiepe ondergrond wordt aangetoond met een studie over een kleine klei-diapier op de Schelde nabij Antwerpen. Zeer hoge resolutie seismische beeldvormingstechnieken, zowel in 2D als 3D, vormen een belangrijke methode in het onderzoek naar munitiedumpplaatsen en mariene archeologische sites, zoals naar bedolven houten scheepswrakken. Ter illustratie hiervan worden verschillende case-studies besproken, uitgevoerd in uiteenlopende omgevingen, gaande van rivieren en kustnabije zones tot de open zee. De seismische beeldvorming wordt vaak verstoord door de aanwezigheid van ondiep gas. De mogelijke impact van gas op het mariene milieu en eventuele constructiewerken vereist echter een betere kennis van deze sedimenten. Een recente studie werd daarom uitgevoerd met betrekking tot de gasrijke sedimenten voor de Belgische kust.

3D seismisch onderzoek

Zeer hoge resolutie (ZHR) seismische metingen vereisen een specifieke strategie. Een optimale benadering is noodgewongen een compromis tussen de behoefte aan hoge resolutie en de beperkingen van de fysische wetten. Een nieuw flexibel opnamesysteem (OPUS3D) werd ontworpen door het RCMG voor kleinschalige studies in ondiep water met beperkte penetratiediepte. Het opnamesysteem bestaat uit 16 ontvangers (onderlinge afstand 2 meter) met een totale spanwijdte van 14 meter. De ruimtelijke spreiding van de ontvangers wordt verzorgd door twee sets van elk drie opblaasbare frames vastgehecht aan een semi-rigide boot (RIB). Door middel van de keuze van de bron, de geometrie van bron en ontvangers, de vaarsnelheid etc. kan het systeem aangepast worden aan de omgeving en het te detecteren voorwerp. Het modulaire systeem is gemakkelijk te gebruiken vanaf kleinere boten, en laat zich gemakkelijk vervoeren in een auto-met-aanhanger. De centraal geplaatste RIB laat bovendien toe om het systeem autonoom te gebruiken in meer beschutte gebieden zoals meren en kanalen.

Een nauwkeurige plaatsbepaling van de akoestische bron en ontvangers is noodzakelijk aangezien kleine bewegingen van het opnamesysteem (bijvoorbeeld veroorzaakt door golven) snel kunnen leiden tot een verslechtering van het seismisch signaal. Met het oog op de vereiste resolutie (< 1 meter) moet de geometrie van de bron-ontvanger posities dan ook met decimeter-precisie gekend zijn. Korte streamers* en een korte bron-ontvanger afstand zullen de onzekerheid in posities verminderen. In beschutte gebieden zal de beweging van het opnamesysteem erg beperkt blijven en kunnen eventuele fouten in de plaatsbepaling genegeerd worden. In minder beschutte gebieden zoals de open zee of gebieden met een sterke stroming zal de stabiliteit van het opnamesysteem verminderen en zijn correcties aangewezen. Een optimaal seismisch signaal vereist een compromis tussen het bemonsteringsinterval (zgn. ‘sampling interval’), ligging en hoek van het object, en de signaalfrequentie. Een bronfrequentie van 2 kHz laat toe om hoeken tot 24 graden correct weer te geven. Om verstoring (zgn ‘aliasing’) van de hogere frequenties te voorkomen moet de lengte tussen de individuele ontvangers (zgn. ‘hydrofonen’) beperkt zijn (< 25 cm). De optimale bin**-dimensie is afhankelijk van de frequentie en de diepte van het te onderzoeken object

(een streamer is de kabel waarin de ontvangers zijn gevat en die achter het schip wordt geslept)*

*(** een bin is een vierkant gebiedje op de zeebodem waarbinnen de seismische sporen worden samengeteld - dit geeft de uiteindelijke 3D ruimtelijke bemonstering van de ondergrond).*

In het kader van het EU project "VHR3D" werden 3D seismische metingen uitgevoerd over een klei-diapier op de Schelde. Door de relatief beschutte omgeving bleef de beweging van het opnamesysteem zeer beperkt en correcties op de posities waren niet nodig. De resulterende beelden tonen de interne structuur van de klei-diapier in groot detail. Horizontale doorsnedes worden gekenmerkt door een groeiend concentrisch patroon. Naar boven toe vertoont de diapier een verstoorde interne structuur, waarschijnlijk een direct gevolg van eerdere verzakkingen. De kleilagen in de omgeving van de diapier worden gekenmerkt door grote aantallen concreties (mergelachtige verhardingen), met een gemiddelde diameter van 0.5 tot 2 meter en een dikte van 20 tot 50 cm. Het was een grote uitdaging om te kijken of deze concreties opgespoord konden worden in de 3D data. Daartoe werden zgn. "horizon slices" gemaakt, horizontale doorsnedes parallel aan een reflectieoppervlak (kleilaag). Het patroon van verschijnende en weer verdwijnende "vlekken" in opeenvolgende doorsneden doet vermoeden dat we hier te doen hebben met concreties of klusters van concreties.

Het onderzoek op de Schelde illustreert duidelijk het belang van zeer hoge resolutie 3D onderzoek voor gedetailleerde geotechnische studies. De ‘cost-efficiency’ van de ontwikkelde methodologie, zonder complexe procedures (niet alleen wat betreft dataopname, maar ook dataverwerking), vormt daarbij een groot voordeel. De resultaten van de metingen geven verder aan dat de nauwkeurige plaatsbepaling van bron en ontvangers (met decimeter-precisie) een cruciale rol speelt in 3D seismische beeldvorming. Door de beschutte omgeving op de Schelde en het feit dat de seismische lijnen parallel werden gevaren aan de stroming, kon een maximale stabiliteit van het meetsysteem bereikt worden, hetgeen resulteerde in een optimale datakwaliteit met grote resolutie.

Onderzoek van munitiestortplaatsen

In zee gedumpte chemische munitie is het onderwerp van groeiende bezorgdheid. De totale hoeveelheid munitie in de Noordzee, Baltische zee en de noordelijke ijszeëen wordt geschat op enkele honderdduizenden ton. De chemische munitie werd vaak gedumpt in ondiep water, in de nabijheid van dichtbevolkte kustgebieden. Een groot aantal ongelukken werd gerapporteerd in verschillende gebieden, meestal met betrekking tot de visserij. Tot op vandaag is erg weinig bekend over de exacte ligging en verspreiding van de munitie in de meeste stortplaatsen. De munitie is vaak bedolven onder een recente sedimentlaag waardoor een snelle opsporing niet voor de hand ligt. Voor een juiste risico-analyse is in de eerste plaats een gedetailleerd beeld van de interne structuur van de stortplaats nodig, niet alleen wat betreft de begraven munitie maar ook de natuurlijke opbouw van de ondergrond.

De Paardenmarkt is een oude munitiestortplaats voor de kust van Knokke-Heist. Na de eerste wereldoorlog werd hier een grote hoeveelheid oorlogsmateriaal gestort. De totale massa wordt geschat op zo'n 35.000 ton waarvan een derde deel chemische munitie. Op hydrografische kaarten wordt het stortgebied voorgesteld als een vijfhoek (met een oppervlakte van ongeveer 3 km2) waarin een anker- en visverbod heerst. Magnetische metingen wijzen op een centrale zone met sterke magnetische afwijkingen, waarschijnlijk gerelateerd aan het gros van de gedumpte munitie, omgeven door een zone met zwakkere afwijkingen. De munitie is volledig begraven onder een paar meter sediment, waarschijnlijk een gevolg van de uitbreiding van de buitenhaven van Zeebrugge die een gevoelige sedimenttoename tot gevolg heeft gehad. Ondiepe reflectoren verwijzen naar de verschillende stadia in het recente sedimentatieproces. De grootste sedimenttoename gebeurde in zuidwestelijke hoek (tot 4 meter) met een geleidelijke afname naar het noorden toe. Recent waargenomen duinstructuren op de zeebodem (tot 1 m hoog) wijzen op een actief sedimentatiemilieu. De detectie van munitie wordt bemoeilijkt door de aanwezigheid van ondiep gas waardoor de akoestische zichtbaarheid beperkt wordt tot een paar

meter. Clusters van diffractiehyperbolen op de akoestische data kunnen hoogstwaarschijnlijk gerelateerd worden aan bedolven munitie. Dit wordt bevestigd door de resultaten van magnetische en gradiometrische metingen. Waarschijnlijk betreft het hier ondiepe munitie; door de geringe penetratiediepte van het seismisch signaal blijft de dieper begraven munitie akoestisch 'onzichtbaar'.

Een tweede studie werd uitgevoerd in de zuidelijke Baltische Zee. Ten oosten van het eiland Bornholm werd hier na WO2 zo'n 32.000 ton chemische munitie gestort. Vier scheepswrakken werden in het stortgebied gevonden. Op verschillende plaatsen werden verhoogde concentraties arsenicum gemeten, onder andere in de nabijheid van de wrakken wat kan betekenen dat sommige wrakken chemische munitie bevatten. In 2006 en 2007 werd gedetailleerd seismisch onderzoek uitgevoerd in het stortgebied, gecombineerd met magnetische metingen. In total werden zeven seismisch-stratigrafische eenheden geïdentificeerd. Deze eenheden weerspiegelen de verschillende fases in de Holocene en laat-glaciale geschiedenis van het gebied. Een groot aantal diapier-vormige ontwateringsstructuren werden waargenomen, waarschijnlijk veroorzaakt door overdruk. De scheepswrakken hebben een lengte tussen de 20 en 50 meter en steken 1 à 2 meter boven de zeebodem uit. De wrakken worden gedeeltelijk bedekt door een dunne laag sediment. Het groot aantal sterke diffracties op de akoestische data duidt op een onregelmatig oppervlak van de wrakken met veel uitstekende delen. Dit werd bevestigd door recente side-scan en video-opnames. Grote objecten werden waargenomen in de nabijheid van de scheepswrakken, het betreft hier waarschijnlijk losgekomen wrakstukken.

Een groot aantal bedolven voorwerpen werd waargenomen op de akoestische data. Naar alle waarschijnlijkheid gaat het hier om gedumpte munitie. De objecten hebben een gemiddelde grootte tussen de 1.5 en 5 meter, in sommige gevallen zelfs tot 10 meter, en liggen niet meer dan 2 meter diep begraven. Ondiepe putstructuren in de zeebodem zijn waarschijnlijk het gevolg van de impact van het dumpen. De magnetische gegevens bevestigen de aanwezigheid van een groot aantal ijzerhoudende objecten in de bodem. In de meeste gevallen was er een goede correlatie tussen de seismische en magnetische data. Grote objecten op de akoestische data kwamen echter niet altijd overeen met grote magnetische anomalieën. Dit is mogelijk een gevolg van het feit dat het ijzeren omhulsel slechts een klein deel (een derde of minder) van het bruto gewicht van deze voorwerpen vormt (het overgrote deel bestaat uit toxische inhoud). De verspreiding van het oorlogsmateriaal is erg heterogeen, en zones met een hoge dichtheid aan voorwerpen wisselen af met grotendeels lege zones. De seismische gegevens bevestigen ook de grote diversiteit aan gestort oorlogsmateriaal, gaande van bommen en granaten tot grote vaten en containers.

De resultaten van deze case-studies illustreren overduidelijk het nut van seismische metingen in munitiedumponderzoek en de toegevoegde waarde van gecombineerde geofysische metingen. Een hoge laterale en vertikale resolutie van de akoestische gegevens zal de detecteerbaarheid van begraven munitie gevoelig vergroten. Simultaan uitgevoerde magnetische en seismische metingen laten niet enkel toe om de exacte ligging, verdeling en diepte van de bedolven munitie in kaart te brengen, maar geven ook informatie met betrekking tot het verspreidingspatroon en het type van gestort materiaal. Samen met de gedetailleerde informatie over de interne geologische structuur van de stortplaats, verkregen uit zeer hoge resolutie akoestische metingen, moet dit uiteindelijk leiden tot een betere risico-analyse van de stortplaats en de mogelijke gevaren voor het milieu. Regelmatige monitoring blijft echter belangrijk om de evolutie van de stortplaats te volgen en eventuele risico's in de toekomst te detecteren (zoals het opnieuw vrijkomen van de munitie door erosie).

Archeologisch onderzoek

De toepassing van mariene akoestische onderzoekstechnieken voor de studie van archeologische sites, meer in het bijzonder bedolven houten scheepswrakken, is gestaag toegenomen over de laatste jaren. De mogelijkheid om begraven houten objecten te detecteren in de zeebodem zal sterk afhangen van het soort hout, de staat van ontbinding en het omringende sediment. In het algemeen is eiken- en dennenhout goed detecteerbaar in de meeste mariene sedimenten. Een toenemende staat van ontbinding van het hout zal aanleiding geven tot een hogere reflectiecoëfficiënt. Ook de grootte en ligging van het houten object kunnen van invloed zijn op de het akoestische beeld. Het potentieel van 2D en 3D seismisch onderzoek wordt geïllustreerd aan de hand van twee studies van bedolven scheepswrakken.

Een eerste studie betreft een zeventiende-eeuws scheepswrak op de Schelde vlakbij Antwerpen. Het wrak werd in het verleden zwaar beschadigd door baggerwerkzaamheden. Verschillende wrakstukken konden waargenomen worden op de 2D seismische data. Een sterke faseomkering van het seismisch signaal duidt op een verregaande staat van ontbinding van het hout. In totaal werden zes wrakstukken gelokaliseerd, verspreid over een afstand van zo'n 150 meter. De wrakstukken zijn begraven onder een halve tot één meter sediment. Uitzonderlijk werd een pseudo-3D verwerking van de éénkanaals-gegevens uitgevoerd. Vertikale en horizontale doorsnedes doorheen het 3D volume tonen de aanwezigheid van begraven wrakstukken, maar de resolutie van de beelden liet niet toe om de exacte vorm en ligging van de wrakstukken te karteren. Hoogst waarschijnlijk is dit een gevolg van de onregelmatige bedekking van meetpunten in het gebied en de grootte van de bins (2x2 m).

Een tweede studie werd uitgevoerd met het flexibel seismisch opnamesysteem OPUS3D over een begraven zeventiende-eeuws scheepswrak in de Waddenzee. Ondanks de beperkte penetratiediepte van de akoestische gegevens (waarschijnlijk door de aanwezigheid van ondiep gas) is het wrak goed waarneembaar op de 2D data. De vorm en ligging van de wrakdelen zijn duidelijk te onderscheiden en bevestigen eerdere informatie van duikers in de jaren negentig toen het wrak nog gedeeltelijk aan de oppervlakte lag. Het wrak ligt op dit moment begraven onder een relatief dunne sedimentlaag van maximum 2 meter. De zwakke faseomkering van het seismisch signaal lijkt te duiden op een minder verregaande staat van ontbinding vergeleken met het wrak in de Schelde. 3D dataverwerking werd uitgevoerd met een bin-afmeting van 0.5x0.5 meter. Nauwkeurige vertikale correcties aan de hand van multibeamgegevens en een geavanceerde ruisfiltering resulteerden in een gevoelige verbetering van het 3D beeld. De wrakstukken zijn duidelijk waarneembaar op de vertikale doorsnedes, maar de exacte ligging is niet éénduidig op de horizontale doorsnedes. Waarschijnlijk liggen kleine afwijkingen in de plaatsbepaling van het opnamesysteem hiervan aan de basis. Maar ook de kromming van de wrakstukken heeft mogelijk geleid tot verstoring van het beeld door meervoudige reflecties.

De resultaten van het onderzoek op de Schelde en in de Waddenzee tonen duidelijk de geschiktheid van zeer hoge resolutie seismische opnames voor wrakkenstudies. De akoestische 'zichtbaarheid' van een bedolven houten wrak wordt grotendeels bepaald door het impedantiecontrast* tussen het hout en het omringende sediment. Als aan deze voorwaarde is voldaan, dan is akoestische detectie van het voorwerp mogelijk, niet alleen in 2D maar ook in 3D, op voorwaarde dat de akoestische bedekking en positioneringsnauwkeurigheid hoog genoeg zijn. Een belangrijke verbetering van de seismische beelden kan verkregen worden door het gebruik van simultane multibeammetingen.
(impedantie is het product van dichtheid en akoestische snelheid)*

Ondiep gas

Ondiep gas kan de seismische metingen ernstig beïnvloeden. De mogelijke impact van ondiep gas op het mariene milieu en eventuele constructiewerken op of in de zeebodem maakt een diepgaandere studie aangewezen. De afgelopen decennia werd voor de Belgische kust een gedetailleerd netwerk van seismische metingen uitgevoerd. De analyse van deze gegevens heeft aangetoond dat een groot deel van de kustnabije zone gekenmerkt wordt door een (al dan niet gedeeltelijk) verstoord seismisch signaal en geringe penetratiediepte, veroorzaakt voor de aanwezigheid van ondiep gas. Het gas heeft waarschijnlijk een biogene oorsprong (afkomstig van de afbraak van organisch materiaal), en de geografische verspreiding van het gas wijst op een mogelijke relatie met een oude veenlaag uit het late Pleistoceen of het vroege Holoceen. Mogelijk heeft ook enige gasvorming plaatsgevonden in de meer recente slibafzettingen.

Een flink aantal gas-gerelateerde fenomenen werd waargenomen op de seismische data: akoestische verstrooiing (zgn 'turbidity') en absorptie (zgn. 'blanking') van het signaal, sterke zeebodemecho's, versterkte reflecties en faseomkering, en interne echo's. De akoestische verstrooiing snijdt vaak scherp door de geologische gelaagdheid heen en wordt lokaal gekenmerkt door trapsgewijze vertikale sprongen die wijzen op verschillende niveaus van opwaartse gasmigratie gerelateerd aan zand- en kleilaagjes. Het gas reikt soms tot de zeebodem, maar er werden geen duidelijke sporen waargenomen van ontsnapping van gas uit de zeebodem. Akoestische snelheid-gerelateerde effecten (zoals een neerwaartse afbuiging van de reflectoren aan de rand van het gasgebied) lijken niet aanwezig. Seismische refractiestudies op de Paardenmarkt suggereren een maximale diepte van 18 meter voor de gasrijke sedimenten.

Al deze seismische karakteristieken wijzen op een zeer lage gasconcentratie, waarschijnlijk lager dan 1%. Dit wordt bevestigd door de akoestische snelheden bekomen uit refractie- en boorgatexperimenten op land en in zee. Waarschijnlijk heeft de lage gasconcentratie weinig invloed op fysische kenmerken van de ondiepe sedimenten (o.a. draagkracht). Een cyclische belasting van de sedimenten veroorzaakt door storm en wind kan de opwaartse beweging van gasbellen beïnvloeden in ondiep water (deze gasbellen zijn erg klein, over het algemeen niet meer dan een paar mm). De resonantiefrequentie van de gasbellen (zgn. 'bubble resonance') verklaart waarschijnlijk de verschillende uitingen van gasrijke sedimenten op sparker en Seistec beelden. De grote overlap van het hoger-frequente Seistec signaal met het resonantiespectrum van de gasbellen veroorzaakt immers een sterkere trilling van de gasbellen en dus een grotere verstrooiing van het signaal.

Verdere ontwikkelingen in onderzoek

Estuaria, op de grens van land en zee, vormen een belangrijke focus van marien onderzoek. Kleine veranderingen in het zeespiegelniveau hebben immers een directe impact op de hydrodynamische processen, sedimenttoevoer en morfologie van zowel supratidale, intertidale en subtidale milieus. De vaak extreem geringe waterdiepte van deze overgangsgebieden vormt een grote uitdaging en vraagt daarom een specifieke aanpak om de land-zee overgang correct in kaart te brengen. Dit kan optimaal gebeuren door de combinatie van metingen op het land en op het water. Een recente studie werd uitgevoerd in het Verdronken Land van Saeftinge in de Westerschelde, waar de grote getijdeverschillen toelaten om verschillende technieken, waaronder seismiek, geo-electrische en electromagnetische metingen, CPT en boringen, te gebruiken bij zeer uiteenlopende waterdieptes. Mariene metingen werden uitgevoerd in de geulen en op zandplaten bij hoog tij, gedurende laag tij werden landmetingen uitgevoerd op schorren, zandplaten en in kleine geulen. De resultaten van deze studie tonen aan dat seismische metingen weliswaar een zeer grote detailinformatie opleveren, maar toch is een combinatie van

complementaire technieken cruciaal om een volledig beeld te geven van de sedimentatieprocessen en de ontwikkeling in actieve estariene milieus. Dit moet uiteindelijk leiden tot een beter inzicht in het gedrag van laaggelegen kustgebieden en laat ons toe om kustlijnontwikkeling, sedimentaanwas en -afslag te modelleren.

De studie van bedolven prehistorische landschappen vormt een belangrijke uitdaging in marien archeologisch onderzoek. De reconstructie van deze submariene landschappen en de mogelijke menselijke impact op de landschappen kan ons helpen een beter beeld te krijgen van hun archeologisch potentieel (zowel wat betreft begraven als herwerkt archeologisch materiaal). De zeespiegelstand was over het algemeen veel lager gedurende het late Pleistoceen en het vroege Holoceen, en het hedendaagse peil werd pas in het late Holoceen bereikt. Plaatselijke zeespiegelschommelingen waren mogelijk door lokale sedimentatie of door menselijke invloed. Waarschijnlijk zijn sommige van deze prehistorische landschappen (gedeeltelijk) verdwenen door erosie, maar hun belang staat inmiddels buiten kijf. In Belgie werd recent een studie aangevat naar het potentieel van zeer hoge resolutie seismische technieken voor de detectie en identificatie van Romeinse artefacten (o.a. dijken, veenwinning) en de kartering van prehistorische getijdengeulen voor de kust van Raversijde, ten westen van Oostende. Dit moet ons toelaten om een beter beeld te krijgen van de complexe laat-Holocene evolutie van het kustgebied en de menselijke impact op dit landschap.

De geofysische uitdaging van ondiepe mariene milieus vraagt om nieuwe technologische ontwikkelingen, gepaard met een zeker pragmatisme en veel creativiteit. De toegevoegde waarde van geïntegreerd multi-parameter onderzoek, waarbij bijvoorbeeld seismische metingen worden gecombineerd met geo-electrische en magnetische metingen, werd duidelijk aangetoond in dit proefschrift. Deze strategie kan nog verder doorgetrokken worden, bijvoorbeeld door het gecombineerd gebruik van akoestische bronnen en ontvangers aan het wateroppervlak en op de zeebodem, en de simultane opname van land- en mariene data met behulp van land- en zeebodemkabels. De integratie en visualisatie van deze verschillende datasets vormt hierbij een grote uitdaging.

ANNEX – THE SEISCAT 3D SEISMIC APPROACH

A.1. Acquisition system "SEISCAT"

In the framework of the EC Hydrocarbons Project 'An integrated approach to the stability evaluation of prospective offshore sites' a first test survey was carried out in 1990 on the Schelde river using the compact 3D acquisition system SEISCAT. The system consisted of an array of 12 short dual-channel streamers and an acoustic source towed from a modified Hobiecat catamaran (Figure A-1). The catamaran frame had a width of 8 m between the two floats (6 m long) and two extension beams yielded the necessary width for the streamer array. The streamer distance of 1 m resulted in a total wing span of the system of 11 m; channel spacing in the streamers was 1 m (Verschuren 1992).

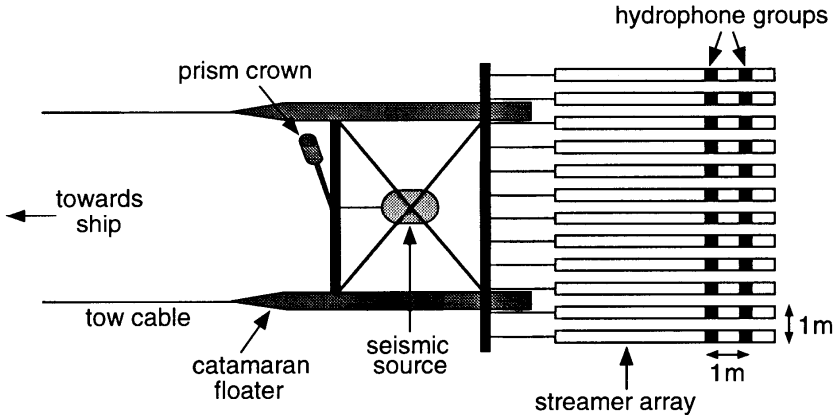

Figure A-1 *Lay-out of the 3D seismic acquisition system 'SEISCAT' (after Henriet et al. 1992).*

A small 3D data volume (50x180 m, penetration ~100 m) was acquired over the clay diapir on the Schelde river in 1990. During the survey the source was attached under the catamaran frame, close to the positioning antenna. The streamers were towed at a short distance behind the catamaran frame, resulting in offsets ranging from 6 to 9 meters. The SEISCAT array was towed 10 m behind the vessel. In order to avoid as much noise as possible the latter sailed on electrical propulsion (Henriet et al. 1992). Both a boomer (EG&G Uniboom) and watergun (Sodera 15 in^3) were used. Seismic data were recorded using an EG&G 2420 recorder. The watergun was fitted with a modified mouthpiece and lashed horizontally to a fender at 0.2 m depth, resulting in improved high frequency content. Both sources have power spectra extending from a few hundred Hz to well over 2000 Hz (Henriet et al. 1992).

Sampling interval was 0.25 ms, shot interval 1 s. An anti-alias filter of 1400 Hz was applied. Positioning was done with an autotracking laser theodolite set up on the river bank, which continuously tracked a crown of reflector prisms mounted on the catamaran frame. This was the best possible option at the time (DGPS-based systems had not yet reached sufficient accuracy level). Positions of the prism (cm precision) were telemetrically transferred to the vessel every two seconds (Henriet et al. 1992). To avoid problems in array stability the seismic tracks were sailed against the current, alternatively forward and backwards, the latter simply by decreasing the speed. This however caused a considerable variation in the absolute velocities over the ground, and shot intervals ranged between 0.5 and 2 m. The combination of low vessel speed, currents and sometimes busy ship traffic also made it difficult to steer along the pre-planned sail tracks (Henriet et al. 1992).

A.2. Initial data processing

Processing of the small-scale 3D data volume implied challenging aspects related to the algorithmic treatment of the data, taking into account both the geotechnical goals and the current processing facilities. Initial processing of the data was carried out using Phoenix Vector software, and focused on a 50x180 m area covering the clay diapir. Boomer and watergun data were sorted in two separate grids of bins using a bin size of 1x1 m. Due to the difficult navigation the coverage was rather variable. Boomer coverage was fairly complete but heterogeneous, with some gaps along the margin, whereas the watergun data were acquired in a narrower zone.

Velocity values for NMO correction were based on a 1D velocity model extracted from geotechnical investigations at the tunnel site (1500 m/s for the water column, 1650 m/s for the entire sediment column) (Heldens 1983). Although the model is a simplification, the limited offset and shallow depth of the target will only allow for extremely small variations in the P-wave velocity that most likely have very little effect on the imaging process. Since tidal action on the river Schelde is large (amplitudes up to 5.5 m), tidal corrections were carried out by adding a timeshift based on the vertical coordinate of the positioning prism crown.

The results after stacking for the boomer data are shown Figure A-2 (the watergun results showed less detail than the boomer data due to lower source frequency and lower data coverage). The vertical section was taken from a central row of bins. The diapiric deformation is clearly visible but its internal facies remains rather chaotic and diffraction hyperbolae were only occasionally observed. The latter is most likely related to the limitation of the sampled frequency band that restricted the possible achieved imaging resolution. Time slices shown in Figure A-2 were taken from the boomer data. The time slices, separated by 0.25 ms, belong to the lower part of the diapir. The concentric reflector pattern of the diapir stands out clearly.

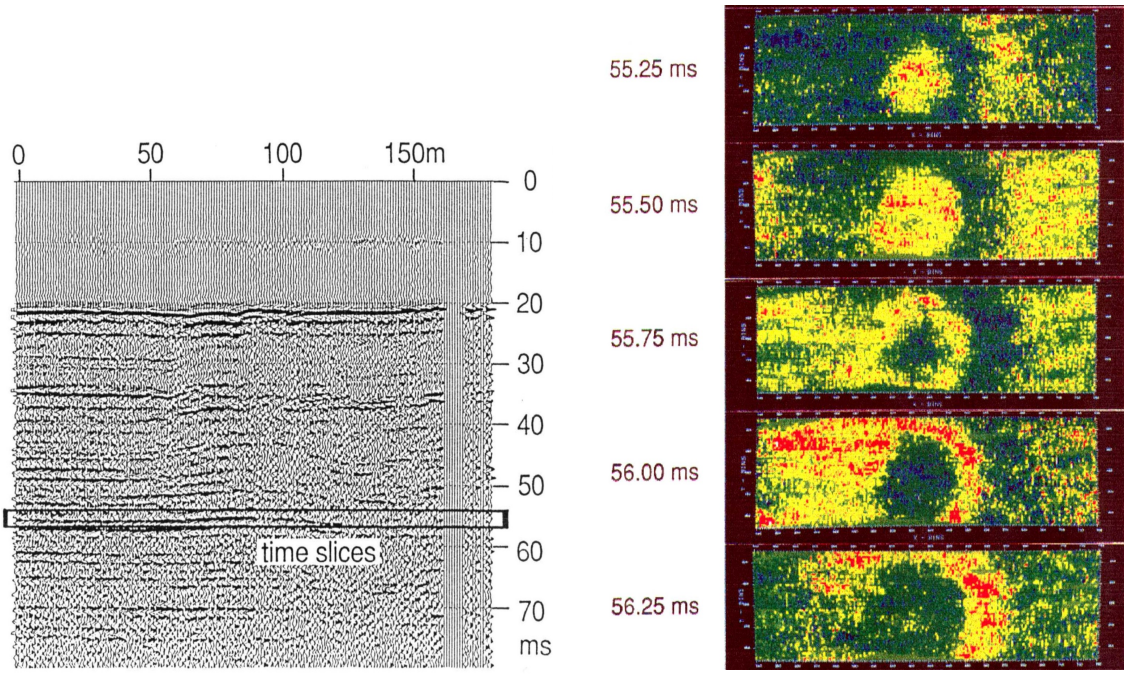

Figure A-2 *1990 stack results (boomer data). Left: Vertical sections along a central row of bins. The black rectangle marks the window of the time slices. Right: Time slices with 0.25 ms interval, showing the concentric reflector pattern over the clay diapir, area dimensions 50x180 m (after Henriet et al. 1992).*

A.3. Advanced data processing - stacking

In 1995-1996 the 3D data were further processed in the framework of the EC MAST-II Fellowship Research Project 'Very high resolution 3D seismic reflection imaging' the 3D data volume was subjected to further processing (Missiaen 1997). Analysis of the watergun data revealed a strong variation in first break arrivals, most likely due to a firing delay caused by failure of the electromagnetic valve of the gun. Due to these static problems, but also the lower frequency content and limited areal coverage, the quality of the watergun data was considerably less compared to the boomer data and further processing focused on the boomer data (Missiaen 1997).

Preliminary processing included bandpass filtering, removal of the direct wave arrivals (muting), tidal and NMO correction (using 1500 for the water column and 1650 m/s for the sediments), and additional multiple removal. Although multiples were suppressed in the stacking process (due to different tidal corrections) they did not disappear completely. A simple deconvolution routine based on multiple prediction submitted to attenuation filtering was therefore applied, which removed the larger part of the river-bed multiple (Missiaen 1997). No amplitude correction was applied, due to the lack of information regarding the acquisition device.

Shot and receiver positions were calculated taking into account the array heading. For each trace the reflection midpoint position was computed. A stack grid was then set out in 1x1 m bins, and the stack bin geometry of each trace midpoint was calculated. The stack fold was fairly good with a maximum of 24 traces per bin, but due to the irregular navigation the coverage was not homogeneous (Figure A-3).

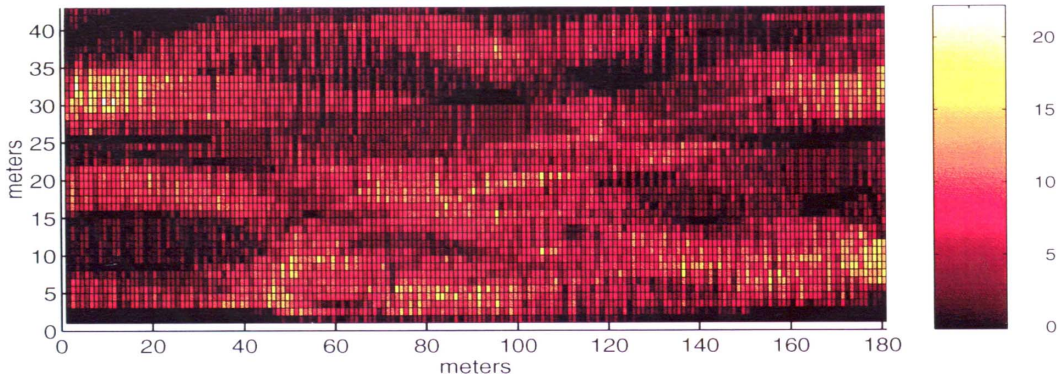

Figure A-3 *Fold coverage of the boomer data in the reduced area, 1990 data (after Missiaen 1997).*

The stacked data still displayed some high frequency variations in first break (seafloor) arrivals. In order to correct for these time delays, and having no bathymetric control, the river-bed reflectors were smoothed by low-passing the first break wavelengths that are larger than the Fresnel zone - thus assuming that the traces had only been shifted in time with a constant value. Although this resulted in a clear improvement in the upper few meters, the data quality decreased dramatically with depth. This suggests that the observed delays were also related to positioning inaccuracies (Missiaen 1997).

The final stack results are shown in Figure A-4. The vertical inline section was chosen from a central row of bins, across the centre of the clay diapir. In general the quality of the stacked section was good in the lower part of the diapir, with a large number of energetic reflectors showing up, but the upper part of the diapir remained disturbed. As was the case for the 1990

results, now the imaging resolution was restricted also by the limitation of the sampled frequency band. Time slices were taken from the lower part of the diapir (indicated by the black arrow on the left), separated by 0.6 ms (~0.5 m). They clearly show the concentric reflector patterns growing towards the base of the diapir. Time slices above those shown in Figure A-4 were less and less coherent, which confirms the chaotic reflector pattern observed on the time section.

The fact that the upper part of the diapir remains very chaotic may be due to gravitational collapses. Indeed the diapir growth may have induced stresses in the less undercompacted upper part of the clayey formation, causing overlying horizons to collapse into the initially undercompacted zone and destroying its internal structure (Verschuren 1992).

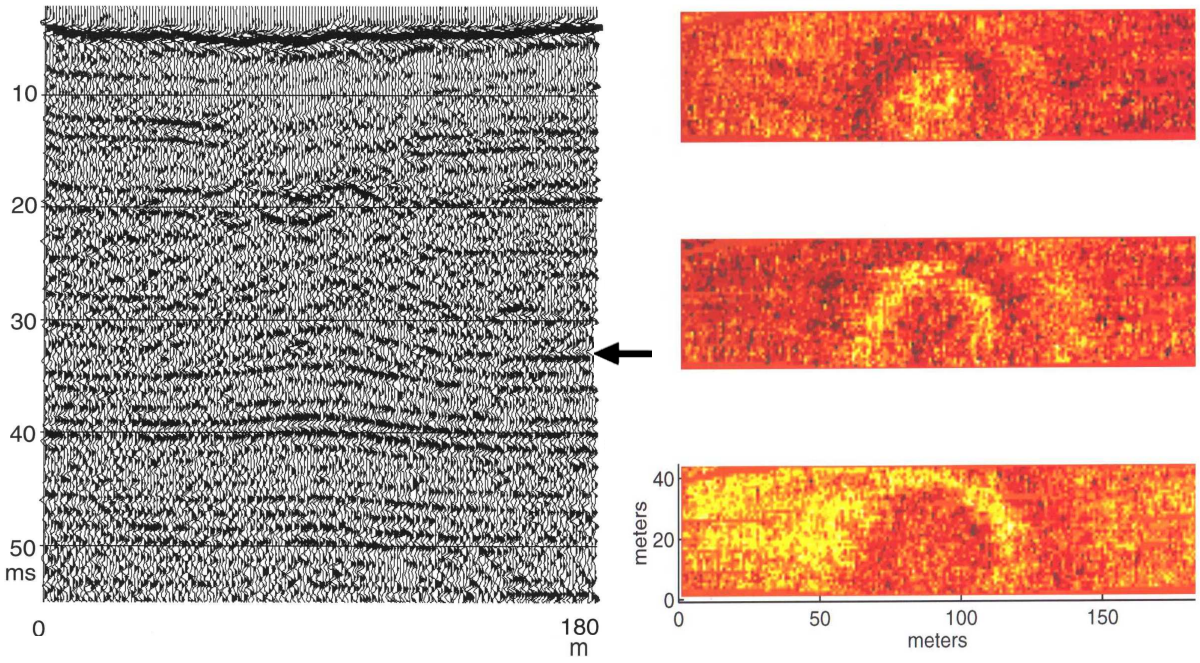

Figure A-4 *1995 stack results (boomer data). Left: Vertical inline section from a central row of bins through the 3D volume. The arrow marks the location of the time slices. Right: Series of consecutive time slices separated by 0.6 ms (~0.5 m).*

A.4. Advanced data processing – 3D migration

In order to fully take into account the 3D nature of the seabed and its near subsurface prestack migration processing was tried. The 3D migration had the reputation of being difficult to use and requiring large computer resources and practical advice for its application in near subsurface seismic data was still in short supply.

The main benefits of migration include the removal of the propagation distortion and noise reduction (Hatton et al. 1986). As the data were not calibrated attention was only paid to the distortion in position. Due to the shallow depth and one-dimensional stratified medium dramatic geometrical changes were not expected. Migration is conventionally carried out after stacking. Poststack migration is less costly as it involves a reduced volume of data, and is often quite robust. Prestack migration gives more accurate results but it has the reputation of being difficult to use and very costly. In shallow subsurface seismics we are mainly interested in the repositioning of the reflectors, and this allows some simplification of the migration algorithm (Missiaen 1997).

The migration method was based on the Kirchhoff summation approach, being economical and easy to handle complex acquisition geometries. It can be interpreted as summing along diffraction curves, every point in the depth section being a possible diffractor. As velocity input a 1D stratified velocity model was used, based on geotechnical investigations nearby. This represents an oversimplification of reality, but seems justified by the shallow environment (Marsset et al. 1998). Using this simple velocity model a 2D time grid was created with 0.1 m intervals, chosen with respect to the average wavelength of the seismic signal (< 1/10). Before actual migration an inverse NMO algorithm was applied to the tidal-corrected zero-offset data.

A horizontal migration grid of 1x1 m bins was created, and for each shot the bin midpoints falling within a spread coverage of 38 m^2 were calculated (a larger spread did not improve the overall distribution) (Marsset et al. 1998). Actual migration was carried out per shot. For each bin within the given spread coverage the offset was computed and travel times were calculated by placing source and receiver within the 2D time grid. Using the 3D Kirchhoff algorithm the energy of the reflector point located at the bin was computed, the weighted sum of the 24 different trace-values resulting in the final migrated trace. Finally the migrated traces were stacked using a 1x1 m grid.

Figure A-5 shows the results after prestack migration. The depth section was chosen from the centre of the diapir. Depth slices (0.5 m interval) were taken from the lower part of the diapir. Reflectors on the depth section seem more coherent than on the stacked time section (see Figure A-4), and the concentric reflector pattern on the depth slices seems to be marked by a slightly higher resolution. Still the uppermost part of the diapir remains chaotic. Due to the 1D stratified velocity model the data improvement was mainly due to noise reduction and smoothing, and in a lesser extent to the repositioning of the reflectors.

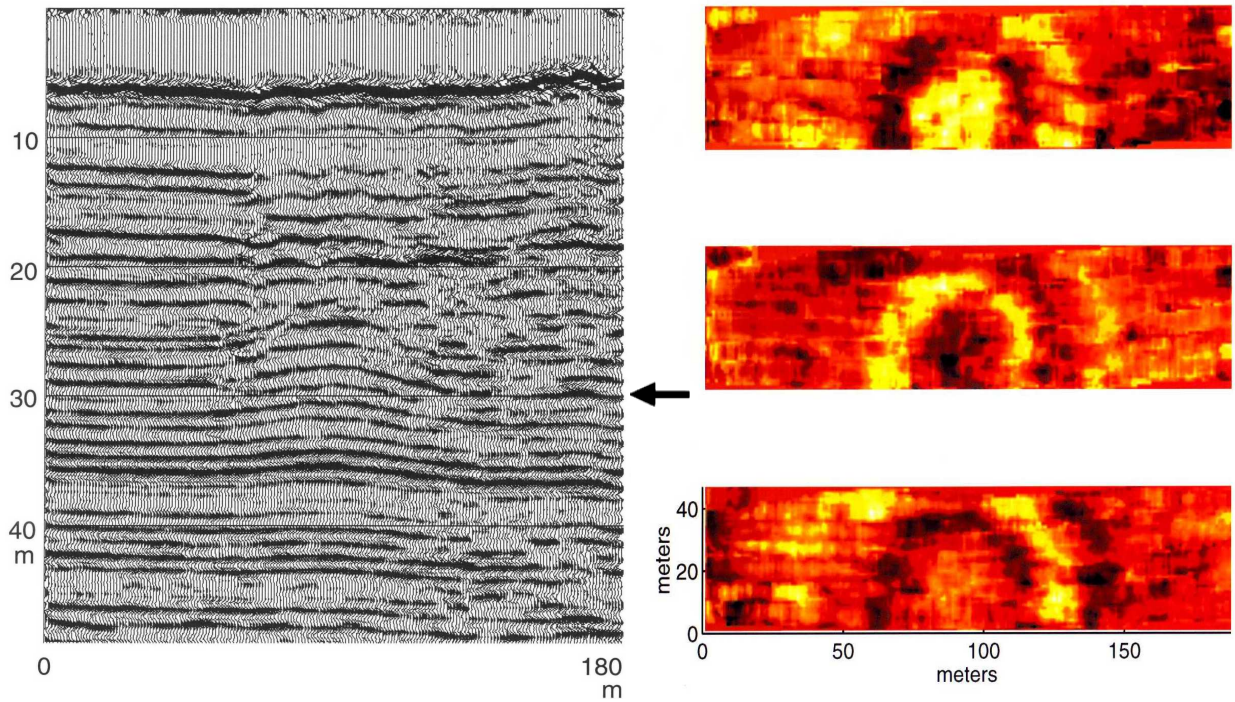

Figure A-5 *1990 stack results with 3D pre-stack migration (boomer data). Left: Depth section from a central row of bins. The arrow indicates the location of the depth slices. Right: Depth slices separated by 0.5 m.*

REFERENCES

Abdulah K.C., Anderson J.B., Coperude S. and Canning A. 1997. Temporal and spatial sampling constraints in high-resolution 3-D seismic surveys. *Marine Geophysical Researches* **19**, 97-113.

Abegg, F. and Anderson, A.L. 1997. The acoustic turbid layer in muddy sediments of Eckernförde Bay, Western Baltic: methane concentration, saturation and bubble characteristics. *Marine Geology* **137**, 137-147.

Anderson, A.L. and Hampton, L.D. 1980. Acoustics of gas-bearing sediments. *J. Acoust. Soc. Am.* **67**(6), 1865-1904.

Anderson, A.L. and Bryant, W.R. 1990. Gassy sediment Occurrence and Properties: Northern Gulf of Mexico. *Geo-Marine Letters* **10**, 209-220.

Anderson, A.L., Abegg, F., Hawkins, J.A. et al. 1998. Bubble populations and acoustic interaction with the gassy floor in Eckernförde Bay. *Continental Shelf Research* **18**, 1807-1838.

Andrén, E., Andrén T. and Sohlenius, G. 2000. The Holocene history of the southwestern Baltic Sea as reflected in a sediment core from the Bornholm Basin. *Boreas* **29**, 233-250.

Andrulewicz, E. 1996. War gases and ammunition in the Polish Economic Zone of the Baltic Sea. In : A.V. Kaffka (ed), Sea-Dumped Chemical Weapons: Aspects, Problems and Solutions. *NATO ASI Series* **7**, 9-15.

Anstey, N.A. 1981. Seismic Prospecting Instruments: Signal Characteristics and Instrument Specifications, Vol 1, Borntraeger, Berlin, 151 pp.

Archie, G.E. 1942. The electrical resistivity log as an aid in determining some reservoir characteristics. *Transactions of the American Institute of Mining, Metallurgical en Petroleum Engineers* **146**, 54-62.

Arnott, S., Dix, J., Best, A. and Gregory, D. 2005. Imaging of buried archaeological materials: the reflection properties of archaeological wood. *Marine Geophysical Researches* **26**, 135-144.

Ashton, C., Bacon, B. et al. 1994. 2D seismic survey design. Oilfield review, April 1994, 19-32.

Baumgartner, F. 1995. A new method for geoelectrical investigations underwater. *Geophysical Prospecting* **44**, 71-98.

Bearden, D.M. 2007. U.S. Disposal of Chemical Weapons in the Ocean: Background and Issues for Congress. CRS Report for Congress. Congressional Research Service, RL33432, 22 pp.

Beddington, J. and Kinloch, A.J. 2005. Munitions Dumped at Sea: A Literature Review. Imperial College, London, 90 pp.

Berkhout, A.J. 1997. Pushing the limits of seismic imaging. *Geophysics* **62**, 937-969.

Best, A., Tuffin, M., Dix, J. and Bull, J. 2004 Tidal height and frequency dependence of acoustic velocity and attenuation in shallow gassy marine sediments. *Journal of Geophysical Research* **109**, B08101, doi:10.1029/2003JB002748.

Björdal, C, Nilsson, T. and Daniel, G. 1999. Microbial decay of waterlogged archaeological wood found in Sweden. *Int. Biodeterioration & Biodegradation* **43**, 63-73.

Blanchette, R. 2000. A review of microbial deterioration found in archaeological wood from different environments. *Int. Biodeterioration & Biodegradation* **46**, 189-204.

BSH 1993. Chemical munitions in the southern and western Baltic Sea. Compilation, Assessment and Recommendations. Bundesamt für Seeschiffahrt und Hydrographie (Federal Maritime and Hydrographic Agency), Hamburg, Germany, 65 pp.

Bull, J. Quinn, R. and Dix, J. 1998. Reflection coefficient calculation from marine high resolution seismic reflection (chirp) data and application to an archaeological case study. *Marine Geophysical Researches* **20**, 1-11.

Caston, G.F. 1979. Wreck marks: indicators of net sand transport. *Marine Geology* **33**, 193-204.

Charlet, F. 2001. Etude de la dynamique sédimentaire et morphologique d'un haut-fond marin: Le Paardenmarkt, Mer du Nord méridionale. Apports d'une étude couplée: granulométrie / outils acoustiques/ modélisation des courants. Msc Thesis (in French), Renard Centre of Marine Geology, University of Gent, 74 pp.

Cherlet, P. 1978. Bepaling van enkele seismische karakteristieken van Tertiaire en Kwartaire sedimenten in Vlaanderen. MSc Thesis (in Dutch), Renard Centre of Marine Geology, University of Gent, 43 pp.

Davies, T.A. and Austin, J.A. 1997. High-resolution 3D seismic reflection and coring techniques applied to late Quaternary deposits on the New Yersey shelf. *Marine Geology* **143**, 137-149.

Demco. 2005. Geoelectrisch Onderzoek op de Paardenmarkt. Internal Report (in Dutch), R05117a, 7 pp.

Decarlo, E.H., Cox, E. and Overfield, M. 2007. Ordnace Reef, WaiAnae, Hawaii. Remote Sensing Survey and Sampling at a Discarded Military Munitions Sea Disposal Site. Final Report. U.S. Department of Commerce, National Marine Sanctuary Program. Marine Sanctuaries Conservation Series NMSP-07-01, 98 pp.

Diviacco, P. and Wardell, N. 2003. Pre-processing of 3D VHR seismic data. Deltech Abstract, 12-13.

DND. 2004. Minister's Response to Petition 50B concerning military dumpsites off the Atlantic coast. Department of National Defence, Canada, 24 June 2004.

Duursma, E. K. (ed). 1999. Dumped chemical weapons in the sea - options. Heineken Foundation for the Environment, 60 pp.

Eisma, D. 1981. Supply and deposition of suspended matter in the North Sea. In: S. Nio, R. Schüttenhelm and Tj. Van Weering (eds.), *Holocene Marine Sedimentation in the North Sea Basin*. Spec. Publ. Int. Ass. Sediment. **5**, 415-428.

Emelyanov, E., Lemke, W., Harff, J., Kramarska, R. and Uscinowicz, S. 1995. Sediment maps of the Western Baltic. *Proceedings of the Third Marine Geological Conference "The Baltic"*, 133-137. Warszawa, Poland, 1995.

Emelyanov, E.M 1996. Chemical components and elements in the suspended matter and sediments of the Western Baltic. *Baltica* **9,** 5-15.

Emelyanov, E.M. and Kravtsov, V.A. 2004. Arsenic in the bottom sediments of the Baltic Sea. Is it dangerous ? In: *International Borders Geoenvironmental Concerns. International workshop*, *"PGJ",* pp. 12-14. Krynica Morska, Poland, pp..

Figueiredo, A.G., Nittrouer, C.A. and de Alencar Costa, E. 1996. Gas-charged sediments in the Amazon submarine delta. *Geo-Marine Letters* **16**, 31-35.

Fleischer, W. 2003. Deutsche Abwurfmunition bis 1945. Motorbuch Verlag Stuttgart, 286 pp.

Floodgate, G.D. and Judd, A.G. 1992. The origin of shallow gas. *Continental Shelf Research* **12**(10), 1145-1156.

Fonnum, F. 1989. An investigation into the sunken chemical ships outside the Norwegian coast. Norwegian Defence Research Establishment, Division for Environmental Technology, Internal Report, 16 pp.

Ford, G., Ottemöller, L. and Baptie, B. 2005. Analysis of Explosions in the BGS Seismic Database in the Area of Beaufort's Dyke, 1992-2004. British Geological Survey Commissioned Report, CR/05/064. 15pp.

Frondorf, M. 1996. *Special study of the sea disposal of chemical munitions by the United States.* In : A.V. Kaffka (ed), Sea-Dumped Chemical Weapons: Aspects, Problems and Solutions. NATO ASI Series, 7, 35-40.

Gardner G.H. 1993. Three dimensional seismic methods: acquisition, processing and interpretation, notes for a short course. Houston Advanced Research Center, 274 pp.

Gorodnitski, A., and Filin, A. 2001. Techniques and results of magnetic detection of dumped weapons in Bornholm and Skagerrak dump sites. In: T. Missiaen & J.-P. Henriet (eds), *Chemical Munition Dump Sites in Coastal Environments*, 53-63.

Granbom, P.O. 1996. Investigation of a dumping area in the Skagerrak 1992. In: A.V. Kaffka (ed), *Sea-Dumped Chemical Weapons: Aspects, Problems and Solutions*. *NATO ASI Series* **7**, 41-48.

Gregory, D.J. 1999. Re-burial of timbers in the marine environment as a means of their long term storage: experimental studies in Lynæs Sands, Denmark. *The International Journal of Nautical Archaeology* **27**(4), 343 - 358.

G-Tec. 1996. Eindrapport Project Paardenmarkt - Fase A2 - Magnetometrie & gradiometrie. Studieopdracht ECS/201/12053 (in Dutch), Federaal Ministerie van Leefmilieu, 28 pp.

G-Tec. 2005. Gevorderde magneto/gradiometrische metingen op testzones op de Paardenmarkt, Eindverslag. Studieopdracht INSPA-22701 (in Dutch), FOD Volksgezondheid, Veiligheid van de Voedselketen en Leefmilieu, 19 pp.

van Ham, N., Duvalois, W. and Sabel, R. 2001. Onderzoek in zee gestorte munitie. TNO Prins Maurits Laboratorium, Internal Report 2001-A6 (in Dutch), 27 pp.

Hart, B.S. and Hamilton, T.S. 1993. High-resolution mapping of shallow gas in unconsolidated sediments beneath the Strait of Georgia, British Columbia. *Geo-Marine Letters* **13**, 49-55.

Hatton L., Worthington, M.H. and Makin J. 1986. Seismic Data Processing. Blackwell Scientific Publications.

HELCOM. 1993a. Report on sea dumping of chemical weapons by the United Kingdom in the Skagerrak waters post World War II. Report submitted by United Kingdom to the Helcom CHEMU Working Group, 2/2/5, 28 September 1993.

HELCOM. 1993b. Report on the availability of correct information on dumped chemical munition on the Swedish Continental Shelf. Report submitted by Sweden to the HELCOM CHEMU Working Group, 1/3, 5 April 1993.

HELCOM. 1993c. Update of a report dated 7 May 1985 concerning environmental, health and safety aspects connected with the dumping of war gas ammunition in the waters around Denmark. Report to the Helsinki Commission from the HELCOM CHEMU Working Group, 14/10/1.

HELCOM. 1993d. Fishing vessel incidents involving dumped chemical munition reported to the Swedish Coast Guard since 1980. Report to the Helsinki Commission from the HELCOM CHEMU Working Group, 2/2/6.

HELCOM. 1993e. National information on dumped chemical munition. Report submitted by Lithuania to the HELCOM CHEMU Working Group, 2/2/7, 28 September 1993.

HELCOM. 1993f. Information on catches of chemical munitions by fishermen. Report submitted by Latvia to the HELCOM CHEMU Working Group, 2/2/2, 8 September 1993.

HELCOM. 1993g. National report on war gases and ammunition dumped in the Polish Economic Zone of the Baltic Sea. Report submitted by Poland to the HELCOM CHEMU Working Group, 2/2/4, 17 September 1993.

HELCOM. 1993h. Complex Analysis of the Hazards related to the captured German Chemical Weapons dumped in the Baltic Sea. Report submitted by Russia to the CHEMU Working Group, 2/2/1/Rev.1 (27 Sept. 1993) as amended 11 Oct. 1993.

HELCOM. 1994. Report on chemical munitions dumped in the Baltic Sea. Report submitted by Denmark to the HELCOM CHEMU Working Group, March 1994, 43 pp.

HELCOM. 1996. Third Periodic Assessment of the State of the Marine Environment of the Baltic Sea, 1989-1993. Executive Summary & Background Document. Balt. Sea Envir. Proc. No 64A & 64B.

HELCOM. 2003. Dumped Chemical Munitions in the Baltic Sea,. Report Nr. 7 submitted by Denmark to the Helsinki Commission, Document 12/3, March 2003, 6 pp.

HELCOM 2005. Press release regarding chemical weapons dumps in the Baltic. Helsinki Commission, May 2, 2005.

www.helcom.fi/press_office/news_helcom/en_GB/ChemicalMunitions1115039886140/

HELCOM 2006. Chemical weapons dumps in the Baltic. Updated report on the dumping sites in the Baltic. Report by Denmark to the Helsinki Commission.

Heldens, P. 1983. Een seismische studie van de klei van Boom en de klei van Ieper. PhD Thesis (in Dutch), Renard Centre of Marine Geology, University of Gent, 237 pp.

Henriet, J.-P., Bastin, A. and De Brouck, J. 1978. Integration of continuous seismic profiling in geotechnical investigations of the Belgian coast. K. V. I. V., 7th Intern. Harbour Congress.

Henriet, J.-P., Monjoie, A. and Schroeder, C. 1986. Shallow seismic investigations in engineering practice in Belgium. *First Break* **4**(5), 29-37.

Henriet, J.P., Verschuren, M. and Versteeg, W. 1992. Very high resolution 3D seismic reflection imaging of small-scale structural deformation. *First Break* **10**(3), 81-88.

Henriet, J.-P. and Winthagen, P. 1996a. Eindrapport Project Paardenmarkt – Fase A3 - Reflectie-seismisch onderzoek. Studieopdracht ECS/201/12053 (in Dutch), Federaal Ministerie van Leefmilieu, 38 pp.

Henriet, J.-P. and Winthaegen, P. 1996b. Studie Paardenmarkt – meer-kanaals seismisch onderzoek. Internal Report (in Dutch), Renard Centre of Marine Geology, University of Gent, 47 pp.

Henriet, J.-P. and Missiaen, T. 2004. Haalbaarheidsstudie 3D onderzoek en diepteboringen (Paardenmarkt site) - Eindrapport. Studieopdracht INS 22473 (in Dutch), Federaal Ministerie van Leefmilieu, 48 pp.

Henriet, J.-P. and Missiaen, T. 2005. Geïntegreerd 3D seismo-electrisch onderzoek op de Paaardenmarkt – Eindrapport. Studieopdracht INS 22693 (in Dutch), Federaal Ministerie van Leefmilieu, 52 pp.

Hobbs, C.H., Blanton, D.B., Gammisch, R.A. and Broadwater, J. 1994. A marine archaeological reconnaissance survey using side-scan sonar, Jamestown, Virginia, USA. *Journal of coastal Research* **10**, 351-359.

Hovland, M. and Judd, A.G. 1988. Seabed pockmarks and seepages: impact on geology, biology and the marine environment. Graham and Trotman, London, 293pp.

HRRT. 2001. Offshore disposal of chemical agents and weapons conducte by the United States. Historical Research and Response Team, U.S. Army Research, Development and Engineering Command, Historical Database Nr. 26, MD21010-5424.

ICRAM. 2006. Research on environmental damage caused by chemical ordnance dumped at sea (R.E.D. C.O.D. Project). Final Scientific Report, October 2006, 277 pp.

Jensen, J.B., Bennike, O., Witkowski, A., Lemke, W. and Kuijpers, A. 1999. Early Holocene history of the southwestern Baltic Sea: the Ancuclus Lake stage. *Boreas* **28**, 437-453.

Judd, A.G. and Hovland, M. 1992. The evidence of shallow gas in marine sediments. *Continental Shelf Research* **12**(10), 1081-1095.

Jurgens, J.A., Blanchette, R.A., and Carlson, D.N. 2003. Evaluating wooden remnants of the *Tektaş Burnu* shipwreck. In: R. Koestler, A. Charola, and F. Nieto-Fernandez (eds), *Art, biology, and conservation: biodeterioration of works of art*. Metropolitan Museum of Modern Art, New York, 390-407.

Kaffka, A. V. (ed). 1995. Sea-Dumped Chemical Weapons: Aspects, Problems and Solutions. *NATO ASI Series* **7**, 170 pp.

Kogan, I. and Paull, C.K. 2004. Coastal seismic wipe-outs – distribution controlled by pore waterc salinity. *Marine Geology* **217**, 161-175.

Kögler, F-C. and Larsen, B. 1979. The West Bornholm basin in the baltic Sea: geological structure and Quaternary sediments. *Boreas* **8**, 1-22.

Köhn, W. 1988. The Holocene transgression of the North Sea as exemplified by the Southern Jade Bay and the Belgian coastline. Internal Report, University of Gent, 42 pp.

Kulturtechnik. 1990. Bericht zur Erfassung und Erkundung der Rüstungsaltlasten in de Nordsee. Kulturtechnik GMBH, Bremen, 118 pp.

Kurata, H. 1980. Lessons learned from the destruction of chemical weapons of the Japanese Imperial Forces. In: *Chemical Weapons Destruction and Conversion*. Stockholm International Peace Research Institute (SIPRI). Taylor and Francis, London.

Lafferty, B., Quinn, R. And Breen, R. 2006. A side-scan and high-resolution Chirp sub-bottom profile study of the natural and anthropogenic sedimentary record of Lower Lough Erne, northwestern Ireland. *Journal of Archaeological Science* **33**, 756-766.

Laga, P. 1966. Geologie in Scheldetunnelwerken. Kleidiapir in de uitgraving voor de spoortunnel onder de E3-weg op de Rechteroever te Antwerpen. *Het Ingenieursblad* **35**, 552-553 (in Dutch).

Laurin, F. 1997. The Baltic and North Sea dumping of chemical weapons: still a threat ? In: T. Stock & K. Lohs (eds), *The challenge of old chemical munitions and toxic armament wastes*. SIPRI Chemical & Biological Warfare Studies, Oxford University Press, 263-278.

Lheureux, V. 1990. L'utilisation du gaz de combat sur le front Belge pendant la guerre 1914-1918. MSc Thesis (in French), Lic. Militaire en Sociale Wetenschappen, Koninklijke Militaire School, Brussel.

Libbrecht, D. 1980. Een onderzoek van de abnormaal lage seismische snelheden in de jong-kwartaire sedimenten van de Oostelijke kustvlakte. MSc Thesis (in Dutch), Renard Centre of Marine Geology, University of Gent, 51 pp.

Loke, M.H. 1999. Electrical imaging surveys for environmental and engineering studies - A practical guide to 2-D and 3-D surveys. Course Notes, 59 pp.

Lurquin, L. 1972. Springtuigen Westrand Appelzakgeul. Nota's ZS3/OPS (134175) en N3/OPS/DOC (114/7/5021) met betrekking tot duikoperaties op de Paardenmarkt. Staf van de Zeemacht, 8 pp.

Magelas. 1996. Eindrapport Project Paardenmarkt - Fase A1 - Side-scan sonar operaties. Studieopdracht ECS/201/12053 (in Dutch), Federaal Ministerie van Leefmilieu, 52 pp.

Magelas. 2003. Monitoring van de munitiestortplaats "Paardenmarkt" met behulp van digitale side-scan sonar en multibeam bathymetrie. Studieopdracht INS 22665 (in Dutch), Federaal Ministerie van Leefmilieu, 38 pp.

Malherbe, B. 1989. A case study of dumping of dredged material in open areas. *Int. Sem. on Environmental Aspects of Dredging*, Nantes, 32 pp.

Malherbe, B. 1991. A case study of dumping of dredged material in open areas. *Terra et Aqua* **45**, 5-32.

Madsen, J.A., Brown, L., McKenna, T., Snyder, S. et al. 2001. Geopgysical characterisation of fresh and saline water distribution in a coastal estuarine setting. SAGEEP meeting Abstract, March 2001, Denver CO.

Manheim, F.T., Krantz, D.E., Snyder, D.S., Bratton, J.F. et al. 2001. Streaming resistivity surveys and core drilling define groundwater discharge into coastal bays of the Delmarva Peninsula. GSA Annual meeting Abstract, pA42.

Marsset, B., Missiaen, T., Noble, M., Versteeg, W. and Henriet, J.P. 1998. Very high resolution 3D marine seismic data processing for geotechnical applications. *Geophysical prospecting* **46**(2), 105-120.

Marsset, B., Henriet, J.-P., Noble, M., Wardell, N. et al. 2001. VHR3D - Very High Resolution 3D seismic Method for Detailed Site Investigation. Mast Project Final Technical Report, MAS3-CT97-0121, 258 pp.

Marsset, B., Thomas, Y., Thereau, E., Didailler, S. et al. 2003. Very high resolution 3D seismic imaging of a complex shelf structure in the Adriatic Sea. *Advances in Natural and Technological Hazards Research* **19**, 441-448.

Mathys, M, Thiessen, O., Theilen, F. and Schmidt, M. 2005. Seismic characterisation of gas-rich near-surface sediments in the Arkona Basin, Western Baltic Sea. *Marine Geophysical Researches* **26**, 207–224.

McGee, T.M. 1991. Seismic reverberations and the remote estimation of properties of underwater soils. *International Journal of Imaging Systems and Technology* **3**, 40-57.

McGhee, M.S., Luyendyk, B.P., and Boegman, D.E. 1968. Location of an ancient Roman shipwreck by modern acoustic techniques - a critical look at marine technology. Marine Technology Society, 4th Annual Conference, Washington D.C.

McGrail, S. 1998. Ancient boats in North-West Europe: the archaeology of water transport to AD 1500. In: B. Cunliffe (ed), *Longman Archaeology series*. Longman, London.

MEDEA. 1997. *Ocean dumping of chemical munitions: environmental effects in arctic areas.* US Government Report, 235 pp.

Mindell, D.A. and Bingham, B. 2000. A high-frequency, narrow-beam subbottom profiler for archaeological applications. Massachusets Institute of Technology Internal Report, MTS-0-933957-28-91.

Ministerie van Openbare Werken. 1978. Trilboringen – Geotechnisch onderzoek van de toegangsgeulen en banken voor de Belgische kust. Internal report (in Dutch), Brussel, 136 pp.

Ministerie van Openbare Werken. 1993. Ecologische impact van baggerspecieoplossingen voor de Belgische kust. Internal report (in Dutch), Brussel, 101 pp.

Missiaen, T., McGee, T., Pearks, D., Ollier, G. and Theilen, F. 1996. An interdisciplinary approach to the evaluation of physical parameters of shallow marine sediments. In: M. De Batist & P. Jacobs (eds.) *The Geology of Siliciclastic Shelf Seas*. Geol. Soc. Spec. Publ. **17**, 299-322.

Missiaen, T. 1997. Very High Resolution 3D Seismic Reflection Imaging. MAST-II Fellowship Research Project, Final Report, 68 pp.

Missiaen, T., Henriet, J.-P. and the Paardenmarkt Project Team. 2001. Paardenmarkt Site Evaluation. OSTC Final Report, Project MN/02/88, 185 pp.

Missiaen, T. and Henriet, J.-P. (eds). 2002. Chemical munition dump sites in coastal environments. OSTC Special Publication, Brussels, 167 pp.

Missiaen T., Versteeg W. and Henriet J.-P. 2002a. A new 3D seismic acquisition system for very high and ultra high resolution shallow water studies. *First Break* **20**(4), 227-232.

Missiaen, T., Murphy, S., Loncke, L. and Henriet, J.-P. 2002b. Very high resolution seismic mapping of shallow gas in the Belgian coastal zone. *Continental Shelf Research* **22**(16), 2291-2301.

Missiaen, T., Henriet, J.-P. and the Paardenmarkt Project Team. 2002c. Chemical munitions off the Belgian coast: an evaluation study. In: T. Missiaen & J.-P. Henriet (eds.), *Chemical munition dump sites in coastal environments*, 65-79.

Missiaen, T., Versteeg, W., Henriet, J.-P., and Lanckneus, J. 2004. Geofysische metingen op de Schelde. Boei 103 (Ketelplaat), Drempel van Frederik, Oosterweel - Eindverslag. Internal Report (in Dutch), Renard Centre of Marine Geology, University of Gent, 44pp.

Missiaen, T. 2005. VHR marine 3D seismics for shallow water investigations: some practical guidelines. *Marine Geophysical Researches* **26**, 145-155.

Missiaen, T., Wardell, N. and Dix, J. (eds). 2005. Subsurface imaging and sediment characterisation in shallow water envirnonments. *Marine Geophysical Researches Special Issue* **26**(2-4), 328 pp.

Missiaen, T. and Versteeg, W. 2006. Very high resolution seismic investigations over a buried wooden shipwreck. *Geologica Belgica Abstracts*, p47.

Missiaen, T. and Noppe, L. 2006. Very high resolution reflection seismic investigations in Bornholm Basin, R/V Shelf 18-29 July 2006. MERCW Project Report (Deliverable D3.1), Renard Centre of Marine Geology, University of Gent, 22 pp.

Missiaen, T. and Paka, V. 2007. Synthesis report of available data regarding CW dumpsites in the Baltic Sea. MERCW Project Report (Deliverable D2.1), Renard Centre of Marine Geology, University of Gent, 62 pp. ISBN 978-951-53-2971-4.

Missiaen, T. and Feller, P. 2007. Very high resolution geophysical investigations in Bornholm Basin, R/V Fritz Reuter 27 June-11 July 2007. MERCW Project Report (Deliverable D2.3), Renard Centre of Marine Geology, University of Gent, 28 pp.

Missiaen, T. and Noppe, L. 2008. Very high resolution seismic study of the Bornholm Basin, southern Baltic Sea. Submitted.

Missiaen, T. and Feller, P. 2008. Very high resolution seismic and magnetic investigations of a chemical munition dumpsite in the Baltic Sea. Submitted.

Missiaen, T., Slob, E. and Donselaar, M.E. 2008a. Comparing different shallow geophysical methods in a tidal estuary, Verdronken Land van Saeftinge, Western Scheldt, The Netherlands. *Netherlands Journal of Geology (NJG)*, accepted.

Missiaen, T., Baeteman, C. and Pieters, M. 2008b. Very high resolution seismic investigations for submerged archeology studies offsore Raversijde, Belgium. In preparation.

Mosher, D. and Law, K. 1996. Application of concurrent marine elektromagnetic and marine seismic high resolution profiling, British Columbia, Canada. *J. Env. Eng. Geophys.* **1**(3), 215–228.

Mosher, D. and Simpkin, P. 1999. Status and trends of marine high-resolution seismic reflection profiling: data acquisition. Geological Survey of Canada contribution number 1999002, 22pp.

Mosher, D., LaPierre, A., Hughes-Clarke, J. and Gilbert, G. 2002. Theoretical comparison of seafloor renders from multibeam and 3D seismic exploration data. Offshore Technology Conference, 6-9 May 2002, Houston, Tx.

Müller C., Milkereit B., Bohlen T. and Theilen F. 2002. Towards high-resolution 3D marine seismics using Boomer sources. *Geophysical Prospecting* **50**, 517-526.

Müller, C., Lübke, H., Woelz, S., Jokisch, T., et al. 2006. Marine 3-D seismic investigation of a late Ertebølle settlement in Wismar Bay (SEAMAP-3D case study). Geophysical Research Abstracts, 8, 08447.

Müller, C., Woelz, S., Jokisch, T., Ersoy, Y et. al. 2007. Ultra-High-Resolution Marine 2D/3D Seismic Investigation of the Limantepe/Carantina Island Archaeological Site (Urla/Turkey). Geophysical Research Abstracts, 9, 10397.

Muribi, M. 1997. Toxicity of mustard gas and two arsenic based warfare agents on Daphnia Magnia. FOI Internal Report, ISSN 1104-9151, April 1997.

Nehring, S. 2005. Warfare-related hazardous sites in German coastal waters - Recommendations for a successful implementation of the EC Water Framework Directive (in German). *Rostock. Meeresbiolog. Beitr*., 14, 109 – 123.

Noppe, L. 2007. Seismisch onderzoek van een dumpplaats in het Bornholmbekken, Baltische Zee. MSc thesis (in Dutch), Renard Centre of Marine Geology, University of Gent, 119 pp.

OSPAR. 2005. Overview of past dumping at sea of chemical weapons and munitions in the OSPAR maritime area. OSPAR Commission Report 2005/222, Biodiversity Series, 13pp.

Paka, V., and Spridonov, M. 2001. Research of dumped chemical weapons made by R/V "Professor Shtokman" in the Gotland, Bornholm & Skagerrak dumpsites. In: T. Missiaen & J.-P. Henriet (eds), *Chemical munition dump sites in coastal environments*, 27-42.

Paka, V. 2004. Sea-dumped Chemical Weapons: state of problem. *Russian Chemical Journal (Journ. of Mendeleev Russian Chemical Society)*, XLVIII **2**, 99-109.

Paka, V. 2006. Pilot Cruise 71 on board R/V Shelf, research area Bornholm Basin & Southern Baltic. MERCW project Deliverable D3.1, December 2006.

Perini, L., Missiaen, T., Ori, G.G. and De Batist, M. 1994. Seismic evidence of glacial to marine sedimentation during the Late Quaternary offshore Bornholm, southern Baltic. *Sedimentary Geology* **102**, 3-21.

Plunkett, G. 2003. Chemical Warfare Agent Sea Dumping off Australia. Third edition. Internal Report, Department of Defence, Australia, ISBN 0642295875, 36 pp.

Politz, F. Zeitbombe Ostsee - Das Giftgas-Erbe auf dem Meerersgrund (in German). Chr. Links Verlag – LinksDruck GmbH, Berlin, 134 pp.

Prentiss, A.M. 1937. Chemicals in war. A treatise on Chemical Warfare. McGraw, NY, 460 pp.

Pulliam J., Austin J.A., et al. 1996. An ultrahigh resolution 3D survey of the shallow subsurface on the continental shelf of New Jersey. *The Leading Edge* **15**, 839-845.

Quinn, R., Bull, J. and Dix, J. 1997a. Imaging wooden artefacts using chirp sources. *Archaeological Prospection* **4**, 25-35.

Quinn, R., Bull, J. and Dix, J. 1997b. The Mary Rose site – geophysical evidence for palaeo-scour marks. *International Journal of Nautical Archaeology* **26**, 3-16.

Quinn, R., Cooper, A. and Williams, B. 2000. Marine geophysical investigation of the inshore coastal waters of Northern Ireland. *International Journal of Nautical Archaeology* **29**(2), 294-298.

Quinn, R., Bree, C. and Forsythe, W. 2002. Integrated geophysical surveys of the French frigate La Surveillante (1797), Bantry bay, Co. Cork, Ireland. *Journal of Archaeological Science* **29**, 413-422.

Rao, T.C. 1988. Geophysical techniques to locate pre-hisroric sites and artifacts on the continental shelf. In: S.R. Rao (ed.), *Marine Archaeology of Indian Ocean Countries*. Nat. Inst. Oceanog., 73-77. Goa, India.

Rapsch, H.-J., and Fisher, U. 2000. Munition im Fischernetz. Altlasten in der Deutschen Bucht. Isensee Verlag, Oldenburg, 80 pp.

Rice, D.D. and Claypool, G.E. 1981. Generation, accumulation, and resource potential of biogenic gas. *AAPG Bulletin* **65**, 5-25.

Richardson, M.D., and Davis, A.M. 1998. Modeling methane-rich sediments of Eckernförde Bay, *Continental Shelf Research* **18**, 1671-1688.

Rijkswaterstaat. 2003. Onderzoekslokaties IMAGO prijsvraag. Rijkswaterstaat Internal Report (in Dutch), 11 pp.

Robb, G.B., Best, A.I., Dix, J.D., Bull, J.M., et al. 2006. The frequency dependence of compressional wave velocity and attenuation coefficient of intertidal marine sediments. *J. Acoust. Soc. Am*. **120**(5), 2526–2537.

Rodacy, P.J., Reber, S.D., Walker, P.K., and Andre, J.V. 2001. Chemical Sensing of Explosive Targets in the Bedford Basin, Halifax Nova Scotia. Report SAND2001-3569, Sandia National Laboratories, 45 pp.

Rogers, A. and Yamamoto, T. 1993. The High Resolution 3-D Seismic Survey System 'Kite'. SEG 60th Annual Meeting, Washington DC, 531-535.

Schittekat, J., Henriet, J.P. and Vandenberghe, N. 1983. Geology and geotechnique of the Scheldt surge barrier – characteristics of an overconsolidated clay. *Proceedings of the 8th International Harbour Congress Antwerpen* **1**, 121- 134.

Scheidhauer, M., Marillier, F. and Dupuy, D. 2005. Development of a system for 3D high-resolution seismic reflection profiling on lakes. *Marine Geophysical Researches* **26**, 183-195.

Schubel, J.R., 1974. Gas bubbles and the acoustically impenetrable, or turbid, character of some estuarine sediments. In: I.R. Kaplan (Ed.) *Marine Science, Vol. 3*. Plenum Press, New York, 275-298.

Schulz-Ohlberg, J., Lemke, W. and Tauber, F. 2001. Tracing dumped chemical munitions in Pomeranian Bay (Baltic Sea) at former transport routes to the dumping areas off Bornholm Island. In: T. Missiaen & J.-P. Henriet (eds), *Chemical Munition Dump Sites in Coastal Environments*, 43-52.

Sheriff, R.E. 1996. Understanding the Fresnel zone. AAPG Explorer, October 1996.

Sheriff, R.E. and Geldart, L.P. 1982. Exploration Seismology, Volume 1, History, theory and data acquisition. Cambridge University Press, 253 pp.

Sheriff, R.E. and Geldart, L.P. 1983. Exploration Seismology, Volume 2, Data-processing and interpretation. Cambridge University Press, 221 pp.

Sills, G.C., Wheeler, S.J., Thomas, S.D., and Gardner, T.N. 1991. Behaviour of offshore soils containing gas bubbles. *Géotechnique* **41**(2), 227-241.

Silva, A.J. and Brandes, H.G. 1998. geotechnical properties and behavior of high-porosity, organic-rich sediment in Eckernförde Bay, Germany. *Continental Shelf Research* **18**, 1917-1938.

Simpkin, P.G. 2005. The Boomer source as a tool for shallow water geophysical exploration. *Marine Geophysical Researches* **26**, 171-181.

SIPRI. 1997. Delayed toxic effects of chemical warfare agents. SIPRI Monograph, Stockholm, 47 pp.

SOAEFD. 1996. Surveys of the Beaufort's Dyke explosives disposal site,November 1995 - July 1996. The Scottish Office of Agriculture, Environment and Fisheries Department, Marine Laboratory, Aberdeen, Scotland, 104 pp.

Staelens, P. 2002. Verwerking van navigatie en deiningscompensatie in 3D seismisch onderzoek met zeer hoge resolutie. MSc thesis (in Dutch), Renard Centre of Marine Geology, University of Gent, 131 pp.

Stock, T. 1996. Sea-dumped chemical weapons and the chemical weapons convention. In: A.V. Kaffka (ed), *Sea-Dumped Chemical Weapons: Aspects, Problems and Solutions*. NATO ASI Series, 7, 49-66.

Stock, T. and Lohs, K. (eds). 1997. The challenge of old chemical munitions and toxic armament wastes. SIPRI Chemical & Biological Warfare Studies, Oxford University Press, 337 pp.

Stucchi, E. and Mazzotti, A. 2003. Reflection and refraction seismic on the great Ancona landslide. *Geophysical Research Abstracts* **5**, 09995.

Theobald, N. 2001. Chemical munitions in the Baltic Sea. In: T. Missiaen & J.-P. Henriet (eds), *Chemical Munition Dump Sites in Coastal Environments*, 95-106.

Thomas, Y., Marsset, B., Didailler, S., Regnault, J.-P., Le Conte, S., et al. 2004. Sismique marine haute résolution 3D: un nouvel outil de reconnaissance à destination de la communauté scientifique (in French*). Comptes Rendus Geosciences* **336**(6), 579-585.

Tijdelijke Vereniging Bergingswerken. 1989a. Magnetometrisch onderzoek op de Paardenmarkt. Internal report (in Dutch), 12 pp.

Tijdelijke Vereniging Bergingswerken. 1989b. Reflectieseismisch onderzoek voor de Belgische kust. Internal report (in Dutch), 14 pp.

TNO-TPD. 2003. IMAGO Project – Plan van aanpak/voorstudie, data acquisitie en data processing. Internal Report DII-RTP-030036 (in Dutch), 45 pp.

Tørnes, J.A., Voie Ø.A., Ljønes, M., Opstad A.M, et al. 2002. Investigation and risk assessment of ships loaded with chemical ammunition scuttled in the Skagerrak. SFT Internal Report TA-1907/2002, 76 pp.

Vandenberghe, N. 1978. Sedimentology of the Boom Clay (Rupelian) in Belgium. Verh. Kon. Acad. Wet., Lett., Schon. Kunsten van België, nr. 147.

Vandenberghe, N. and Laga, P. 1986. The septaria of the Boom Clay (Rupelian) and its type area in Belgium. *Aardkundige mededelingen* **3**, 229-238.

van den Brenk, S., Romijn, R. and Missiaen, T. 2003. Eindrapport IMAGO - Rapport, Prijsvraag en onderzoek Wadenzee. RDIJ rapport nr. 2003-13c, ISBN 90 36913233 (in Dutch), 80 pp.

Vardy, M., Dix, J., Henstock, T., Bull, J. and Gutowski, M. 2006. High-Resolution 3D Seismic Chirp Volumes: A Case Study in Small Object Detection. Eos Trans. *AGU 87(52) fall Meet. Suppl*. Abstract NS31B-1577.

Verbeeck, P. 2004. Akoestische en sedimentologische karakterisering van een oude munitiedump-plaats: de Paardenmarkt site, Belgisch Continentaal Plat. MSc thesis (in Dutch), Renard Centre of Marine Geology, University of Gent, 103 pp.

Verbeek, N. 1995. Aspects of high resolution marine seismics. PhD thesis, University of Utrecht, 134 pp.

Vermeer, G. 1999. Factors affecting spatial resolution. *Geophysics* **64**(3), 942-953.

Verschuren, M. 1992. An integrated approach to clay tectonic deformation. PhD Thesis, Renard Centre of Marine Geology, University of Gent, 359 pp.

Voipio, A. (ed.). 1981. The Baltic Sea. Elsevier Oceanography Series, 30, 418pp.

Waleij, A., Ahlberg, M., Muribi, M. and Erikson, J. 2001. Ecotoxicity of mustard gas, Clark I, Clark II and the metabolite tetraphenyldiarsine oxide occurring in sea-dumped chemical munition. In: T. Missiaen & J.-P. Henriet (eds), *Chemical Munition Dump Sites in Coastal Environments*, 121-132.

Wardell N., Diviacco P. and Sinceri, R. 2002. Pre-processing techniques for marine very high resolution 3D (VHR3D) seismic data. *First Break* **20**(7), 457-466.

Westley, K., Dix, J.K. and Quinn, R. 2004. A Re-assessment of the Archaeological Potential of Continetal Shelves. Final Report. Aggregates Level Sustainability Fund Project 3362. English Heritage Report, 236 pp.

Wheeler, S.J. 1988. The undrained shear strength of soils containing large gas bubbles. *Géotechnique* **38**(3), 399-413.

Wheeler, S.J. 1990. Movement of large gas bubbles in unsaturated fine-grained sediments. *Marine Geotechnology* **9**, 113-129.

Wheeler, S.J., Sills, G.C., Sham, W.K., Duffy, S.M. and Boden, D.G. 1990. The influence of gas on geotechnical properties of fdine-grained sediments. *Underwater Technology* **17**(3), 11-16.

Wilkens, R.H. and Richardson, M.D. 1998. The influence of gas bubbles on sediment acoustic properties: in situ, laboratory, and theoretical results from Eckernförde Bay, Baltic Sea. *Continental Shelf Research* **18**(14–15), 1859–1892.

Winterhalter, B. 2001. The BASYS coring site in the North Central Baltic Sea Basin – a geological description. *Baltica* **14**, 9-17.

Winthagen, P. 1996. Paardenmarkt Study: Multichannel seismic investigation. Internal report, Renard Centre of Marine Geology, University of Gent, 38 pp.

Wunderlich, J., Wendt, G. and Müller, S. 2005. High-resolution echo-sounding and detection of embedded archaeological objects with nonlinear sub-bottom profilers. *Marine Geophysical Researches* **26**, 123-133.

Yilmaz, Ö. 1987. Seismic data processing. Society of Exploration Geophysics, Tulsa, Oklahoma, 526 pp.

Zgur, F., Baradello, L., Del Negro, E., Marino, B. and Nieto, D. 2003. A seismic acquisition system for transition zone high resolution surveys. *DelTech International Workshop Abstract Book*, 5-9 May 2003, Venice, 83-84.

Zhurbas, V. 2007. A robust numerical/analytical model of dispersion of a non-conservative tracer released in a bottom layer boundary. MERCW Project Report (Deliverable 4.3), 14pp.

Zhurbas, V., Stipa, T., Malkki, P., Paka, V. Golenko, N. et al. 2004. Generation of Subsurface Cyclonic Eddies in the Southeast Baltic Sea: Observations and Numerical Experiments. *J. Geophys.Res*. **109**, C05033, doi:10.1029/2003JC002074.